REPORT DOCUMENTATION PAGE

Form Approved
OMB No. 0704-0188

PLEASE DO NOT RETURN YOUR FORM TO THE ABOVE ADDRESS.

1. REPORT DATE *(DD-MM-YYYY)*	2. REPORT TYPE	3. DATES COVERED *(From - To)*
31-08-2006	Final	1 July 2003- 30 June 2006

4. TITLE AND SUBTITLE
Nonlinear Wave Propagation

5a. CONTRACT NUMBER

5b. GRANT NUMBER
F49620-03-1-0250

5c. PROGRAM ELEMENT NUMBER

6. AUTHOR(S)
Mark J. Ablowitz

5d. PROJECT NUMBER

5e. TASK NUMBER

5f. WORK UNIT NUMBER

7. PERFORMING ORGANIZATION NAME(S) AND ADDRESS(ES)
Department of Applied Mathematics
University of Colorado
Campus Box 526
Boulder, CO 80309-0526

8. PERFORMING ORGANIZATION REPORT NUMBER
1536810

9. SPONSORING/MONITORING AGENCY NAME(S) AND ADDRESS(ES)
Air Force Office of Scientific Research
875 North Randolph St., Rm 3112
Arlington, VA 22203

10. SPONSOR/MONITOR'S ACRONYM(S)

11. SPONSORING/MONITORING AGENCY REPORT NUMBER

12. DISTRIBUTION AVAILABILITY STATEMENT
DISTRIBUTION A. Approved for public release; distribution unlimited.

13. SUPPLEMENTARY NOTES

14. ABSTRACT
The dynamics and properties of mode locked lasers, such as Titanium:sapphire lasers, that produce ultrashort pulses were modeled and comparisons with experiments carried out. An important characteristic of short pulse lasers is the carrier-envelope phase (CEP) slip which is the phase offset between carrier and envelope from pulse to pulse in the pulse train. Control of the phase slip allows researchers to stabilize trains of ultrashort pulses, which are very useful in applications. Accurate models of the slip were obtained. New asymptotic and computational methods describing observed phenomena in photonic lattices were developed. Research in quadratic optical materials has led to novel asymptotic systems of equations. In certain parameter regimes stable localized pulse solutions are found and in other cases the equations have unstable and singular solutions. The possibility of such solutions indicates situations when extreme damage to the optical crystal can occur. New numerical schemes to compute localized states to a broad class of nonlinear systems have been developed. From 1 July 2003 to 30 June 2006, 8 papers were published or accepted in refereed journals, 2 book chapters were published and 19 invited lectures were given.

15. SUBJECT TERMS
nonlinear wave propagation

INSTRUCTIONS FOR COMPLETING SF 298

16. SECURITY CLASSIFICATION OF:			17. LIMITATION OF ABSTRACT	18. NUMBER OF PAGES	19a. NAME OF RESPONSIBLE PERSON
a. REPORT U	b. ABSTRACT U	c. THIS PAGE U	U	26	19b. TELEPONE NUMBER (*Include area code)*

Nonlinear Wave Propagation
AFOSR Grant/Contract # F49620-03-1-0250
Final Report
1 July 2003 – 30 June 2006

August 31, 2006

Mark J. Ablowitz
Department of Applied Mathematics
University of Colorado
Boulder, CO 80309-0526
Phone: 303-492-5502
Fax:303-492-4066
email address: mark.ablowitz@colorado.edu

OBJECTIVES

To carry out fundamental and wide ranging research investigations involving the nonlinear wave propagation that arise in physically significant systems. Applications include modelling and computational studies of wave phenomena in nonlinear optics, solutions of physically significant nonlinear equations, direct and inverse scattering, and the development of new computational methods for investigation of physical systems.

STATUS OF EFFORT

The research program of the PI in the field of nonlinear wave propagation is broad based and very active. There have been a number of important research contributions carried out as part of the effort funded by the Air Force. During the period 1 July 2003 – 30 June 2006, 8 papers were published or accepted for publication in refereed journals, 2 book chapters/conference proceedings were published and 19 invited lectures were given. The key results and research directions are described below in the section on accomplishments/new findings. Full details can be found in our research papers which are also given at the end of this report. Specific research investigations carried out by the PI and colleagues included the following studies.

The dynamics and properties of mode locked lasers that produce ultrashort pulses were investigated. Titanium:sapphire (Ti:sapphire or Ti:s) lasers are often used to produce ultrashort pulses, typically on the order of a few femtoseconds. There are other mode locked lasers which produce ultrashort pulses, such as Sr-Forsterite and fiber lasers, but Ti:s lasers have better stability characteristics. These mode-locked lasers generate a regularly spaced train of ultrashort pulses separated by one cavity round-trip time. A Ti:s laser consists of a Ti:sapphire crystal which exhibits a nonlinear Kerr response and has a large normal group-velocity dispersion (GVD). The Ti:s laser systems also have a set of prisms and/or mirrors specially designed to have large anomalous GVD in order to largely compensate for the normal GVD of the crystal. Recent experiments conducted at the University of Colorado, in collaboration with our group demonstrated that such lasers are well approximated by dispersion managed (DM) systems and the intra-cavity pulse was found to be described by a dispersion managed soliton. An important characteristic of short pulse lasers analyzed in our work is the carrier-envelope phase (CEP) slip. The CEP slip is the change of the phase offset between carrier and envelope from pulse to pulse in the pulse train. This slip is equal to the phase slip that the intra-cavity pulse accumulates over one cavity round-trip before being emitted from the output coupler. The intra-cavity slip is induced by the nonlinearity and dispersion of the cavity. Control of the phase slip allows researchers to stabilize trains of ultrashort pulses which are very useful in applications. Noise effects due to spontaneous emission were also studied. Improved understanding of the phase slip and noise characteristics will help experimentalists improve the characterisitcs/stabilization of the pulse train. Applications of Ti:sapphire laser systems include new and enhanced methods for optical signal processing and greatly improved timing and measuring devices.

Investigations of pulse propagation in photonic lattices were carried out. In recent years there has been important experimental research on discrete optical wave-guides and the propagation of their nonlinear modes. Nonlinear waves in waveguide arrays have attracted special

attention due to their experimental realizability. Early experimental observation of nonlinear lattice modes in optical waveguide arrays demonstrated that at sufficiently high power, a laser beam could be self-trapped inside the waveguide. This demonstrated the formation of a lattice soliton. Importantly, these waveguides can be constructed on extremely small scales. Experimentalists now have been able to construct one and two dimensional lattices by interference of laser beams. This is a significant advantage since the background lattice structure does not need to be mechanically fabricated. Lattice nonlinear Schrodinger equations provide excellent models. We developed new asymptotic and computational methods which describe observed phenomena and found localized pulse solutions to two-dimensional optical lattices with both regular and irregular lattice backgrounds. Applications of photonic lattices include all-optical switching, steering, blocking and routing of lattice-discrete solitons in two-dimensional networks.

Research involving quadratic, or so-called $\chi^{(2)}$, nonlinear optical materials has led to new asymptotic systems of equations. Detailed calculations indicate that in certain parameter regimes there are stable localized pulse solutions and in other cases the equations have unstable and singular solutions. The possibility of such singular solutions indicates situations when extreme damage to the underlying optical crystal is possible.

New numerical schemes to compute localized states, or solitary waves to a broad class of nonlinear systems have been developed. The essential steps involve renormalizing the unknown variables, transforming the underlying nonlinear equation into Fourier space and determining nonlinear algebraic equations which couple to the nonlocal integral equation in Fourier space. The coupling prevents the numerical scheme from diverging. The nonlinear mode is determined from a convergent fixed point iteration scheme. The computational methods allow us to find mutidimensional localized pulse solutions to the governing systems.

ACCOMPLISHMENTS/NEW FINDINGS

Dynamics of ultra-short laser pulses and frequency combs

Research breakthroughs over the past few years with mode locked lasers, such as Ti:sapphire lasers, have enabled scientists to generate regularly spaced trains of ultrashort pulses, separated by one cavity round-trip time. Fig. 1 below shows a schematic of a mode locked Ti:sapphire laser and the emitted pulse train. Typical values for a Ti:sapphire mode locked laser are pulse width: $\tau = 10$ fs $= 10^{-14}$ sec and repetition time: $T_{\rm rep} = 10$ ns $= 10^{-8}$ sec.

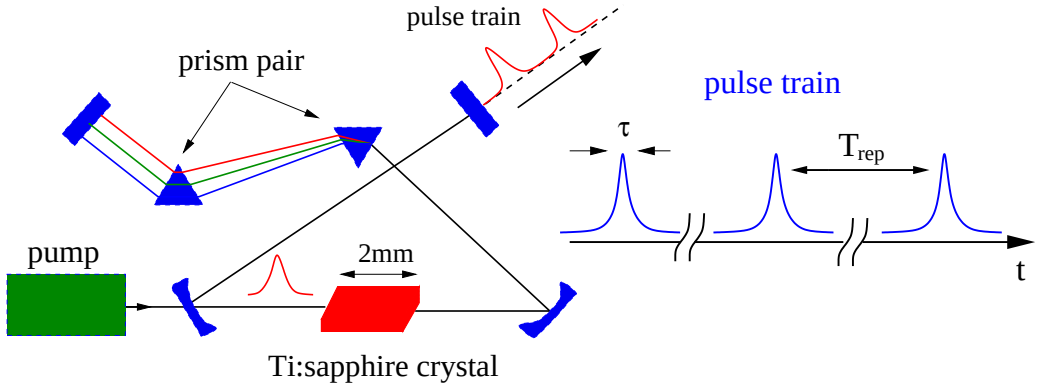

Figure 1: Ti:sapphire laser (left) and the emitted pulse train (right).

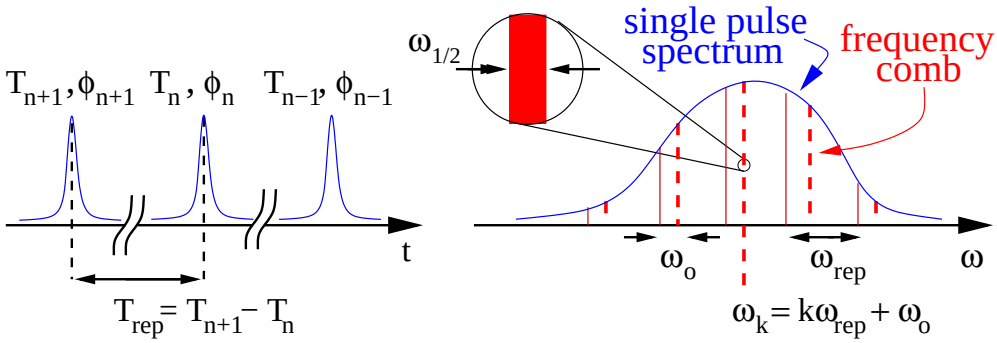

Figure 2: Schematic of a pulse train (left) and its spectrum –frequency comb (right).

Associated with the spectrum of the pulse train is a frequency comb, whose frequencies are separated by the laser's repetition frequency $f_{\rm rep} = \frac{1}{T_{\rm rep}} = 100$ MHz; $\omega_{\rm rep} = 2\pi f_{\rm rep}$; see Figure 2 above. In this figure T_n, ϕ_n are the center time and phase of the nth pulse. In the absence of noise, the pulse's spectrum determines the bandwidth, while the repetition-time,

$T_{rep} = T_{n+1} - T_n$, and overall phase slip, $\Delta\phi = \phi_{n+1} - \phi_n$, determine the comb function in frequency space. The frequency of the k'th comb line (enumerated around the center frequency) is $\omega_k = k\omega_{\rm rep} + \omega_o$, where $\omega_{\rm rep} = 2\pi/T_{rep}$ and $\omega_o = \Delta\phi\omega_{\rm rep}/2\pi$ are the repetition and offset frequencies which are indepicted in Fig. 2. The linewidth ($\omega_{1/2}$ in the inset) is the FWHM (full width half maximum) of the comb function around each comb frequency. In the deterministic case, for a large number of pulses $N >> 1$, the linewidth can estimated to be $\omega_{1/2} = O(\frac{1}{NT_{\rm rep}})$. Additional noise leads to jitter in the center time T_n, and phase ϕ_n, which in turn, broadens the FWHM of the comb lines.

As indicated above, modelocked lasers such as Ti:sapphire (Ti:s) laser systems (see Fig. 1) generate trains of optical pulses, whose spectrum consists of frequency comb lines (see Fig. 2). Important progress in the development of extremely stable optical oscillators has been made possible by the use of controlled femtosecond frequency combs. To date the most stable frequency combs have been generated by Ti:s laser systems, but other less expensive lasers such as Sr:Forsterite lasers are also being intensively studied. We have been working with faculty in the Department of Physics at the University of Colorado on this research.

i) Carrier-envelope phase slip

Ti:s lasers produce pulses as short as a few femtoseconds; typically 10 fs. These modelocked lasers generate a regularly spaced train of ultrashort pulses separated by one cavity round-trip time The phase slip is the change of the phase offset between carrier and envelope from pulse to pulse in the pulse train which accumulates over one cavity round-trip, before being emitted from the output coupler. Fig. 3 depicts the **physical origin of the** carrier envelope phase (CEP) shift. The intra-cavity slip is induced by the nonlinearity and dispersion of the cavity.

A typical Ti:s laser, such as the one depicted in Fig. 1, consists of a Ti:sapphire crystal that has a nonlinear Kerr response as well as large normal group-velocity dispersion (GVD),

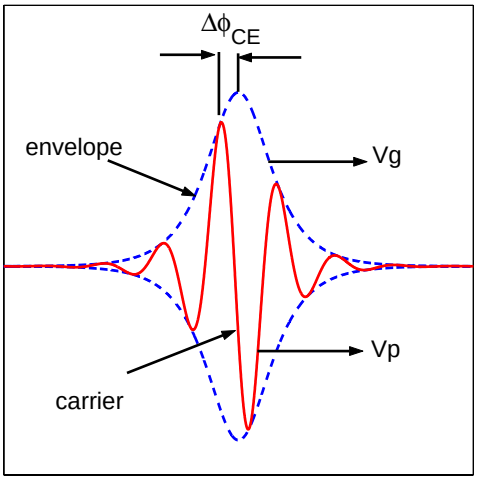

Figure 3: The carrier-envelope phase, $\Delta\phi_{CE} \equiv \Delta\phi$, changes during propagation, because the envelope propagates at the group velocity while the carrier wave propagates at the phase velocity.

and a set of prisms and mirrors specially designed to have large anomalous GVD. The pump laser excites the Ti:Sapphire crystal, causing it to lase and the pulse undergoes large changes inside the Ti:sapphire cavity . The combined contributions to the phase slip depends on the nonlinear phase and nonlinear dispersion in the cavity.

This crystal induces a nonlinear effect as well as large **normal** GVD. On the other hand, the mirror and prisms induce large **anomalous** GVD that nearly balances the normal GVD of crystal. Therefore, the cavity has a small net-GVD (average dispersion) over one round-trip. The pulse bounces between the mirrors and output coupler and is "sampled" every round-trip at the output coupler (which transmits only 6% of the energy). When the laser is mode-locked a regularly-spaced ultrashort pulse train is emitted from the cavity. To model the intra-cavity pulse dynamics we employed the following perturbed NLS equation (after non-dimensionalization) for the pulse-envelopes $u(z,t)$:

$$iu_z + \frac{D(\zeta)}{2}u_{tt} + g(\zeta)|u|^2u = -i\epsilon g(\zeta)(|u|^2u)_t \tag{1}$$

where the normalized linear dispersion coefficient is given by $D(z) =< D > +l_c^{-1}\Delta(z/l_c)$, with $\zeta = z/l_c$, $< D >$ the average dispersion (net GVD), Δ the deviation from the average,

and l_c the laser-design map length. Typically for mode-locked Ti:Sapphire lasers $l_c \ll 1$. Nonlinearity-management means that $g = 1$ inside the Ti:sapphire crystal and $g = 0$ outside the crystal, i.e., we have linear propagation inside the prisms and mirrors. It is useful to define the map strength $s = \Delta_1/4$ (for a symmetric map), where Δ_1 is the GVD of the crystal after subtracting the net GVD. This map strength thus measures the variation of the intra-cavity GVD. The term on the right-hand side, often called the "shock" term, corresponds to small nonlinear dispersion arising form the Kerr effect. We focus on the shock term, first because it is particularly important for shorter pulses. In addition, the shock term induces a nonlinear change in the phase slip, an intriguing phenomenon that is consistent with observed experimental dependence of the slip on pulse energy (pump power).

The nonlinear contribution to the phase slip is the difference between the nonlinear phase and timing shifts accumulated over one cavity round-trip. We found the nonlinear slip, i.e., the slip induced by nonlinear phase and nonlinear dispersion effects, to be well-approximated by

$$\delta_{\mathrm{NL}} \approx 3\bar{k}'' L/\tau_0^2 s,$$

where $\bar{k}''$ is average-cavity GVD and L is the optical cavity length. This result shows that the phase slip that is induced by nonlinear-dispersion reduces to zero with strong dispersion-management, which is consistent with the insensitivity of the slip to pulse energy with strong dispersion management. We also considered additional effects on the slip such as third-order dispersion (TOD), which can be modeled by adding $[i\bar{k}'''/(6\gamma P^*\tau_0^3)]u_{ttt}$ (normalized) to the right-hand side of Eq. (1), where $\bar{k}'''$ is the average TOD coefficient, i.e., the net TOD per round-trip of the cavity. For TOD we found that $\delta_{\mathrm{TOD}} \approx -\omega\bar{k}''' L/\tau_0^2 s$.

Thus the laser cavity is modeled by a dispersion and nonlinearity managed nonlinear Schrödinger equation (perturbed NLS), that takes nonlinear phase (self-phase modulation) and small nonlinear dispersion into account. In our paper: "Carrier-envelope phase slip of ultra-short dispersion managed solitons", M.J. Ablowitz, B. Ilan and S. Cundiff, *Optics Let-*

ters, **29** (2004) 1808, we developed a detailed asymptotic theory which gave analytic results that described the carrier-envelope phase shift in this dispersion-managed NLS equation.

Control of the carrier envelope phase shift is important in applications. It is a key aspect to obtain highly stable optical oscillators.

ii) Comparison of theory with recent experiments

Motivated by the theory we developed, experiments were performed in the Dept. of Physics at the University of Colorado. It was found that the theory agrees with experiments remarkably well. In Fig. 4 the full width half maximum (FWHM) is plotted vs. the average pulse energy for various values of the net group delay dispersion (GDD). The dashed lines are the theoretical values. This experimental research validates the model we have introduced and demonstrates that dispersion management concepts are broadly applicable. The above work was published in: "Dynamics of Nonlinear and Dispersion managed Solitons" , Q. Quraishi, S. Cundiff, B. Ilan and M.J. Ablowitz, *Physical Review Letters* **94** (2005), 243904.

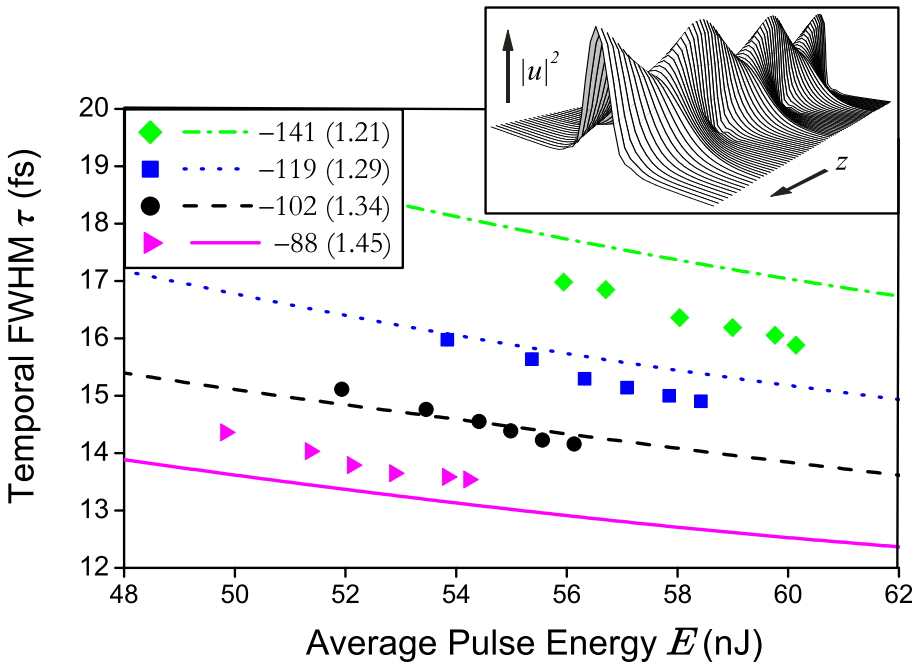

Figure 4: Fundamental pulse parameters in a modelocked Titanium:sapphire laser. The points are the measured temporal FWHM at four values of the average cavity GDD. The curves are the solutions of the Dispersion Managed NLS equation. The legend states the GDD values in fs^2. The errors for the GDD are approximately 1% and the errors for the τ values are negligible on the scale shown. Inset shows the breathing dynamics of a dispersion managed soliton $|u|^2$ as it propagates along z.

iii) Noise induced linewidth in frequency combs

As mentioned earlier, modelocked Ti:s lasers generate trains of optical pulses, whose spectrum consists of frequency comb lines. These combs are represented by evenly-spaced frequencies and an offset frequency that is proportional to the carrier envelope phase (see Fig. 2). The conversion between optical and microwave frequencies requires stabilization of the carrier envelope phase slip which is usually carried out by a feedback mechanism. We investigated the effect of random processes on these frequency combs.

Random physical effects can induce a linewidth, or uncertainty, in a comb line frequency. Some random effects, such as thermal fluctuations, can, in principle, be minimized. However, as far back as 1958 Schawlow and Townes discovered that the linewidth, or monochromaticity, of a single-mode continuous-wave (cw) laser is fundamentally limited by the random process of amplified spontaneous emission (**ASE**) in the lasing medium. We studied the limits of frequency combs associated with modelocked lasers in the presence of ASE noise and obtained a remarkable scaling law result. In particular, we analyzed the frequency combs generated by trains of pulses emitted from mode-locked lasers when the center-time and phase of the pulses undergo noise-induced random walk, which in turn broadens the comb lines. Detailed asymptotic analysis and computation of the ensemble-averaged spectrum has revealed a time-frequency duality, whereby the increase of the standard deviation of the center-time with pulse number, and the increase of the linewidth with frequency, occur with inversely proportional exponents. More precisely, when the standard deviation of the center-time jitter of the n'th pulse scales as $n^{p/2}$, where p is a jitter-exponent, the linewidth of the k'th comb line scales as $k^{2/p}$. The linear-dispersionless system ($p = 1$) and pure nonlinear soliton ($p = 3$) dynamics in lasers are found as special cases of this time-frequency duality relation. This work was published in: "Noise induced linewidth in frequency combs", M.J. Ablowitz, B. Ilan and S. Cundiff, *Optics Letters* **31** (2006) 1875.

Although this result was derived for mode locked lasers, the general nature of the result

indicates that it can be applied to the stochastic dynamics associated with other frequency combs as well.

Nonlinear Optics in Waveguide arrays and photonic lattices

Nonlinear light wave propagation in photonic lattices, or periodic optical waveguides, is an active and interesting area of research. This is due, in part, to the realization that photonic lattices can be constructed on extremely small scales of only a few microns in size. Hence they allow the possibility of manipulation and navigation of lightwaves on small scales. Localized nonlinear optical pulses which occur on one and two dimensional backgrounds have been investigated. These backgrounds can be either fabricated mechanically such as those comprised of AlGaAs materials or all-optically using photo-refractive materials where the photonic structures are constructed via interference of two or more plane waves.

An array of coupled optical waveguides is a setting that is a convenient laboratory for experimental observations. Such a system, as depicted in Figure 5, is typically composed of three layers of AlGaAs material: a substrate with refractive index n_0, a core with higher index (n_1) and surface with index n_0. By etching the surface of the waveguide, one forms a periodic structure which is called a waveguide array. Self-trapping of light in the "y"(i.e., vertical) direction is due to total internal reflection. On the other hand, the beam will diffract in the lateral "x" direction unless it is balanced by nonlinearity. Typically, such a waveguide array is composed of 40-60 single-mode individual waveguides each being 4-5 microns in width and 4-6 millimeters in length. Such small scale structures could be embedded in a large scale environment and can be used to guide light in a controllable manner.

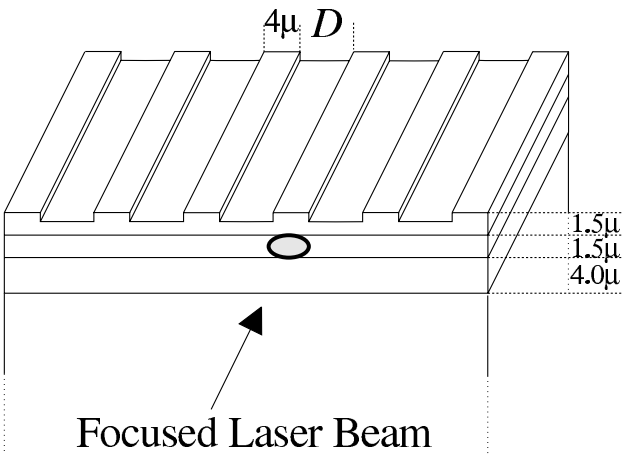

Figure 5: One-dimensional AlGaAs waveguide structure. It is composed of three layers of AlGaAs material: a substrate with refractive index n_0, a core with higher index (n_1) and surface with index n_0. By etching the surface of the waveguide, one forms a periodic structure which is called a waveguide array.

Motivated by these experiments we undertook wide ranging studies of discrete scalar and vector nonlinear Schrodinger (NLS) systems. From first principles, employing asymptotic analysis, new equations governing discrete systems in nonlinear optical arrays as well as discrete diffraction managed systems have been derived. In particular we derived the following vector diffraction-managed discrete NLS equation

$$
\begin{aligned}
i\frac{\partial A_n}{\partial z} + D(z)(A_{n+1} + A_{n-1}) + (|A_n|^2 + b|B_n|^2)A_n + cB_n^2 A_n^* = 0 \\
i\frac{\partial B_n}{\partial z} + D(z)(B_{n+1} + B_{n-1}) + (b|A_n|^2 + |B_n|^2)B_n + cA_n^2 B_n^* = 0
\end{aligned} \tag{2}
$$

where A_n, B_n are the slowly varying envelopes of the two underlying polarization fields at site n; b, c are cross-phase and four-wave-mixing coefficients respectively and D(z) is the varying diffraction term in the array. The, concept of diffraction management means that the waveguide array is alternately directed "positively" and "negatively" as a function of waveguide number over the propagation distance of the fiber.

In general, it is difficult to find solutions to discrete equations. New and effective methods have been developed in the Fourier domain to find localized and stationary and travelling wave pulse solutions to the governing both continuous and discrete equations. These methods are described in detail later in this report. The methods are robust and apply to a variety of equations; there is no need for the equations to be integrable. Travelling wave solutions pose certain difficulties in discrete problems. Unlike continuous equations, in general one does not expect to be able to find "uniformly" travelling soliton wave solutions to discrete equations. But over short scales we find that approximate travelling optical pulses can be obtained; they persist and are stable over the experimental regime. We have applied the above analysis to a waveguide array which is a discrete diffraction managed system. Using discrete Fourier methods we have obtained a nonlocal integral equation which governs the wave propagation in the discrete system and have found a class of discrete diffraction managed solitons as special solutions of this system. The theory has also been extended to

include vector discrete systems and the interaction effects of travelling discrete solitons have been analyzed. We have found that discrete constant and diffraction managed NLS equations and their vector analogues exhibit novel soliton propagation and interaction properties. By appropriately modifying the waveguide properties, one can change the control properties of soliton interactions and switching characteristics. This work was pulished in: "Discrete spatial solitons in a diffraction managed nonlinear waveguide array: a unified approach", M.J. Ablowitz and Z. Musslimani, *Physica D*, **184**, (2003) 276; "Discrete scalar and vector diffraction-managed nonlinear Schrödinger equations", M. J. Ablowitz, Z. Musslimani, *Nonlinear Physics: Theory and Experiment. II*, Eds. M.J. Ablowitz, M. Boiti, F. Pempinelli and B. Prinari, 319, World Scientific, Singapore, 2003 and "Nonlinear waves and (interesting) applications", M.J. Ablowitz, T.Hirooka, and Z. Musslimani, Nonlinear dynamics from lasers to butterflies, Eds. R. Ball and N. Akhmediev, World Scientific, 2003.

When the lattice system varies slowly in the transverse direction (y, below), we have derived new asymptotic multidimensional systems from Maxwell's equations. When the wavelength of the transverse modulation is much larger than the period of the longitudinal grating, the dynamics of wave propagating in such media was found to be governed by a semi-continuous NLS equation with the addition of an anomalous/normal bulk diffraction term and an external "optical trapping potential". The equation is given by

$$i\frac{\partial A_n}{\partial z} + D(A_{n+1} + A_{n-1}) + \gamma\frac{\partial^2 A_n}{\partial y^2} + V_n(y)A_n + a|A_n|^2 A_n = 0 \tag{3}$$

where A_n is the slowly varying envelope of the electromagnetic field fields at site n, D is the diffraction coefficient, γ is constant, $V_n(y)$ is related to the varying transverse index of refraction and a is the self-phase coefficient. Equation (3) describes wave propagation in a multidimensional transversely modulated optically induced waveguide array. Using our new numerical techniques (described later in this report) we find localized modes and we established that they are stable. This work was published in: "Wave dynamics in optically modulated waveguide arrays", M.J. Ablowitz, K. Julien, Z. Musslimani and M. Weinstein,

Physical Review E **71** (2005), 055602.

In two-dimensional photonic lattice applications, a nonlinear Schrödinger equation with an external potential, derivable from Maxwell's equations, is the governing equation. Recently we have begun a collaboration with faculty in the Electrical Engineering Department at the University of Colorado. They have been constructing defect and dislocated photonic lattice systems in the laboratory. By a defect we mean that only one or two lattice sites are affected by either removing a small number of sites or enhancing the amplitude of these sites. On the other hand a dislocated photonic lattice system has one line of sites merging with another (see e.g. Fig. 6 -left) or a row pinching off etc. These dislocation structures are typical of what is often seen in nature. Remarkably, using our newly developed numerical methods we can find localized modes to the underlying nonlinear systems. It strongly suggests that localized pulses can propagate in complex lattice environments.

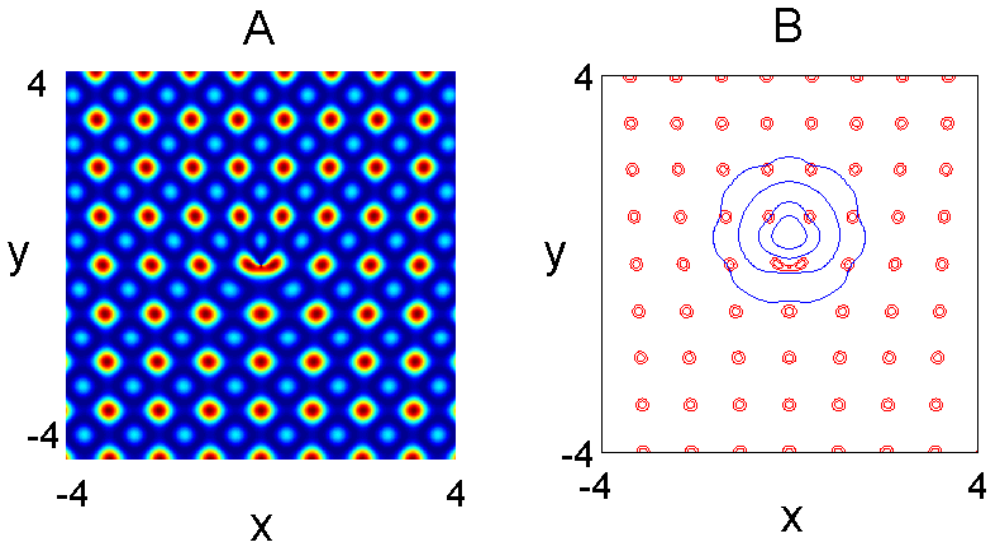

Figure 6: Left: contour plot of a dislocated two-dimensional lattice: the center vertical array of lattice cells splits into two separate arrays ("edge dislocation"). Right: contours of a soltion solution on this dislocated lattice.

In our recent work: "Solitons in two-dimensional lattices possessing defects, dislocations and quasicrystal structures", M. J. Ablowitz, B. Ilan, E. Schonbrun, and R. Piestun, 2006,

which was recently accepted by Physical Review E, Rapid Communications, we constructed by computational means, nonlinear localized pulses for a range of photonic lattices. The contours of a typical soliton solution on a dislocated lattice is depicted in Fig. 6 -right. To date most investigators have considered regular lattices. In our research we have considered irregular background lattices which have localized defects, edge dislocations such as the one mentioned above where two sequences of lattice maximum merge into one, and quasi-crystal lattice backgrounds. Our calculations show that we can obtain localized modes in all these cases. Potential applications involve beam management, pulse shaping, optical switching and the development of logic devices.

Nonlinear optics: multi-dimensional pulse propagation in $\chi^{(2)}$ optical materials

In many applications the leading nonlinear polarization effect in an optical material is quadratic; they are referred to as "$\chi^{(2)}$" materials. We have found that in multidimensional nonresonant $\chi^{(2)}$ materials, the nonlinear equation governing the slowly varying envelope of quasi-monochromatic wave trains is not the NLS equation but rather a coupled nonlinear system involving both the optical field and mean terms. We call these equations NLSM systems (M stands for the mean contribution). In water waves similar scalar systems were derived in 1969 by Benney and Roskes. A few years later, a special case of this system was found to be integrable. The latter system is frequently referred to as the Davey-Stewartson (DS) system.

In $\chi^{(2)}$ optical materials, we derived both scalar and a vector NLSM systems directly from Maxwell's equations. The vector NLSM systems generalize to multidimensions the well known 1+1 vector NLS equations. Such vector multidimensional systems are new in mathematical physics; there is no analog in water waves. Investigations of the scalar NLSM system has shown that localized optical pulse solutions can be constructed. These localized pulses are induced by their interaction with mean terms that have nontrivial boundary values. Hence the localized pulses are boundary induced. Such solutions are similar to the

ones that are known to exist for the Davey-Stewartson system; however in the optics problem the system is not integrable. These findings suggest that stable localized multidimensional pulses are a reproducible feature of these NLSM systems. In the future we will extend our analysis to spatial nonlinear optics where the boundary behavior can be more readily controlled. Potential applications using such pulses include beam steering, pulse shaping, terrahertz imaging and spatio-temporal light bullets.

In our recent published research,"Wave collapse in nonlocal nonlinear Schrödinger systems", M.J. Ablowitz, I. Bakirtas, and B. Ilan, *Physica D* **207** (2005), 230, we found that the $\chi^{(2)}$ optical system could admit wave collapse for a suitable ranges of parameter and initial data. This indicates that intense optical pulses can occur in these systems. We believe that experimentalists will be able to observe this phenomena since the analagous situation was recently observed in cubic nonlinear media. These theoretical results indicate that in this range of parameters researchers must be careful in their experiments not to damage the underlying optical crystal.

The NLSM system of equations possesses nonlocal-nonlinear coupling between a dynamic field that is associated with the first harmonic (with a "cascaded" effect from the second harmonic), and a static field that is associated with the mean term (i.e., the zero'th harmonic). The general NLSM system that we analyzed can be written in the following non-dimensional form,

$$\begin{aligned} iu_z + \frac{1}{2}(\sigma_1 u_{xx} + u_{yy}) + \sigma_2 u|u|^2 - \rho u\phi_x &= 0, \\ \phi_{xx} + \nu\phi_{yy} &= \left(|u|^2\right)_x , \end{aligned} \tag{4}$$

where $u(x, y, z)$ corresponds to the field associated with the first-harmonic, $\phi(x, y, z)$ corresponds to the mean field, σ_1 and σ_2 are ± 1, and ν and ρ are real constants that depend on the physical parameters. It can be proven that the system (4) can admit collapse of localized waves when $\sigma_1 = \sigma_2 = 1$ and $\nu > 0$. In that case, the above governing equations reduce to

$$iu_z + \frac{1}{2}\Delta u + |u|^2 u - \rho u \phi_x = 0 \ , \tag{5a}$$

$$\phi_{xx} + \nu \phi_{yy} = (|u|^2)_x \ , \tag{5b}$$

where $\nu > 0$ and ρ is real, and the initial conditions are $u(x, y, 0) = u_0(x, y)$, $\phi(x, y, 0) = \phi_0(x, y)$, such that equation (5b) is satisfied at $z = 0$, i.e., $\phi_{0,xx} + \nu \phi_{0,yy} = (|u_0|^2)_x$.

It is important to note that our numerical solutions indicate that the solution tends to the steady state mode found from the above NLSM system (5). The steady solution is obtained by assuming a solution of the form $u(x, y, z) = F(x, y)e^{i\lambda z}$ and $\phi(x, y, z) = G(x, y)$, where F and G are real functions and λ is a positive real number. Substituting this ansatz into equations (5) gives

$$-\lambda F + \frac{1}{2}\Delta F + F^3 - \rho F G_x = 0 \ , \tag{6a}$$

$$G_{xx} + \nu G_{yy} = (F^2)_x \ . \tag{6b}$$

We are currently investigating whether localized optical pulses can be obtained when we have an underlying optical lattice. We are also investigating the possibility of light navigation and optical switching.

New numerical methods to find localized solutions to nonlinear equations

Localized states, or solitary waves, in nonlinear media are of considerable interest to the scientific community and are especially important in optical sciences and fluid mechanics. They have been demonstrated to exist in a wide range of physical systems both in continuous and discrete setting. Such nonlinear modes usually form due to balance between diffraction or dispersion and nonlinearity. A central issue for these types of nonlinear guided waves is how to compute the localized states which generally involve solving nonlinear partial differential or difference equations.

To date, various techniques have been used such as shooting and relaxation techniques and methods to find nonlinear modes (fundamental and higher order excited states) which

utilize the concept: a solitary wave forms when the optical field induces a waveguide structure or self-induced potential well via the nonlinearity and "self-traps".

Another method, introduced by Petviashvili in 1976, constructs localized solutions to nonlinear systems by transforming to Fourier space and determining a "convergence factor" based upon the homogeneity of the nonlinearity. It was first used to find solutions of the two-dimensional Korteweg-deVries equation (usually referred to as the Kadomtsev-Petviashvili equation). Recently we have significantly extended this method to find localized solutions in a wide variety of interesting systems – e.g. dispersion managed and diffraction managed discrete systems (see discussion earlier in this report and "Discrete spatial solitons in a diffraction managed nonlinear waveguide array: a unified approach", M.J. Ablowitz and Z. Musslimani, *Physica D*, **184**, (2003) 276-303). However, Petviashvili's method usually converges only when underlying equation has a fixed power nonlinearity; i.e. when it has a fixed homogeneity. But, many problems involve nonlinearities with different homogeneities, such as for example, saturable nonlinearity in nonlinear Schrödinger type systems or many types of coupled nonlinear systems.

In recent work we have developed a new numerical scheme to compute localized states, or solitons, in nonlinear waveguides for more general systems than those with a single fixed nonlinear term. The idea behind the method is to transform the underlying equation governing the soliton, such as a nonlinear Schrödinger-type equation, into Fourier space and determine a nonlinear nonlocal integral equation coupled to an algebraic equation. The algebraic equation is solved by numerical nonlinear equation root finding techniques and the integral equation is solved iteratively. The coupling prevents the numerical scheme from diverging. The nonlinear guided mode is then determined from a convergent fixed point iteration scheme. The method works when we have relatively simple nonlinearities as in the NLS equation and more difficult systems where the nonlinearity arises in a complex manner. We have considered numerous cases such as the defect and dislocated photonic lattices

and optically modulated wave guide arrays mentioned above. The method has proven to be extremely powerful. This work was published in: "A spectral renormalization method to compute nonlinear self-localized solutions to nonlinear systems", M.J. Ablowitz and Z. Musslimani, *Optics Letters* **30** (2005), 2140.

The essence of the method is to: i) transform the underlying equation governing the soliton into Fourier space (this part is the same as Petviashvili (1976); ii) re-normalize variables and iii) determine an algebraic system which is coupled to a nonlinear integral equation. This leads to a nonlinear nonlocal integral equation (or system of integral equations) coupled to an algebraic equation (or system). The coupling is found to prevent the numerical scheme from diverging. We have found the method of coupling to be effective and straight forward to implement. The localized pulse is determined from a convergent fixed point iteration scheme.

We describe the method using the following scalar nonlinear Schrödinger like equation

$$i\frac{\partial U}{\partial z} + \nabla^2 U + V(\mathbf{x})U + N\Big(|U|^2, a(\mathbf{x})\Big)U = 0, \tag{7}$$

where z is the propagation direction; N is the nonlinearity that can depend on both intensity and inhomogenieties $a(\mathbf{x})$ and $V(\mathbf{x})$ models an optical lattice. Here, $\nabla^2 = \frac{\partial^2}{\partial x^2} + \frac{\partial^2}{\partial y^2}$. A special class of soliton solution can be constructed by assuming $U(\mathbf{x}, z) = u(\mathbf{x}; \mu)e^{i\mu z}$ where μ is the propagation constant or the soliton eigenvalue. Substituting the above ansatz into equation (7) we get

$$-\mu u + \nabla^2 u + V(\mathbf{x})u + N\Big(|u|^2, a(\mathbf{x})\Big)u = 0\ . \tag{8}$$

This is a nonlinear eigenvalue problem for u and μ which is suplemented with the following boundary conditions:

$$u \longrightarrow 0 \text{ as } |r| \longrightarrow +\infty$$

where $r^2 = x^2 + y^2$. The spectral renormalization (SPRZ) scheme is based on Fourier analysis which transforms equation (8) into nonlocal equation which is solved using an iteration

scheme. First we define the Fourier transform $\mathcal{F}$ and its inverse $\mathcal{F}^{-1}$

$$\begin{aligned} \hat{u}(\mathbf{k}) &= \mathcal{F}[u(\mathbf{x})] \\ &= \int_{-\infty}^{+\infty}\int_{-\infty}^{+\infty} u(\mathbf{x}) e^{-i(k_x x + k_y y)} d\mathbf{x} \,, \end{aligned} \tag{9}$$

$$\begin{aligned} u(\mathbf{x}) &= \mathcal{F}^{-1}[\hat{u}(\mathbf{k})] \\ &= \frac{1}{(2\pi)^2}\int_{-\infty}^{+\infty}\int_{-\infty}^{+\infty} \hat{u}(\mathbf{k}) e^{+i(k_x x + k_y y)} d\mathbf{k} \,, \end{aligned} \tag{10}$$

where $d\mathbf{x} = dxdy$ and $d\mathbf{k} = dk_x dk_y$. Applying the Fourier transform on equation (8) leads to

$$\hat{u}(\mathbf{k}) = \frac{\mathcal{F}[Vu] + \mathcal{F}[N(|u|^2, a(\mathbf{x}))u]}{\mu + |\mathbf{k}|^2} \,. \tag{11}$$

The idea underlying this method is to construct a condition which limits the amplitude under iteration from either growing without bound or tending to zero. This is accomplished by introducing a new field variable (i.e. renormalizing the field variable)

$$u(\mathbf{x}) = \lambda w(\mathbf{x}) \,, \qquad \hat{u}(\mathbf{k}) = \lambda \hat{w}(\mathbf{k}) \,, \tag{12}$$

where $\lambda \neq 0$ is a constant to be determined. Then function $\hat{w}$ satisfies

$$\hat{w}(\mathbf{k}) = \frac{1}{\lambda}\frac{\mathcal{F}[\lambda V w] + \mathcal{F}[N(\lambda^2|w|^2, a(x))w]}{\mu + |\mathbf{k}|^2} \equiv Q_\lambda[\hat{w}(\mathbf{k})] \,. \tag{13}$$

Multiplying equation (13) by $\hat{w}^*(\mathbf{k})$ and integrating over the entire (k_x, k_y) space we find the relation

$$\int_{-\infty}^{+\infty} |\hat{w}(\mathbf{k})|^2 d\mathbf{k} = \int_{-\infty}^{+\infty} \hat{w}^*(\mathbf{k}) Q_\lambda[\hat{w}(\mathbf{k})] d\mathbf{k} \,. \tag{14}$$

Equation (14) provides an algebraic condition on the constant λ which, in general we denote by

$$G(\lambda) = 0 \,. \tag{15}$$

To obtain the desired solution, we iterate Eqs. (13) and (15) as follows:

$$\hat{w}_{m+1}(\mathbf{k}) = \frac{1}{\lambda_m}\frac{\mathcal{F}[\lambda_m V w_m] + \mathcal{F}[N(\lambda_m^2|w_m|^2, a(x))\lambda_m w_m]}{\mu + |\mathbf{k}|^2} \quad , \tag{16}$$

$$G(\lambda_m) = 0 \quad , \tag{17}$$

where a localized initial function $w_0(\mathbf{x})$ begins the iteration procedure. The scheme is relatively insensitive to the initial function.

Note that it is possible that the algebraic equation (17) can admit more than one "root" or even complex solutions. In that case, one might need to exclude some solutions depending upon the physics at hand. Knowing the weakly nonlinear limit is very useful in this regard.

Thus the idea behind the method is to transform the underlying equation governing the localized mode, such as a nonlinear Scrödinger-type equation, into Fourier space, renormalize variables and then determine a nonlinear nonlocal integral equation coupled to an algebraic equation. The coupling is found to prevent the numerical scheme from diverging. The nonlinear guided mode is then obtained from a convergent fixed point iteration scheme. This method has already found wide applications in nonlinear optics, water waves, internal waves and related fields such as Bose-Einstein condensation.

PERSONNEL SUPPORTED

- Faculty: Mark J. Ablowitz
- Post-Doctoral Associates: B. Ilan
- Other (please list role) None

PUBLICATIONS

- **SUBMITTED**
  - **Books/Book Chapters:**
  - None
  - **Journals** None
  - **Conference Procedings:** None
- **ACCEPTED/PUBLISHED**
  - **Books/Book Chapters**

1. Discrete scalar and vector diffraction-managed nonlinear Schrödinger equations, M. J. Ablowitz, and Z. Musslimani, *Nonlinear Physics: Theory and Experiment. II*, Eds. M.J. Ablowitz, M. Boiti, F. Pempinelli and B. Prinari, p. 319–332, World Scientific, Singapore, 2003.
2. Nonlinear waves and (interesting) applications, M.J. Ablowitz, T.Hirooka, and Z. Musslimani, Nonlinear dynamics from lasers to butterflies, Eds. R. Ball and N. Akhmediev, World Scientific, 2003.

  - **Journals**

1. Discrete spatial solitons in a diffraction managed nonlinear waveguide array: a unified approach, M.J. Ablowitz and Z. Musslimani, *Physica D*, **184**, (2003) 276-303.

2. Carrier-envelope phase slip of ultrashort dispersion managed solitons, M.J. Ablowitz, B. Ilan and S. Cundiff, *Optics Letters*, **29** (2004) 1808-1820.
3. Dynamics of nonlinear and dispersion managed soltions, Q. Quraishi, S. Cundiff, B. Ilan and M.J. Ablowitz. *Physical Review Letters* **94** (2005), 243904.
4. Spectral renormalization method to compute nonlinear self-localized solutions to nonlinear systems, M.J. Ablowitz, Z. Musslimani, *Optics letters* **30** (2005), 2140-2142.
5. Wave dynamics in optically modulated waveguide arrays, M.J. Ablowitz, K. Julien, Z. Musslimani and M. Weinstein, *Physical Review E* **71** (2005), 055602.
6. Wave collapse in nonlocal nonlinear Schrödinger systems, M.J. Ablowitz, I. Bakirtas, and B. Ilan, *Physica D* **207** (2005), p. 230-253..
7. Noise induced linewidth in frequency combs, M.J. Ablowitz, B. Ilan and S. Cundiff, *Optics Letters* **31** (2006) p. 1875-1877.
8. Solitons in two-dimensional lattices possessing defects, dislocations and quasicrystal structures, M. J. Ablowitz, B. Ilan, E. Schonbrun, and R. Piestun, accepted *Physical Review E, Rapid Communications*, 2006.

– **Conferences**

INTERACTIONS/TRANSITIONS

- Participation/Presentations At Meetings, Conferences, Seminars, etc.

1. Department of Mathematics, Loughborough University, U.K., Differential and Difference Equations in the Complex Domain, June 27-July 1, 2003; "Discrete and continuous nonlinear Schrödinger equations", July 1, 2003.
2. Department of Applied Mathematics, Cambridge University, U.K., July 1-4, 2003. "Investigations in nonlinear optics and water waves".

3. Advanced NATO Research Workshop, Nonlinear Waves, Classical and Quantum Systems, Estoril, Portugal, July 12-19, 2003, "Discrete and continuous nonlinear Schrödinger equations", July 12, 2003.

4. Nonlinear Guided Waves and Their Applications, March 28-31, 2004, "Theory of carrier-envelope phase slip for ultra-short dispersion managed solitons", March 30, 2004.

5. Department of Physics, University of Rome, Italy, June 12-17, 2004, "Nonlinear waves in optics", June 16, 2004.

6. Conference: Mathematical Methods in Nonlinear Optics, July 19-24, 2004, Edinburgh, U.K., "Dispersion managed nonlinear Schrödinger systems" July 19, 2004.

7. AFOSR Workshop: Nonlinear Optics, University of Arizona, September 9-11, 2004, "Carrier envelope phase slip for ultrashort optical pulses", September 10, 2004.

8. Conference, Singularities in Materials and Mathematical Applications, Institute for Mathematics and Applications, University of Minnesota, October 25-29, 2004, "Wave collapse in nonlocal nonlinear Schrödinger Systems", October 26, 2004.

9. Conference Nonlinear Waves and Applications, University of Tokyo, Tokyo, Japan, February 14-18, 2005, "Wave collapse in nonlocal nonlinear Schrödinger systems", February 14, 2005.

10. Department of Mathematics, University of Wyoming, "WWW: waves, water and the web", February 24, 2005.

11. Department of Mathematics, Rutgers University, "Solitary waves: from optics to water waves", September 15, 2005.

12. Department of Mathematics, Yale University, "Solitary waves: from optics to water waves", September 19, 2005.

13. AFOSR Workshop: Nonlinear Optics, University of Arizona, October 4-5, 2005, "Ultrashort Optical Pulses: Dynamics and Noise", September 5, 2005.

14. Department of Applied Mathematics, University of Colorado, "What you always wanted to know about solitons but...", March 17, 2006.

15. Conference "Nonlinearity and randomness in complex systems", SUNY Buffalo, March 31 - April 2 2006; "Solitary waves: from optics to fluid dynamics", March 31, 2006.

16. Department of Mathematics, University of Massachusetts, "Solitary waves: from optics to fluid dynamics", April 25, 2006.

17. Department of Mechanical Engineering, University of Rochester, "What you always wanted to know about solitons but...", May 5, 2006.

18. Conference: Frontiers in Applied Mathematics, Tsinghua University, Beijing, China, June 8,9, 2006; "Solitary waves: from optics to water waves", June 9, 2006.

19. Conference: Nonlinear Physics Theory and Experiment, Gallipolli, Italy June 22-July 1, 2006, "Solitary waves: from optics to fluids", June 23, 2006.

- **Consultative and Advisory Functions to Other Laboratories and Agencies:** None

- **Transitions:** none

NEW DISCOVERIES, INVENTIONS, OR PATENT DISCLOSURES: None

HONORS/AWARDS: Named as one of the most highly cited people in the field of Mathematics by the ISI Web of Science, 2003-present.

Available online at www.sciencedirect.com
SCIENCE DIRECT®
Physica D 184 (2003) 276–303
PHYSICA D
www.elsevier.com/locate/physd

Discrete spatial solitons in a diffraction-managed nonlinear waveguide array: a unified approach

Mark J. Ablowitz*, Ziad H. Musslimani

Department of Applied Mathematics, University of Colorado at Boulder, Campus Box 526, Boulder, CO 80309-0526, USA

Abstract

Localized, stable nonlinear waves, often referred to as solitons, are of broad interest in mathematics and physics. They are found in both continuous and discrete media. In this paper, a unified method is presented which is used to describe the propagation of linearly polarized light as well as two polarization modes in a diffraction-managed nonlinear waveguide array. In the regime of normal diffraction, both stationary and moving discrete solitons are analyzed using the Fourier transform method. The numerical results based on a modified Neumann iteration scheme as well as renormalization techniques, indicate that traveling wave solutions are unlikely to exist. An asymptotic equation is derived from first principles which governs the propagation of electromagnetic waves in a waveguide array in the presence of both normal and anomalous diffraction. This is termed diffraction management. The theory is then extended to the vector case of coupled polarization modes.

Keywords: Nonlinear waves; Discrete spatial soliton; Diffraction

1. Introduction

Dynamics of discrete nonlinear systems dates back to the mid-fifties when Fermi, Pasta and Ulam (FPU) studied dynamics of nonlinear springs [1]. Apart from the fact that the work of FPU motivated the discovery of solitons, it also stimulated considerable interest in the study of discrete nonlinear media which possesses self-confined structures (discrete solitary waves). Such waves are localized modes of nonlinear lattices that form when "discrete diffraction" is balanced by nonlinearity. In physics a soliton usually denotes a stable localized wave structure, i.e., solitary wave. We shall use the term soliton in this broader sense (i.e., they do not necessarily interact elastically). Discrete solitons have been demonstrated to exist in a wide range of physical systems [2–5]. For example, atomic chains [6,7] (discrete lattices) with an on-site cubic nonlinearities, molecular crystals [8], biophysical systems [9], electrical lattices [10], and recently in arrays of coupled nonlinear optical waveguides [11,12]. An array of coupled optical waveguides is a setting that represents a convenient laboratory for experimental observations.

The first theoretical prediction of discrete solitons in an optical waveguide array was reported by Christodoulides and Joseph [13]. Later, many theoretical studies of discrete solitons in a waveguide array reported switching, steering and other collision properties of these solitons [14–19] (see also the review papers [20,21]). In all the above cases, the

* Corresponding author.
E-mail address: markjab@newton.colorado.edu (M.J. Ablowitz).

0167-2789/$ – see front matter © 2003 Elsevier B.V. All rights reserved.
doi:10.1016/S0167-2789(03)00226-4

localized modes are solutions of the well known discrete nonlinear Schrödinger (DNLS) equation which describes beam propagation in Kerr nonlinear media (according to coupled mode theory). Discrete bright and dark solitons have also been found in quadratic media [22], in some cases, their properties differ from their Kerr counterparts [23].

In fact, the DNLS equation (and its "cousins" such as diffraction-managed discrete nonlinear Schrödinger (DM-DNLS) or DNLS with a potential such as discrete BEC) is "asymptotically universal". Namely it is the discrete equation which emerges from either a weakly nonlinear Helmholtz equation with a suitable "potential" or a weakly nonlinear continuous NLS equation with a suitable potential where the following terms are in balance:

(i) Slow variation in either distance (waveguide array) or time (for BEC);
(ii) linear terms induced by a potential which can be viewed as asymptotically separated localized potentials (sometimes called the "tight binding approximation");
(iii) nonlinearity.

It took almost a decade until self-trapping of light in discrete nonlinear waveguide array was experimentally observed [11,12]. When a low intensity beam is injected into one or a few waveguides, the propagating field spreads over the adjacent waveguides hence experiencing discrete diffraction. However, at sufficiently high power, the beam self-traps to form a localized state (a soliton) in the center waveguides. Subsequently, many interesting properties of nonlinear lattices and discrete solitons were reported. For example, the experimental observation of linear and nonlinear Bloch oscillations in: AlGaAs waveguides [24], polymer waveguides [25] and in an array of curved optical waveguides [26]. Discrete systems have unique properties that are absent in continuous media such as the possibility of producing *anomalous* diffraction [27]. Hence, self-focusing and defocusing processes can be achieved in the same medium (structure) and wavelength. This also leads to the possibility of observing discrete dark solitons in self-focusing Kerr media [28]. The recent experimental observations of discrete solitons [11] and diffraction management [27] have motivated further interests in discrete solitons in nonlinear lattices. This includes the newly proposed model of discrete diffraction-managed nonlinear Schrödinger equation [29,30] whose width and peak amplitude vary periodically, optical spatial solitons in nonlinear photonic crystals [31–33] and the possibility of creating discrete solitons in Bose–Einstein condensation [34]. Also, recently, it was shown that discrete solitons in two-dimensional networks of nonlinear waveguides can be used to realize intelligent functional operations such as blocking, routing, logic functions and time gating [35–38]. In addition, spatiotemporal discrete solitons have been recently suggested in nonlinear chains of coupled microcavities embedded in photonic crystal structures [39].

In this paper, we introduce the Fourier transform method to analyze both stationary and moving solitons in nonlinear lattices. The essence of the method is to transform the DNLS equation governing the solitary wave into Fourier space, where the wave function is smooth, and then deal with a nonlinear nonlocal integral equation for which we employ a rapidly convergent numerical scheme to find solutions. A key advantage of the method is to transform a differential-delay equation into an integral equation for which computational methods are effective. Mathematically, the method also provides a foundation upon which an analytic theory describing solitons in nonlinear lattices can be constructed. We shall consider in this paper two important models: the DNLS equation and the DM-DNLS equation. Applying this method to the first model, shows that approximate traveling solitons possess a nontrivial nonlinear "chirp". Moreover, our results (both numerical and analytical) indicate that, unlike the integrable case [40], a continuous exact traveling wave (TW) solution is unlikely to exist [41]. In the limit of small velocity, we develop a fully discrete perturbation theory and show that slowly but not uniformly moving discrete solitons are indeed "chirped". An asymptotic equation is derived from first principles which governs the propagation of electromagnetic waves in a waveguide array in the presence of both normal and anomalous diffraction. This is related to the second model of DM-DNLS equation. The theory is then extended to the vector case of coupled polarization modes.

The new results of this paper can be summarized as follows:

- The derivation of the DNLS equation based on asymptotic multiple scale theory starting, e.g., from the Helmholtz equation.
- The derivation of the scalar DM-DNLS equation from first principles. Using multiple scale asymptotic theory it is found that the most general equation that governs the dynamics of light propagating in a diffraction-managed waveguide array is

$$\mathrm{i}\frac{\partial E_n}{\partial z} + \mathcal{C}(z)E_{n+1} + \mathcal{C}^*(z)E_{n-1} + \nu|E_n|^2E_n = 0,$$

  where E_n is the slowly varying envelope of the electric field at site n, ν a constant that measures the nonlinear refractive index, $\mathcal{C}(z)$ a complex periodic function and $*$ the complex conjugate.
- The derivation from first principles of the vector DM-DNLS equation which includes self and cross-phase modulation as well as four-wave mixing (FWM) terms:

$$\mathrm{i}\frac{\partial A_n}{\partial z} + k_{\mathrm{wg}}A_n + \mathcal{C}(z)A_{n+1} + \mathcal{C}^*(z)A_{n-1} + (|A_n|^2 + b_1|B_n|^2)A_n + \eta_1 B_n^2 A_n^* = 0,$$
$$\mathrm{i}\frac{\partial B_n}{\partial z} + k_{\mathrm{wg}}B_n + \mathcal{C}(z)B_{n+1} + \mathcal{C}^*(z)B_{n-1} + (|B_n|^2 + b_2|A_n|^2)B_n + \eta_2 A_n^2 B_n^* = 0,$$

  where A_n, B_n are the slowly varying envelopes of the two polarization fields at site n, b the cross-phase modulation coefficient and η the strength of FWM term. We note that even the derivation of the constant diffraction case is new.
- A numerical scheme based on renormalization of suitable norms to solve the nonlinear integral equation governing solitons is proposed.
- Based on asymptotic and numerical evidence, we conclude that it is unlikely that a *uniformly* moving TW exists for the DNLS equation.
- The derivation of a new discrete nonlinear Schrödinger type equation.

The paper is organized as follows. In Section 2 we formulate the basic physical model and describe the asymptotic analysis that leads to the DNLS equation. Linear propagation is discussed in both normal and anomalous regimes. In Section 3 we introduce the discrete Fourier transform method to find soliton solutions and show how one can obtain approximate TW solutions. Two numerical schemes are introduced. The first is based on modified Neumann iteration and the second on renormalization. Analytical analysis of TWs based on asymptotic theory is provided in Section 4 which further support our conjecture that *exact* TWs may not exist. Next, we set up in Section 5 a physical model that describes the propagation of two interacting optical fields in a nonlinear waveguide array with varying diffraction. Moreover, the general scalar as well as vector equation governing diffraction management is derived from first principles based on asymptotic theory.

2. Waveguide array

As mentioned above, an array of coupled optical waveguides is a setting that represents a convenient laboratory for experimental observations and theoretical predictions. Such system (see Fig. 1) is typically composed of three layers of AlGaAs material: a substrate with refractive index n_0, a core with higher index (n_1) and surface with index n_0. By etching the surface of the waveguide, one forms a periodic structure which is called a waveguide array. Self-trapping of light in the "y" (i.e., vertical) direction is possible (even in the linear regime) by virtue of the principle of total internal reflection. On the other hand, the beam will diffract in the "x"-direction unless it is

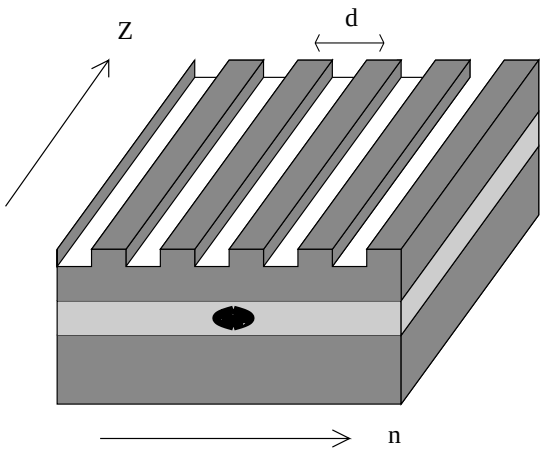

Fig. 1. AlGaAs waveguide structure. It is composed of three layers of AlGaAs material: a substrate with refractive index n_0, a core with higher index (n_1) and surface with index n_0. By etching the surface of the waveguide, one forms a periodic structure which is called a waveguide array.

balanced by nonlinearity. In the following we describe the propagation of light in such a periodic structure both in the linear and nonlinear regimes.

2.1. Linear and nonlinear propagation

If the full width at half maximum (FWHM), τ, of the optical field is small compared to the distance, d, between adjacent waveguides, then the propagating beams across each single waveguide do not "feel" each other. Therefore, the amplitude of each beam evolves independently according to the linear wave equation:

$$\frac{\mathrm{d}^2\psi_0}{\mathrm{d}x^2} + [k_0^2 f_0^2(x) - \lambda_0^2]\psi_0 = 0, \tag{2.1}$$

where k_0 is the wavenumber of the optical field in vacuum, f_0^2 the refractive index of a single waveguide and λ_0 the lowest eigenvalue (propagation constant) that corresponds to the ground state ψ_0 (a bell shape eigenfunction). In this respect we have assumed that a single waveguide supports only a single mode. The more intricate situation of multimode waveguide is also possible in which case $\lambda_0 \to \lambda_j$ and $\psi_0 \to \psi_j$ where j is the number of modes occupied by a single waveguide. On the other hand when τ is on the order of d or larger, then there is a significant overlap between modes of adjacent waveguide (see Fig. 2). In either case, the beam's amplitude is not constant in z anymore. Moreover, when the intensity of the incident beam is sufficiently high then the refractive index of the medium will depend on the intensity which for Kerr media is proportional to the intensity. In this case, the evolution of the total field's amplitude $\mathbf{\Psi}$ follows from Maxwell equations (see details in Section 5.3):

$$\left(\frac{\partial^2}{\partial z^2} + \frac{\partial^2}{\partial x^2}\right)\mathbf{\Psi} + (k_0^2 f^2(x) + \delta|\mathbf{\Psi}|^2)\mathbf{\Psi} = 0, \tag{2.2}$$

where $f^2(x)$ represents the refractive index of the entire structure and δ a small parameter to be determined later. If the overlap between adjacent modes is "small", which is valid in the regime $\mu \equiv \tau/d \ll 1$, we expect the power exchange to be slow. By introducing a slow scale $Z = \varepsilon z$ (ε is a small parameter to be determined later) we

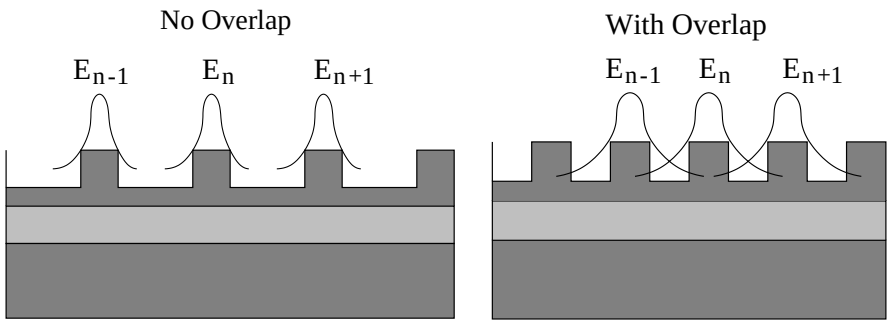

Fig. 2. Cross-section of the waveguide array and mode overlap.

approximate the solution to Eq. (2.2) as a multiscale perturbation series:

$$\Psi = \sum_{m=-\infty}^{+\infty} E_m(Z)\psi_m(x)\exp(-\mathrm{i}\lambda_0 z). \tag{2.3}$$

In this notation, $\psi_m(x) = \psi_0(x - md)$ and $f_m^2(x) = f_0^2(x - md)$. Substituting the ansatz (2.3) into Eq. (2.2), we find

$$\sum_{m=-\infty}^{+\infty}\Bigg[-2\mathrm{i}\varepsilon\lambda_0\psi_m\frac{\partial E_m}{\partial Z} + \varepsilon^2\psi_m\frac{\partial^2 E_m}{\partial Z^2} + \left(\frac{\mathrm{d}^2\psi_m}{\mathrm{d}x^2} + k_0^2 f^2\psi_m - \lambda_0^2\psi_m\right)E_m + \delta\sum_{m',m''} E_m E_{m'} E_{m''}^*\psi_m\psi_{m'}\psi_{m''}^*\Bigg]\mathrm{e}^{-\mathrm{i}\lambda_0 z} = 0. \tag{2.4}$$

Using Eq. (2.1) in the above equation, multiplying Eq. (2.4) by $\psi_n^*\exp(\mathrm{i}\lambda_0 z)$ and integrating over x yields the following:

$$\sum_{m=-\infty}^{+\infty}\Bigg[\left(-2\mathrm{i}\varepsilon\lambda_0\frac{\partial E_m}{\partial Z} + \varepsilon^2\frac{\partial^2 E_m}{\partial Z^2}\right)\int_{-\infty}^{+\infty}\mathrm{d}x\,\psi_m\psi_n^* + k_0^2 E_m\int_{-\infty}^{+\infty}\mathrm{d}x\,\Delta f_m^2\psi_m\psi_n^* + \delta\sum_{m',m''} E_m E_{m'} E_{m''}^*\int_{-\infty}^{+\infty}\mathrm{d}x\,\psi_n^*\psi_m\psi_{m'}\psi_{m''}^*\Bigg] = 0. \tag{2.5}$$

Here, $\Delta f_m^2 \equiv f^2 - f_m^2$ which measures the deviation of the total refractive index from each individual waveguide. As mentioned earlier, the overlap integral between adjacent waveguides is an important measure in determining the dynamic evolution of the modes. With this in mind we shall *assume* that the overlap integrals appearing in Eq. (2.5) can be approximated by

$$\int \mathrm{d}x\,\psi_m\psi_{m+N}^* = a_N\varepsilon^N, \qquad \int \mathrm{d}x\,\Delta f_m^2|\psi_m|^2 = c_0\varepsilon, \qquad \int \mathrm{d}x\,\Delta f_m^2\psi_m^*\psi_{m\pm1} = c_1\varepsilon. \tag{2.6}$$

In order to understand the idea behind this scaling, we will assume that the mode at waveguide m can be modeled by

$$\psi_m(x) = \operatorname{sech}\kappa(x - md), \tag{2.7}$$

where $\kappa = 1/\tau$ and τ is the FWHM. The reason for this choice is only to simplify the analysis. In fact, the real modes of a step index waveguide has exponential behavior which is close to a sech-like mode. Other choices of eigenfunctions with different exponential decays are possible, e.g., $\psi_m(x) = \exp[-(x - md)^2/\tau^2]$ but the basic ordering mechanism remains the same. A straightforward calculation shows that

$$\int_{-\infty}^{+\infty} \mathrm{d}x\, \psi_m \psi_n^* = c\, \mathrm{e}^{-|n-m|/\mu} \tag{2.8}$$

with c being a constant of order 1. Since $\mu \ll 1$, then the choice $\varepsilon = \exp(-1/\mu)$ provides a measure for the order of magnitude for the overlap integral. Restricting the sum in Eq. (2.5) to nearest neighbors, i.e., $m = n, n \pm 1$ (which contribute to the order ε equation) and assuming that the only order 1 contribution comes from the nonlinear term is when $m = n = m' = m''$ and that

$$\int_{-\infty}^{+\infty} \mathrm{d}x\, |\psi_n|^4 = g_{\mathrm{nl}},$$

we find that to $\mathrm{O}(\varepsilon)$ the nonlinear evolution of E_n is given by

$$-2\mathrm{i}\lambda_0 a_0 \frac{\partial E_n}{\partial Z} + k_0^2 c_0 E_n + k_0^2 c_1 (E_{n+1} + E_{n-1}) + g_{\mathrm{nl}} |E_n|^2 E_n = 0, \tag{2.9}$$

where we have taken $\delta = \varepsilon$ to ensure maximal balance. By defining a new variables $\tilde{z} = Z/(2\lambda_0 a_0)$, $k_0^2 c_1 = C$, $E_n = \tilde{E}_n^* \exp(-\mathrm{i}k_0^2 c_0 \tilde{z})$ we find that $\tilde{E}_n$ satisfies (dropping the tilde)

$$\mathrm{i}\frac{\partial E_n}{\partial z} + C(E_{n+1} + E_{n-1}) + g_{\mathrm{nl}} |E_n|^2 E_n = 0. \tag{2.10}$$

To put the DNLS equation in dimensionless form, we define

$$E_n = \sqrt{P_*}\phi_n \exp(2\mathrm{i}Cz), \qquad z' = \frac{z}{z_{\mathrm{nl}}} \tag{2.11}$$

with P_* and z_{nl} being the characteristic power and z_{nl} the nonlinear length scale. Then ϕ_n satisfies

$$\mathrm{i}\frac{\mathrm{d}\phi_n}{\mathrm{d}z} + \frac{1}{h^2}(\phi_{n+1} + \phi_{n-1} - 2\phi_n) + |\phi_n|^2 \phi_n = 0 \tag{2.12}$$

with $z_{\mathrm{nl}} C = 1/h^2$ and $z_{\mathrm{nl}} = 1/(g_{\mathrm{nl}} P_*)$. In the DNLS equation there are two important length scales: the diffraction and nonlinear length scales, respectively, defined by $L_{\mathrm{D}} \sim 1/C$ and $z_{\mathrm{nl}} = 1/(g_{\mathrm{nl}} P_*)$. Solitons which are self-confined and invariant structures are expected to form when $L_{\mathrm{D}} \sim z_{\mathrm{nl}}$.

2.2. New discrete nonlinear Schrödinger type equation

We begin as before with the nonlinear Helmholtz equation with modulated Kerr coefficient:

$$\left(\frac{\partial^2}{\partial z^2} + \frac{\partial^2}{\partial x^2}\right)\boldsymbol{\Psi} + (k_0^2 f^2(x) + \delta(x)|\boldsymbol{\Psi}|^2)\boldsymbol{\Psi} = 0, \tag{2.13}$$

where $f^2(x)$ is defined before, and $\delta(x)$ measures the local change of nonlinear refractive index along the transverse direction. Importantly, note that as compared to Eq. (2.2), we now assume the nonlinear coefficient to be a spatially dependent function. Moreover, we shall assume here, that the nonlinear index change $\delta(x)$ is an odd function relative to each waveguide (i.e., $\delta(x) \to \delta(x - nd) = -\delta(-x + nd)$). Following the reasoning outlined before, we

approximate the solution to Eq. (2.13) via a multiscale perturbation series given in Eq. (2.3). In this case, the linear part remains the same but the nonlinear contribution changes to

$$\mathcal{N} = \sum_{m=-\infty}^{+\infty} \sum_{m',m''} E_m E_{m'} E^*_{m''} \delta(x) \psi_m \psi_{m'} \psi^*_{m''} \, \mathrm{e}^{-\mathrm{i}\lambda_0 z}. \tag{2.14}$$

Multiplying Eq. (2.14) by $\psi^*_n \exp(\mathrm{i}\lambda_0 z)$ and integrating over x yields the following:

$$\mathcal{I} = \int_{-\infty}^{+\infty} \mathrm{d}x \, \mathcal{N} \psi^*_n \exp(\mathrm{i}\lambda_0 z) = \sum_{m=-\infty}^{+\infty} \sum_{m',m''} E_m E_{m'} E^*_{m''} \int_{-\infty}^{+\infty} \mathrm{d}x \, \delta(x) \psi^*_n \psi_m \psi_{m'} \psi^*_{m''}. \tag{2.15}$$

Since $\delta(x)$ is an odd function then there is no on-site contribution, i.e.:

$$\mathcal{I}_{m=m'=m''=n} = |E_n|^2 E_n \int_{-\infty}^{+\infty} \mathrm{d}x \, \delta(x) |\psi_n|^4 = 0.$$

Therefore, the leading order contribution comes by setting $m = n \pm 1, m' = m'' = n$; $m = m'' = n, m' = n \pm 1$; $m = m' = n, m'' = n \pm 1$. The nonlinearity in each of the cases is

$$\mathcal{I}_{m=n\pm1,m'=m''=n} = \mathcal{I}_{m=m''=n,m'=n\pm1} = \pm |E_n|^2 E_{n\pm1} \int_{-\infty}^{+\infty} \mathrm{d}x \, \delta(x) \psi^*_n |\psi_n|^2 \psi_{n\pm1},$$

$$\mathcal{I}_{m=m'=n,m''=n\pm1} = \pm E_n^2 E^*_{n\pm1} \int_{-\infty}^{+\infty} \mathrm{d}x \, \delta(x) |\psi_n|^2 \psi_n \psi^*_{n\pm1}.$$

The linear portion follows the same derivation as in Section 2.1 and we shall assume that the waveguide function $f^2(x)$ is $\mathrm{O}(\varepsilon)$, and $Z = \varepsilon^2 z$, $\delta(x) = \mathrm{O}(\varepsilon)$. Combining all the linear and nonlinear terms, we find

$$\begin{aligned} &-2\mathrm{i}\lambda_0 a_0 \varepsilon^2 \frac{\partial E_n}{\partial Z} + k_0^2 c_0 \varepsilon E_n + k_0^2 c_1 \varepsilon^2 (E_{n+1} + E_{n-1}) + 2Q_1 \varepsilon^2 |E_n|^2 (E_{n+1} - E_{n-1}) \\ &\quad + Q_2 \varepsilon^2 E_n^2 (E^*_{n+1} - E^*_{n-1}) = 0, \end{aligned} \tag{2.16}$$

where

$$a_0 = \int_{-\infty}^{+\infty} \mathrm{d}x \, |\psi_n(x)|^2, \qquad c_0\varepsilon = \int_{-\infty}^{+\infty} \mathrm{d}x \, (f^2 - f_n^2) |\psi_n(x)|^2,$$

$$c_1\varepsilon^2 = \int_{-\infty}^{+\infty} \mathrm{d}x \, (f^2 - f_{n+1}^2) \psi_n(x) \psi_{n+1}(x), \qquad Q_1\varepsilon^2 = \int_{-\infty}^{+\infty} \mathrm{d}x \, \delta(x) |\psi_n(x)|^2 \psi^*_n(x) \psi_{n+1}(x),$$

$$Q_2\varepsilon^2 = \int_{-\infty}^{+\infty} \mathrm{d}x \, \delta(x) |\psi_n(x)|^2 \psi_n(x) \psi^*_{n+1}(x).$$

By defining new variables $\tilde{z} = Z/(2\lambda_0 a_0)$, $k_0^2 c_1 = C$, $E_n = \tilde{E}^*_n \exp(-\mathrm{i}k_0^2 c_0 \tilde{z}/\varepsilon)$, we find that $\tilde{E}_n$ satisfies

$$\mathrm{i}\frac{\partial \tilde{E}_n}{\partial z} + C(\tilde{E}_{n+1} + \tilde{E}_{n-1}) + 2Q_1 |\tilde{E}_n|^2 (\tilde{E}_{n+1} - \tilde{E}_{n-1}) + Q_2 \tilde{E}_n^2 (\tilde{E}^*_{n+1} - \tilde{E}^*_{n-1}) = 0. \tag{2.17}$$

2.3. Diffraction properties of a waveguide array

In this section we consider the basic properties of discrete diffraction of a linear array of waveguides emphasizing the recent discovery of anomalous diffraction [11]. However, we consider first propagation of light in bulk linear

and homogeneous media which is governed by the linear Helmholtz equation:

$$\nabla^2 \mathsf{E} + k^2 \mathsf{E} = 0, \quad \nabla^2 = \frac{\partial^2}{\partial x^2} + \frac{\partial^2}{\partial z^2}, \tag{2.18}$$

where E is the amplitude of the electric field. If we assume a solution of the form $\mathsf{E} = a \exp[\mathrm{i}(k_z z + k_x x)]$ then we find $k_z = \sqrt{k^2 - k_x^2}$. In the paraxial approximation ($k_x/k \ll 1$), the diffraction relation reads $k_z \approx k - k_x^2/2k$. Then the group velocity is defined by $\partial k_z/\partial k_x \approx -k_x/k$ which says that each transverse component k_x travels at different rates hence beam will diffract. A measure for the rate of diffraction is $\partial^2 k_z/\partial k_x^2$ which for plane waves is $\approx -1/k < 0$. Since all plane waves have this definite negative sign for diffraction, it is referred to as normal diffraction regime. Note that this is exactly the opposite from dispersion in which the normal regime is positive. Next, we discuss linear propagation of light in a waveguide array. As mentioned in Section 2.1, the dynamics of the beam's amplitude $E_n(z)$ at waveguide number n follows Eq. (2.10). In this case, when an extended state or cw mode of the form

$$E_n(z) = A \exp[\mathrm{i}(k_z z - n k_x d)] \tag{2.19}$$

is inserted into Eq. (2.10) it yields the following diffraction relation:

$$k_z = 2C \cos(k_x d). \tag{2.20}$$

In close analogy to the definition of dispersion, discrete diffraction is given by $k_z'' = -2Cd^2 \cos(k_x d)$. Since the diffraction relation is periodic in Fourier space, we shall restrict the discussion for wavenumbers in the interval $|k_x d| \leq \pi$. In that region, the diffraction is *normal* for wavenumbers k_x satisfying $-\pi/2 < k_x d \leq \pi/2$ ($k_z'' < 0$) and is *anomalous* in the range $\pi/2 < |k_x d| \leq \pi$. Moreover, contrary to the bulk case, diffraction can even vanish when $k_x d = \pm\pi/2$. In practice, the sign and value of the diffraction can be controlled and manipulated by launching light at a particular angle γ or equivalently by tilting the waveguide array. The relation between k_x, k_z and the tilt angle is given by $\sin\gamma = k_x/k$. This in turn allows the possibility of achieving a "self-defocusing" (with *positive* Kerr coefficient) regime which leads to the formation of discrete dark solitons [28]. To understand more about diffraction management we consider three typical cases for which light enters the central waveguide array at different angles, say, $k_x d = 0, \pi/2$ and π. When $k_x d = 0$ then light tunnels between adjacent waveguides giving rise to discrete diffraction. The phase front in this case has a concave (negative) curvature. On the other hand, if $k_x d = \pi$, then diffusion of light still occurs but this time the phase front has convex (positive) curvature. Finally, at $k_x d = \pi/2$ the diffraction vanishes (even though light can couple to different waveguides) and in the absence of any higher order diffraction the phase front looks almost flat (see Fig. 3).

3. Stationary and moving solitons: Fourier transform method

In this section, we introduce a new method to obtain both stationary and moving solitons for the DNLS equation. The essence of the method is to transform the DNLS equation governing the solitary wave into Fourier space, where the wave function is smooth, and then deal with a nonlinear nonlocal integral equation for which we employ a rapidly convergent numerical scheme to find solutions. A key advantage of the method is to transform a differential-delay equation into an integral equation for which computational methods are effective (see also Refs. [42,43]). Mathematically, the method also provides a foundation upon which an analytic theory describing solitons in nonlinear lattices can be constructed. Moreover, the method is applicable to continuous problems.

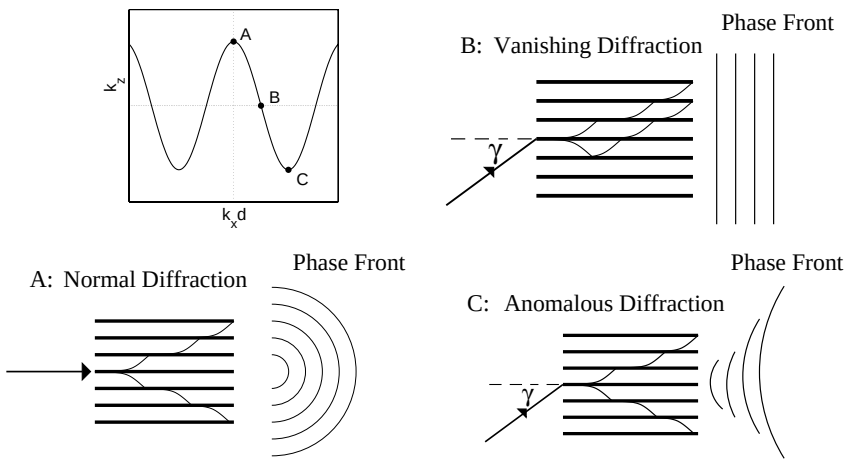

Fig. 3. Diffraction relation (top left) showing three typical examples of diffraction scenarios: (A) Normal in which the phase front is concave; (B) vanishing diffraction in which the phase front is almost flat; (C) anomalous diffraction with convex phase front.

3.1. Stationary solutions

We look for a stationary solution to Eq. (2.12) in the form

$$\phi_n = F_n \exp(\mathrm{i}\omega z) \tag{3.1}$$

with F_n being real valued function and ω a real eigenvalue. Then F_n satisfies

$$-\omega F_n + \frac{1}{h^2}(F_{n+1} + F_{n-1} - 2F_n) + F_n^3 = 0. \tag{3.2}$$

Eq. (3.2) can be solved using Newton iteration scheme by which one gives initial values for F_0 and F_1 and then iterate. However, our aim here is to provide a different approach based on the Fourier transform method in which a discrete equation is transformed into an integral equation. To this end, we use the transform defined by

$$\hat{u}(w,t) = \sum_{n=-\infty}^{+\infty} u_n w^{-n} \tag{3.3}$$

with the inverse transform given as

$$u_n(t) = \frac{1}{2\pi\mathrm{i}} \oint_{\mathcal{C}_0} \hat{u}(w,t) w^{n-1}\,\mathrm{d}w, \tag{3.4}$$

where w is a complex number and $\mathcal{C}_0$ the unit circle. If we let $w = \mathrm{e}^{\mathrm{i}qh}$ then Eq. (3.4) coincides with the discrete Fourier transform

$$\hat{u}(q) = \sum_{m=-\infty}^{+\infty} u_m\,\mathrm{e}^{-\mathrm{i}qmh}, \qquad u_m = \frac{h}{2\pi}\int_{-\pi/h}^{\pi/h} \hat{u}(q)\,\mathrm{e}^{\mathrm{i}qmh}\,\mathrm{d}q. \tag{3.5}$$

Applying the discrete Fourier transform in Eq. (3.2) leads to the following nonlinear integral equation:

$$\hat{F}(q) = \frac{h^2}{4\pi^2\Omega(q)} \iint_{\mathbb{D}^2} \mathrm{d}q_1\,\mathrm{d}q_2 \hat{F}(q_1)\hat{F}(q_2)\hat{F}(q-q_1-q_2) \equiv \mathcal{K}_\omega[\hat{F}(q)], \tag{3.6}$$

where $\mathbb{D}^2 = \mathbb{D} \times \mathbb{D}$ and $\mathbb{D} = [-\pi/h, \pi/h]$. Here, $\Omega(q) = \omega + 2(1 - \cos(hq))/h^2$ corresponds to the frequency of the linear excitations. The important conclusion is that the soliton can be viewed as a fixed point of an infinite-dimensional nonlinear functional. To numerically find the fixed point, one might start with an initial guess for $\hat{F}(q)$ and iterate Eq. (3.6) using

$$\hat{F}_{n+1}(q) = \mathcal{K}_\omega[\hat{F}_n(q)], \quad n \geq 0. \tag{3.7}$$

However, if the norm of $\hat{F}(q)$ is "large" then the iteration based on Eq. (3.7) will diverge while it will converge to zero for small norm. This is because the right hand side of Eq. (3.7) has degree 3 whereas the left hand side is suggested of degree 1. To overcome this difficulty, we employ instead, a modified Neumann iteration scheme and consider a new equation

$$\hat{F}_{n+1}(q) = \left(\frac{\langle \hat{F}_n, \hat{F}_n \rangle}{\langle \hat{F}_n, \mathcal{K}_\omega \rangle} \right)^{3/2} \mathcal{K}_\omega[\hat{F}_n(q)], \quad n \geq 0, \tag{3.8}$$

where the inner product $\langle \cdot \rangle$ is defined by

$$\langle \hat{f}, \hat{g} \rangle \equiv \int_{\mathbb{D}} \hat{f}(q)\hat{g}(q)\,\mathrm{d}q. \tag{3.9}$$

The factor 3/2 is chosen to make the right hand side of Eq. (3.8) of degree 0 which yields convergence of the scheme [42,43]. When F_m is real and even, it implies that $\hat{F}(q)$ is also real. Clearly when $\hat{F}_n(q) \to \hat{F}_s(q)$ as $n \to \infty$ then $\langle \hat{F}_n, \hat{F}_n \rangle / \langle \hat{F}_n, \mathcal{K}_\omega \rangle \to 1$ and in turn $\hat{F}_s(q)$ will be the solution to Eq. (3.6). Fig. 4 shows a typical solution to (3.6) both in the Fourier domain (Fig. 4a) and in physical space (Fig. 4b) for different values of lattice spacing h. The proposed scheme converges linearly as can be seen in Fig. 5 where the relative error between successive iterations E_n^F defined by

$$E_n^F = \log |E_n - E_{n-1}| \tag{3.10}$$

is plotted for different values of lattice spacing h and typical parameter value $\omega = 1$. In order to shed more light on the property of the solution, we will consider for comparison the IDNLS given by [40]

$$\mathrm{i}\frac{\partial u_n}{\partial t} + \frac{1}{h^2}(u_{n+1} + u_{n-1} - 2u_n) + |u_n|^2(u_{n+1} + u_{n-1}) = 0, \tag{3.11}$$

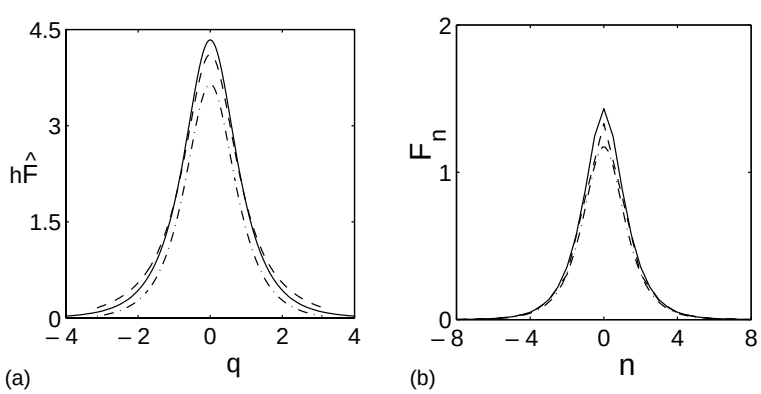

Fig. 4. Mode profiles obtained with $\omega = 1$ in Fourier space (a), for $h = 0.5$ (solid), $h = 1$ (dashed) and $h = 1$ (dashed-dotted) for the integrable case. (b) Soliton shape in physical space for $h = 0.5$ (solid), $h = 1$ (dashed) and for the integrable case at $h = 1$ (dashed-dotted).

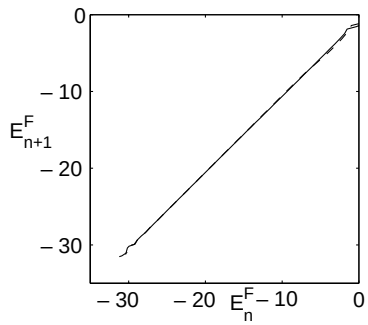

Fig. 5. Plot of the relative error E_n^F between successive iterations for $h = 0.5$ (solid) and $h = 1$ (dashed) with $\omega = 1$.

which possesses an exact TW solution of the form

$$u_n(t) = \frac{\sin(h)}{h}\,\mathrm{sech}(nh - Vt)\exp[-\mathrm{i}(\beta nh - \omega t)], \tag{3.12}$$

$$\omega = \frac{2}{h^2}[\cos(\beta h)\cos(h) - 1], \qquad V = -\frac{2}{h^2}\sin(\beta h)\sin(h). \tag{3.13}$$

Consider first the case when the soliton is stationary ($V = 0$). The method of discrete Fourier transform rapidly converges when applied to Eq. (3.11) and agrees with Eq. (3.12) (see Fig. 4). What is also remarkable about the solution (3.12) is that it forms a *continuous* function, i.e., the solution is not only defined at the grid pints $n = 0, \pm 1, \pm 2, \ldots$ but also it can be defined off the grid points (e.g., $n = 1.234$). This suggests that Eq. (3.11) can be embedded in a larger class of differential-delay equations in which the discrete variable n can be considered as a *continuous* variable without affecting the solution. With this extension in mind, we could search for a stationary solutions for Eq. (3.11) (with $n \equiv \xi$ being a continuous variable) by applying the continuous Fourier transform:

$$\hat{u}(q) = \int_{-\infty}^{+\infty} u(\xi)\,\mathrm{e}^{-\mathrm{i}q\xi}\,\mathrm{d}\xi, \qquad u(\xi) = \frac{1}{2\pi}\int_{-\infty}^{+\infty} \hat{u}(q)\,\mathrm{e}^{\mathrm{i}q\xi}\,\mathrm{d}q, \tag{3.14}$$

which can be obtained from Eq. (3.5) by taking the limit $h \to 0$ with fixed $nh = \xi$. The important question we ask is: does a continuous stationary solution exist for the DNLS equation as well? To partially answer this question we applied the continuous Fourier transform in Eq. (3.2) (to find stationary solution). The only change from Eq. (3.6) is that $\mathbb{D}^2 \to \mathbb{R}^2$. We found that the numerical scheme based on (3.8) does not converge which indicates that a continuous stationary localized solution to the DNLS may not exist. On the other hand we did find numerically that a continuous Fourier transform solution to Eq. (3.11) converged rapidly. As we will see later, this will have a direct impact on the TW problem.

3.2. Remarks

Below we make some comments on the proposed scheme for discrete systems outlining its usefulness.

- The numerical scheme based on Eq. (3.8) can be replaced by one in which the convergent factors belong to L^1:

$$\|\hat{F}\|_1 \equiv \int_{\mathbb{D}} \hat{F}(q)\,\mathrm{d}q. \tag{3.15}$$

In this case, the iteration scheme takes the form

$$\hat{F}_{n+1}(q) = \left(\frac{\|\hat{F}_n\|_1}{\|\mathcal{K}_\omega\|_1}\right)^{3/2} \mathcal{K}_\omega[\hat{F}_n(q)], \quad n \geq 0. \tag{3.16}$$

- Finding stationary solutions for multidimensional continuous partial differential equations (PDEs) using the above scheme is straightforward.
- Applying the Fourier transform technique to higher order continuous or discrete systems only results in a modification of the linear dispersion relation from, e.g., $\cos(qh) \to \cos(qh) + \cos(2qh)$.
- The proposed technique is natural for diffraction-managed systems in which an infinite-dimensional nonlinear integral equation must be solved. Applying direct methods such as Newton iteration would be difficult on such diffraction-managed equations.

3.3. Numerical iteration based on energy renormalization

We next highlight a different approach based on energy renormalization to solve Eq. (3.6). As we have seen before, one reason why simple iteration scheme does not converge is because the right and left hand side of (3.6) have different homogeneity. An alternative method is to renormalize the wave function $\hat{F}(q)$ at each iteration stage by its L^∞ (maximum) or L^2 norm, respectively, defined by

$$\|\hat{F}\|_\infty \equiv \max_{q\in\mathbb{D}} |\hat{F}(q)|, \tag{3.17}$$

$$\|\hat{F}\|_2 \equiv \left(\int_{\mathbb{D}} |\hat{F}(q)|^2 \,\mathrm{d}q\right)^{1/2}. \tag{3.18}$$

In this case the beam amplitude remains always finite. For discrete problems, the choice of the maximum norm is particularly natural since the problem is restricted to a finite domain in q space. To implement this scheme, we start with a localized guess, $\hat{\mathsf{F}}_0(q)$ and compute its norm $\|\hat{\mathsf{F}}_0\|$ (by $\|\cdot\|$ we mean either $\|\cdot\|_\infty$ or $\|\cdot\|_2$). We then define the renormalized function $\hat{\mathcal{F}}_0(q) = \hat{\mathsf{F}}_0(q)/\|\hat{\mathsf{F}}_0\|$. Then from Eq. (3.6) we compute $\hat{\mathsf{F}}_1(q)$ and, in general, the mth iteration takes the form

$$\hat{\mathsf{F}}_{m+1}(q) = \frac{h^2}{4\pi^2\Omega(q)} \iint_{\mathbb{D}^2} \mathrm{d}q_1\,\mathrm{d}q_2 \hat{\mathcal{F}}_m(q_1)\hat{\mathcal{F}}_m(q_2)\hat{\mathcal{F}}_m(q-q_1-q_2), \tag{3.19}$$

$$\hat{\mathcal{F}}_m(q) = \frac{\hat{\mathsf{F}}_m(q)}{\|\hat{\mathsf{F}}_m\|}. \tag{3.20}$$

Note that as $m \to \infty$ the scheme based on Eq. (3.20) converges, i.e.:

$$\lim_{m\to\infty} \|\hat{\mathcal{F}}_m - \hat{\mathcal{F}}_s\| = 0, \tag{3.21}$$

where $\hat{\mathcal{F}}_s$ and $\hat{\mathsf{F}}_s = \|\hat{\mathsf{F}}_s\|\hat{\mathcal{F}}_s$ is the exact solution to Eq. (3.20). Importantly, Eq. (3.6) admits the following scaling property: if $\hat{F}(q) = \varkappa\hat{F}'(q)$ then $\hat{F}'(q) = \varkappa^2\mathcal{K}_\omega[\hat{F}'(q)]$ is also a solution. In light of this scaling property we find that $\hat{\mathcal{F}}_s$ and $\hat{\mathsf{F}}_s$ are also solutions to Eq. (3.6). We have compared the solution obtained by this method with the previous technique and with the IDNLS solution and found excellent agreement.

3.4. Do discrete TWs exist or not?

Finding analytical TW solutions for a continuous PDE and for differential-delay equations in particular, is a challenging problem. For some PDEs, TWs can be readily obtained by making use of either Galilean or Lorentz

invariance. However, for general discrete systems, such a symmetry does not exist. An additional source of difficulty that arises when dealing with differential-delay systems is the lack of quadrature. In this section, we describe a method to obtain TW solutions for discrete systems which is applicable to many discrete models such as FPU lattice, sine-Gordon to name a few. However, here we will focus our attention to TW of the DNLS model. Unlike the IDNLS in which exact continuous traveling solitons are known, there are no known explicit solutions for DNLS solitons. Previous studies of TWs for the DNLS equation employed various techniques and ansatz [44–46]. One method is to write the DNLS as a perturbed IDNLS [47] and use perturbation theory, based on inverse scattering, to gain some insight to the solution. However, this method is limited to moderately confined wave functions and cannot be used as a constructive method. Another technique is to use the "exact" stationary solutions discussed in Section 3.2 and, based on what we know from continuous NLS theory, employ a linear phase tilt:

$$\phi_n = F_n \exp(\mathrm{i}\beta n h) \tag{3.22}$$

with F_n being the stationary solution found before and β the beam "velocity" or phase tilt. However, by doing so, we do not obtain a uniformly moving solitary wave (as can be seen in Fig. 6 where the top of the beam oscillates). This is even more clear when we zoom in on small amplitude where radiation modes are seen to be emitted during propagation (see Fig. 7). Our analysis, which is based on the discrete Fourier methods, reveals another fundamental distinction from the IDNLS traveling solitons: there are approximate TW solutions which are "multimode" discrete solitons, i.e., a single mode (sech-like shape) does not propagate without significant radiation [48]. In fact the modes we found are characterized by having a nonlinear "chirp". To formulate the analysis, we look for traveling localized modes in the form

$$\phi_n(z) = u(\xi)\exp[-\mathrm{i}(\beta n h - \omega z)], \quad \xi = nh - Vz \tag{3.23}$$

with V and ω being the soliton velocity and wavenumber shift, respectively. Assuming u is complex, i.e., $u(\xi) = F(\xi) + \mathrm{i}G(\xi)$ (with F, G being real), then Eq. (2.12) takes the form

$$V\frac{\mathrm{d}G}{\mathrm{d}\xi} + \mathcal{D}_1 F + \mathcal{D}_2 G + (F^2+G^2)F = \omega F, \qquad -V\frac{\mathrm{d}F}{\mathrm{d}\xi} + \mathcal{D}_1 G - \mathcal{D}_2 F + (F^2+G^2)G = \omega G, \tag{3.24}$$

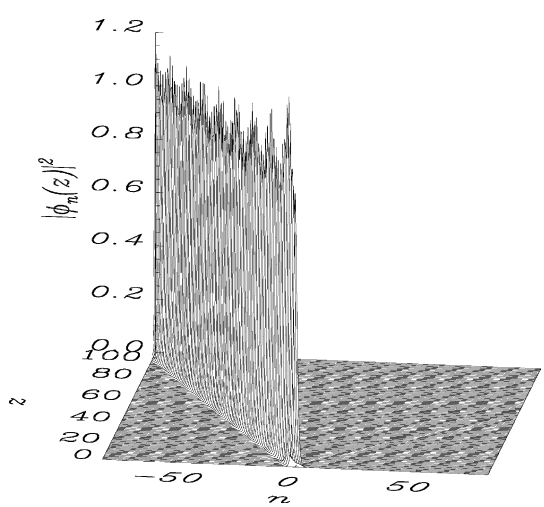

Fig. 6. Evolution of the stationary solution in physical domain for $\omega = 1$ and $h = 0.5$ obtained by direct numerical simulation by employing a linear phase tilt (or velocity) with $\beta = 0.5$.

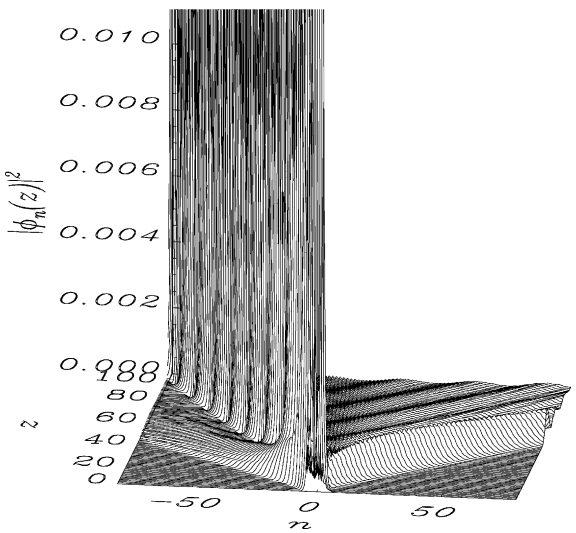

Fig. 7. The same as in Fig. 6 but zoomed to small amplitude. Radiation modes are clearly seen which leads to a nonuniform moving beam.

where the linear operators $\mathcal{D}_1$ and $\mathcal{D}_2$ are defined by

$$\mathcal{D}_1 f \equiv \frac{1}{h^2}[\cos(\beta h)(E_+ + E_-)f - 2f], \qquad \mathcal{D}_2 g \equiv \frac{\sin(\beta h)}{h^2}(E_+ - E_-)g \tag{3.25}$$

with $E_\pm \mathcal{S}(\xi) \equiv \mathcal{S}(\xi \pm h)$. To find the mode shapes and soliton velocity, we proceed as before by taking the discrete Fourier transform of Eq. (3.24) which yields the following iteration scheme:

$$\hat{F}_{n+1}(q) = \frac{\Omega_2(q)}{\Omega_1(q)}\tilde{G}_n(q) + \left(\frac{\alpha_1}{\beta_1}\right)^{3/2}\mathcal{Q}_1[\hat{F}_n, \tilde{G}_n], \qquad \tilde{G}_{n+1}(q) = \frac{\Omega_2(q)}{\Omega_1(q)}\hat{F}_n(q) + \left(\frac{\alpha_2}{\beta_2}\right)^{3/2}\mathcal{Q}_2[\hat{F}_n, \tilde{G}_n], \tag{3.26}$$

where $\hat{F}(q)$ and $\hat{G}(q) \equiv -\mathrm{i}\tilde{G}(q)$ are the Fourier transforms of $F(\xi)$ and $G(\xi)$, respectively, and

$$\mathcal{Q}_1[\hat{F}, \tilde{G}] = \frac{h^2}{4\pi^2\Omega_1(q)}(\hat{F} * \hat{F} * \hat{F} - \tilde{G} * \tilde{G} * \hat{F}), \qquad \mathcal{Q}_2[\hat{F}, \tilde{G}] = \frac{h^2}{4\pi^2\Omega_1(q)}(\hat{F} * \hat{F} * \tilde{G} - \tilde{G} * \tilde{G} * \tilde{G}), \tag{3.27}$$

where $*$ denotes a convolution:

$$f * g = \int_{\mathbb{D}} f(k)g(q-k)\,\mathrm{d}k.$$

The convergence factors α_j and β_j, $j = 1, 2$ are given by

$$\alpha_1 = \left\langle \hat{F}_n, \hat{F}_n - \frac{\Omega_2\tilde{G}_n}{\Omega_1}\right\rangle, \qquad \alpha_2 = \left\langle \tilde{G}_n, \tilde{G}_n - \frac{\Omega_2\hat{F}_n}{\Omega_1}\right\rangle, \qquad \beta_1 = \langle \hat{F}_n, \mathcal{Q}_1\rangle, \qquad \beta_2 = \langle \tilde{G}_n, \mathcal{Q}_2\rangle$$

with

$$\Omega_1(q) = \omega + \frac{2}{h^2}[1 - \cos(hq)\cos(\beta h)], \qquad \Omega_2(q) = \frac{2}{h^2}\sin(hq)\sin(\beta h) + Vq. \tag{3.28}$$

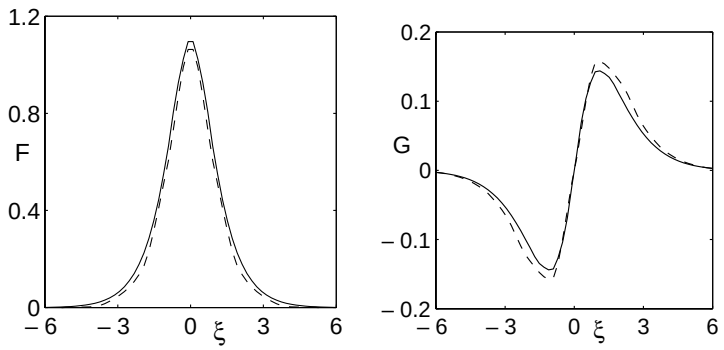

Fig. 8. Mode shapes in physical space for $\omega = 1$ and $\beta = 0.5$. Solid line corresponds to $h = 0.5$ and velocity $V = -0.25$ whereas dashed line for $h = 1$ and $V = -0.155$.

The next stage would be to iterate Eq. (3.26). However, Eq. (3.26) form a system of two equations with *three* unknowns, $\hat{F}$, $\tilde{G}$ and V. Therefore, we need to add an extra condition to match the number of variables with the number of equations. By doing so, we proceed as follows. For a given set of parameters h, ω and $\beta > 0$, the mode shapes and soliton velocity are found by iterating Eq. (3.26) with an initial guess, e.g., $\hat{F}_0(q) = \mathrm{sech}(q)$, $\tilde{G}_0(q) = \mathrm{sech}(q)\tanh(q)$ and $V = V_* < 0$. The iterations are carried out until the condition $|\mathcal{E}_j| \equiv |\alpha_j - \beta_j| < \epsilon$ $(j = 1, 2)$ is satisfied with $\epsilon > 0$ being a prescribed tolerance. However, unlike the stationary case, here, the soliton velocity is still to be determined. For any choice of $V_* < 0$ if $|\mathcal{E}_j| \not< \epsilon$, we seek a different value of V_* at which $\mathcal{E}_j$ changes sign. Then, we use the bisection method to change V_* in order to locate the correct velocity V and modes $\hat{F}$, $\tilde{G}$ for each ω, β and h. Typical soliton modes are shown in Fig. 8.

At this stage it is useful to make some further comments on the Fourier transform. Since ξ is a continuous variable it implies that Eq. (3.24) are continuous equations in ξ. Therefore it seems natural to use the *continuous* Fourier transform rather than discrete. However, when we apply the *continuous* Fourier transform in Eq. (3.24), we find that the numerical scheme based on Eq. (3.26) with $\pi/h \to \infty$ does not converge to a solution. This is a strong indication that, as opposed to the integrable case, a *true continuous* stationary or TW solutions to the DNLS model does not exist. By continuous solution we mean a solution that can be defined off the lattice points which is *necessary* when discussing TWs on lattices. In fact, the perturbation analysis presented below supports this observation as it *fails* to give consistent results off the grid points. To support these founding, let us take the continuous limit on the DNLS which yields

$$\mathrm{i}\frac{\partial \phi}{\partial z} + \phi_{xx} + \alpha_4 \phi_{xxxx} + |\phi|^2 \phi = 0, \tag{3.29}$$

where $\alpha_4 = h^2/12$. Importantly, it was shown in [49] that Eq. (3.29) with $\alpha_4 > 0$ lacks exact soliton solutions whereas it possess closed form solution for $\alpha_4 < 0$ [50]. Moreover, in this case the asymptotic behavior of the solution to Eq. (3.29) in the limit $0 < \alpha_4 \ll 1$ is [49]

$$\phi \sim \mathrm{sech}(\xi) + \mathrm{O}(\mathrm{e}^{-\Upsilon/|h|}) P(\xi, z),$$

with $\xi = x - Vz$ and Υ being a positive constant with $P(\xi, z)$ being a concrete function of *both* ξ and z (see Eq. (16) of Ref. [49]). This means that for $h = 0.1$ (as an example), the nonstationary correction to the exact solution (when $\alpha_4 = 0$) is exponentially small and cannot be captured in numerical simulations. These results differ from those of [51,52] in which a "continuous" traveling solitary waves were reported using Fourier series expansions with finite period L while *assuming convergence* as $L \to \infty$.

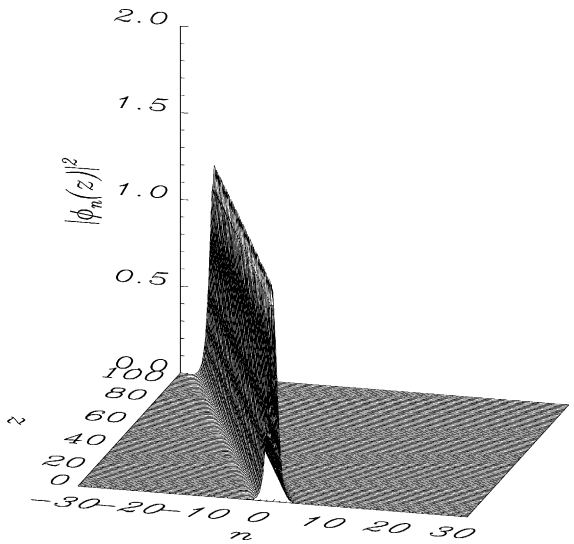

Fig. 9. Evolution of a moderately localized soliton in physical domain for $\beta = 0.5$, $V = -0.25$, $\omega = 1$ and $h = 0.5$ obtained by direct numerical simulation.

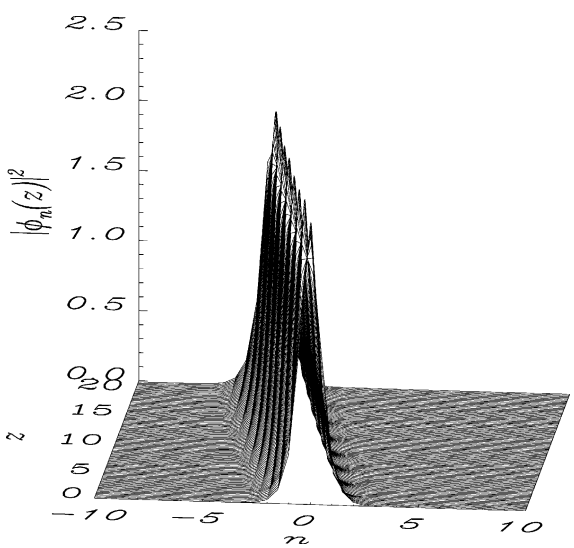

Fig. 10. Evolution of a strongly localized soliton in physical domain for $\beta = 0.5$, $V = -0.2$, $\omega = 2$ and $h = 0.5$ obtained by direct numerical simulation.

Although Eq. (3.26) can be solved numerically with high accuracy, the resulting solutions are only obtained at the discrete locations $\xi = nh$, while all real values of ξ are called upon in a TW solution. So the question we want to ask is: what happen to the modes found above when they propagate across the arrays? To answer this question, we simulated Eq. (2.12) using $\phi_n(z = 0) = u(nh)\,\mathrm{e}^{-\mathrm{i}\beta nh}$ as an initial condition with $u(nh) = F_{\mathrm{TW}}(nh) + \mathrm{i}G_{\mathrm{TW}}(nh)$ being the solutions obtained from (3.26). When a moderately localized mode[1] is launched, the beam moved across the

[1] Moderate localization obtains when the FWHM of the intensity is 4–6 lattice sites; strong localization occurs when FWHM = 1–3 lattice sites.

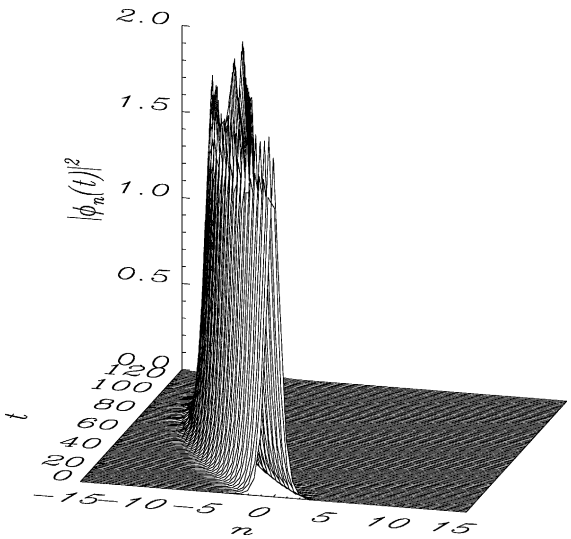

Fig. 11. Evolution of a strongly localized soliton in physical domain for large distance. Contrary to Fig. 10, in which the beam travels for short distance, here after some distance, the beam starts to decelerate. Parameters are: $\beta = 0.5$, $V = -0.2$, $\omega = 2$ and $h = 0.5$.

waveguides undistorted (Fig. 9) over 100 normalized z-units. This corresponds, according to the experimental data reported in [11], to 120 mm (recall that the waveguides used in [11] were 6 mm in length). On the other hand, strongly localized modes travel essentially undistorted for shorter distances (around 20 normalized z-units, see Fig. 10) which corresponds to 24 mm. Noticeably, during propagation there was a change of 0.0133%/mm(0.245%/mm) in the soliton velocity for moderately (strongly) localized modes in which case strongly localized mode slows down and eventually relaxes to a stationary state (see Fig. 11). This behavior depends crucially on the initial amplitude. Higher amplitude solitons are less "mobile" than lower amplitude beams. The discrete Fourier transform yields a useful, but nonuniform TW solution.

4. Asymptotic theory for discrete TWs

4.1. Perturbation expansion around stationary solutions

We have seen in Section 3.4, that TWs with nonuniform speed can be numerically constructed by means of the Fourier iteration method. These solutions can move over short distances without drastic change in their shape or speed. However, strongly localized modes will immediately start decelerating and emitting radiation. Our conclusion from Section 3.4 was that uniform TWs for the DNLS equation are unlikely to exist. To give further support to this belief, we consider the case in which the solitons move slowly. We develop a fully discrete perturbation theory for finite amplitudes. It is important to note that our perturbative approach is fundamentally different than the perturbation methods based on inverse scattering theory (cf. [47]). We begin by taking $\beta = \epsilon\beta_1 + \mathrm{O}(\epsilon^2)$, $\epsilon \ll 1$, and expand the soliton velocity, frequency and the wave functions in a power series in ϵ:

$$F = F_0 + \epsilon F_1 + \epsilon^2 F_2 + \mathrm{O}(\epsilon^3), \qquad G = \epsilon G_1 + \epsilon^2 G_2 + \mathrm{O}(\epsilon^3), \tag{4.1}$$

$$V = \epsilon V_1 + \epsilon^2 V_2 + \mathrm{O}(\epsilon^3), \qquad \omega = \omega_s + \epsilon\omega_1 + \epsilon^2\omega_2 + \mathrm{O}(\epsilon^3). \tag{4.2}$$

Substituting Eqs. (4.1) and (4.2) into Eq. (3.26), we find that to leading order (ϵ^0), F_0 satisfies the stationary equation and is even in ξ:

$$\mathcal{L}_1 F_0(\xi) = 0. \tag{4.3}$$

The order ϵ equations for F_1 and G_1 are given by

$$\mathcal{L}_1 F_1 = \omega_1 F_0, \tag{4.4}$$

$$\mathcal{L}_2 G_1 = V_1 \frac{\mathrm{d}F_0}{\mathrm{d}\xi} + \frac{\beta_1}{h}(E_+ - E_-)F_0 \tag{4.5}$$

and the order ϵ^2 system is

$$\mathcal{L}_2 G_2 = \omega_1 G_1 + V_1 \frac{\mathrm{d}F_1}{\mathrm{d}\xi} + V_2 \frac{\mathrm{d}F_0}{\mathrm{d}\xi} - 2F_0 F_1 G_1 + \frac{\beta_1}{h}(E_+ - E_-)F_1, \tag{4.6}$$

$$\mathcal{L}_1 F_2 = \omega_1 F_1 + \omega_2 F_0 - V_1 \frac{\mathrm{d}G_1}{\mathrm{d}\xi} - F_0 G_1^2 - 3F_0 F_1^2 + \frac{\beta_1^2}{2}(E_+ + E_-)F_0 - \frac{\beta_1}{h}(E_+ - E_-)G_1, \tag{4.7}$$

where the linear operators $\mathcal{L}_1$ and $\mathcal{L}_2$ are defined by

$$\mathcal{L}_1 \mathcal{S} \equiv -\omega_s \mathcal{S} + \frac{1}{h^2}(E_+ + E_- - 2)\mathcal{S} + 3F_0^2 \mathcal{S}, \qquad \mathcal{L}_2 \mathcal{S} \equiv -\omega_s \mathcal{S} + \frac{1}{h^2}(E_+ + E_- - 2)\mathcal{S} + F_0^2 \mathcal{S}. \tag{4.8}$$

Next we solve the system of equations at each order in ϵ. By taking $\omega_1 \partial/\partial\omega_s$ in Eq. (4.3) we find that solution to F_1 is given by

$$F_1 = \omega_1 \frac{\partial F_0}{\partial \omega_s} + c_1 \frac{\partial F_0}{\partial \xi}. \tag{4.9}$$

To solve equation in (4.5), we make the ansatz:

$$G_1 = V_1 A + \beta_1 \xi F_0 + c_2 F_0, \tag{4.10}$$

where c_1 and c_2 are arbitrary constants and A satisfies

$$\mathcal{L}_2 A = \frac{\partial F_0}{\partial \xi}, \tag{4.11}$$

which can be solved either numerically by Fourier transform method or by reduction of order method. Note that $A(\xi)$ is an anti-symmetric function.

4.2. Solvability conditions at $O(\epsilon)$

The velocity $V_1(\beta_1)$ and frequency shift ω_1, are determined by a solvability condition at order ϵ^2 which is the discrete analog of Green's identity. We start first with the order ϵ equations. Let $W(\xi)$ be a solution to the homogeneous equation, $\mathcal{L}_1 W(\xi) = 0$. Multiplying Eq. (4.4) by $W(\xi)$ and subtracting $F_1(\xi)\mathcal{L}_1 W(\xi) = 0$ we find

$$\Delta_\xi[Y(\xi)] = h^2 \omega_1 W(\xi) F_0(\xi), \tag{4.12}$$

where $Y(\xi) = W(\xi - h)F_1(\xi) - F(\xi - h)W(\xi)$ and Δ_ξ is defined by $\Delta_\xi[\mathcal{S}(\xi)] = \mathcal{S}(\xi + h) - \mathcal{S}(\xi)$. An important identity which will be used frequently is the discrete analog of Green's identity

$$\sum_{\ell=-\infty}^{+\infty} [S(\xi + \ell h) - S(\xi + (\ell - 1)h)] = 0$$

with $\ell \in \mathbb{Z}$. Since $W = \mathrm{d}F_0/\mathrm{d}\xi$, summing over all integers in Eq. (4.12) and using the discrete Green's identity we find

$$\omega_1 \sum_{\ell=-\infty}^{+\infty} \left(F_0 \frac{\mathrm{d}F_0}{\mathrm{d}\xi} \right)\Big|_{\xi+\ell h} = 0. \tag{4.13}$$

Importantly, if ξ is not restricted to the grid points then the sum in Eq. (4.13) is generally not zero. We shall consider the case in which $\xi \in \mathbb{Z}$ otherwise, as we will see below, no TW solution is obtained. With this assumption in mind, the solvability condition at order ϵ is satisfied and at this stage ω_1 is an arbitrary constant. Similarly, we find that the solvability condition for Eq. (4.5) reads

$$\sum_{\ell=-\infty}^{+\infty} F_0(\xi+\ell h) \left[V_1 \frac{\mathrm{d}F_0}{\mathrm{d}\xi}\Big|_{\xi+\ell h} + \frac{\beta_1}{h} \left(F_0(\xi+(\ell+1)h) - F_0(\xi+(\ell-1)h) \right) \right] = 0. \tag{4.14}$$

As before, if we are off the grid points then the sum in (4.14) does not necessarily vanish and as a result the velocity will depend on ξ. Therefore, we restrict the sum to the lattice points which is consistent with the discrete Fourier transform.

4.3. Solvability conditions at $O(\epsilon^2)$

Next we consider the solvability conditions to the $\mathrm{O}(\epsilon^2)$ equations which will determine the velocity V_1 and frequency ω_1. The solvability conditions for Eqs. (4.6) and (4.7), respectively, read

$$\begin{aligned} \sum_{\ell=-\infty}^{+\infty} F_0(\xi+\ell h) \Bigg[& V_1 \frac{\mathrm{d}F_1}{\mathrm{d}\xi}\Big|_{\xi+\ell h} + V_2 \frac{\mathrm{d}F_0}{\mathrm{d}\xi}\Big|_{\xi+\ell h} + \frac{\beta_1}{h}(F_1(\xi+(\ell+1)h) - F_1(\xi+(\ell-1)h)) \\ & + \omega_1 G_1(\xi+\ell h) - 2F_0(\xi+\ell h)F_1(\xi+\ell h)G_1(\xi+\ell h) \Bigg] = 0, \end{aligned} \tag{4.15}$$

$$\begin{aligned} \sum_{\ell=-\infty}^{+\infty} F_0(\xi+\ell h) \Bigg[& \omega_1 F_1(\xi+\ell h) + \omega_2 F_0(\xi+\ell h) - V_1 \frac{\mathrm{d}G_1}{\mathrm{d}\xi}\Big|_{\xi+\ell h} - F_0(\xi+\ell h)G_1^2(\xi+\ell h) \\ & - 3F_0(\xi+\ell h)F_1^2(\xi+\ell h) + \frac{\beta_1^2}{2}(F_0(\xi+(\ell+1)h) + F_0(\xi+(\ell-1)h)) \\ & - \frac{\beta_1}{h}(G_1(\xi+(\ell+1)h) - G_1(\xi+(\ell-1)h)) \Bigg] = 0. \end{aligned} \tag{4.16}$$

Substituting the expressions for F_1 and G_1 [see Eqs. (4.9) and (4.10)] in Eqs. (4.15) and (4.16) and using the fact that the function $A(\xi)$ is anti-symmetric we find

$$\begin{bmatrix} \mathbb{A}_{11} & \mathbb{A}_{12} \\ \mathbb{A}_{21} & \mathbb{A}_{22} \end{bmatrix} \begin{bmatrix} c_1 \\ c_2 \end{bmatrix} = 0, \tag{4.17}$$

where

$$\mathbb{A}_{11} = V_1 \sum_{\ell=-\infty}^{+\infty} F_0(\xi+\ell h)\left[\left.\frac{\mathrm{d}^2F_0}{\mathrm{d}\xi^2}\right|_{\xi+\ell h} + \frac{\beta_1}{h}\left(\left.\frac{\mathrm{d}F_0}{\mathrm{d}\xi}\right|_{\xi+(\ell+1)h} - \left.\frac{\mathrm{d}F_0}{\mathrm{d}\xi}\right|_{\xi+(\ell-1)h}\right)\right]$$
$$- 2V_1 \sum_{\ell=-\infty}^{+\infty} A(\xi+\ell h)F_0^2(\xi+\ell h)\left.\frac{\mathrm{d}F_0}{\mathrm{d}\xi}\right|_{\xi+\ell h} - 2\beta_1 \sum_{\ell=-\infty}^{+\infty} (\xi+\ell h)F_0^3(\xi+\ell h)\left.\frac{\mathrm{d}F_0}{\mathrm{d}\xi}\right|_{\xi+\ell h},$$

$$\mathbb{A}_{12} = \omega_1 \sum_{\ell=-\infty}^{+\infty} F_0^2(\xi+\ell h) - 2\omega_1 \sum_{\ell=-\infty}^{+\infty} F_0^3(\xi+\ell h)\frac{\mathrm{d}F_0}{d\omega_s}(\xi+\ell h),$$

$$\mathbb{A}_{21} = \omega_1 \sum_{\ell=-\infty}^{+\infty} \left.\left(\frac{\mathrm{d}F_0}{\mathrm{d}\xi}\right)^2\right|_{\xi+\ell h} - 6\omega_1 \sum_{\ell=-\infty}^{+\infty} \left.\left(\frac{\mathrm{d}F_0}{\mathrm{d}\xi}\right)^2\right|_{\xi+\ell h} F_0(\xi+\ell h)\frac{\mathrm{d}F_0}{\mathrm{d}\omega_s}(\xi+\ell h),$$

$$\mathbb{A}_{22} = -\sum_{\ell=-\infty}^{+\infty} \left.\frac{\mathrm{d}F_0}{\mathrm{d}\xi}\right|_{\xi+\ell h} [2\beta_1(\xi+\ell h)F_0^3(\xi+\ell h) + 2V_1A(\xi+\ell h)F_0^2(\xi+\ell h)]$$
$$- \frac{\beta_1}{h}\sum_{\ell=-\infty}^{+\infty} \left.\frac{\mathrm{d}F_0}{\mathrm{d}\xi}\right|_{\xi+\ell h} (F_0(\xi+(\ell+1)h) - F_0(\xi+(\ell-1)h)) - V_1 \sum_{\ell=-\infty}^{+\infty} \left.\left(\frac{\mathrm{d}F_0}{\mathrm{d}\xi}\right)^2\right|_{\xi+\ell h}.$$

The dependence of the velocity on β_1 will be determined by requiring that the determinant of the matrix equation (4.17) vanish. By restricting the sum to the lattice points, $\xi = \xi_\ell \equiv \ell h$, which is consistent with the discrete Fourier transform we find that the results are consistent if $\omega_1 = 0$ in which case the velocity is given by

$$V_1 = -\frac{a_1}{a_2}\beta_1, \qquad a_1(h) = \sum_{\ell\in\mathbb{Z}} \left.\frac{\mathrm{d}F_0}{\mathrm{d}\xi}\right|_{\xi_\ell}\left[2\xi_l F_0^3(\xi_l) + \frac{1}{h}(E_+ - E_-)F_0(\xi_l)\right],$$
$$a_2(h) = \sum_{\ell\in\mathbb{Z}} \left.\frac{\mathrm{d}F_0}{\mathrm{d}\xi}\right|_{\xi_\ell}\left[2A(\xi_\ell)F_0^2(\xi_\ell) + \left.\frac{\mathrm{d}F_0}{\mathrm{d}\xi}\right|_{\xi_\ell}\right]. \tag{4.18}$$

We compared these semi-analytical results with direct numerical simulation for the fully discrete case and found a good agreement for distances z of order 1. However, for longer distances, the theory needs to be modified. Moreover, in the limit $h \to 0$ we retrieve the known result $V_1 = -2\beta_1$, $G_1(\xi) \to 0$.

5. Nonlinear diffraction management

5.1. Heuristic approach

Let us begin the analysis by considering an infinite array of weakly coupled optical waveguides with equal separation d. We have seen that the equation which governs the evolution of a singly polarized beam in a nonlinear waveguide array follows the discrete NLS equation. A natural generalization to two interacting electric fields $E_n^{(1)}$ and $E_n^{(2)}$, is given by [13,29,30,53,54]

$$\frac{\mathrm{d}E_n^{(j)}}{\mathrm{d}z} = \mathrm{i}C(E_{n+1}^{(j)} + E_{n-1}^{(j)}) + \mathrm{i}k_{\mathrm{w}}^{(j)}E_n^{(j)} + \mathrm{i}(\boldsymbol{\kappa}\mathcal{E}_n)_j E_n^{(j)}, \quad j = 1, 2, \tag{5.1}$$

where $\boldsymbol{\kappa}$ is a 2×2 matrix with κ_{jj} and κ_{jl}, $j \neq l$ the self and cross-phase modulation coefficients, respectively, that result from the nonlinear index change, $\mathcal{E}_n = (|E_n^{(1)}|^2, |E_n^{(2)}|^2)^{\mathrm{T}}$, C a coupling constant, z the propagation distance

and $k_{\mathrm{w}}^{(1,2)}$ the propagation constants of the waveguides. When a cw modes of the form

$$E_n^{(1,2)}(z) = A_{1,2}\exp[\mathrm{i}(k_z z - nk_x d)] \tag{5.2}$$

is inserted into the linearized version of Eq. (5.1) it yields

$$k_z = k_{\mathrm{w}}^{(1,2)} + 2C\cos(k_x d), \qquad k_z'' = -2Cd^2\cos(k_x d), \tag{5.3}$$

where, as mentioned earlier, discrete diffraction is given by k_z''. An important consequence of Eq. (5.3) is that k_z'' can have a negative sign if $\pi/2 < |k_x d| \leq \pi$, hence, a light beam can experience anomalous diffraction. Experimentally, the sign and local value of the diffraction can be controlled and manipulated by launching light at a particular angle with respect to the normal to the waveguides or equivalently by tilting the waveguide array. To build a nonlinear model of diffraction management, we use a cascade of different segments of the waveguide, each piece being tilted by an angle zero and γ_{w}, respectively. The actual physical angle γ_{w} (the waveguide tilt angle) is related to the wavenumber k_x by the relation [27] $\sin\gamma_{\mathrm{w}} = k_x/k$ where $k = 2\pi n_0/\lambda_0$ ($\lambda_0 = 1.53\,\mu\mathrm{m}$ is the central wavelength in vacuum and we take $n_0 = 3.3$ to be the linear refractive index). In this way, we generate a waveguide array with alternating diffraction. Next, we define the dimensionless amplitudes $U_n^{(j)}$ ($U_n^{(1)} \equiv U_n$, $U_n^{(2)} \equiv V_n$) by

$$E_n^{(j)} = \sqrt{P_*}U_n^{(j)}\,\mathrm{e}^{\mathrm{i}(k_{\mathrm{w}}^{(j)}+2C)z}, \qquad z' = \frac{z}{z_*}, \tag{5.4}$$

where $P_* = \max(|U_n|^2_{\max}, |V_n|^2_{\max})$ is the characteristic power and z_* the nonlinear length scale. Substituting these quantities into Eq. (5.1) yields the following (dropping the prime) diffraction-managed vector DNLS equations [29,30]:

$$\begin{aligned}
&\mathrm{i}\frac{\mathrm{d}U_n}{\mathrm{d}z} + \frac{D(z/z_{\mathrm{w}})}{2h^2}(U_{n+1} + U_{n-1} - 2U_n) + (|U_n|^2 + \eta|V_n|^2)U_n = 0,\\
&\mathrm{i}\frac{\mathrm{d}V_n}{\mathrm{d}z} + \frac{D(z/z_{\mathrm{w}})}{2h^2}(V_{n+1} + V_{n-1} - 2V_n) + (\eta|U_n|^2 + |V_n|^2)V_n = 0,
\end{aligned} \tag{5.5}$$

where $\eta = \kappa_{12}/\kappa_{11}$ (we take $\kappa_{11} = \kappa_{22}, \kappa_{12} = \kappa_{21}$) and $z_* = 1/(\kappa_{11}P_*)$. We choose $z_* C\cos(k_x d) = D(z/z_{\mathrm{w}})/(2h^2)$ where $D(z/z_{\mathrm{w}})$ is a piecewise constant periodic function that measures the local value of diffraction. Here $z_{\mathrm{w}} \equiv 2L/z_*$ with L being the physical length of each waveguide segment (see Fig. 12(a) for schematic representation). Eq. (5.5) describe the dynamical evolution of coupled beams in a Kerr medium with varying diffraction. When the "effective" nonlinearity balances the average diffraction then bright vector discrete solitons can form. The dependence of the coupling constant C on the waveguide width (ℓ) and separation (d) is given by (for AlGaAs waveguide) $C = (0.00984/\ell)\exp(-0.22d)$ (see Eq. 13.8-10, pp. 523 of Ref. [55]). Therefore, the coupling constant C that corresponds to the experimental data reported in [28] (for 2.5 μm waveguide separation and width) is found

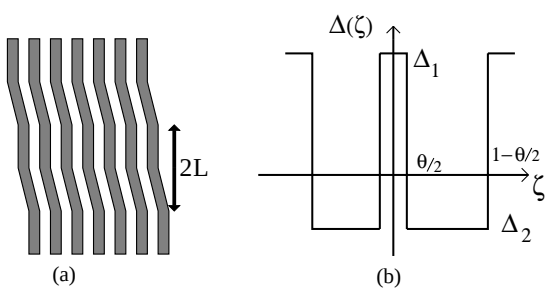

Fig. 12. Schematic presentation of the waveguide array (a) and the diffraction map (b).

to be $C = 2.27\,\mathrm{mm}^{-1}$. For typical power $P_* \approx 300\,\mathrm{W}$; typical nonlinear Kerr coefficient $\kappa_{11} = 3.6\,\mathrm{m}^{-1}\,\mathrm{W}^{-1}$ and typical waveguide length $L \approx 100\,\mu\mathrm{m}$ we find $z_* \approx 1\,\mathrm{mm}$ and $z_\mathrm{w} \approx 0.2$, which suggests the use of asymptotic theory based on small z_w. Such asymptotic analysis was developed in [29,30] for both the scalar and vector cases where the diffraction function $D = \delta_1 + \Delta/z_\mathrm{w}$ with Δ being a piecewise constant function (see Fig. 12(b)). Model (5.5) admits stationary soliton solution even when z_w is of order 1.

5.2. Asymptotic theory for diffraction management

5.2.1. Renormalization

We have seen in the preceding section how can we build, based on physical heuristic arguments, a model that incorporate both normal and anomalous diffraction. The key idea in formulating a model of diffraction management, is to use a cascade of different segments of waveguide, each piece being tilted by an angle zero and γ, respectively. Here, we give a derivation of the model, in the scalar case, based on asymptotic theory. Two approaches are given. The first is based on perturbation expansion using a renormalized eigen-mode of each single waveguide, whereas in the second we expand around eigenfunction of an untilted waveguide. It is clear from Fig. 12(a) that each single waveguide is not stationary. As a result, the evolution of the beam's amplitude is governed by

$$\left(\frac{\partial^2}{\partial z^2} + \frac{\partial^2}{\partial x^2}\right)\boldsymbol{\Psi} + k_0^2 f^2(X)\boldsymbol{\Psi} = 0, \quad X = x - \frac{\alpha}{\varepsilon}\int_0^Z \mathsf{D}(Z')\,\mathrm{d}Z', \tag{5.6}$$

whereas before, $Z = \varepsilon z$; α is a small parameter to be determined later and $\mathsf{D}(Z)$ a *piecewise constant* periodic function that measures the local value of diffraction. When the waveguides are well separated then the dynamics of each mode ψ_m in waveguide f_m^2 is decoupled and is given by

$$(\alpha^2\mathsf{D}^2(Z) + 1)\frac{\mathrm{d}^2\psi_m}{\mathrm{d}X^2} + (k_0^2 f_m^2(X) - \lambda_0^2)\psi_m = 0. \tag{5.7}$$

However when the waveguides are at close proximity, we approximate the solution to Eq. (5.6) as a multiscale perturbation series:

$$\boldsymbol{\Psi} = \sum_{m=-\infty}^{+\infty} \mathsf{E}_m(Z)\psi_m(X)\,\mathrm{e}^{-\mathrm{i}\lambda_0 z}. \tag{5.8}$$

Substituting the ansatz (5.8) into Eq. (5.6), we find

$$\sum_{m=-\infty}^{+\infty}\left[-2\mathrm{i}\varepsilon\lambda_0\psi_m\frac{\partial\mathsf{E}_m}{\partial Z} + \varepsilon^2\psi_m\frac{\partial^2\mathsf{E}_m}{\partial Z^2} + \left((\alpha^2\mathsf{D}^2+1)\frac{\mathrm{d}^2\psi_m}{\mathrm{d}X^2} + k_0^2 f^2\psi_m - \lambda_0^2\psi_m\right)\mathsf{E}_m \right.$$
$$\left. + 2\mathrm{i}\alpha\lambda_0\mathsf{D}\mathsf{E}_m\frac{\mathrm{d}\psi_m}{\mathrm{d}X} - 2\alpha\varepsilon\mathsf{D}\frac{\partial\mathsf{E}_m}{\partial Z}\frac{\mathrm{d}\psi_m}{\mathrm{d}X} - \alpha\varepsilon\mathsf{E}_m\frac{\mathrm{d}\mathsf{D}}{\mathrm{d}Z}\frac{\mathrm{d}\psi_m}{\mathrm{d}X}\right]\mathrm{e}^{-\mathrm{i}\lambda_0 z} = 0. \tag{5.9}$$

Using Eq. (5.7) in the above equation, multiplying Eq. (5.9) by $\psi_n^*\exp(\mathrm{i}\lambda_0 z)$ and integrating over X yields the following:

$$\sum_{m=-\infty}^{+\infty}\left[\left(-2\mathrm{i}\varepsilon\lambda_0\frac{\partial\mathsf{E}_m}{\partial Z} + \varepsilon^2\frac{\partial^2\mathsf{E}_m}{\partial Z^2}\right)\int_{-\infty}^{+\infty}\mathrm{d}X\,\psi_m\psi_n^* + k_0^2\mathsf{E}_m\int_{-\infty}^{+\infty}\mathrm{d}X\,\Delta f_m^2\psi_m\psi_n^*\right.$$
$$\left. + 2\mathrm{i}\alpha\lambda_0\mathsf{D}\mathsf{E}_m\int_{-\infty}^{+\infty}\mathrm{d}X\frac{\mathrm{d}\psi_m}{\mathrm{d}X}\psi_n^* - \varepsilon\alpha\left(2\mathsf{D}\frac{\partial\mathsf{E}_m}{\partial Z} + \mathsf{E}_m\frac{\mathrm{d}\mathsf{D}}{\mathrm{d}Z}\right)\int_{-\infty}^{+\infty}\mathrm{d}X\frac{\mathrm{d}\psi_m}{\mathrm{d}X}\psi_n^*\right] = 0. \tag{5.10}$$

Similar to the arguments we presented before, we shall assume that the overlap integrals follow the scaling given in Eq. (2.6) and that $\alpha = \mathrm{O}(\mu)$. In close analogy to the calculations given before, we find that for a sech-like mode (Eq. (2.7)) profile we have

$$\int_{-\infty}^{+\infty} \mathrm{d}X \frac{\mathrm{d}\psi_m}{\mathrm{d}X}\psi_n^* = \frac{b}{\mu}\mathrm{e}^{-|n-m|/\mu}, \tag{5.11}$$

where b is a constant. Restricting the sum in Eq. (5.10) to the nearest neighbors, i.e., $m = n, n \pm 1$ and by defining $\tilde{z} = Z/(2\lambda_c a_0)$, $k_0^2 c_1 = C_1$, $2\lambda_c b\mathsf{D} = \tilde{\mathsf{D}}$; $\mathsf{E}_n = \tilde{\mathsf{E}}_n^* \exp(-\mathrm{i}k_0^2 c_0 \tilde{z})$ we find that E_n satisfies (dropping the tilde)

$$\mathrm{i}\frac{\partial \mathsf{E}_n}{\partial z} + C_1(\mathsf{E}_{n+1} + \mathsf{E}_{n-1}) + \mathrm{i}\mathsf{D}(z)(\mathsf{E}_{n+1} - \mathsf{E}_{n-1}) = 0. \tag{5.12}$$

The constant diffraction case, i.e., Eq. (2.10) is recovered when $\mathsf{D} = 0$. Eq. (5.12) is the general dynamical equation that governs the evolution of optical beam in a diffraction-managed linear waveguide array. However, when the intensity of the incident beam is sufficiently high then the refractive index of the medium will depend on the intensity which for Kerr media is proportional to the intensity. Therefore, by following the same procedure outlined in Section 2.1 we find that the general evolution equation for the optical field in a diffraction-managed nonlinear waveguide array is governed by

$$\mathrm{i}\frac{\partial \mathsf{E}_n}{\partial z} + C_1(\mathsf{E}_{n+1} + \mathsf{E}_{n-1}) + \mathrm{i}\mathsf{D}(z)(\mathsf{E}_{n+1} - \mathsf{E}_{n-1}) + g_{\mathrm{nl}}|\mathsf{E}_n|^2\mathsf{E}_n = 0. \tag{5.12}$$

In the case of strong diffraction for which $\max|\mathsf{D}(z)| \gg |C_1|$ (recall that $\mathsf{D}(z)$ is a piecewise constant function) and by defining $\mathsf{E}_n = E_n \exp(-\mathrm{i}\pi n/2)$, Eq. (5.12) reduces to

$$\mathrm{i}\frac{\partial E_n}{\partial z} + \mathsf{D}(z)(E_{n+1} + E_{n-1}) + g_{\mathrm{nl}}|E_n|^2 E_n = 0. \tag{5.13}$$

5.2.2. Direct approach

In this section, we give a different approach to derive a model for diffraction management. We approximate the solution to Eq. (5.6) again as a multiscale perturbation series:

$$\boldsymbol{\Psi} = \sum_{m=-\infty}^{+\infty} \mathsf{E}_m(Z)\psi_m(X)\,\mathrm{e}^{\mathrm{i}[\varphi_m(z)-\lambda_0 z]}, \tag{5.14}$$

where the the phase $\varphi_m(z)$ will be chosen later. Substituting the ansatz (5.14) into Eq. (5.6), we find

$$\begin{aligned}\sum_{m=-\infty}^{+\infty} \mathrm{e}^{\mathrm{i}[\varphi_m(z)-\lambda_0 z]} \Bigg[& \mathsf{E}_m \frac{\mathrm{d}^2\psi_m}{\mathrm{d}X^2}(1+\alpha^2\mathsf{D}^2) + k_0^2 f^2 \mathsf{E}_m\psi_m + 2\mathrm{i}\left(\frac{\mathrm{d}\varphi_m}{\mathrm{d}z} - \lambda_0\right)\left(\varepsilon\frac{\partial \mathsf{E}_m}{\partial Z}\psi_m - \alpha\mathsf{D}\frac{\mathrm{d}\psi_m}{\mathrm{d}X}\mathsf{E}_m\right) \\ & - \left(\frac{\mathrm{d}\varphi_m}{\mathrm{d}z} - \lambda_0\right)^2 \mathsf{E}_m\psi_m - 2\alpha\varepsilon\mathsf{D}\frac{\partial \mathsf{E}_m}{\partial Z}\frac{\mathrm{d}\psi_m}{\mathrm{d}X} - \alpha\varepsilon\mathsf{E}_m\frac{\mathrm{d}\mathsf{D}}{\mathrm{d}Z}\frac{\mathrm{d}\psi_m}{\mathrm{d}X} + \mathrm{i}\frac{\mathrm{d}^2\varphi_m}{\mathrm{d}z^2}\mathsf{E}_m\psi_m + \varepsilon^2\frac{\partial \mathsf{E}_m}{\partial Z}\psi_m \Bigg] = 0.\end{aligned} \tag{5.15}$$

Using Eq. (2.1) and multiplying Eq. (5.15) by $\psi_n^* \exp[-\mathrm{i}\varphi_n(z)]$ and integrating over $-\infty < X < \infty$ yields the following equation (ignoring the order ε^2 term):

$$\sum_{m=-\infty}^{+\infty} \mathrm{e}^{\mathrm{i}[\varphi_m(z)-\varphi_n(z)]} \left\{ \mathsf{E}_m \int \mathrm{d}X\, \psi_m \psi_n^* \left[\alpha^2 \mathsf{D}^2 (\lambda_0^2 - k_0^2 f_m^2) + k_0^2 \Delta f_m^2 - \left(\frac{\mathrm{d}\varphi_m}{\mathrm{d}z} \right)^2 + 2\lambda_0 \frac{\mathrm{d}\varphi_m}{\mathrm{d}z} + \mathrm{i} \frac{\mathrm{d}^2 \varphi_m}{\mathrm{d}z^2} \right] \right.$$
$$- \alpha \left[\mathsf{E}_m \left(2\mathrm{i} \left(\frac{\mathrm{d}\varphi_m}{\mathrm{d}z} - \lambda_0 \right) \mathsf{D} + \frac{\mathrm{d}\mathsf{D}}{\mathrm{d}Z} \right) + 2\varepsilon \mathsf{D} \frac{\partial \mathsf{E}_m}{\partial Z} \right]$$
$$\left. \times \int \mathrm{d}X\, \frac{\mathrm{d}\psi_m}{\mathrm{d}X} \psi_n^* + 2\mathrm{i}\varepsilon \left(\frac{\mathrm{d}\varphi_m}{\mathrm{d}z} - \lambda_0 \right) \frac{\partial \mathsf{E}_m}{\partial Z} \int \mathrm{d}X\, \psi_m \psi_n^* \right\} = 0.$$

Until now the phase factor φ_m is arbitrary. Therefore, we shall choose the phase in such a way that

$$\alpha^2 \mathsf{D}^2 \int_{-\infty}^{+\infty} \mathrm{d}X (\lambda_0^2 - k_0^2 f_m^2) |\psi_m|^2 = \left[\left(\frac{\mathrm{d}\varphi_m}{\mathrm{d}z} \right)^2 - 2\lambda_0 \frac{\mathrm{d}\varphi_m}{\mathrm{d}z} \right] \int_{-\infty}^{+\infty} \mathrm{d}X\, |\psi_m|^2. \tag{5.16}$$

Eq. (5.16) implies that

$$\frac{\mathrm{d}\varphi_m}{\mathrm{d}z} = \mathrm{O}(\alpha^2), \qquad \left(\frac{\mathrm{d}\varphi_m}{\mathrm{d}z} \right)^2 = \mathrm{O}(\alpha^4), \qquad \frac{\mathrm{d}^2 \varphi_m}{\mathrm{d}z^2} = \mathrm{O}(\alpha\varepsilon). \tag{5.17}$$

The localized nature of the waveguides indicates that φ_m is independent of m, i.e., it is the same for all waveguides. With this scaling in mind and by taking as before $\alpha = \mathrm{O}(\mu)$, we recover Eq. (5.12).

5.3. Asymptotic theory for vector diffraction management

In this section we present a derivation of the vector DM-DNLS equation starting from the nonlinear vector Helmholtz equations which is obtained from Maxwell's equations. The propagation of an intense laser beam in a Kerr medium is described by the vector Helmholtz equations:

$$\left(\frac{\partial^2}{\partial x^2} + \frac{\partial^2}{\partial z^2} \right) \mathbf{E} + \delta \nabla (\nabla \cdot \mathbf{P}_{\mathrm{NL}}) + k_0^2 f^2(x) \mathbf{E} + \delta \mathbf{P}_{\mathrm{NL}} = 0. \tag{5.18}$$

The nonlinear polarization $\mathbf{P}_{\mathrm{NL}}$ can be expressed in terms of the electric field as

$$\mathbf{P}_{\mathrm{NL}} = (\mathbf{E} \cdot \mathbf{E}^*)\mathbf{E} + \gamma (\mathbf{E} \cdot \mathbf{E}) \mathbf{E}^*, \tag{5.19}$$

where γ is a constant related to the third order nonlinear susceptibility [56]. Since we are interested in interaction between two coupled laser beams, we shall assume that each one is initially linearly polarized and mutually orthogonal, i.e.:

$$\mathbf{E}(x, z) = \mathcal{E}_1(x, z)\hat{\mathbf{x}} + \mathcal{E}_2(x, z)\hat{\mathbf{y}} + \mathcal{E}_3(x, z)\hat{\mathbf{y}}. \tag{5.20}$$

In this case, the nonlinear polarization takes the form

$$\mathbf{P}_{\mathrm{NL}} = P_{\mathrm{NL}}^{(1)} \hat{\mathbf{x}} + P_{\mathrm{NL}}^{(2)} \hat{\mathbf{y}} + P_{\mathrm{NL}}^{(3)} \hat{\mathbf{z}}, \tag{5.21}$$

where

$$P_{\mathrm{NL}}^{(1)} = ((1+\gamma)|\mathcal{E}_1|^2 + |\mathcal{E}_2|^2)\mathcal{E}_1 + \gamma \mathcal{E}_2^2 \mathcal{E}_1^* + \gamma \mathcal{E}_3^2 \mathcal{E}_1^*, \tag{5.22}$$

$$P_{\mathrm{NL}}^{(2)} = (|\mathcal{E}_1|^2 + (1+\gamma)|\mathcal{E}_2|^2)\mathcal{E}_2 + \gamma \mathcal{E}_1^2 \mathcal{E}_2^* + \gamma \mathcal{E}_3^2 \mathcal{E}_2^*, \tag{5.23}$$

$$P_{\mathrm{NL}}^{(3)} = (|\mathcal{E}_1|^2 + |\mathcal{E}_2|^2 + (1+\gamma)|\mathcal{E}_3|^2)\mathcal{E}_3 + \gamma \mathcal{E}_1^2 \mathcal{E}_3^* + \gamma \mathcal{E}_2^2 \mathcal{E}_3^*. \tag{5.24}$$

Substituting the expression for $\mathbf{E}$ in Eq. (5.18) and taking into account the nonlinear polarization, leads to the coupled system:

$$\left(\frac{\partial^2}{\partial x^2}+\frac{\partial^2}{\partial z^2}\right)\mathcal{E}_1+\delta\frac{\partial^2 P_{\mathrm{NL}}^{(1)}}{\partial x^2}+k_0^2 f^2(x)\mathcal{E}_1+\delta P_{\mathrm{NL}}^{(1)}=0, \tag{5.25}$$

$$\left(\frac{\partial^2}{\partial x^2}+\frac{\partial^2}{\partial z^2}\right)\mathcal{E}_2+k_0^2 f^2(x)\mathcal{E}_2+\delta P_{\mathrm{NL}}^{(2)}=0, \tag{5.26}$$

$$\left(\frac{\partial^2}{\partial x^2}+\frac{\partial^2}{\partial z^2}\right)\mathcal{E}_3+\delta\frac{\partial^2 P_{\mathrm{NL}}^{(1)}}{\partial x\partial z}+\delta\frac{\partial^2 P_{\mathrm{NL}}^{(3)}}{\partial z^2}+k_0^2 f^2(x)\mathcal{E}_3+\delta P_{\mathrm{NL}}^{(3)}=0. \tag{5.27}$$

In this work, we are interested in interaction of two mutually orthogonal beams. However, if we initially assume that $\mathcal{E}_3=0$, then the source term $\partial^2 P_{\mathrm{NL}}^{(1)}/\partial x\partial z$ appearing in Eq. (5.27) will eventually generate a nonzero $\mathcal{E}_3$ component. In fact, this additional term (due to nonlinear polarization) is of order δ. Hence, we are justified in neglecting $\mathcal{E}_3$ as compared to $\mathcal{E}_1$ and $\mathcal{E}_2$. Next we follow the same expansion as mentioned earlier and let

$$\mathcal{E}_1=\sum_{m=-\infty}^{+\infty}A_m(Z)\psi_m(X)\,\mathrm{e}^{-\mathrm{i}\lambda_0 z},\qquad \mathcal{E}_2=\sum_{m=-\infty}^{+\infty}B_m(Z)\psi_m(X)\,\mathrm{e}^{-\mathrm{i}\lambda_0 z}, \tag{5.28}$$

where X has been defined in Eq. (5.6). The expansion of the linear terms is already given in (5.12) with the addition of on-site terms $k_{\mathrm{wg}}A_n$ and $k_{\mathrm{wg}}B_n$. Therefore, we focus the attention below solely on the nonlinear terms and in particular give an estimate on the order of magnitude of $\partial^2 P_{\mathrm{NL}}^{(1)}/\partial x^2$. Substituting the ansatz (5.28) into Eqs. (5.25) and (5.26); multiplying by $\psi_n^*\exp(\mathrm{i}\lambda_0 z)$ and integrating over X yields the following result for the nonlinear terms:

$$\begin{aligned}\int_{-\infty}^{+\infty}\mathrm{d}X P_{\mathrm{NL}}^{(1)}\psi_n^*\,\mathrm{e}^{\mathrm{i}\lambda_0 z}&=(1+\gamma)\sum_{m,m',m''}A_mA_{m'}A_{m''}^*\int_{-\infty}^{+\infty}\mathrm{d}X\,\psi_m\psi_{m'}\psi_{m''}^*\psi_n^*\\&\quad+\sum_{j,j',j''}B_jB_{j'}^*A_{j''}\int_{-\infty}^{+\infty}\mathrm{d}X\,\psi_j\psi_{j'}\psi_{j''}^*\psi_n^*+\gamma\sum_{l,l',l''}B_lB_{l'}A_{l''}^*\int_{-\infty}^{+\infty}\mathrm{d}X\,\psi_l\psi_{l'}\psi_{l''}^*\psi_n^*.\end{aligned} \tag{5.29}$$

$$\begin{aligned}\int_{-\infty}^{+\infty}\mathrm{d}X P_{\mathrm{NL}}^{(2)}\psi_n^*\,\mathrm{e}^{\mathrm{i}\lambda_0 z}&=\sum_{m,m',m''}A_mA_{m'}^*B_{m''}\int_{-\infty}^{+\infty}\mathrm{d}X\,\psi_m\psi_{m'}\psi_{m''}^*\psi_n^*+(1+\gamma)\sum_{j,j',j''}B_jB_{j'}B_{j''}^*\\&\quad\times\int_{-\infty}^{+\infty}\mathrm{d}X\,\psi_j\psi_{j'}\psi_{j''}^*\psi_n^*+\gamma\sum_{l,l',l''}A_lA_{l'}B_{l''}^*\int_{-\infty}^{+\infty}\mathrm{d}X\,\psi_l\psi_{l'}\psi_{l''}^*\psi_n^*.\end{aligned} \tag{5.30}$$

Due to the assumption of widely separated waveguides, the only order 1 contribution comes from the nonlinear term when $m=m'=m''=n$. We therefore find that to $\mathrm{O}(\varepsilon)$ the nonlinear evolution of A_n and B_n is given by (taking $\delta=\varepsilon$)

$$\mathrm{i}\frac{\partial A_n}{\partial z}+k_{\mathrm{wg}}A_n+\mathcal{C}(z)A_{n+1}+\mathcal{C}^*(z)A_{n-1}+(\tilde{a}_1|A_n|^2+\tilde{b}_1|B_n|^2)A_n+\tilde{\eta}_1B_n^2A_n^*=0, \tag{5.31}$$

$$\mathrm{i}\frac{\partial B_n}{\partial z}+k_{\mathrm{wg}}B_n+\mathcal{C}(z)B_{n+1}+\mathcal{C}^*(z)B_{n-1}+(\tilde{a}_2|B_n|^2+\tilde{b}_2|A_n|^2)B_n+\tilde{\eta}_2A_n^2B_n^*=0, \tag{5.32}$$

where the coefficients $\tilde{a}_1,\tilde{a}_2,\tilde{b}_1,\tilde{b}_2,\tilde{\eta}_1,\tilde{\eta}_2$ are given by

$$\tilde{a}_1=(1+\gamma)\eta_{\mathrm{nl}}+\gamma_{\mathrm{nl}},\quad \tilde{b}_1=\eta_{\mathrm{nl}}+\gamma_{\mathrm{nl}},\quad \tilde{a}_2=(1+\gamma)\eta_{\mathrm{nl}},\quad \tilde{b}_2=\eta_{\mathrm{nl}},\quad \tilde{\eta}_1=\gamma\eta_{\mathrm{nl}}+\gamma_{\mathrm{nl}},\quad \tilde{\eta}_2=\gamma\eta_{\mathrm{nl}},$$

and

$$\int_{-\infty}^{+\infty} \mathrm{d}X\, |\psi_n|^4 = \eta_{\mathrm{nl}}, \qquad \int_{-\infty}^{+\infty} \mathrm{d}X \frac{\partial^2}{\partial X^2}(|\psi_n|^2\psi_n)\psi_n^* = \gamma_{\mathrm{nl}}.$$

By rescaling the field amplitudes, i.e., $A_n = \tilde{A}_n/\sqrt{\tilde{a}_1}$, $B_n = \tilde{B}_n/\sqrt{\tilde{a}_2}$ we find the system (dropping the tilde):

$$\mathrm{i}\frac{\partial A_n}{\partial z} + k_{\mathrm{wg}}A_n + \mathcal{C}(z)A_{n+1} + \mathcal{C}^*(z)A_{n-1} + (|A_n|^2 + b_1|B_n|^2)A_n + \eta_1 B_n^2 A_n^* = 0,$$
$$\mathrm{i}\frac{\partial B_n}{\partial z} + k_{\mathrm{wg}}B_n + \mathcal{C}(z)B_{n+1} + \mathcal{C}^*(z)B_{n-1} + (|B_n|^2 + b_2|A_n|^2)B_n + \eta_2 A_n^2 B_n^* = 0,$$

with $b_1 = \tilde{b}_1/\tilde{a}_2$, $b_2 = \tilde{b}_2/\tilde{a}_1$, $\eta_1 = \tilde{\eta}_1/\tilde{a}_2$, $\eta_2 = \tilde{\eta}_2/\tilde{a}_1$ (see also Section 1).

6. Conclusions

Localized, stable nonlinear waves, often referred to as solitons, are of broad interest in mathematics and physics. They are found in both continuous and discrete media. In this paper, a unified method is presented which is used to obtain soliton solutions to discrete problems. In recent experiments, discrete solitons were observed in an optical waveguide array. The fundamental governing system is the scalar DNLS equation. A suitable modification of this system describes diffraction-managed solitons.

In this paper we have derived and investigated scalar and vector discrete diffraction-managed systems. The proposed vector model describes propagation of two polarization modes interacting in a waveguide array with Kerr nonlinearity in the presence of varying diffraction. The coupling of the two fields is described via a cross-phase modulation coefficient. In the regime of normal diffraction, both stationary and moving discrete solitons are analyzed using the Fourier transform method. The results indicate that a continuous stationary solution and a TW solutions with uniform velocity are unlikely to exist. In the presence of both normal and anomalous diffraction a model is developed from first principles that governs the propagation of two polarization modes interacting in a nonlinear waveguide array via cross-phase modulation coupling.

Acknowledgements

MJA is partially supported by the Air Force Office of Scientific Research, under grant number F49620-03-1-0250, and NSF under grant number DMS-0070792.

References

[1] E. Fermi, J. Pasta, S. Ulam, Studies of nonlinear problems, Los Alamos Report LA1940, 1955.
[2] O.M. Braun, Y.S. Kivshar, Nonlinear dynamics of the Frenkel–Kontorova model, Phys. Rep. 306 (1998) 1–108.
[3] D. Henning, G.P. Tsironis, Wave transmission in nonlinear lattices, Phys. Rep. 307 (1999) 333–432.
[4] S. Flach, C.R. Willis, Discrete breathers, Phys. Rep. 295 (1998) 181–264.
[5] F. Lederer, J.S. Aitchison, Discrete solitons in nonlinear waveguide arrays, in: V.E. Zakharov, S. Wabnitz (Eds.), Les Houches Workshop on Optical Solitons, Springer, Berlin, 1999, pp. 349–365.
[6] A.C. Scott, L. Macneil, Binding-energy versus nonlinearity for a small stationary soliton, Phys. Lett. A 98 (1983) 87–88.
[7] A.J. Sievers, S. Takeno, Intrinsic localized modes in anharmonic crystals, Phys. Rev. Lett. 61 (1988) 970–973.
[8] W.P. Su, J.R. Schieffer, A.J. Heeger, Solitons in polyacetylene, Phys. Rev. Lett. 42 (1979) 698–1701.
[9] A.S. Davydov, Theory of contraction of proteins under their excitation, J. Theor. Biol. 38 (1973) 559–569.

[10] P. Marquii, J.M. Bilbaut, M. Remoissenet, Observation of nonlinear localized modes in an electrical lattice, Phys. Rev. E 51 (1995) 6127–6133.
[11] H. Eisenberg, Y. Silberberg, R. Morandotti, in: A. Boyd, J. Aitchison (Eds.), Discrete Spatial Optical Solitons in Waveguide Arrays, Phys. Rev. Lett. 81 (1998) 3383–3386.
[12] R. Morandotti, U. Peschel, J. Aitchison, H. Eisenberg, Y. Silberberg, Dynamics of discrete solitons in optical waveguide array, Phys. Rev. Lett. 83 (1999) 2726–2729.
[13] D.N. Christodoulides, R.J. Joseph, Discrete self-focusing in nonlinear arrays of coupled wave-guides, Opt. Lett. 13 (1988) 794–796.
[14] Y.S. Kivshar, Self-localization in arrays of defocusing waveguides, Opt. Lett. 18 (1993) 1147–1149.
[15] W. Krolikowski, Y.S. Kivshar, Soliton-based optical switching in waveguide arrays, J. Opt. Soc. Am. B 13 (1996) 876–887.
[16] A.B. Aceves, C. De Angelis, S. Trillo, S. Wabnitz, Storage and steering of self-trapped discrete solitons in nonlinear wave-guide arrays, Opt. Lett. 19 (1994) 332–334.
[17] B. Malomed, M.I. Weinsrein, Soliton dynamics in the discrete nonlinear Schrödinger equations, Phys. Lett. A 220 (1996) 91–96.
[18] A.B. Aceves, C. De Angelis, T. Peschel, R. Muschall, F. Lederer, S. Trillo, S. Wabnitz, Discrete self-trapping, soliton interactions, and beam steering in nonlinear waveguide arrays, Phys. Rev. E 53 (1996) 1172–1189.
[19] A.B. Aceves, C. De Angelis, A.M. Rubenchik, S.K. Turitsyn, Multidimensional solitons in fiber arrays, Opt. Lett. 19 (1994) 329–331.
[20] F. Lederer, S. Darmanyan, A. Kobyakov, Discrete solitons, in: S. Trillo, W. Torruellas (Eds.), Spatial Solitons, Springer, Berlin, 2001, pp. 267–290.
[21] P.G. Kevrekidis, K.Ø. Rasmussen, A.R. Bishop, The discrete nonlinear Schrödinger equation: a survey of recent results, Int. J. Mod. Phys. B 15 (2001) 2833–2900.
[22] T. Peschel, U. Peschel, F. Lederer, Discrete bright solitary waves in quadratically nonlinear media, Phys. Rev. E 57 (1998) 1127–1133.
[23] S. Darmanyan, A. Kobyakov, F. Lederer, Strongly localized modes in discrete systems with quadratic nonlinearity, Phys. Rev. E 57 (1998) 2344–2349.
[24] R. Morandotti, U. Peschel, J. Aitchison, H. Eisenberg, in: Y. Silberberg (Ed.), Experimental Observation of Linear and Nonlinear Optical Bloch Oscillations, Phys. Rev. Lett. 83 (1999) 4756–4759.
[25] T. Pertsch, P. Dannberg, W. Elflein, A. Bräuer, F. Lederer, Optical bloch oscillations in temperature tuned waveguide arrays, Phys. Rev. Lett. 83 (1999) 4752–4755.
[26] G. Lenz, I. Talanina, C. Martijn de Sterke, Bloch oscillations in an array of curved optical waveguides, Phys. Rev. Lett. 83 (1999) 963–966.
[27] H. Eisenberg, Y. Silberberg, R. Morandotti, J. Aitchison, Diffraction management, Phys. Rev. Lett. 85 (2000) 1863–1866.
[28] R. Morandotti, H. Eisenberg, Y. Silberberg, M. Sorel, J. Aitchison, Self-focusing and defocusing in waveguide arrays, Phys. Rev. Lett. 86 (2001) 3296–3299.
[29] M.J. Ablowitz, Z.H. Musslimani, Discrete diffraction managed spatial solitons, Phys. Rev. Lett. 87 (2001) 254102.
[30] M.J. Ablowitz, Z.H. Musslimani, Discrete vector spatial solitons in a nonlinear waveguide array, Phys. Rev. E 65 (2002) 056618.
[31] S.F. Mingaleev, Y.S. Kivshar, Self-trapping and stable localized modes in nonlinear photonic crystals, Phys. Rev. Lett. 86 (2001) 5474–5477.
[32] A.A. Sukhorukov, Y.S. Kivshar, Nonlinear localized waves in a periodic medium, Phys. Rev. Lett. 87 (2001) 083901.
[33] A.A. Sukhorukov, Y.S. Kivshar, Spatial optical solitons in nonlinear photonic crystals, Phys. Rev. E 65 (2002) 036609.
[34] A. Trombettoni, A. Smerzi, Discrete solitons and breathers with dilute Bose–Einstein condensates, Phys. Rev. Lett. 86 (2001) 2353–2356.
[35] D.N. Christodoulides, E.D. Eugenieva, Blocking and routing discrete solitons in two-dimensional networks of nonlinear waveguide arrays, Phys. Rev. Lett. 87 (2001) 233901.
[36] D.N. Christodoulides, E.D. Eugenieva, Minimizing bending losses in two-dimensional discrete soliton networks, Opt. Lett. 26 (2001) 1876–1878.
[37] E.D. Eugenieva, N.K. Efremidis, D.N. Christodoulides, Design of switching junctions for two-dimensional discrete soliton, Opt. Lett. 26 (2001) 1978–1980.
[38] E.D. Eugenieva, N.K. Efremidis, D.N. Christodoulides, Opt. Photonics News 12 (2001) 57.
[39] D.N. Christodoulides, N.K. Efremidis, Discrete temporal solitons along a chain of nonlinear coupled microcavities embedded in photonic crystals, Opt. Lett. 27 (2002) 568–570.
[40] M.J. Ablowitz, J.F. Ladik, Nonlinear differential-difference equations and Fourier-analysis, J. Math. Phys. 17 (1976) 1011–1018.
[41] M. Peyrard, M.D. Kruskal, Kink dynamics in the highly discrete sine-Gordon system, Physica D 14 (1984) 88–102.
[42] V.I. Petviashvili, Equation of an extraordinary soliton, Sov. J. Plasma Phys. 2 (257) (1976).
[43] M.J. Ablowitz, G. Biondini, Multiscale pulse dynamics in communication systems with strong dispersion management, Opt. Lett. 23 (1998) 1668–1670.
[44] S. Flach, K. Kladko, Moving discrete breathers?, Physica D 127 (1999) 61–72.
[45] S. Flach, Y. Zolotaryuk, K. Kladko, Moving lattice kinks and pulses: an inverse method, Phys. Rev. E 59 (1999) 6105–6115.
[46] S. Aubry, T. Cretegny, Mobility and reactivity of discrete breathers, Physica D 119 (1998) 34–46.
[47] Ch. Claude, Y.S. Kivshar, O. Kluth, K.H. Spatschek, Moving localized modes in nonlinear lattices, Phys. Rev. B 47 (1993) 14228–14232.
[48] M.J. Ablowitz, Z.H. Musslimani, G. Biondini, Methods for discrete solitons in nonlinear lattices, Phys. Rev. E 65 (2002) 026602.
[49] V.I. Karpman, Evolution of solitons described by higher-order nonlinear Schrodinger equations, Phys. Lett. A 244 (1998) 397–400.
[50] M. Karlsson, A. Höök, Soliton-like pulses governed by fourth order dispersion in optical fibers, Opt. Commun. 104 (1994) 303–307.
[51] H. Feddersen, Lecture Notes in Physics, Springer, Berlin, 1991, pp. 159–167.

[52] D.B. Duncan, J.C. Eilbeck, H. Feddersen, J.A.D. Wattis, Solitons on lattices, Physica D 68 (1993) 1–11.
[53] S. Darmanyan, A. Kobyakov, E. Schmidt, F. Lederer, Strongly localized vectorial modes in nonlinear waveguide arrays, Phys. Rev. E 57 (1998) 3520–3530.
[54] S. Somekh, E. Garmire, A. Yariv, H.L. Garvin, R.G. Hunsperger, Channel optical waveguide directional couplers, Appl. Phys. Lett. 22 (1973) 46–47.
[55] A. Yariv, Optical Electronics, 5th ed., Oxford University Press, Oxford, 1997.
[56] R.W. Boyed, Nonlinear Optics, Wiley, New York, 1992.

Carrier-envelope phase slip of ultrashort dispersion-managed solitons

Mark J. Ablowitz and Boaz Ilan

Department of Applied Mathematics, University of Colorado, Boulder, Colorado 80309-0526

Steven T. Cundiff

JILA, National Institute of Standards and Technology and University of Colorado, Boulder, Colorado 80309-0440

Received March 8, 2004

The carrier-envelope phase slip of an ultrashort pulse circulating in a mode-locked Ti:sapphire laser is analyzed. The laser cavity is modeled by a dispersion- and nonlinearity-managed nonlinear Schrödinger equation. The combined contributions to the phase slip induced by nonlinear phase and nonlinear dispersion are found to approach zero for strong dispersion maps. The dependence of the slip on third-order dispersion is found as well. The analytical results are verified using numerical simulations. © 2004 Optical Society of America

OCIS codes: 190.5530, 320.7110.

Mode-locked Ti:sapphire lasers generate a regularly spaced train of pulses separated by one cavity round-trip time. The carrier-envelope phase slip (CEPS) is the change from pulse-to-pulse of the phase offset between the envelope and the carrier waves. Controlling the phase slip has been the subject of recent experimental efforts in optical frequency metrology, carrier-envelope phase coherence, and extreme nonlinear optics.[1–4] In a recent seminal contribution Haus and Ippen[5] studied the CEPS for classical and dispersion-managed (DM) solitons, the latter being waveguide solutions of a perturbed DM nonlinear Schrödinger equation. DM solitons are a key element to describing Ti:sapphire lasers.[6] In this Letter an asymptotic theory governing the propagation of DM and nonlinearity-managed solitons is applied to a model of the laser. Applying multiple-scales analysis yields a relation for the nonlinear change of the phase velocity over one cavity round trip. In our model we treat nonlinear dispersion (the shock term) and third-order dispersion (TOD) as small perturbations. They induce changes in the group velocity that are found using conservation-law methods. The nonlinear slip induced by the combined effects is found to approach zero as $O(1/s)$, where s is the cavity's map strength. In addition, it is found that the CEPS can be controlled by changing the average group-velocity dispersion (GVD) and TOD in the laser. Our analytical results agree with numerical simulations and display the explicit dependence of the phase slip on physical parameters.

Typically, the electromagnetic field of a pulse is decomposed into a rapidly oscillating carrier wave $\exp[i(kz - \omega t)] = \exp[i(1/v_p - t/z)\omega z]$ that is modulated by a slowly varying envelope. Here z is the propagation direction, t is time, $k(\omega) = \omega n(\omega)/c$ is the center wave number, where ω is the center frequency, $n(\omega)$ is the linear index of refraction, and c is light speed in vacuum. During propagation the carrier slips through the envelope, because the carrier propagates at phase velocity $v_p = \omega/k$ while the envelope propagates at group velocity $v_g = 1/k'(\omega)$. Thus the linear contribution to the slip of the carrier-envelope phase offset is given (mod 2π) by $\delta_{\text{linear}} = (v_p{}^{-1} - v_g{}^{-1})\omega L = -c^{-1}\omega^2 n'(\omega)L$, where L is the propagation distance. In addition, when an intense pulse propagates in a Kerr medium (such as sapphire) there is a nonlinear contribution to the phase slip. To study the nonlinear slip we recall that the propagation of the envelope is well described by the classical nonlinear Schrödinger (NLS) equation

$$iA_z - \frac{k''}{2}A_{\tau\tau} + \gamma|A|^2A = -i\omega^{-1}\gamma(|A|^2A)_\tau, \qquad (1)$$

where $A(z,\tau)$ is the slowly varying envelope, $\tau = t - z/v_g$ is the retarded-time frame, k'' is the GVD coefficient, $\gamma = n_2\omega/cA_{\text{eff}}$ is the nonlinear coefficient, where n_2 is the Kerr (nonlinear) refractive index, and A_{eff} is the effective cross-sectional area of the pulse, and the term on the right-hand side, often called the shock term, corresponds to nonlinear dispersion arising from the Kerr effect. We focus on the shock term first because it becomes larger with shorter pulses. Indeed, the shock term scales as $\epsilon|A|^3$, where $\epsilon \equiv 2\pi/\omega\tau_0$ and τ_0 is the pulse width. For example, at $\lambda = 800$ nm and $\tau_0 = 20$ fs one has $\omega/2\pi = 400$ THz and $\epsilon \approx 0.13$. In addition, the shock term induces a nonlinear change in the CEPS, a phenomenon that is consistent with the dependence of the CEPS on pulse energy (pump power).[1,4] Without the shock term and when k'' is a negative constant, Eq. (1) has the soliton solution

$$A(z,\tau) = A_0\,\text{sech}(\tau/\tau_0 - T)\exp[i\phi(z)],$$
$$\phi(z) \equiv \gamma|A_0|^2 z/2, \qquad (2)$$

where A_0 is amplitude and T corresponds to a time shift of the pulse center. Self-phase modulation is described by $\phi(z)$, which, in turn, induces a nonlinear change in the phase velocity as $\Delta(1/v_p) = \phi'(z)/\omega = \gamma|A_0|^2/2\omega$. The timing shift corresponds to a change

0146-9592/04/151808-03$15.00/0

in the group velocity as $\Delta(1/v_g) = T'(z)\tau_0$. The normalized nonlinear contribution to the CEPS was defined in Ref. 5 as

$$\tilde{\delta}_{\mathrm{NL}} \equiv \frac{\Delta(1/v_p) - \Delta(1/v_g)}{\Delta(1/v_p)} = 1 - \frac{T'(z)}{\epsilon\phi'(z)}. \tag{3}$$

For classical solitons the shock term gives[5] $T'(z) = \epsilon\gamma|A_0|^2$. Thus $\tilde{\delta}_{\mathrm{NL}} = -1$, which means that for classical solitons the nonlinear change in ${v_g}^{-1}$ is twice as large that of ${v_p}^{-1}$.

For a regularly spaced train of pulses, such as those emitted from a mode-locked Ti:sapphire laser, the CEPS refers to the change of the phase offset between carrier and envelope from pulse to pulse, which is the phase slip that each pulse accumulates over one cavity round trip, before being sampled at the output coupler. The linear contribution to the CEPS is thus $\delta_{\mathrm{linear}} = -c^{-1}\omega^2 \sum_m {n_m}'(\omega) L_m$, where the summation is carried over all the cavity elements (crystal, prisms, etc.). In addition, the nonlinear contribution to the CEPS is the difference between the nonlinear phase and the timing shifts accumulated over one cavity round trip. In normalized form it is given by the average of Eq. (3):

$$\tilde{\delta}_{\mathrm{NL}} = 1 - \frac{\langle T'(z)\rangle}{\epsilon\langle\phi'(z)\rangle}, \tag{4}$$

where $\langle\,\rangle$ stands for the average over one cavity round trip. A typical Ti:sapphire laser consists of a Ti:sapphire crystal that has a Kerr response as well as large normal GVD and a set of prisms and (or) mirrors especially designed to have large anomalous GVD. Hence such lasers are well described as DM systems,[6] which have been heavily studied in telecommunications. Let us recall some of the results of these studies. For further analysis we normalize the variables as $\tilde{z} = z/\zeta^*$, $\tilde{t} = \tau/\tau_0$, $D(z) = -k''(\zeta)/k''^*$, and $u(z,t) = A(\zeta,\tau)/\sqrt{P^*}$, where P^* is the characteristic pulse peak power, $\zeta^* = 1/\gamma P^*$ is the (average) nonlinear length, and $k''^* = {\tau_0}^2/\zeta^*$. After dropping the tildes, we can describe the pulse propagation using the perturbed NLS[7]:

$$iu_z(z,t) + \frac{D(\zeta)}{2}u_{tt} + g(\zeta)\,|u|^2 u = -i\epsilon g(\zeta)\,(|u|^2 u)_t, \tag{5}$$

where $\zeta = z/l_c$ is the fast variable, l_c is the normalized (with respect to ζ^*) optical length of the cavity, $D(\zeta) = \overline{D} + {l_c}^{-1}\Delta(\zeta)$ is the dispersion map, where $\overline{D}$ is the average dispersion and $\Delta(\zeta)/l_c$ is the large and rapidly varying dispersion with zero average path, and the right-hand side corresponds to the shock term. A lumped model of a cavity consists of a symmetric two-step dispersion map, i.e., $\Delta(\zeta) = \Delta_1 > 0$ for $\zeta \in \{[0, \theta/2), [1 - \theta/2, 1)\}$ and $\Delta(\zeta) = \Delta_2 < 0$ for $\zeta \in [\theta/2, 1 - \theta/2)$, subject to $\Delta_1\theta + \Delta_2(1-\theta) = 0$, with period extension for $\zeta > 1$. To model a Ti:sapphire laser we choose $\theta = 0.75$ and a managed nonlinearity: $g(z) = 1$ in the normal GVD section and $g(z) = 0$ in the anomalous GVD section [see Fig. 1(a)]. It is useful to define $C(\zeta) = \int_0^\zeta \Delta(\zeta')\mathrm{d}\zeta'$ as well as to map strength $s = \Delta_1\theta/2$. Classical NLS equation (1) corresponds to $s = 0$ and $C(\zeta) \equiv 0$. Ti:sapphire systems, however, operate in the strong DM regime, which corresponds to large-variance GVD (s) and small average GVD ($\overline{D}$).

The two small parameters in Eq. (5) are ϵ (weak nonlinear dispersion) and l_c (short nonlinear length). Let us treat the shock term perturbatively by first considering the unperturbed model, i.e., when $\epsilon = 0$. Since $l_c \ll 1$ one can apply the method of multiple scales to Eq. (5). With this method it was previously shown[7] that, to leading order, $\hat{u}(z,\omega) \sim \hat{U}(\omega, z)\exp[-i/2\omega^2 C(\zeta)]$, where $\hat{h}(\omega) \equiv F\{h(t)\} = \int h(t)\exp(i\omega t)\mathrm{d}t$. A solvability condition for $O(l_c)$ leads to the DMNLS (averaged) equation:

$$i\frac{\partial\hat{U}}{\partial z} - \frac{\overline{D}}{2}\omega^2\hat{U} + \langle J[\hat{u}]\rangle = 0, \tag{6}$$

where $J[\hat{u}] = g(\zeta)\exp[i/2\omega^2 C(\zeta)]F\{|u|^2 u\}$. Equation (6) is a nonlocal (integral) equation that governs the averaged dynamics of the solutions of Eq. (5). Looking for a DM soliton of the form $\hat{U}(z,\omega) = \hat{f}(\omega)\exp(i\phi z)$, where $\phi(z) = \lambda^2 z/2$, leads to the following equation:

$$-\frac{\lambda^2}{2}\hat{f}(\omega) - \frac{\overline{D}}{2}\omega^2\hat{f} + \langle J[\hat{f}]\rangle\exp(-i\lambda^2 z/2) = 0. \tag{7}$$

Taking the inverse Fourier transform, multiplying by $(f + tf_t)$, and integrating leads to

$$\frac{\lambda^2}{2} = \frac{2}{W}\left\langle\int F^{-1}\{J[\hat{f}]\}(f + tf_t)\mathrm{d}t\right\rangle - \frac{3\overline{D}}{2W}\int (f_t)^2\mathrm{d}t, \tag{8}$$

where $W = \int f^2\mathrm{d}t$ is energy. With strong dispersion management $f(t)$ can be approximated with a Gaussian,[7] which is helpful for gaining insight into the physics, by assigning specific pulse parameters. Thus, substituting $f(t) \approx a(2\pi b)^{-1/2}\exp(-t^2/2b)$ into Eq. (8) gives the result that

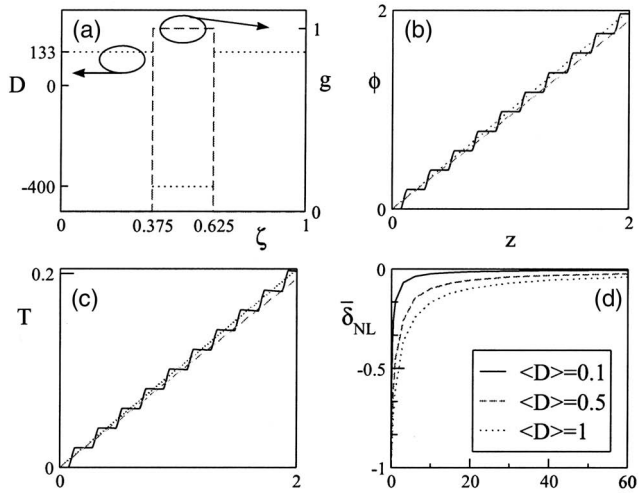

Fig. 1. (a) Dispersion [$D(\zeta)$, dotted lines] and nonlinearity maps [$g(\zeta)$, dashed lines] used in (b) and (c). (b) Numerical phase [Eq. (6), solid curve], $\lambda^2 z/2$ (dotted curve) and ${\lambda_G}^2 z/2$ (dashed curve). (c) Numerical timing shift [Eq. (6), solid curve], average slope with Eq. (10) (dotted curve), and with Eq. (11), below (dashed curve). (d) Normalized CEPS (12) with $\lambda = \sqrt{2}$, $\theta = 0.75$, for three values of $\overline{D}$.

$$\langle \phi'(z) \rangle = \frac{\lambda^2}{2} \approx \frac{{\lambda_G}^2}{2} \equiv \frac{a^2(1-\theta)q(x)}{\sqrt{8}\,\pi b} - \frac{3\overline{D}}{4b}, \qquad (9)$$

where

$$q(x) \equiv \frac{\sinh^{-1}(x/2)}{x} + \frac{2}{(4+x^2)^{1/2}}, \qquad x = \frac{2s}{b}.$$

Equation (7) can be solved numerically using a fixed-point method,[7] which for strong dispersion management gives the result that x grows monotonically to 7.9. Therefore, $q(x)$ decreases monotonically to 0.51, $b \approx s/3.95$, and $a \approx 1.46\lambda[s/(1-\theta)]^{1/2}$. Equation (9) thus shows that with strong dispersion management the average nonlinear phase shift decreases to a (energy-dependent) constant.

To find the timing shift induced by the shock term we use the conservation law for timing corresponding to Eq. (5), which, after averaging, gives us, to leading order,

$$\langle T'(z) \rangle = -\frac{2\epsilon}{W l_c}\left\langle \Delta(\zeta)\mathrm{Im}\iint |u|^2 u {u_{tt}}^* \mathrm{d}t\mathrm{d}z \right\rangle + \frac{3\epsilon}{2W}\left\langle \int |u|^4 \mathrm{d}t \right\rangle, \qquad (10)$$

where $u(z,t) = F^{-1}\{\hat{f}(\omega)\exp[-i\omega^2 C(\zeta)/2]\}$. Note that the shock term conserves energy, i.e., $W =$ constant. Using the Gaussian ansatz leads to

$$\langle T'(z) \rangle \approx \frac{\epsilon a^2(1-\theta)q(x)}{\sqrt{8}\,\pi b}, \qquad (11)$$

which shows that the average timing shift decreases to a constant with strong dispersion management. We note that the shock term induces an $O(l_c)$ phase change as well, which, however, is negligible compared with Eq. (9).

To verify the analytic results we solve Eq. (5) numerically with $\epsilon = 0.1$, $l_c = 0.2$, $\overline{D} = 0.1$, $s = 10$, $\theta = 0.75$, and initial conditions $\hat{u}(0,\omega) = \hat{f}(\omega)$, where $\hat{f}(\omega)$ is the solution of Eq. (7) with $\overline{D} = 0.1$, $s = 10$, and $\lambda = \sqrt{2}$. Figure 1(b) shows that the slope of the numerically recovered phase (after unwrapping), i.e., $\phi(z) = \arg[\hat{u}(z,0)]$, is almost indistinguishable from $\lambda^2/2$ during propagation and agrees well with ${\lambda_G}^2/2$ calculated using Eq. (9). Figure 1(c) shows that the averaged slope of the numerical timing shift $[T(z) \equiv W^{-1}\int t|u|^2]$ is precisely that obtained with Eq. (10) and is in good agreement with Eq. (11). Note that the CEPS (4) depends on the phase and timing shifts accumulated over one round trip and hence on the average slopes of $\phi(z)$ and $T(z)$.

Remarkably, the first term on the right-hand side of Eq. (9) times ϵ is the same as Eq. (11). Thus, combining these results with Eq. (4) we arrive at

$$\tilde{\delta}_{\mathrm{NL}} \approx \frac{1}{1 - \sqrt{2}\,a^2(1-\theta)q(x)/3\pi\overline{D}} \approx \frac{1}{1 - \lambda^2 s/6\overline{D}}. \qquad (12)$$

Hence $\tilde{\delta}_{\mathrm{NL}}$ approaches zero monotonically as $O(1/s)$ [see Fig. 1(d)]. This means that, unlike classical solitons, the combined contributions of the nonlinear phase and the shock term to the phase slip nearly cancel each other with strong dispersion management. We note that Ref. 5 obtained $\tilde{\delta}_{\mathrm{NL}}$ approaches -0.1, presumably because a rather large $\overline{D}$ was used. Indeed, Fig. 1(d) shows that with larger values of $\overline{D}$ the slip saturates at larger s, whereas with smaller $\overline{D}$ the slip becomes roughly independent of map strength, a conclusion that may be useful for controlling the slip. The unnormalized form of the slip equation (12) is $\delta_{\mathrm{NL}} \equiv (\langle\phi'\rangle - \epsilon^{-1}\langle T'\rangle)\gamma P^* L \approx -3\overline{k}''L/{\tau_0}^2 s$, where $\overline{k}''$ is the average-cavity GVD and L is the cavity length. This result is consistent with the insensitivity of the slip to pulse energy with strong dispersion management.[4] In that case, however, one should consider additional effects on the slip. One such effect is TOD, which can be modeled by adding $[i\overline{k}'''/(6\gamma P^* {\tau_0}^3)]u_{ttt}$ to the right-hand side of Eq. (5), where $\overline{k}'''$ is the average TOD coefficient. Using a similar analysis leads to $\delta_{\mathrm{TOD}} \approx -\omega\overline{k}'''L/{\tau_0}^2 s$.

We remark that the asymptotic methods used here on a nonlinear DM model are different from the analysis in Ref. 5, which was based on a linear DM model with effective parameters. Our methods are accurate and display an explicit dependence of the CEPS on physical parameters.

To conclude, our results indicate that for stronger dispersion management the nonlinear phase slip becomes insensitive to map strength and tends to zero.

This research was partially supported by the U.S. Air Force Office of Scientific Research under grant F-49620-03-1-0250. B. Ilan's e-mail address is boaz@colorado.edu.

References

1. L. Xu, Ch. Spielmann, A. Poppe, T. Brabec, F. Krausz, and T. W. Hänsch, Opt. Lett. **21,** 2008 (1996).
2. D. J. Jones, S. A. Diddams, J. K. Ranka, A. Stentz, R. S. Windeler, J. L. Hall, and S. T. Cundiff, Science **288,** 635 (2000).
3. T. Brabec and F. Krausz, Rev. Mod. Phys. **72,** 545 (2000).
4. K. W. Holman, R. J. Jones, A. Marian, S. T. Cundiff, and J. Ye, Opt. Lett. **28,** 851 (2003).
5. H. A. Haus and E. P. Ippen, Opt. Lett. **26,** 1654 (2001).
6. Y. Chen, F. X. Kärtner, U. Morgner, S. H. Cho, H. A. Haus, E. P. Ippen, and J. G. Fujimoto, J. Opt. Soc. Am. B **16,** 1999 (1999).
7. M. J. Ablowitz and G. Biondini, Opt. Lett. **23,** 1668 (1998).

Dynamics of Nonlinear and Dispersion Managed Solitons

Qudsia Quraishi,[1,*] Steven T. Cundiff,[2] Boaz Ilan,[3] and Mark J. Ablowitz[3]

[1]*Department of Physics, University of Colorado, National Institute of Standards and Technology, and JILA, Boulder, Colorado 80309-0440, USA*

[2]*JILA, National Institute of Standards and Technology, and the University of Colorado, Boulder, Colorado 80309-0440, USA*

[3]*Department of Applied Mathematics, University of Colorado, Boulder, Colorado 80309-0526, USA*

(Received 28 February 2005; published 23 June 2005)

The relation between the fundamental parameters of energy and temporal duration of ultrashort pulses, under the condition of varying the average dispersion, are demonstrated both theoretically and experimentally in a solid-state femtosecond mode-locked laser. An asymptotic theory for nonlinear and dispersion managed solitons agrees well with the experimental data and demonstrates that the dominant factor in the pulse dynamics arises from the equilibrium established between the nonlinear Kerr effect and linear dispersion.

DOI: 10.1103/PhysRevLett.94.243904 PACS numbers: 42.65.Tg, 42.60.Fc, 42.65.Re, 42.65.Sf

Solitons are fascinating nonlinear phenomena that arise widely in physics. Solitons have a finite, localized energy and propagate unchanged. They form from the competition between linear dispersion and the nonlinear index of refraction. Surprisingly, when the sign of the linear dispersion periodically varies, as in long distance fiber communications, a new breed of soliton forms. The change in the sign of the dispersion causes these so-called dispersion managed (DM) solitons to temporally broaden and recompress or ''breathe'' as they propagate [1]. The prevalence of DM solitons has generated significant research toward understanding their behavior [2–5].

To experimentally characterize the propagation dynamics of DM solitons, a medium amenable to systematic changes in the linear dispersion is required. Such characterization has proven difficult partly because of the complexity in systematically varying the linear dispersion. The ultrashort optical pulses propagating in solid-state mode-locked lasers are also dispersion managed. However, the method by which these pulses are dispersion managed allows for systematic control over the cavity dispersion and thus, provides a near ideal environment to undertake such studies. In addition, these pulses experience a periodicity in the nonlinear refractive index, known as nonlinear management. Recent theoretical work in understanding their dynamics has shown novel behavior that is distinct from that of classical solitons [4]. Here, we report the first experimental demonstration of the systematic varying of the group velocity dispersion for a nonlinear and dispersion managed soliton. We show remarkable agreement between experiments and the DM theory of solitons for the scaling of the fundamental pulse properties of energy and temporal duration for the ultrashort pulses in a mode-locked laser. This study advances the understanding of the dynamics of the DM system in ultrashort pulsed mode-locked lasers, which have numerous important applications that rely upon pulse stability [6–10].

In the classical theory of solitons, the nonlinear Schrödinger equation (NLS) governing the pulse envelope $u(z, t)$ in an optical fiber is

$$iu_z(z, t) - \frac{\beta''}{2} u_{tt}(z, t) + \gamma_0 |u(z, t)|^2 u(z, t) = 0, \qquad (1)$$

where β'' is the group velocity dispersion (GVD) coefficient, t is the retarded time (with respect to the group delay), and $\gamma_0 = n_2\omega/cA_{\text{eff}}$ is the nonlinear coefficient for an effective transverse area A_{eff} of the beam, with center frequency ω, propagating in the z direction through a medium with a Kerr nonlinear refractive index n_2, where c is the speed of light [11]. The soliton solution for constant anomalous dispersion, $\beta'' < 0$, is $u(z, t) = A\text{sech}\,(\frac{c_0 t}{\tau}) e^{i\gamma_0 |A|^2 z/2}$, where $c_0 = 2\text{sech}^{-1}\,(1/\sqrt{2})$, A is the real-valued amplitude, and τ is the temporal FWHM. The intensity is $|A|^2 = P/A_{\text{eff}}$, where $P = E/\tau$ is the pulse power with energy $E = \int |u|^2 dt$. For the theory of classical solitons (CS), the relation between these fundamental parameters is

$$\tau = \frac{2c_0|\beta''|}{\gamma_0 E}. \qquad (2)$$

This scaling for classical solitons was observed in optical fibers [12]. No such relation has been experimentally demonstrated for DM solitons.

In the nonlinear and dispersion managed theory, $u(z, t)$ satisfies Eq. (1) with periodically varying GVD and nonlinear coefficients. Using a dispersion managed model, it was shown that stable pulses can form in a mode-locked laser [4]. A mode-locked laser is a pulsed laser that emits a periodic sequence of optical pulses where the pulses are spaced by the cavity round-trip time (the group delay, τ_g). Figure 1(a) is a schematic of a 92.8 MHz repetition-rate Kerr-lens mode-locked (KLM) Ti:sapphire laser pumped by a solid-state frequency-doubled Nd:YVO_4 laser.

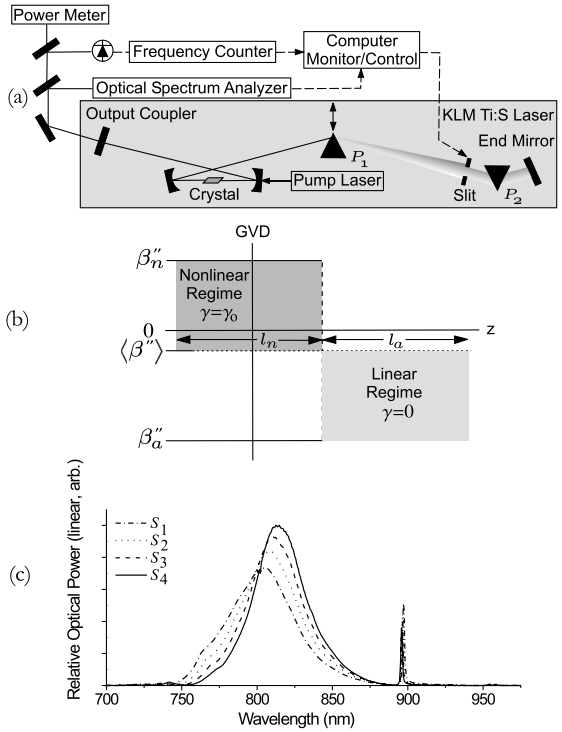

FIG. 1. (a) Schematic of a mode-locked Ti:sapphire laser, with the measurement setup. The position of the slit near prism P_2 is computer controlled to set the center frequency of mode-locked operation. (b) Schematic of the nonlinear normal GVD propagation due to the Kerr nonlinearity in the crystal and linear anomalous GVD propagation in the prism sequence. (c) Spectral profiles at four positions of the prism P_1 resulting in four different GDD values. The dash-dotted line S_1 corresponds to the most prism insertion. The spectrum narrowed as the prism was pulled out of the beam. The solid line S_4 corresponds to the least prism insertion. The sharp feature at 900 nm may be the result of the cavity mirror reflectivity characteristics.

Since such a laser can generate ultrashort pulses ($\lesssim$20 fs), the average dispersion in the cavity must be relatively small to sustain this pulse [13]. In one cavity round-trip, the pulse propagates through cavity elements with different signs of dispersion. The most significant contributions to the linear dispersion come from the normal dispersion β_n'' in the region of length l_n in the Ti:sapphire crystal, and the *compensating* anomalous dispersion β_a'' in region of length l_a in the prism sequence. For sustained, stable mode locking, the intensity of the pulse at the crystal center, after it has experienced this linear dispersion compensation, is now sufficiently high for the nonlinear Kerr effects (self- focusing and self-phase modulation) to occur so that the mode-locked operation is preferred over the continuous wave operation. For such a dispersion map the GVD, averaged over one round-trip in the cavity, $\langle\beta''\rangle$, is used to define the round-trip group delay dispersion (GDD); that is, $\langle\beta''\rangle l_t = \beta_n'' l_n + \beta_a'' l_a$, where $l_t = l_n + l_a$ is the total optical length of the cavity, as seen in Fig. 1(b). Indeed, by this definition of the round-trip GDD, the two shaded regions in Fig. 1(b) are of equal area. All other cavity elements, including air and the cavity mirrors, irrespective of their sign of GDD, only contribute to the net linear dispersion compensation provided by the cavity prism sequence and so, for simplicity, we take $l_a = l_n$.

To model this dispersion map, β'' in Eq. (1) is replaced by the local GVD, $\beta''(z)$. It is convenient to introduce the GDD variance of the dispersion map. This variance is known as the map strength s where $s = |\beta_i'' l_i - \frac{1}{2}\langle\beta''\rangle l_t|$, which is independent of the replacement of i with n or a. In the DM theory, s arises naturally as a physically relevant and theoretically important parameter [14,15]. The *reduced* map strength $M = s/(\langle\beta''\rangle l_t)$ is the relative strength of the GDD variance with respect to the round-trip GDD. The nonlinearity must also be managed in the theory, with the replacement $\gamma = \gamma_0$ in the crystal and $\gamma = 0$ elsewhere, so now $\gamma = \gamma(z)$. This nonlinear and dispersion managed equation is referred to as the perturbed NLS (PNLS),

$$iu_z(z,t) - \frac{\beta''(z)}{2}u_{tt}(z,t) + \gamma(z)|u(z,t)|^2 u(z,t) = 0. \quad (3)$$

Figure 1(b) shows the nonlinear and dispersion maps of the laser in one cavity round-trip. For the DM theory, three experimental input parameters, $\langle\beta''\rangle l_t$, γ_0, and s, are required to model the fundamental propagation dynamics.

To characterize the experimental relation between the fundamental pulse properties, we recorded E as a function of τ for various values of the average cavity GDD, $\langle\beta''\rangle l_t$. In the mode-locked laser, dispersion causes the group delay of the pulse ($\tau_g = 1/f_{\text{rep}}$, where f_{rep} is the repetition rate) to depend upon the center frequency ω of the mode-locked spectrum. Actively controlling the center frequency through the use of a slit in the cavity, positioned after the prism P_1, permits one to map $\tau_g(\omega)$ and thus, to measure the round-trip GDD [Fig. 1(a)] [16]. For a given prism P_1 insertion, the slit near P_2 was situated in the cavity beam with the slit opening adjusted to reduce the bandwidth while still permitting mode locking. The slit was then translated transversely to the beam and at each slit position the spectrum was recorded with an optical spectrum analyzer and f_{rep} was measured by an RF frequency counter. The center frequency was calculated from the first moment of the recorded optical spectrum. The GDD is given by the linear coefficient of a least-squares fit to these data. From this measured value of the GDD, the anomalous GDD of the prism sequence and s are calculated. Since the nonlinearity occurs in a small region (within the Rayleigh range of the beam focus) in the Ti:sapphire crystal (length of 2.3 mm), we set $l_n = 0.5$ mm so $\beta_n'' l_n = +30$ fs^2($\beta_n'' = +60$ fs^2/mm). To minimize the cavity GDD for more stable mode locking, we use dispersion compensated mirrors (DCM) [17]. Since the prism sequence (and DCMs) provide dispersion compensation up to second order, higher order contributions are minimized by using prisms

made of CaF_2. Drift of the repetition rate arising from cavity length fluctuations can disturb or even prohibit the measurement of the GDD. This drift has been observed to vary linearly with time and was minimized by isolating the laser in a plexiglass enclosure. Additionally, the data acquisition was automated so that the GDD was measured in less than 60 sec and corrected for the drift.

To systematically change the cavity GDD, the first prism P_1 was successively translated into the beam [Fig. 1(a)]. The (fixed) separation between the prisms determines the amount of anomalous compensation, while each prism's individual differential insertion into the beam determines the added normal dispersion [Fig. 1(c)]. For each GDD setting, the pump laser power was used to control the intracavity pulse energy E and was ramped through the full stability range of mode locking.

To gain insight into the fundamental governing dynamics, an asymptotic analysis may be undertaken. The quantity l_n/l_0, where $l_0 = 1/(\gamma_0 P)$, is a measure of the length over which the nonlinearity causes a 2π-phase shift in the pulse. A perturbative expansion of the PNLS [Eq. (3)] to first order in l_n/l_0 yields the dispersion managed nonlinear Schrödinger equation (DMNLS)

$$i\hat{U}_z(z,\omega) + \frac{\langle\beta''\rangle}{2}\omega^2\hat{U}(z,\omega) + \frac{\gamma_0}{2}\iint_{-\infty}^{+\infty}\frac{\sin(\omega_1\omega_2 s)}{\omega_1\omega_2 s} \times \hat{U}(z,\omega+\omega_1)\hat{U}(z,\omega+\omega_2) \times \hat{U}^*(z,\omega+\omega_1+\omega_2)d\omega_1 d\omega_2 = 0. \quad (4)$$

The nonlinear management yields the factor of $1/2$ in the nonlocal term and so doubles the pulse energy as compared to the usual DM solitons with a constant nonlinear coefficient. The DMNLS is a nonlocal equation and admits localized stable solutions known as DM solitons,

$$\hat{U}(z,\omega) = e^{i(\lambda^2/2)z}\hat{f}(\omega), \quad (5)$$

where λ^2 is a constant and $\hat{f}(\omega)$ is real and symmetric [14]. When these solutions seed the PNLS, they remain localized and stable while acquiring an additional phase term. This frequency dependent phase introduces a chirp in the pulse, with a period related to the periodicity of the dispersion map. As the DM soliton propagates from the center of the normal region, it temporally broadens and then recompresses until it reaches the center of the anomalous region, whereupon it begins to broaden again, thereby breathing, as seen in the inset in Fig. 2, whereas the classical soliton does not breathe. The full (PNLS) solution, written in terms of the DM soliton is

$$u(z,t) = \mathcal{F}^{-1}[\hat{U}(z,\omega)e^{-i(\omega^2/2)\int_0^z[\beta_i''(z)-\langle\beta''\rangle]}]. \quad (6)$$

The DMNLS, unlike the PNLS, has constant coefficients. Another significant advantage of the DMNLS is that the rapidly varying phase associated with the breathing is removed and the DM soliton solution is readily obtained.

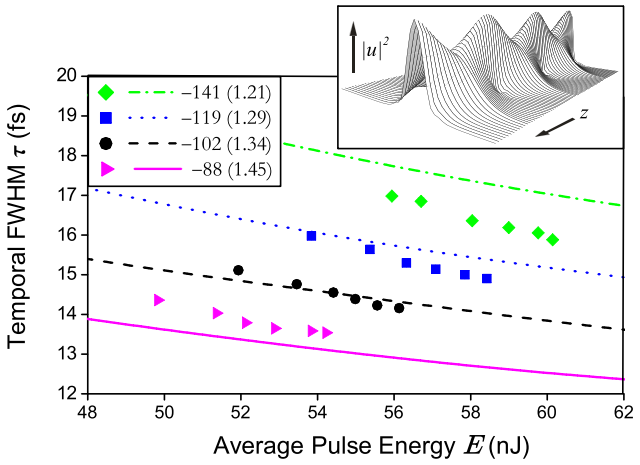

FIG. 2 (color online). Scaling of the fundamental pulse parameters in a mode-locked Ti:sapphire laser. The points are the measured temporal FWHM at the four values of the average cavity GDD. The curves are the solutions of Eq. (4), where one data point (54.4 nJ, 14.6 fs) was used to fit γ_0. The legend states both the GDD values in fs^2 (and the corresponding M values). The errors for the GDD are approximately 1% and the errors for the τ values are negligible on the scale shown. The spectra in Fig. 1(c) correspond to each of the highest E values (S_1 corresponds to the point at 54.2 nJ). The inset shows the breathing dynamics of a dispersion managed soliton $|u|^2$ [Eq. (6)] propagating along z.

Thus, the energy E and the temporal FWHM τ are calculated from Eq. (5).

The experimental data for the temporal FWHM dependence upon the intracavity pulse energy for four values of the GDD are plotted in Fig. 2. Since the theoretical model predicts the pulse duration at the crystal center ($z = 0$), the width τ for each E setting was determined assuming a transform-limited optical spectrum. In this regime, as the GDD becomes more anomalous, the pulse requires higher energies to remain stably mode locked. The theoretical curves are plotted in Fig. 2 where each is distinguished by the value of the reduced map strength, M. Given that the mechanisms for mode locking are not included in the model, the curves show remarkable agreement with the data and accurately predict the pulse dynamics over a broad range of parameters.

In generating the theoretical nonlinear and dispersion managed solutions, only one fitting parameter is used. The experimental uncertainty in the effective area A_{eff} of the beam at the center of the crystal requires that the nonlinear coefficient γ_0 be fit to match the data ($n_2 = 3.2 \times 10^{-8}$ mm^2/MW). Fitting one experimental data point, we find $A_{\text{eff}} = 200$ μm^2 and so $\gamma_0 = 1.26(mm \cdot MW)^{-1}$. Since our model uses only one fitting parameter, here we have explicitly determined γ_0 for an ultrashort pulsed mode-locked laser.

The formation of a mode-locked pulse in a Ti:sapphire laser requires gain and loss mechanisms that have so far

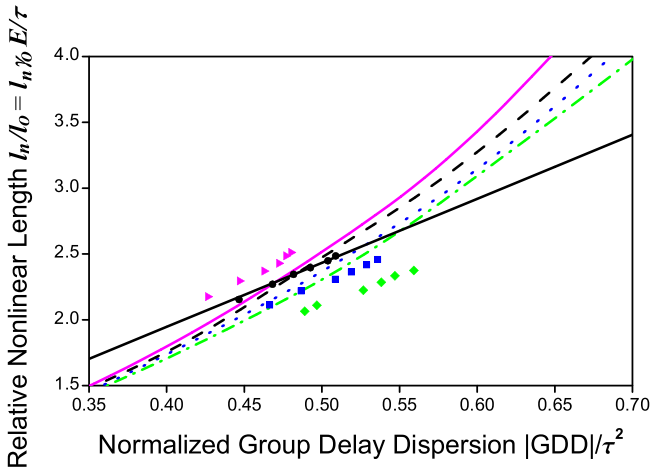

FIG. 3 (color online). Plot of the scaling of the asymptotic parameter with the normalized GDD, where the reduced map strength M is fixed for each of the theoretical curves. The solid line corresponds to the CS theory using Eq. (2) where one data point was used to fit γ_0. The curves are from the nonlinear and dispersion managed theory [Eq. (4)] and correspond to the same M values (with their respective colors and line types) as those given in Fig. 2. The experimental data are those from Fig. 2, with the appropriate scaling each pair of E and GDD with τ.

been neglected in the model. Such effects typically include saturable absorption, saturable gain, and spectral filtering and, when included in the theoretical model, the governing equation is called the master equation for mode locking [18]. We have included saturable absorption and gain in the theoretical model (in the PNLS) and have confirmed that the predictions are largely insensitive to these processes. Consequently, this simplifies the theory for the understanding of the propagation of pulses in mode-locked lasers, establishing that though these gain and loss processes are necessary to generate the pulse, the pulse's subsequent dynamics is well governed by the DM theory [Eq. (4)]. Hence, the pulse's behavior is dominated by the competing mechanisms of the Kerr nonlinearity and linear dispersion.

For the CS theory ($s = 0$) there is a fixed relationship between l_n/l_0 and the normalized GDD, $|\langle\beta''\rangle|l_t/\tau^2$, as seen in Eq. (2). In the DM theory, the additional parameter of s changes this relation and predicts the separation between the curves observed experimentally, as seen in Fig. 3. The CS line was obtained by fitting γ_0 in Eq. (2) to one data point. As the energy E vanishes, the soliton is not sustained, and hence, the DM (and CS) curves converge to zero (not shown). We also note that the Ti:sapphire laser is in a regime where l_n/l_0 is $\mathcal{O}(1)$. Nevertheless, our asymptotic theory for this regime still agrees with the direct numerical simulations to the PNLS equation.

In summary, for the solitons propagating in mode-locked Ti:sapphire lasers, the agreement between the PNLS and the experimental data demonstrates that the dominant factor in the pulse dynamics is the equilibrium established between the Kerr nonlinearity and the linear dispersion. We have used an asymptotic theory developed for the PNLS to predict the dynamics of these solitons using only one fitting parameter in the model to generate the theoretical curves. This study shows that the dispersion management concepts originally developed in fiber communications apply in a much broader context.

This research was partially supported by the U.S. Air Force Office of Scientific Research under Grant No. 1-49620-03-1-0250. The work at JILA was supported by the NSF, NIST, and the University of Colorado, Department of Physics.

*Electronic address: quraishi@colorado.edu

[1] C. Lin, H. Kogelnik, and L. G. Cohen, Opt. Lett. **5**, 476 (1980).
[2] F. O. Ilday, J. R. Buckley, W. G. Clark, and F. W. Wise, Phys. Rev. Lett. **92**, 213902 (2004).
[3] M. Suzuki and N. Edagawa, J. Lightwave Technol. **21**, 916 (2003).
[4] Y. Chen, F. X. Kärtner, U. Morgner, S. H. Cho, H. A. Haus, E. P. Ippen, and J. G. Fujimoto, J. Opt. Soc. Am. B **16**, 1999 (1999).
[5] N. Smith, F. Knox, N. Doran, K. Blow, and I. Bennion, Electron. Lett. **32**, 54 (1996).
[6] D. Meshulach and Y. Silberberg, Nature (London) **396**, 239 (1998).
[7] S. A. Diddams *et al.*, Science **293**, 825 (2001).
[8] Th. Udem, R. Holzwarth, and T. W. Hänsch, Nature (London) **416**, 233 (2002).
[9] *Femtosecond Optical Frequency Comb Technology*, edited by J. Ye and S. T. Cundiff (Springer, New York, 2004).
[10] *Ultrafast Phenomena XIV*, edited by T. Kobayashi, T. Okada, T. Kobayashi, K. A. Nelson, and S. De Silvestri (Springer, New York, 2004), Vol. 79.
[11] A. Hasegawa and F. D. Tappert, Appl. Phys. Lett. **23**, 142 (1973).
[12] L. F. Mollenauer and R. H. Stolen, Opt. Lett. **9**, 13 (1984).
[13] M. T. Asaki, C. P. Huang, D. Garvey, J. Zhou, H. C. Kapteyn, and M. M. Murnane, Opt. Lett. **18**, 977 (1998).
[14] M. J. Ablowitz and G. Biondini, Opt. Lett. **23**, 1668 (1998).
[15] M. J. Ablowitz, B. Ilan, and S. T. Cundiff, Opt. Lett. **29**, 1808 (2004).
[16] W. H. Knox and J. P. Gordon, J. Opt. Soc. Am. B **10**, 2071 (1993).
[17] G. Tempea, F. Krausz, C. Spielmann, and K. Ferencz, IEEE J. Sel. Top. Quantum Electron. **4**, 193 (1998).
[18] H. Haus, IEEE J. Sel. Top. Quantum Electron. **6**, 1173 (2000).

Spectral renormalization method for computing self-localized solutions to nonlinear systems

Mark J. Ablowitz

Department of Applied Mathematics, University of Colorado, Campus Box 526, Boulder, Colorado 80309-0526

Ziad H. Musslimani

Department of Mathematics, University of Central Florida, Orlando, Florida, 32816

Received February 10, 2005

A new numerical scheme for computing self-localized states—or solitons—of nonlinear waveguides is proposed. The idea behind the method is to transform the underlying equation governing the soliton, such as a nonlinear Schrödinger-type equation, into Fourier space and determine a nonlinear nonlocal integral equation coupled to an algebraic equation. The coupling prevents the numerical scheme from diverging. The nonlinear guided mode is then determined from a convergent fixed point iteration scheme. This spectral renormalization method can find wide applications in nonlinear optics and related fields such as Bose–Einstein condensation and fluid mechanics. © 2005 Optical Society of America

OCIS codes: 000.0000, 000.2690.

Optical spatial or temporal solitons in nonlinear media have attracted considerable attention in the scientific community. They have been demonstrated to exist in a wide range of physical systems in both continuous and discrete settings.[1–3] Such nonlinear modes can form as a result of a balance between diffraction or dispersion and nonlinearity. A central issue for these types of nonlinear guided waves is how to compute localized, i.e., soliton, solutions, which generally involve solving nonlinear ordinary or partial differential equations or difference equations. Various techniques have been used, e.g., shooting and relaxation techniques and the self-consistency method, to find nonlinear modes that utilize the concept that a soliton forms when the optical field induces a waveguide structure via the nonlinearity and self-traps itself (see, e.g., Refs. 4–6). Another method, introduced by Petviashvili,[7] for constructing localized solutions of a nonlinear system is based on transforming to Fourier space and determining a convergence factor based upon the degree (homogeneity) of a single nonlinear term (e.g., $|U|^pU$ has homogeneity $p+1$). While it was first used to find localized solutions in the two-dimensional Korteweg–deVries equation (usually referred to as the Kadomtsev–Petviashvili equation[8,9]), the method has been significantly extended and has been used to find localized solutions in a wide variety of interesting systems, e.g., dispersion-managed[10] and discrete diffraction-managed[11,12] nonlinear Schrödinger equations, dark and gray solitons,[13] and lattice vortices.[14] This method often is successful only when the underlying equation contains nonlinearity with fixed homogeneity. However, many physically interesting problems involve nonlinearities with different homogeneities, such as cubic–quintic, or even lack any homogeneity, as in saturable nonlinearity.

In this Letter we describe a novel spectral renormalization scheme with which we can compute localized solutions in nonlinear waveguides. The essence of the method is to transform the underlying equation that governs the soliton (e.g., nonlinear Schrödinger type) into Fourier space and find a nonlinear nonlocal integral equation (or system of integral equations) coupled to an algebraic equation (or system). The coupling prevents the numerical scheme from diverging. The nonlinear guided mode is then obtained from an iteration scheme, which in the cases we have investigated converges rapidly. The advantages of the present method are that (i) it can be applied to a large class of physically interesting problems including those in which the self-consistency method fails, as is the case for second-harmonic generation, (ii) it is relatively easy to implement (e.g., compared with relaxation methods), (iii) it can handle higher-order nonlinearities with different homogeneities, and (iv) it is spectrally efficient. Moreover, this method can find wide applications in nonlinear optics, Bose–Einstein condensation, and fluid dynamics. We begin by considering a scalar nonlinear Schrödinger-like equation:

$$i\frac{\partial U}{\partial z} + \nabla^2 U - V(\mathbf{x})U + N(|U|^2)U = 0, \tag{1}$$

where U is the envelope proportional to the electric field, z is the propagation direction, N is a nonlinearity that depends on intensity, $V(\mathbf{x})$ models an optical lattice, $\mathbf{x}=(x,y)$, and $\nabla^2=\partial^2/\partial x^2+\partial^2/\partial y^2$. A special class of soliton solution can be constructed by assuming that $U(\mathbf{x},z)=u(\mathbf{x};\mu)\exp(i\mu z)$, where μ is the propagation constant or the soliton eigenvalue. Substituting the above ansatz into Eq. (1), we get

$$-\mu u + \nabla^2 u - V(\mathbf{x})u + N(|u|^2)u = 0. \tag{2}$$

This is a nonlinear eigenvalue problem for u and μ that is supplemented with the boundary condition $u \to 0$ as $|r| \to +\infty$, where $r^2=x^2+y^2$. The scheme is based on Fourier analysis, which transforms Eq. (2) into a nonlocal equation that will then be solved using a convergent iteration. Define the Fourier transform $\mathcal{F}$ by

0146-9592/05/162140-3/$15.00

$$\hat{u}(\mathbf{k}) = \mathcal{F}[u(\mathbf{x})] = \int_{-\infty}^{+\infty}\int_{-\infty}^{+\infty} u(\mathbf{x})\exp[i(k_x x + k_y y)]\mathrm{d}\mathbf{x}, \tag{3}$$

where $\mathrm{d}\mathbf{x}=\mathrm{d}x\mathrm{d}y$. First, consider the case with no optical potential or external defect ($V=0$), for which $\mu>0$. Applying the Fourier transform to Eq. (2) leads to

$$\hat{u}(\mathbf{k}) = \frac{\mathcal{F}[N(|u|^2)u]}{\mu + |\mathbf{k}|^2}. \tag{4}$$

The idea is to construct a condition that limits the amplitude under iteration from either growing without bound or tending to zero. This is accomplished by introducing of a new field variable, $u(\mathbf{x})=\lambda w(\mathbf{x})$, $\hat{u}(\mathbf{k})=\lambda\hat{w}(\mathbf{k})$, where $\lambda\neq 0$ is a constant to be determined. Then the function $\hat{w}$ satisfies

$$\hat{w}(\mathbf{k}) = \frac{\mathcal{F}[N(|\lambda|^2|w|^2)w]}{\mu + |\mathbf{k}|^2} \equiv Q_\lambda[\hat{w}(\mathbf{k})]. \tag{5}$$

Multiplying Eq. (5) by $\hat{w}^*(\mathbf{k})$ and integrating over the entire $\mathbf{k}$ space, we find the relation

$$G(\lambda) \equiv \int_{-\infty}^{+\infty} |\hat{w}(\mathbf{k})|^2\mathrm{d}\mathbf{k} - \int_{-\infty}^{+\infty} \hat{w}^*(\mathbf{k})Q_\lambda[\hat{w}(\mathbf{k})]\mathrm{d}\mathbf{k} = 0, \tag{6}$$

providing an algebraic condition on the constant λ. Finally, the desired solution is obtained by iterating Eq. (5):

$$\hat{w}_{m+1}(\mathbf{k}) = \frac{\mathcal{F}[N(|\lambda_m|^2|w_m|^2)w_m]}{\mu + |\mathbf{k}|^2} \tag{7}$$

for $m\geqslant 1$; λ_m denotes the solution to $G(\lambda_m)=0$ at iteration m. Other variants of Eq. (6) are possible. But what is crucial is to solve Eq. (7) coupled to an algebraic-type equation that is obtained from Eq. (5) by imposing an integral identity such as Eq. (6). We name this method spectral renormalization. It is straightforward to implement Eq. (7): Initially we guess a function $w_1(\mathbf{x})$ [e.g., a Gaussian or sech-like profile], which from Eq. (6) yields λ_1 that satisfies $G(\lambda_1)=0$. Then, from Eq. (7), we obtain $\hat{w}_2(\mathbf{k})$, which from the inverse, Fourier transform leads to $w_2(\mathbf{x})$. The iteration continues until convergence is achieved. The procedure described above reproduces the results presented elsewhere.[12] Knowing the weakly nonlinear limit is very useful in this regard. Before presenting specific examples, we explain how to construct localized solutions in the presence of an external defect ($V\neq 0$). In this case, $\mu<0(\mu\equiv -|\mu|)$. But dividing by the expression $|\mu|-|\mathbf{k}|^2$ leads to a singularity. To avoid this, we add to and subtract from Eq. (2) the term $ru(\mathbf{x})$, where r is a positive constant, and then take the Fourier transform. This leads to

$$\hat{u}(\mathbf{k}) = \frac{(r+|\mu|)\hat{u}}{r+|\mathbf{k}|^2} - \frac{\mathcal{F}[Vu]-\mathcal{F}[N(|u|^2)u]}{r+|\mathbf{k}|^2} \equiv R[\hat{u}(\mathbf{k})]. \tag{8}$$

Following the change of variable $u(\mathbf{x})=\lambda w(\mathbf{x})$ the iteration scheme takes the form $\hat{w}_{m+1}(\mathbf{k})=R[\lambda_m\hat{w}_m(\mathbf{k})]$, with λ_m given by the relation

$$\int_{-\infty}^{+\infty} |\hat{w}_m(\mathbf{k})|^2\mathrm{d}\mathbf{k} - \int_{-\infty}^{+\infty} \hat{w}_m^*(\mathbf{k})R[\lambda_m\hat{w}_m(\mathbf{k})]\mathrm{d}\mathbf{k} = 0. \tag{9}$$

To illustrate the method in a prototypical problem we consider photorefractive lattice solitons in self-focusing saturable nonlinearity, for which $V(\mathbf{x})=I_0[\cos^2(x)+\cos^2(y)]$ and $N(|u|^2)=-1/(1+|u|^2)$. These photorefractive solitons were observed experimentally for the first time by Segev's group.[15] The lattice modes were originally found using the self-consistency method.[16] The reason for our showing this example is to delineate a situation in which the nonlinearity does not have a well-defined homogeneity. For the fully saturable case, the iteration scheme reads as

$$\hat{w}_{m+1}(\mathbf{k}) = \frac{(r+|\mu|)}{r+|\mathbf{k}|^2}\hat{w}_m - \frac{\mathcal{F}[Vw_m]}{r+|\mathbf{k}|^2} + \frac{1}{r+|\mathbf{k}|^2}\mathcal{F}\left[\frac{w_m}{1+|\lambda_m|^2|w_m|^2}\right], \tag{10}$$

where λ_m are obtained from iterating Eq. (9) by using standard nonlinear algebraic equation solvers, e.g., the Newton method. A typical example of a fundamental discrete soliton that corresponds to the parameters $I_0=1$ and $\mu=0.8$ is shown in Fig. 1. We have verified the stationarity of the mode by using direct numerical simulation in Eq. (1). We can readily generalize the above method to include more than one field. In that case, Eq. (2) is replaced by M coupled stationary nonlinear Schrödinger-like equations that are solvable using the same idea outlined above.

Another interesting case that arises in many applications is that of second-harmonic generation. The system of equations governing stationary soliton states[17–21] is

$$-\nu A + W(\mathbf{x})A + \nabla^2 A + AB = 0, \tag{11}$$

$$-4\nu B + 4W(\mathbf{x})B + \nabla^2 B + \frac{A^2}{2} = 0, \tag{12}$$

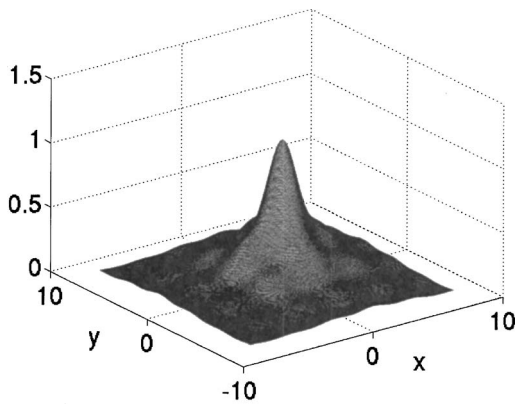

Fig. 1. Fundamental lattice soliton obtained by iterating Eq. (10) for $I_0=1$ and $|\mu|=0.8$.

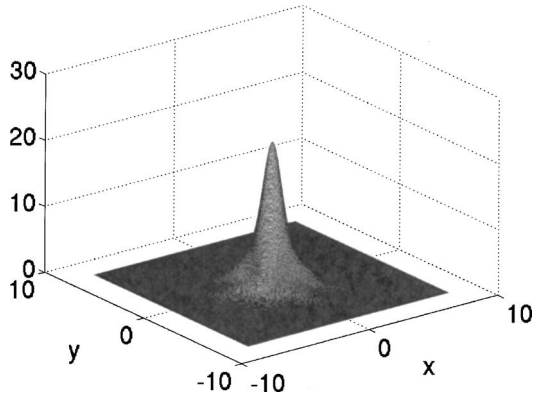

Fig. 2. Fundamental harmonic $|A|$ for $W_0=2$ and $\nu=2$.

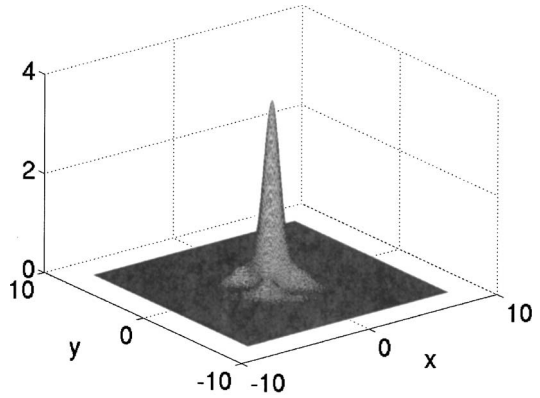

Fig. 3. Second harmonic $|B|$ for $W_0=2$ and $\nu=2$.

where $\nu>0$ is the soliton propagation constant and the lattice potential is given by $W(\mathbf{x}) = W_0 \cos(2x)\cos(2y)$. Following a similar procedure, we adopt the change of variables $A=\lambda_1\psi$, $B=\lambda_2\phi$. In this case the iteration scheme takes the form

$$\hat{\psi}_{m+1} = \frac{\mathcal{F}[W\psi_m] + \lambda_{2m}\mathcal{F}[\psi_m\phi_m]}{\nu + |\mathbf{k}|^2}, \tag{13}$$

$$\hat{\phi}_{m+1} = \frac{4\mathcal{F}[W\phi_m] + (\lambda_{1m}^2/\lambda_{2m})\mathcal{F}[\psi_m^2/2]}{4\nu + |\mathbf{k}|^2}. \tag{14}$$

The convergence factors λ_{1m} and λ_{2m} satisfy the coupled system

$$\lambda_{2m} = -\frac{\int_{-\infty}^{+\infty} d\mathbf{k}[(\nu + |\mathbf{k}|^2)|\hat{\psi}_m|^2 - \hat{\psi}_m^*\mathcal{F}[W\psi_m]]}{\int_{-\infty}^{+\infty} d\mathbf{k}\hat{\psi}_m^*\mathcal{F}[\psi_m\phi_m]},$$

$$\lambda_{1m}^2 = \frac{\lambda_{2m}\int_{-\infty}^{+\infty} d\mathbf{k}[(4\nu + |\mathbf{k}|^2)|\hat{\phi}_m|^2 - 4\hat{\phi}_m^*\mathcal{F}[W\phi_m]]}{\int_{-\infty}^{+\infty} d\mathbf{k}\hat{\phi}_m^*\mathcal{F}[\psi_m^2/2]}.$$

Typical examples of quadratic lattice solitons are shown in Figs. 2 and 3.

In conclusion, we have developed a novel numerical scheme with which to compute self-localized states of nonlinear waveguides that is flexible and can be applied to many nonlinear systems. As prototypical examples, we considered photorefractive saturable nonlinearity, which lacks the property of homogeneity and second-harmonic generation. We have shown how to find lattice solitons by using this spectral renormalization method.

This research was partially supported by the U.S. Air Force Office of Scientific Research under grant F-49620-03-1-0250 and by National Science Foundation grant DMS-0303756. Z. H. Musslimani's e-mail address is zmuslima@mail.ucf.edu.

References

1. G. Stegeman and M. Segev, Science **286**, 1518 (1999).
2. D. N. Christodoulides, F. Lederer, and Y. Silberberg, Nature **424**, 817 (2003).
3. G. P. Agrawal, *Nonlinear Fiber Optics*, 3rd ed. (Elsevier, 2001).
4. A. W. Snyder, D. J. Mitchell, L. Polodian, and F. Ladouceur, Opt. Lett. **16**, 21 (1991).
5. M. Mitchell, M. Segev, T. H. Coskun, and D. N. Christodoulides, Phys. Rev. Lett. **79**, 4990 (1997).
6. O. Cohen, T. Schwartz, J. W. Fleischer, M. Segev, and D. N. Christodoulides, Phys. Rev. Lett. **91**, 113901 (2003).
7. V. I. Petviashvili, Sov. J. Plasma Phys. **2**, 257 (1976).
8. B. B. Kadomtsev and V. I. Petviashvili, Sov. Phys. Dokl. **15**, 539 (1970).
9. M. J. Ablowitz and H. Segur, *Solitons and the Inverse Scattering Transform* (Society for Industrial and Applied Mathematics, 1981).
10. M. J. Ablowitz and G. Biondini, Opt. Lett. **23**, 1668 (1998)
11. M. J. Ablowitz and Z. H. Musslimani, Phys. Rev. Lett. **87**, 254102 (2001).
12. M. J. Ablowitz and Z. H. Musslimani, Physica D **184**, 276 (2003).
13. M. J. Ablowitz and Z. H. Musslimani, Phys. Rev. E **67**, 025601(R) (2003).
14. Z. H. Musslimani and J. Yang, J. Opt. Soc. Am. B **21**, 973 (2004).
15. J. W. Fleischer, M. Segev, N. K. Efremidis, and D. N. Christodoulides, Nature **422**, 147 (2003).
16. N. K. Efremidis, D. N. Christodoulides, J. W. Fleischer, O. Cohen, and M. Segev, Phys. Rev. Lett. **91**, 213906 (2003).
17. A. Fratalocchi, G. Assanto, K. A. Brzdakiewicz, and M. A. Karpierz, Opt. Lett. **29**, 1530 (2004).
18. T. Peschel, U. Peschel, and F. Lederer, Phys. Rev. E **57**, 1127 (1998).
19. S. Darmanyan, A. Kobyakov, and F. Lederer, Phys. Rev. E **57**, 2344 (1998).
20. R. Iwanow, R. Schiek, G. I. Stegeman, T. Pertsch, F. Lederer, Y. Min, and W. Sohler, Phys. Rev. Lett. **93**, 113902 (2004).
21. Z. Xu, Y. V. Kartashov, L. Crasovan, D. Mihalache, and L. Torner, Phys. Rev. E **71**, 016616 (2005).

PHYSICAL REVIEW E **71**, 055602(R) (2005)

Wave dynamics in optically modulated waveguide arrays

Mark J. Ablowitz,[1] Keith Julien,[1] Ziad H. Musslimani,[2] and Michael I. Weinstein[3]
[1]*Department of Applied Mathematics, University of Colorado, Campus Box 526, Boulder, Colorado 80309-0526, USA*
[2]*Department of Mathematics, University of Central Florida, Orlando, Florida 32816, USA*
[3]*Department of Applied Physics and Applied Mathematics, Columbia University, 200 S.W. Mudd - MC4701 New York, New York 10027, USA*

(Received 20 January 2005; published 11 May 2005)

A model describing wave propagation in optically modulated waveguide arrays is proposed. In the weakly guided regime, a two-dimensional semidiscrete nonlinear Schrödinger equation with the addition of a bulk diffraction term and an external "optical trap" is derived from first principles, i.e., Maxwell equations. When the nonlinearity is of the defocusing type, a family of *unstaggered* localized modes are numerically constructed. It is shown that the equation with an induced potential is well-posed and gives rise to localized dynamically stable nonlinear modes. The derived model is of the Gross-Pitaevskii type, a nonlinear Schrödinger equation with a linear optical potential, which also models Bose-Einstein condensates in a magnetic trap.

DOI: 10.1103/PhysRevE.71.055602 PACS number(s): 42.65.Wi

Wave propagation in nonlinear periodic structures displays unique phenomena that are absent in homogeneous media. The interplay between periodicity and nonlinearity can lead to the formation of discrete or lattice solitons, which were predicted theoretically in the context of optical waveguide arrays [1] and then experimentally observed in [2]. Until recently, discrete solitons were considered experimentally in one-dimensional geometry [2]. However, by making use of the photorefractive screening nonlinearity one can "write" either one- or higher-dimensional optical waveguide arrays by interfering pairs of plane waves [3]. Indeed, such localized structures were experimentally observed in two-dimensional geometries [4].

In this paper we study wave propagation in optically modulated waveguide arrays, starting from the full time-harmonic three-dimensional Maxwell's equations. For the case where the periodic modulation along the y direction is much larger than the periodic modulation along the x direction we derive, using multiscale asymptotic analysis, a semidiscrete nonlinear Schrödinger equation with the addition of bulk diffraction term and an external "optical trap." When the nonlinearity is of the defocusing type (where in the absence of modulation no finite energy solitons are known) *unstaggered* localized modes are numerically constructed. The fundamental properties such as the well-posedness of the equation, existence, and the dynamical stability associated with a special class of localized wave solutions, i.e., stationary wave, or ground state, are discussed. The semidiscrete model is derived from the scalar nonlinear Helmholtz equation. Below we briefly outline the justification for neglecting vectorial effects under certain physical assumptions. A more general and detailed study of scalar and vector semidiscrete nonlinear Schrödinger (NLS) type models will be given elsewhere.

We begin by considering the three-dimensional Maxwell equations governing time-harmonic solutions of frequency ω_0

$$\nabla^2\mathbf{E} - \nabla(\nabla\cdot\mathbf{E}) + k_0^2(\mathbf{E}+\mathbf{P}) = 0, \quad k_0 = \frac{\omega_0}{c}. \tag{1}$$

Here, $\nabla = \partial_x\hat{\mathbf{i}} + \partial_y\hat{\mathbf{j}} + \partial_z\hat{\mathbf{k}}$, $\mathbf{E} = \mathbf{E}(\mathbf{x};\omega_0)$ denotes the *complex* envelope of the electric field, $\mathbf{P} = \mathbf{P}(\mathbf{E}(\mathbf{x});\omega_0)$ denotes the polarization field, containing both linear and nonlinear responses; we further assume the nonlinear polarization to be of Kerr type [5] where the second component of the polarization is given by

$$P_2 = \chi E_2 + \delta((|E_1|^2 + (1+\gamma)|E_2|^2 + |E_3|^2)E_2 + \gamma(E_1^2 + E_3^2)E_2^*); \tag{2}$$

where γ is a constant, δ is proportional to the nonlinear index change of refraction, and χ is a function of x and y; the other polarization components are found by cyclically changing the indices $(1\to 2\to 3\to 1)$. We consider propagation in the z direction through a photonic structure (invariant in z) having nontrivial spatial variations in the (x,y) plane due to χ. A schematic of the kind of transverse structure we consider is given in Fig. 1. This structure has a rapid periodic variation in x and a slow modulation in y. In nondimensional terms, this corresponds to the assumed form $\chi = \chi(x,\varepsilon^{1/2}y)$, where ε is a small dimensionless parameter. The period in x is of order 1 whereas a typical distance in y is of order $\varepsilon^{-1/2}$. We further assume that the nondimensional nonlinear index of refraction is small in size $[O(\varepsilon)]$. Then, analysis of Maxwell's equations (1) shows that $E_3/E_2 = O(\varepsilon)$ and $E_1/E_2 = O(\varepsilon^{3/2})$ and to leading order

$$\partial_z E_3 = -\partial_y E_2. \tag{3}$$

Then the second component of Maxwell's equations (1) leads to the following nonlinear Helmholtz equation

$$\nabla^2\Psi + f^2(x,y)\Psi + \varepsilon\eta|\Psi|^2\Psi = 0, \tag{4}$$

where Ψ is the envelope wave function, which is proportional to the optical field E_2 $(\nabla^2 = \partial_x^2 + \partial_y^2 + \partial_z^2)$. $f^2(x,y) = 1+\chi$ is the linear refractive index of the waveguide structure, η is proportional to δ and $\operatorname{sgn}\eta = +1$ and $\operatorname{sgn}\eta = -1$ correspond to, respectively, the cases of self-focusing and self-defocusing

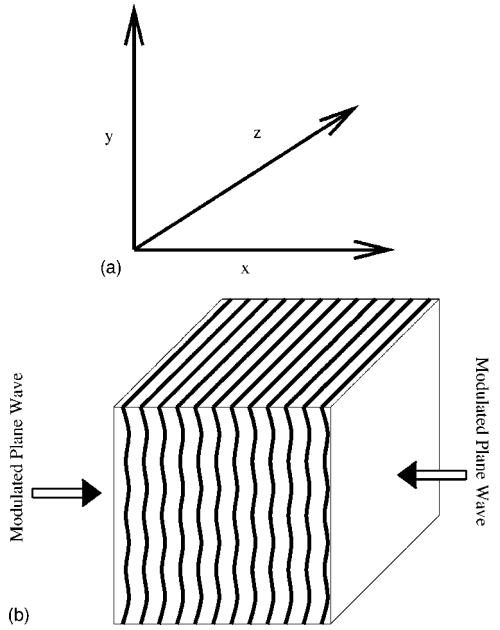

FIG. 1. A typical modulated waveguide array.

nonlinearity. We assume that the linear refractive index appearing in (4) takes the form

$$f^2(x,y) = \mathcal{F}^2(x) + \varepsilon\, a\mathcal{F}_p^2(x,\varepsilon^{1/2}y), \tag{5}$$

where $a=\pm 1$. $\mathcal{F}^2(x)$ is the refractive index of a grating structure in the x longitudinal coordinate, which may be viewed as a superposition of spatial translates of a basic waveguide with index profile $F_0^2(x)$, which we assume to be single moded. Thus, $\mathcal{F}^2(x)\sim\Sigma_m F_m^2(x)$, $F_m(x)=F_0(x-mD)$. Here, $\varepsilon\mathcal{F}_p^2(x,\varepsilon^{1/2}y)$ is a weak modulation of refractive index (slow in y and fast in x). One can create a photonic structure of this type by illuminating a photorefractive crystal with a pair of interfering one-dimensional plane waves weakly modulated along the y direction with a wavelength larger than the wavelength along the x direction. We now analyze wave propagation in a nonlinear optical two-dimensional array and discuss the physical phenomena that result.

We exploit the weak nonlinearity (small ε) in (4) and (5) to construct a multiple scale expansion of the envelope, Ψ. We seek Ψ as a superposition of $x-$ translates of the isolated single mode wave function with slowly varying amplitudes [6]

$$\Psi \approx \sum_{m=-\infty}^{+\infty} A_m(Z,Y)\psi_m(x)e^{i\mu z}, \tag{6}$$

where $Z=\varepsilon z$ and $Y=\varepsilon^{1/2}y$ are slow propagation and modulation scales, respectively. Here, $\psi(x)$ is the single waveguide mode and μ its corresponding eigenvalue

$$\frac{d^2\psi}{dx^2} + (F_0^2(x) - \mu^2)\psi = 0, \tag{7}$$

and $\psi_m(x)=\psi(x-mD)$. Substituting the expansion (6) into the Helmholtz equation (4) and making use of (7), we find that the corrections to (6) are small provided the projections of

$$\sum_{m=-\infty}^{+\infty}\left[2i\varepsilon\mu\psi_m\frac{\partial A_m}{\partial Z} + \psi_m(\mathcal{F}^2(x) - F_m^2(x))A_m + \varepsilon\psi_m\frac{\partial^2 A_m}{\partial Y^2} + a\varepsilon\mathcal{F}_p^2(x,Y)\psi_m A_m + \varepsilon\eta\sum_{m',m''=-\infty}^{+\infty}\psi_m\psi_{m'}\psi_{m''}^* A_m A_{m'} A_{m''}^*\right] = 0, \tag{8}$$

onto all ψ_j are of order $\varepsilon^\delta, \delta>1$. This yields (see also [6])

$$i\frac{\partial A_n}{\partial Z} + C(A_{n+1} + A_{n-1}) + \gamma\frac{\partial^2 A_n}{\partial Y^2} + aV_n(Y)A_n + \kappa|A_n|^2 A_n = 0, \tag{9}$$

where $\varepsilon C = 1/c_0\int(\mathcal{F}^2(x) - F_{n\pm1}^2(x))\psi_{n\pm1}\psi_n^* dx$, $V_n(Y) = 1/c_0\int\mathcal{F}_p^2(x,Y)|\psi_n|^2 dx$, $\kappa=\eta/c_0\int|\psi_n|^4 dx$, and $c_0 = 2\mu\int|\psi_n|^2 dx$; $\gamma=1/(2\mu)$. Note that we are considering the regime where only nearest neighbor waveguides contribute to order ε. Equation (9) governs the slow evolution of A_n in a weakly modulated optically induced waveguide array. Next we examine linear propagation and then highlight some physical nonlinear phenomena that are predicted by the model (9). For the ideal one-dimensional waveguide array [$\gamma=\kappa=V_n(Y)\equiv 0$], the propagating field experiences discrete diffraction due to optical tunneling to adjacent sites and exhibits a typical discrete diffraction pattern with the intensity mainly concentrated in the outer lobes [7]. However, in the presence of modulation ($\gamma\neq 0$ and $V_n\neq 0$), and in the quasi-two-dimensional configuration (when modulating along the y direction), the waveguide action prevents the beam from diffracting. It should also be noted that a similar derivation in the case when two fields are initially present, i.e., nontrivial E_1, E_2 leads to a vector system whose first component satisfies,

$$i\frac{\partial A_n^{(1)}}{\partial Z} + C(A_{n+1}^{(1)} + A_{n-1}^{(1)}) + \gamma\frac{\partial^2 A_n^{(1)}}{\partial Y^2} + aV_n(Y)A_n^{(1)} + \kappa[(1+\gamma)|A_n^{(1)}|^2 + |A_n^{(2)}|^2]A_n^{(1)} + \gamma A_n^{(1)^2}A_n^{(2)*} = 0, \tag{10}$$

and the second equation is obtained by cyclically changing the indices ($1\to 2\to 1$). In a future publication we will give the derivation in detail. We now discuss the results obtained for the model (9) which are depicted in Figs. 2–4. First, in both self-focusing and self-defocusing cases, propagating beams of any finite power do not collapse or filament. This is in contrast to the continuum analog, the two-dimensional cubic-focusing NLS equation, whose solutions with sufficient initial power are well known to develop singularities at a finite distance into a bulk Kerr propagation medium [8]. That the semidiscrete character inhibits collapse, (see Fig. 4), can be understood by an argument based on the conserved integrals of (9)

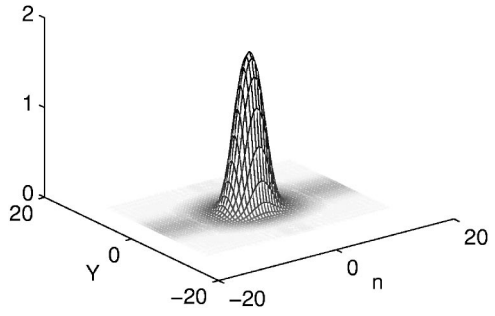

FIG. 2. Localized semidiscrete, two-dimensional soliton solution to Eq. (12) in the presence of a semidiscrete two-dimensional trap ($\alpha=\beta=1/2$) for the defocusing nonlinearity. The parameters are $C=2$, $\nu=4$, $\gamma=1$, and $\kappa=-1$.

$$\mathcal{N}=\sum_n \int |A_n|^2 dY$$

$$\mathcal{H}=C\sum_n \int |A_{n+1}-A_n|^2+|\partial_Y A_n|^2-aV_n|A_n|^2-\frac{\kappa}{2}|A_n|^4 dY.$$

That no singularity can form as the wave form propagates through increasing Z is a direct consequence of the $Z-$ independence of $\mathcal{N}$ and $\mathcal{H}$ and the semidiscrete Sobelev-Gagliardo-Nirenberg inequality (dSNG) for functions $f_n(Y)$ defined on the integer lattice times the real continuum [9–11]: Let $\vec{f}=(f_n(Y))$, $\tau\vec{f}=(f_{n+1}(Y))$ and $\|\vec{f}\|_p^p=\Sigma_n\int|f_n|^p dY$. Then, there is a universal constant $C_*>0$ such that for all $\vec{f}$

$$\|\vec{f}\|_4^4 \leqslant C_*\|\partial_Y\vec{f}\|_2\|\vec{f}-\tau\vec{f}\|_2\|\vec{f}\|_2^2. \tag{11}$$

In particular, the Z independence of $\mathcal{N}$ and $\mathcal{H}$ and the inequality (11) together imply upper bounds on $\|\partial_Y\vec{f}(Z)\|_2$ and $|\vec{f}(Z,Y)|$ in terms of $\mathcal{H}$ and $\mathcal{N}$ (which are independent of Z and Y). These bounds break down when passing to the continuum limit. It should be remarked that in the defocusing case, $\gamma\kappa<0$, when $V_n(Y)\equiv 0$, there are no localized nonlinear modes. In this case, a finite energy concentration diffractively spreads and attenuates in amplitude. However, the optical trapping potential, $V_n(Y)$, introduces the possibility of stable bright solitonlike states. Indeed, the existence and importance of such *nonlinear defect modes* has been studied in the context of a plasma model [12] and in the trapping of nonlinear pulses in fiber gratings with localized defects [13]. Such nonlinear defect modes are solutions to Eq. (9) of the form $A_n=B_n e^{-i\nu Z}$ and satisfy

$$\nu B_n+C(B_{n+1}+B_{n-1})+\gamma\frac{\partial^2 B_n}{\partial Y^2}-V_n(Y)B_n+\kappa|B_n|^2B_n=0, \tag{12}$$

where $\nu>0$ is the propagation constant. In the above, we took $a=-1$ and $\eta=-1$. The existence and stability of these states follows from their variational characterization as local minima of the energy functional $\mathcal{H}$ subject to fixed total power, $\mathcal{N}$. Here too, the inequality (11) plays a role in that it implies the boundedness from below of the constrained energy. For simplicity, in our numerics we consider a perturbed index, which is locally parabolic (which can be induced by a weak sinusoidal refractive index), $\mathcal{F}_p^2(x,Y)=\tilde{\alpha}x^2+\tilde{\beta}Y^2$ leading to the induced potential

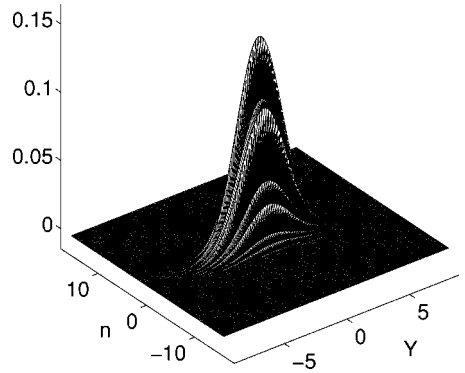

FIG. 3. Localized semidiscrete, two-dimensional soliton solution to Eq. (12) in the presence of a one-dimensional "discrete trap" ($\alpha=1/2$; $\beta=0.1$) for the defocusing nonlinearity. The parameters are $C=2$, $\nu=4$, $\gamma=1$, and $\kappa=-1$.

$$V_n(Y)=\alpha n^2+\beta Y^2. \tag{13}$$

To numerically construct the bound states solutions to Eq. (12) we first define the Fourier transform $\mathbb{F}$ and its inverse $\mathbb{F}^{-1}$

$$\hat{B}(k,q)=\mathbb{F}[B_n(Y)]=\sum_{n=-\infty}^{+\infty}\int_{-\infty}^{+\infty}B_n(Y)e^{-i(qn+kY)}dY, \tag{14}$$

$$B_n(Y)=\mathbb{F}^{-1}[\hat{B}(k,q)]=\frac{1}{(2\pi)^2}\int_{-\infty}^{+\infty}\int_{-\pi}^{+\pi}\hat{B}(k,q)e^{+i(qn+kY)}dkdq. \tag{15}$$

The idea of the method (see also Ref. [14]) is to make the change of variables: $B_n(Y)=\theta Q_n(Y)$, $\hat{B}(k,q)=\theta\hat{Q}(k,q)$, where $\theta\neq 0$ is a constant to be determined from a consistency condition. Taking the Fourier transform on Eq. (12) and using the above change of variables we get

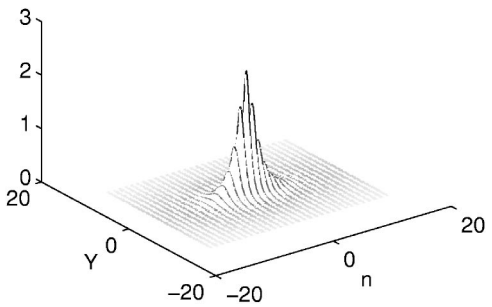

FIG. 4. Localized semidiscrete, two-dimensional soliton solution to Eq. (12) without a trap [$V_n(Y)\equiv 0$] for the focusing nonlinearity. The parameters are $C=2$, $\nu=1$, $\gamma=1$, and $\kappa=+1$.

$$\Omega(k,q)\hat{Q}(k,q) - \mathbb{F}[V_n(Y)Q_n(Y)] = -\theta^2\mathbb{F}[\kappa|Q_n|^2Q_n], \tag{16}$$

where $\Omega(k,q)=\nu+2C\cos(q)-\gamma k^2$. Multiplying Eq. (16) by $\hat{Q}^*(k,q)$ and integrating over the (k,q) space, we find

$$\theta^2 = \frac{-\int \hat{Q}^*(k,q)\{\Omega(k,q)\hat{Q}(k,q) - \mathbb{F}[V_n(Y)Q_n(Y)]\}dkdq}{\int \hat{Q}^*(k,q)\mathbb{F}[\kappa|Q_n|^2Q_n]dkdq}. \tag{17}$$

Since $\Omega(k,q)$ vanishes for $\nu=-2C\cos(q)+\gamma k^2$, we add and subtract $(r+2C)\hat{Q}(k,q)$ in Eq. (16) where r is an arbitrary positive number. Then the iteration will take the following form:

$$\hat{Q}^{(m+1)} = \frac{r+\nu+2C}{r+2C[1-\cos(q)]+\gamma k^2}\hat{Q}^{(m)}(k,q) - \frac{\mathbb{F}[V_n(Y)Q_n^{(m)}(Y)] - (\theta^{(m)})^2\mathbb{F}[\kappa|Q_n^{(m)}|^2Q_n^{(m)}]}{r+2C[1-\cos(q)]+\gamma k^2}, \tag{18}$$

where $\theta^{(m)}$ is defined by the right-hand side of (17) with Q set equal to $Q^{(m)}$. Typical examples of self-localized beams are shown in Figs. 2–4. In Fig. 2 we have a trap in both n and Y and the mode is localized *equally* in both directions. In Fig. 3, we depict a trap with $\alpha=1/2$ and $\beta=0.1$, which is much longer in the Y direction than the discrete n. We also note that when the trap is only a function of n ($\beta=0$), the corresponding mode is only localized in the n direction; similarly it turns out that when the trap is localized in the y direction (e.g., $\alpha=0$) then the mode is only localized in the Y direction. Finally we find that when the trap is "turned off" $V_n=0$—then we find a new localized mode in the focusing nonlinear case when $\gamma\kappa=1$ (see Fig. 4).

In conclusion, a model describing wave propagation in optically modulated waveguide arrays is derived from Maxwell's equations. In the weakly guided regime, a discrete nonlinear Schrödinger equation with the addition of a bulk diffraction term and an external "optical trapping potential" is derived. In the defocusing regime, where in the absence of modulation no finite energy solitons are known, the induced optical trap prevents the beam from defocusing, resulting in a stable unstaggered localized mode. These results also establish a connection to the modeling of Bose-Einstein condensation where discrete optical lattices with a potential induced by a magnetic trap have been studied (cf. [15]).

M.J.A. was partially supported by the Air Force Office of Scientific Research under Grant No. F-49620-03-1-0250 and by the NSF under Grant No. DMS-0303756 M.I.W. was partially supported by the NSF under Grant No. DMS-0412305. K.J. acknowledges partial support from the University of Colorado.

[1] D. N. Christodoulides and R. J. Joseph, Opt. Lett. **13**, 794 (1988).
[2] H. Eisenberg, Y. Silberberg, R. Morandotti, A. Boyd, and J. Aitchison, Phys. Rev. Lett. **81**, 3383 (1998).
[3] N. Efremidis, S. Sears, D. N. Christodoulides, J. Fleischer, and M. Segev, Phys. Rev. E **66**, 046602 (2002).
[4] J. Fleischer, M. Segev, N. Efremidis, and D. N. Christodoulides, Nature (London) **422**, 147 (2003).
[5] R. W. Boyd, *Nonlinear Optics*, 2nd ed. (Academic Press, SanDiego, CA, 2003).
[6] M. J. Ablowitz and Z. H. Musslimani, Physica D **184**, 276 (2003).
[7] A. Yariv, *Optical Electronics in Modern Communications* (Oxford University Press, Oxford, 1997).
[8] P. L. Kelley, Phys. Rev. Lett. **15**, 1005 (1965).
[9] M. I. Weinstein and B. Yeary, Phys. Lett. A **222**, 157 (1996).
[10] M. I. Weinstein, Nonlinearity **12**, 673 (1999).
[11] B. Yeary, Ph.D. thesis, University of Michigan, 1996 (unpublished).
[12] H. A. Rose and M. I. Weinstein, Physica D **30**, 207 (1988).
[13] R. H. Goodman, R. E. Slusher, and M. I. Weinstein, J. Opt. Soc. Am. B **19**, 1635 (2002).
[14] M. J. Ablowitz and Z. H. Musslimani, Opt. Lett.(to be published).
[15] P. Meystre, *Atom Optics* (Springer, Berlin, 2001).

Available online at www.sciencedirect.com
SCIENCE DIRECT®
Physica D 207 (2005) 230–253
PHYSICA D
www.elsevier.com/locate/physd

Wave collapse in a class of nonlocal nonlinear Schrödinger equations

Mark Ablowitz[a], İlkay Bakırtaş[b], Boaz Ilan[a,*]

[a] *Department of Applied Mathematics, University of Colorado, Campus Box 526, Boulder, CO 80309-0526, USA*
[b] *Department of Mathematics, Istanbul Technical University, Maslak 34469, Istanbul, Turkey*

Received 10 October 2004; received in revised form 30 March 2005; accepted 3 June 2005
Available online 22 June 2005
Communicated by A.C. Newell

Abstract

Wave collapse is investigated in nonlocal nonlinear Schrödinger (NLS) systems, where a nonlocal potential is coupled to an underlying mean term. Such systems, here referred to as NLS-Mean (NLSM) systems, are also known as Benney–Roskes or Davey–Stewartson type and they arise in studies of shallow water waves and nonlinear optics. The role of the ground-state in global-existence theory is elucidated. The ground-state is computed using a fixed-point method. The critical-powers for collapse predicted by the Virial Theorem, global-existence theory, and by direct numerical simulations of the NLSM are found to be in good agreement with each other for a wide range of parameters. The ground-state profile in the water-wave case is found to be generically narrower along the direction of propagation, whereas in the optics case it is generically wider along the axis of linear polarization. In addition, numerical simulations show that NLSM collapse occurs with a quasi self-similar profile that is a modulation of the corresponding astigmatic ground-state, which is in the same spirit as in NLS collapse. It is also found that NLSM collapse can be arrested by small nonlinear saturation.

Keywords: Blowup; Singularity formation; Modulated nonlinear waves

1. Introduction

Nonlinear waves problems are of wide physical and mathematical interest and arise in a variety of scientific fields such as nonlinear optics, fluid dynamics, plasma physics, etc. (cf. [7,36]). The solutions of the governing nonlinear

* Corresponding author. Tel.: +1 303 492 4543; +1 303 492 4066.
E-mail address: boaz@colorado.edu (B. Ilan).

0167-2789/$ – see front matter © 2005 Elsevier B.V. All rights reserved.
doi:10.1016/j.physd.2005.06.001

waves equations often exhibit important phenomena, such as stable localized waves (e.g., solitons), self-similar structures, chaotic dynamics and wave singularities such as shock waves (derivative discontinuities) and/or wave collapse (i.e., blowup) where the solution tends to infinity in finite time or finite propagation distance. A prototypical equation that arises in *cubic media*, such as Kerr media in optics, is the (2+1)D focusing cubic nonlinear Schrödinger equation (NLS),

$$\mathrm{i}u_z(x, y, z) + \tfrac{1}{2}\Delta u + |u|^2 u = 0, \qquad u(x, y, 0) = u_0(x, y), \tag{1}$$

where u is the slowly-varying envelope of the wave, z is the direction of propagation,[1] (x, y) are the transverse directions, $\Delta u \equiv u_{xx} + u_{yy}$, and u_0 is the initial conditions. Remarkably, in 1965 Kelley [23] carried out direct numerical calculations of (1) that indicated the possibility of wave collapse. In 1970, Vlasov et al. [34] proved that solutions of Eq. (1) satisfy the following "Virial Theorem" (also called Variance Identity)

$$\frac{\mathrm{d}^2}{\mathrm{d}z^2}\int (x^2 + y^2)|u|^2 = 4H, \qquad H = \frac{1}{2}\int (|\nabla u_0|^2 - |u_0|^4), \tag{2}$$

where $\nabla \equiv (\partial_x, \partial_y)$, the integrations are carried over the (x, y) plane, and H, which is a constant of motion, is the Hamiltonian of Eq. (1). Using the Virial Theorem, Vlasov et al. concluded that the solution of the NLS can become singular in finite distance (or time), because a positive-definite quantity could become negative for initial conditions satisfying $H < 0$. On the other hand, Weinstein [35] showed that when the power (which is also conserved) is sufficiently small, i.e., $N = \int |u_0|^2 = \text{constant} < N_c \approx 1.8623\pi$, the solution exists globally, i.e., for all $z > 0$. Therefore, a *sufficient condition* for collapse is $H < 0$ while a *necessary condition* for collapse is $N > N_c$. Weinstein also found that the *ground-state* of the NLS plays an important role in the collapse theory. This ground-state is a "stationary" solution of the form $u = R(r)\,\mathrm{e}^{\mathrm{i}z}$, such that R is radially-symmetric, positive, and monotonically decaying. Papanicolaou et al. [27] studied the singularity structure near the collapse point and showed asymptotically and numerically that collapse occurs with a (quasi) self-similar profile. The readers are referred to [30] for a comprehensive review of related studies. Recent research by Merle and Raphael [26] further elaborated on the collapse behavior of NLS Eq. (1) and related equations, allowing for detailed understanding of the self-similar asymptotic profile. Furthermore, Gaeta and coworkers [24] recently carried out detailed optical experiments in cubic media that reveal the nature of the singularity formation and showed experimentally that collapse occurs with a self-similar profile.

On the other hand, there are considerably fewer studies of wave collapse that arises in nonlinear media, whose governing system of equations have *quadratic nonlinearities*, such as water waves and $\chi^{(2)}$ nonlinear-optical media. Here we discuss a class of such systems, denoted as NLS-Mean (NLSM) systems, which are sometimes referred to as Benney and Roskes [8] or Davey and Stewartson [13] type. The physical derivation of NLSM systems in water waves and nonlinear optics is reviewed in Section 2. Broadly speaking, the derivation of NLSM systems is based on an expansion of the slowly-varying (i.e., quasi-monochromatic) wave amplitude in the first and second harmonics of the fundamental frequency, as well as a mean term that corresponds to the zeroth harmonic. This leads to a system of equations that describes the nonlocal-nonlinear coupling between a dynamic field that is associated with the first harmonic (with a "cascaded" effect from the second harmonic), and a static field that is associated with the mean term (i.e., the zeroth harmonic). For the physical models considered in this study, the general NLSM system can be written in the following non-dimensional form,

$$\mathrm{i}u_z + \tfrac{1}{2}(\sigma_1 u_{xx} + u_{yy}) + \sigma_2 u|u|^2 - \rho u\phi_x = 0, \quad \phi_{xx} + \nu\phi_{yy} = (|u|^2)_x, \tag{3}$$

where $u(x, y, t)$ corresponds to the field associated with the first-harmonic, $\phi(x, y, t)$ corresponds to the mean field, σ_1 and σ_2 are ± 1, and ν and ρ are real constants that depend on the physical parameters. It is well-known

[1] In this study z plays the role of the evolution variable (i.e., like time).

that System (3) can admit collapse of localized waves when $\sigma_1 = \sigma_2 = 1$ and $\nu > 0$. In that case, the governing equations are

$$iu_z + \tfrac{1}{2}\Delta u + |u|^2 u - \rho u \phi_x = 0, \tag{4a}$$

$$\phi_{xx} + \nu \phi_{yy} = (|u|^2)_x, \tag{4b}$$

where $\nu > 0$ and ρ is real, and the initial conditions are $u(x, y, 0) = u_0(x, y)$, $\phi(x, y, 0) = \phi_0(x, y)$, such that Eq. (4b) is satisfied at $z = 0$, i.e., $\phi_{0,xx} + \nu\phi_{0,yy} = (|u_0|^2)_x$. The goal of this study is to further investigate the collapse dynamics in the NLSM System (4).

We note that System (4) reduces to the classical NLS Eq. (1) when $\rho = 0$, because in that case the mean field ϕ does not couple to the harmonic field u in Eq. (4a). In addition, when $\nu = 0$ Eq. (4b) gives that $\phi_x = |u|^2$ and, therefore, Eq. (4a) reduces to a classical NLS Eq. (1) with the cubic term $(1 - \rho)|u|^2 u$. As we shall see, in optics $\rho > 0$, whereas in water waves $\rho < 0$. In either case, i.e., when $\rho \neq 0$, the NLSM System (4) is a nonlocal system of equations. Indeed, since $\nu > 0$, Eq. (4b) can be solved as

$$\phi(x, y, z) = \int_{-\infty}^{\infty} G(x - x', y - y') \frac{\partial}{\partial x'} |u(x', y', z)|^2 \, dx' \, dy',$$

where $G(x, y)$ is the usual Green's function. For Eq. (4b) $G(x, y) = (4\pi)^{-1} \log(x^2 + y^2/\nu)$, which corresponds to a strongly-nonlocal function ϕ. While one might have expected the strong-nonlocality in the NLSM to arrest the collapse process, generally speaking, that is not the case for System (4). Moreover, there is a striking mathematical similarity between collapse dynamics in the NLS and NLSM cases.

The paper is organized as follows:

(1) In Section 2 NLSM systems in water waves and in nonlinear optics are discussed.
(2) In Section 3 the theory of collapse and global existence in NLS and NLSM equations is reviewed. In addition, the Hamiltonian is used to explain why collapse in the case of water waves ($\rho < 0$) is relatively easier to attain, and also occurs more quickly, than in the case of nonlinear optics ($\rho > 0$).
(3) Using global existence theory and numerical calculations of the ground-state, in Section 4 the necessary condition for collapse is explored in terms of the parameters ν and ρ in the NLSM System (4). Using the Virial Theorem and the Hamiltonian, a sufficient condition for collapse is found for Gaussian input beams, explicitly in terms of ν, ρ, and the input power. These theoretical results are found to be consistent with numerical simulations of the NLSM System (4) and are also consistent with the numerical results of Crasovan et al. [12] for nonlinear optics ($\rho > 0$). In addition, the effect of input astigmatism in the initial conditions on the critical power for collapse is studied (Section 4.1]). Furthermore, in Section 4.2 it is shown that the NLSM can admit collapse even without the cubic term [i.e., without $|u|^2 u$ in Eq. (4a)].
(4) In Section 5 the astigmatism of the NLSM ground-state is explored in the (ν, ρ) parameter space. It is found that the ground-state is relatively more astigmatic for nonlinear optics ($\rho > 0$) than for water waves ($\rho < 0$). In addition, the dependence of the astigmatism of the ground-state on ν is found to be weaker than its dependence on ρ.
(5) In Section 6 simulations of the NLSM System (4) show that the collapsing solution is well described by a quasi self-similar profile that is given in terms of a modulation of the corresponding ground state, a result that is in the same spirit as for the NLS equation and also strengthens the results of Papanicolaou et al. [28]. However, in [28] the ground-state itself was not computed and, in turn, it was not shown numerically that the asymptotic profile approaches the corresponding ground-state. In this study numerical simulations directly show that the collapsing wave approaches a quasi self-similar modulation of the corresponding ground-state. To calculate the ground-state a fixed-point algorithm is used, which has been previously applied in dispersion-managed NLS theory (see Appendix C).

(6) In Section 7 numerical simulations are used to show that NLSM collapse can be arrested by a small saturation of the cubic nonlinearity, a phenomenon that can be explained using the results of Fibich and Papanicolaou [19] for the the perturbed NLS.

2. NLSM systems in water waves and nonlinear optics

Below we review some of the main results from the derivations of NLSM systems, with an emphasis on collapse.

2.1. Water waves

In the context of free-surface gravity-capillary water waves, NLSM equations result from a weakly-nonlinear quasi-monochromatic expansion of the velocity potential as

$$\phi(x, y, t) \sim \varepsilon[\tilde{A}\mathrm{e}^{\mathrm{i}(kx-wt)} + \text{c.c.} + \tilde{\Phi}] + \varepsilon^2[\tilde{A}_2\mathrm{e}^{2\mathrm{i}(kx-wt)} + \text{c.c.}] + \cdots, \tag{5}$$

where x is the direction of propagation, y the transverse direction, t the time, $\varepsilon \ll 1$ a measure of the (weak) nonlinearity, $\tilde{A}$, $\tilde{A}_2$, and $\tilde{\Phi}$ are slowly varying functions of (x, y, t), which correspond to the coefficients of the first, second, and zeroth harmonics, respectively, "c.c." denotes complex conjugate of the term to its left, and the frequency ω satisfies the dispersion relation $\omega^2(\kappa) = (g\kappa + T\kappa^3)\tanh(\kappa h)$, where g is the gravity acceleration, T is the surface tension coefficient, and $\kappa = \sqrt{k^2 + l^2}$, where (k, l) are the wave-numbers in the (x, y) directions, respectively. Substituting the wave expansion (5) into the water-wave equations (i.e., Euler's equation with a free surface) and assuming slow modulations of the field in the x and y directions results in a nonlinearly-coupled system for $\tilde{A}$ and $\tilde{\Phi}$. After non-dimensionalization, i.e., $(A, \Phi) = (\tilde{A}, \tilde{\Phi})k^2/\sqrt{gh}$, one finds the general NLSM system [6]

$$\mathrm{i}A_\tau + \lambda A_{\xi\xi} + \mu A_{\eta\eta} = \chi|A|^2A + \chi_1 A\Phi_\xi, \tag{6a}$$

$$\alpha\Phi_{\xi\xi} + \Phi_{\eta\eta} = -\beta(|A|^2)_\xi, \tag{6b}$$

where $\xi = \varepsilon k(x - c_\mathrm{g}t)$, $\eta = \varepsilon l y$ and $\tau = \varepsilon^2\sqrt{gk}\,t$ are dimensionless coordinates, and $c_\mathrm{g} = \partial\omega/\partial k$ is group velocity. The coefficients $\lambda, \mu \geq 0$, χ, $\chi_1 \geq 0$, α and $\beta \geq 0$ are suitable functions of h, T, k, c_g, and the second-order dispersion coefficients $\partial^2\omega/\partial k^2$ and $\partial^2\omega/\partial l^2$. We note that in the derivation of System (6) $\tilde{A}_2$ is expressed in terms of $\tilde{A}$, which accounts for the fact that A_2 does not appear explicitly in the resulting system.[2]

NLSM equations were originally obtained by Benney and Roskes [8] in their study of the instability of wave packets in water of finite depth h, without surface tension. In 1974, Davey and Stewartson [13] studied the evolution of a 3D wave packet in water of finite depth and obtained a different, although equivalent, form of these equations. In 1975 Ablowitz and Haberman [4] studied the integrability of systems such as (6). These integrable systems correspond to the Benney–Roskes equations in the shallow water limit. In 1977, Djordevic and Reddekopp [14] extended the results of Benney and Roskes to include surface tension. Subsequently, Ablowitz and Segur [6] investigated System (6) or, equivalently, System (3). They showed that the shallow water limit, i.e., $h \to 0$, corresponds to $\sigma_1 \to -\nu = \pm 1$, and $\rho \to 2$ in System (3). The resulting equations agreed with those obtained by Ablowitz and Haberman [4]. Hence, the shallow-water limit of System (6) is integrable and can be obtained from an associated compatible linear scattering system. In [21] these reduced equations were linearized by the inverse scattering transform (see also [3]).

Subsequently, Ablowitz and Segur [6] studied the NLSM System (6) in the non-integrable case. In this parameter regime, System (6) can be transformed by a rescaling of variables to System (3) with $\sigma_1 = \sigma_2 = 1$ and $\nu > 0$, i.e.,

[2] A similar observation holds in the optics case mentioned below.

the so called focusing elliptic–elliptic case, which, physically speaking, requires sufficiently large surface tension. They found that System (6) preserves the Hamiltonian

$$H = \int \left[\lambda \left| \frac{\partial A}{\partial \xi} \right|^2 + \mu \left| \frac{\partial A}{\partial \eta} \right|^2 \right] - \frac{1}{2} \int \left[(-\chi)|A|^4 + \frac{\alpha \chi_1}{\beta} (\Phi_\xi)^2 + \frac{\chi_1}{\beta} (\Phi_\eta)^2 \right], \tag{7}$$

where the first and second integrals correspond to the second-derivative and the nonlinear terms in Eq. (6a), respectively, and the integrations are carried over the (ξ, η) plane. When, in addition to the physical requirements $\mu \geq 0$, $\beta \geq 0$, and $\chi_1 \geq 0$, one has that $\lambda > 0$, $-\chi > 0$, and $\alpha > 0$, the first and second integral terms in (7) are positive and negative-definite, respectively. This corresponds to the self-focusing regime. Clearly, in that case $H < 0$ is possible for sufficiently large initial conditions.[3] Furthermore they proved that the following Virial Theorem holds

$$\frac{\partial^2}{\partial \tau^2} \int \left(\frac{\xi^2}{\lambda} + \frac{\eta^2}{\mu} \right) |A|^2 = 8H.$$

As can be seen, if $H < 0$, the moment of inertia vanishes at a finite time. In that case, as for the NLS case mentioned above, this indicates finite-distance singularity formation. We note that in the same study collapse solutions with the self-similar profile were also investigated, i.e., with $|A| \sim L^{-1} f(\frac{x}{L}, \frac{y}{L})$, where $L = L(t)$ approaches zero during the collapse.

2.2. Nonlinear optics

The electric polarization field of intense laser beams propagating in optical media an be expanded in powers of the electric field as

$$P = \chi^{(1)} \times E + \chi^{(2)} \times E \times E + \chi^{(3)} \times E \times E \times E + \cdots, \tag{8}$$

where $E = (E_1, E_2, E_3)$ the electric field vector and $\chi^{(j)}$ are the susceptibility tensor coefficients of the medium. In isotropic Kerr media, where the nonlinear response of the material depends cubically [i.e., through $\chi^{(3)}$ and when $\chi^{(2)} \equiv 0$] and instantaneously on the applied field, the dynamics of a quasi-monochromatic optical pulse is governed by the NLS Eq. (1) (cf. [9,23,31]). It turns out that NLSM type equations also arise in nonlinear optics when studying media with a non-zero $\chi^{(2)}$ [even when $\chi^{(3)} \equiv 0$], i.e., materials that have a *quadratic* nonlinear response. Such materials are anisotropic, e.g., crystals whose optical refraction has a preferred direction.

Ablowitz et al. [1,2] found, from first principles, that NLSM type equations describe the evolution of the electromagnetic field in such quadratically [i.e., $\chi^{(2)}$] polarized media. Both scalar and vector (3+1)D NLS systems were obtained. Briefly, in this derivation one assumes a quasi-monochromatic expansion of the x component of the electromagnetic field (which is primarily linearly-polarized), with the fundamental harmonic, second-harmonic, and a mean term as

$$E_1 \sim \varepsilon [A\, \mathrm{e}^{\mathrm{i}(kx-\omega t)} + \text{c.c.}] + \varepsilon^2 [A_2\, \mathrm{e}^{2\mathrm{i}(kx-\omega t)} + \text{c.c.} + \phi_x] + \cdots, \tag{9}$$

where A, A_2, and ϕ are slowly varying functions of (x, y, t), which correspond to the first, second, and zeroth harmonics, respectively. Using a polarization field of the form (8) in Maxwell's equations leads to the system of equations

$$[2\mathrm{i}k\partial_Z + (1 - \alpha_{x,1})\partial_{XX} + \partial_{YY} - kk''\partial_{TT} + M_{x,1}|A|^2 + M_{x,0}\phi_x]A = 0, \tag{10a}$$

$$[(1 - \alpha_{x,0})\partial_{XX} + \partial_{YY} + s_x\partial_{TT}]\phi_x - \alpha_{y,0}\partial_{XY}\phi_y = (N_{x,1}\partial_{TT} - N_{x,2}\partial_{XX})|A|^2, \tag{10b}$$

[3] Note that from Eq. (6b) Φ scales as $|A|^2$, so all the terms in the second integral of (7) scale like $|A|^4$.

where $\alpha_{x,0}$, $\alpha_{x,1}$, $\alpha_{y,0}$, and s_x depend on the linear polarization term $\chi^{(1)}$; $M_{x,0}$, $N_{x,1}$, and $N_{x,2}$ depend on the nonlinear polarization terms $\chi^{(2)}$ and $\chi^{(3)}$; and $M_{x,1}$ depends on products of $\chi^{(2)}$ and $\chi^{(3)}$. Physically speaking, the dependence of $M_{x,1}$ on $\chi^{(2)}$ and $\chi^{(3)}$ corresponds to the fact that the second-harmonic (i.e., $\tilde{A}_2$) is coupled to the first harmonic (i.e., $\tilde{A}_1$), a process that is sometimes referred to as "optical rectification" or "cascaded" optical effect. However, as in the water-wave case, here too $\tilde{A}_2$ is expressed in terms of $\tilde{A}$, which is why A_2 does not appear explicitly in the resulting system (10). In addition, similar to the water-wave case, the term with $M_{x,0}$ in System (10a) couples the mean field to the first-harmonic field. Interestingly, when the time dependence in these equations is neglected ($\partial_T \equiv 0$) and for media with a special symmetry class such that $\alpha_{y,0} = 0$, it can be seen that, after proper rescaling, the governing system of equation is given by System (4). In [32] these equations were further elucidated and the coefficients described in terms of the electro-optic effect.

From the point of view of perturbation analysis, it is interesting to remark that in the expansion of the field in the case of water-waves [i.e., Eq. (5)], the mean term $\tilde{\Phi}$ appears as an $O(\varepsilon)$ term, whereas in the in the case of optics [i.e., Eq. (9)], the mean term ϕ_x appears as an $O(\varepsilon^2)$ term. However, the physically measurable quantity in water waves is $\tilde{\Phi}_x$, which scales like $O(\varepsilon^2)$, because $\tilde{\Phi}$ is slowly-varying. Therefore, the expansions in the water-wave and optics cases are, in fact, analogous from the viewpoint of perturbation analysis.

Wave collapse in such NLSM systems was recently investigated numerically by Crasovan et al. [12]. They solved the following normalized system of equations,

$$\mathrm{i}U_z + \tfrac{1}{2}\Delta U + |U|^2 U - \rho UV = 0, \tag{11a}$$

$$V_{xx} + \nu V_{yy} = (|U|^2)_{xx}, \tag{11b}$$

where U is the normalized amplitude of the envelope of the electric field, V the normalized static field, ρ a coupling constant that comes from the combined optical rectification and electro-optic effects, and ν corresponds to the anisotropy coefficient of the medium. They solved System (11) numerically with Gaussian initial conditions for U. The regions of collapse were investigated for various values of the parameters ρ and ν. We note that System (11) is a simple mathematical modification of the NLSM System (4). Indeed, starting with the NLSM System (4), taking the derivative of Eq. (4b) with respect to x, and defining the new variable (potential) $V = \phi_x$, one finds that the resulting system is identical to (11).

3. Global existence, collapse, and the ground-state

We begin by briefly outlining some of the known results for the NLS and NLSM equations. Two conserved quantities for the NLS Eq. (1) and NLSM System (4) are the power, i.e.,

$$N(u) = \int |u|^2 = N(u_0), \tag{12}$$

where the integrations (here and below) are carried over the (x, y) plane, and the Hamiltonian, i.e.,

$$H_{\mathrm{NLS}}(u) = \frac{1}{2}\int |\nabla u|^2 - \frac{1}{2}\int |u|^4 = H_{\mathrm{NLS}}(u_0),$$

$$H_{\mathrm{NLSM}}(u, \phi) = \frac{1}{2}\int |\nabla u|^2 - \frac{1}{2}\int |u|^4 + \frac{\rho}{2}\int (\phi_x^2 + \nu\phi_y^2) = H_{\mathrm{NLSM}}(u_0, \phi_0), \tag{13}$$

where H_{NLS} and H_{NLSM} correspond to Eq. (1) and System (4), respectively, and ϕ in (13) is obtained from Eq. (4b). In addition, the Virial Theorem holds (cf. [6]),

$$\frac{\partial^2}{\partial z^2}\int (x^2 + y^2)|u|^2 = 4H, \tag{14}$$

where H is the corresponding Hamiltonian, i.e., either H_{NLS} or H_{NLSM}. We are interested in the localized-decaying case, when u and ϕ vanish sufficiently rapidly at infinity to be in the Sobolev space H_1, i.e., $\int |u|^2 + \int |\nabla u|^2 < \infty$ and similarly for ϕ. We note that within the context of the water-wave problem (i.e., $\rho < 0$), existence and well-posedness of solutions of System (4) were studied in [22]. Singularity formation corresponds to finite-time (or finite-distance) blowup in H_1. Since the L_2 norm is conserved (12), blowup in H_1 amounts to $\lim_{z\to Z_c} \int |\nabla u|^2 = \infty$, where Z_c is the collapse distance. In fact, it is well-known in NLS and NLSM theories that when a singularity occurs, the peak amplitude of the wave blows-up as well, i.e., $\lim_{z\to Z_c} \max_{(x,y)} |u(x, y, z)| = \infty$.

When $H < 0$ it follows from the Virial Theorem (14) that the solution becomes singular in finite time. This gives a *sufficient condition* for collapse. On the other hand, a *necessary condition* for collapse can be obtained using the associated ground-state, as reviewed below. We note that the Hamiltonian (13) is comprised of three integrals, the first of which is positive definite, the second negative definite, and, when $\nu \geq 0$, the third integral is definite with a sign that is determined by ρ. Generally speaking, NLS (and NLSM) theory shows that the positive-definite terms correspond to defocusing mechanisms, while the negative-definite terms correspond to focusing mechanisms. Thus, it follows that when $\rho > 0$, i.e., in the optics case, the coupling to the mean field corresponds to a self-defocusing mechanism, while when $\rho < 0$, i.e., the water-wave case, it corresponds to a self-focusing effect in addition to the cubic term in the NLS Eq. (1). In other words, loosely speaking, one can expect that self-focusing in the water-wave case is "easier" to attain than in the optics case (see Sections 4 and 6 for details).

A stationary solution of the NLSM System (4) is a solution of the form $u(x, y, z) = F(x, y)\, \mathrm{e}^{\mathrm{i}\lambda z}$ and $\phi(x, y, z) = G(x, y)$, where F and G are real functions and λ is a positive real number. Substituting this ansatz into System (4) gives

$$-\lambda F + \tfrac{1}{2}\Delta F + F^3 - \rho F G_x = 0, \tag{15a}$$

$$G_{xx} + \nu G_{yy} = (F^2)_x. \tag{15b}$$

Similarly, the NLS stationary solutions, which are obtained by substituting $u = R(x, y)\, \mathrm{e}^{\mathrm{i}\lambda z}$ into the NLS Eq. (1), satisfy

$$-\lambda R + \tfrac{1}{2}\Delta R + R^3 = 0. \tag{16}$$

The *ground-state* of the NLS[4] can be defined as a solution in H_1 of Eq. (16) for a given λ having minimal power of all the nontrivial solutions. The existence and uniqueness of the ground state have been proven, as also the fact that it is radially-symmetric, positive, and monotonically decaying (see [30]). Since $R(r; \lambda) = \sqrt{\lambda} R(\sqrt{\lambda}\, r; 1)$, it suffices to consider the case $\lambda = 1$, for which the solution is henceforth denoted by R. Furthermore, Weinstein [35] proved that the NLS ground-state is a minimizer of a Gagliardo-Nirenberg inequality that is associated with the NLS Hamiltonian. To be precise, the functional

$$J(u) = \frac{\|u\|_2^2\, \|\nabla u\|_2^2}{\|u\|_4^4}, \qquad \|u\|_p^p \equiv \int |u|^p,$$

attains its minimum for $u \in H_1$ when $u(x, y) = R(r)$, where R is the ground-state of Eq. (16) and $J(R) = 2/N_c$, where $N_c \equiv \int R^2$. Moreover, Weinstein proved that when $N < N_c$, the NLS solution exists globally (i.e., for all $z > 0$) in H_1. In addition, it is not difficult to show (cf. Appendix A) that any stationary solution, in particular the ground-state, admits a zero Hamiltonian, i.e., $H_{\mathrm{NLS}}(R) = 0$. These results can be used to explain why the ground-state may be considered to be on the borderline between existence and collapse. Indeed, consider the initial conditions $u_0 = (1 + \varepsilon)R(r)$ with $\varepsilon =$ constant. When $\varepsilon < 0$ then $N < N_c$ and, therefore, the solution exists globally. On the other hand, when $\varepsilon > 0$ then $H < 0$ and, therefore, finite-distance collapse is guaranteed by the Virial Theorem

[4] R, the NLS ground-state, is sometimes referred to as the Townes profile.

(cf. [35]). We note that $N \geq N_c$ is only a necessary condition for collapse, i.e., there are solutions with $N > N_c$ that exist globally.

Similarly to the NLS case, the ground-state of System (15) can be defined as the nontrivial solution (F, G) in H_1, such that F has minimal power. Cipolatti [10] proved the existence of the ground-state. In the same spirit as for the NLS, Papanicolaou et al. [28] defined the ground-state as the minimizer the associated functional[5]

$$J(u) = \frac{\|u\|_2^2 \, \|\nabla u\|_2^2}{\int [|u|^4 + \mathcal{B}(u) u^{*2}]}, \qquad \mathcal{B}(u) \equiv \mathcal{F}^{-1}\left[\frac{\rho k_x^2}{k_x^2 + \nu k_y^2} \mathcal{F}[|u|^2]\right],$$

where $\mathcal{F}$ and $\mathcal{F}^{-1}$ denote the Fourier Transform operator and its inverse, respectively (see Appendix B). They extended global existence theory to the NLSM and proved the following.

Theorem 3.1. *Consider System (4) with initial conditions $u_0 \in H_1$. Let F be the nontrivial minimizer of $J(u)$ above, and let N_c be defined as*

$$N_c(\nu, \rho) \equiv \int F^2(x, y; \nu, \rho). \tag{17}$$

Then F is a positive function and, therefore, $N_c > 0$. In addition, if $\int |u_0|^2 < N_c$ the solution of System (4) exists in H_1 for all $z > 0$.

In other words, solutions of the NLSM System (4) exist globally when their power is smaller than the power of the corresponding ground-state.

On the other hand, since the ground-state is a stationary solution, in analogy to $H_{\mathrm{NLS}}(R) = 0$, one has also (see Appendix A)

Proposition 3.2. *Let (F, G) be a solution of System (15). Then*

$$H_{\mathrm{NLSM}}(F, G) \equiv \frac{1}{2}\int (\nabla F)^2 - \frac{1}{2}\int F^4 + \frac{\rho}{2}\int (\nabla_\nu G)^2 = 0, \tag{18}$$

where $(\nabla_\nu G)^2 \equiv G_x^2 + \nu G_y^2$.

Therefore, it follows from Theorem 3.1, the Virial Theorem (14), and Proposition 3.2 that, as in the NLS case, the NLSM ground-state is neutrally-stable and may be considered to be on the borderline between global existence and collapse.

4. Collapse and global-existence regions

In this section System (4) is considered with the Gaussian initial conditions

$$u_0^G(x, y) = \sqrt{\frac{2N}{\pi}}\, \mathrm{e}^{-(x^2+y^2)}, \tag{19}$$

where $N = N(G)$ is the input power of u_0^G. The collapse and global-existence regions in the NLSM System (4) are explored in the (N, ν, ρ) parameter space using the results obtained from the Virial Theorem (14), the global-existence Theorem (3.1), and direct (2+1)D numerical simulations of the NLSM System (4).

[5] Note that from Eq. (4b) $\phi_x = \rho^{-1}\mathcal{B}(u)$.

The critical power $N_c(\nu, \rho)$ is calculated from the ground-state [see Eq. (17)], which is found by using a numerical method that is explained in Appendix C. For the NLSM simulations a standard fourth order accurate Runge-Kutta integration is used, with a fourth order accurate spatial finite-difference stencil. The computational domain is a truncation of the (x, y) plane with Dirichlet boundary-conditions at $|x| = L$ and $|y| = L$, where L is taken sufficiently large, so to assure that the results are independent of reflections from the outer boundaries.

Substituting the initial-conditions (19) into the NLSM Hamiltonian (13) gives (see Appendix B)

$$H(u_0^G, \phi_0^G) = N - \left(1 - \frac{\rho}{1+\sqrt{\nu}}\right)\frac{N^2}{2\pi}. \tag{20}$$

It follows from (20) and the Virial Theorem (14) that for the Gaussian initial conditions (19) there is a *threshold power* for which $H = 0$, given by

$$N_c^H(\nu, \rho) \equiv \frac{2\pi}{1 - \rho/(1+\sqrt{\nu})}, \tag{21}$$

such that when $N > N_c^H$ then $H < 0$ and, therefore, the solution collapses at finite distance. We note that this condition makes sense only when $0 < N_H < \infty$, which implies $\rho < 1 + \sqrt{\nu}$. Conversely, when either $\rho \geq 1 + \sqrt{\nu}$ (no matter how large N) or $N \leq N_c^H$, then $H \geq 0$, in which case collapse is not guaranteed by the Virial Theorem.

Fig. 1 compares the critical power for collapse, N_c (17), the threshold-power N_c^H (21), and the "actual" power for collapse found from numerical simulations of the NLSM System (4), where the latter is obtained by gradually increasing the input power (or amplitude), i.e., N in the initial conditions (19), until the solution undergoes collapse. This figure also shows that for $\nu = 0.5$ and $-1 \leq \rho \leq 1$, N_c^H (21) is quite close to N_c, which, in turn, is very close to the numerically obtained threshold power for collapse in the NLSM System (4). For example, for the classical NLS (i.e., $\rho = 0$) the discrepancy between $N_c(R) \approx 1.86\pi$ and $N_c^H(R) = 2\pi$ is approximately 7% (see also [16]). In addition, in this entire parameter regime the discrepancy between N_c and the numerically-obtained threshold power is less than 2%. Furthermore, this figure shows that the change in the critical power with ρ is more pronounced for $\rho > 0$ than for $\rho < 0$. Similarly, Fig. 2 shows that for a wide range of the parameters, N_c^H (21) is a good approximation of N_c, which, in turn, is a good approximation of the numerically-obtained power for collapse. Furthermore, this figure shows that the critical power is weakly-dependent on ν, for either sign of ρ.

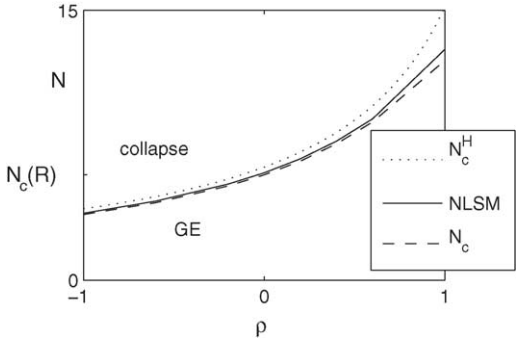

Fig. 1. The critical power for collapse as a function of ρ for $\nu = 0.5$ ($\rho < 0$ for water-waves and $\rho > 0$ for optics). N_c is obtained from the power of the ground-state [i.e., Eq. (17), dashes], N_c^H corresponds to $H = 0$ [i.e., Eq. (21), dotted], and the threshold power for collapse obtained by numerically integrating the NLSM [i.e., System (4) with (19), solid]. "GE" denotes global existence and "NLSM" denotes numerical simulations of System (4).

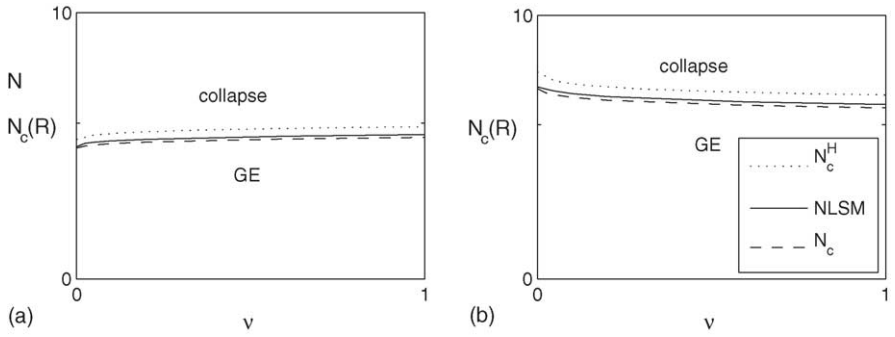

Fig. 2. Same as Fig. 1 with: (a) $\rho = -0.2$ and varying ν; (b) $\rho = 0.2$ and varying ν.

An alternative way of using Eq. (20) is to fix N and allow ν and ρ to vary. Thus, for a fixed N there is a *separatrix curve* in the (ν, ρ) plane for which $H = 0$, given by

$$\rho_c^H(N, \nu) \equiv \left(1 - \frac{2\pi}{N}\right)(1 + \sqrt{\nu}), \tag{22}$$

such that when $\rho < \rho_c^H$ then $H < 0$ and collapse is guaranteed by the Virial Theorem. These separatrix curves are depicted in Fig 3, which is consistent in the case of $\rho > 0$ with the results of Crasovan et al. [12].

As discussed in Section 3, larger (more positive) values of ρ correspond to more defocusing. In fact, the results in this section show that when $\rho < 0$, or when $\rho > 0$ and sufficiently small, the defocusing effect induced by the coupling to the mean field is weaker than the focusing effect induced by the cubic term in Eq. (4a). In that case, collapse is guaranteed by the Virial Theorem for sufficiently large input power. On the other hand, when $\rho > 0$ and is sufficiently large, the defocusing effect induced by the coupling to the mean field can overcome the focusing effect induced by the cubic term in Eq. (4a). In that case, the NLSM can effectively behave as a defocusing NLS-type equation, i.e., like Eq. (1) with a negative sign before the cubic term.

We emphasize that $H \geq 0$ does not imply GE, because $H < 0$ is only a sufficient condition for collapse, not a necessary one. Nevertheless, owing to their explicitness and apparent accuracy, conditions (21) and (22) can be useful for predicting for the boundary in the (N, ν, ρ) space between the regions of collapse and GE. On the

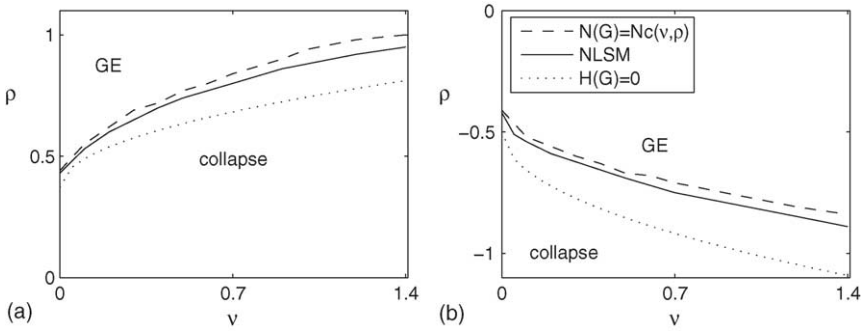

Fig. 3. The regions in the (ν, ρ) plane corresponding to collapse and global-existence (GE). Equating the power of the ground-state, $N_c(\nu, \rho)$ [i.e., Eq. (17)], to the power $N(G)$ of the initial conditions (19) [dashes, denoted by $N(G) = N(\nu, \rho)$ in the legend], ρ_c^H obtained from $H = 0$ [i.e., Eq. (22), dotted, denoted by $H(G) = 0$ in the legend], and using numerical simulations of the NLSM [i.e., System (4), solid] for: (a) nonlinear optics (i.e., $\rho > 0$) and the initial conditions (19) with the fixed input power $N(G) = 10$; (b) water waves (i.e., $\rho < 0$) and the initial conditions (19) with $N(G) = 4\pi/3$.

other hand, the condition derived from GE theory appears to be more accurate in the following sense: the actual (numerical) critical power appears to be slightly closer to N_c than to N_c^H. We note that in [16] a similar conclusion was reached for the NLS Eq. (1) when using Gaussian as well as other types of initial conditions.

4.1. Input astigmatism

It is interesting generalize the results above to the case when the initial conditions are astigmatic. To do that, consider the astigmatic Gaussian initial conditions

$$u_0^E(x, y) = \sqrt{\frac{2EN}{\pi}}\, \mathrm{e}^{-[(Ex)^2+y^2]}, \tag{23}$$

where N is the input power and E is input ellipticity. Here $E = 1$ corresponds to radial symmetry, whereas $0 < E < 1$ and $E > 1$ correspond to relative elongation along the x and y axes, respectively.

Similar to Eq. (20), one arrives at (see Appendix B)

$$H(u_0^E, \phi_0^E) = \frac{1+E^2}{2}N - \left(1 - \frac{\rho}{1+\sqrt{\nu}/E}\right)\frac{EN^2}{2\pi}. \tag{24}$$

Thus, denoting

$$N_c^H(\nu, \rho, E) \equiv \frac{(E+1/E)\pi}{1-\rho/(1+\sqrt{\nu}/E)}, \tag{25}$$

it follows that when $N > N_c^H$ then $H < 0$ and, therefore, the solution collapses at finite distance. This condition makes sense only when $0 < N_H < \infty$, which implies that $\rho < 1 + \sqrt{\nu}/E$.

Generally speaking, N_c^H increases with astigmatism. For example, let us consider the optics case with $0 < \rho < 1 + \sqrt{\nu}/E$ with an input beam (23) that is "focused" along the x direction, i.e., has $E > 1$. As E increases it will approach the value $E_c = \sqrt{\nu}/(\rho - 1)$, for which $N_c^H = \infty$. Physically speaking, this results suggests that as the input beam becomes narrower along the x-axis, the critical power for collapse increases, making the collapse more difficult to attain. This conclusion is consistent with the numerical observations of Crasovan et al. [12] in the optics case, and is in the same spirit as the results of Fibich and Ilan [17] for the NLS case (i.e., $\rho = 0$).

In addition, for a given power N, the separatrix curve in the (ν, ρ) plane for which $H = 0$ is given by

$$\rho_c^H(N, \nu, E) \equiv \left[1 - \frac{(E+1/E)\pi}{N}\right]\left(1 + \frac{\sqrt{\nu}}{E}\right), \tag{26}$$

such that when $\rho < \rho_c^H$ then $H < 0$ and, therefore, collapse is guaranteed by the Virial Theorem.

4.2. Related NLSM-type system

Consider the NLSM System (4) without the cubic term, i.e.,

$$\mathrm{i}u_z + \tfrac{1}{2}\Delta u - \rho u\phi_x = 0, \tag{27a}$$

$$\phi_{xx} + \nu\phi_{yy} = (|u|^2)_x. \tag{27b}$$

One might expect that the nature of collapse in the NLSM-type System (27) would be similar to the NLSM System (4). Indeed, the analysis of System (27) is quite similar to that in Sections 3 and 4. The only difference is that the Hamiltonian corresponding to (27) is like (13), but without the second "self-focusing" integral, that is,

$$H(u, \phi) = \frac{1}{2}\int |\nabla u|^2 + \frac{\rho}{2}\int (\phi_x^2 + \nu\phi_y^2).$$

Since the Virial Theorem (14) remains unchanged, collapse is possible in System (27) whenever $\rho < 0$ and the initial conditions are sufficiently large. Furthermore, substituting the initial-conditions (19) into the Hamiltonian above gives

$$H(u_0, \phi_0) = N + \frac{\rho}{1+\sqrt{\nu}} \frac{N^2}{2\pi}.$$

It follows that the threshold power for which $H = 0$ is given by

$$N_c^H(\nu, \rho) \equiv -\frac{2\pi(1+\sqrt{\nu})}{\rho}.$$

Thus, similar to the NLSM case, the Virial Theorem guarantees that the solution of System (27) undergoes finite-distance collapse when $N > N_c^H$. To conclude, although the cubic term in the NLSM System (4) is self-focusing, its presence is not necessary for collapse to occur. In other words, collapse can occur even in the case when the nonlinearity is strictly and strongly nonlocal.

5. Astigmatic ground-states

Below we study how the astigmatism of the ground-state depends on ρ and ν. The astigmatism is recovered from the ground-state as

$$e(F) \equiv \frac{\int |(F^2)_x|}{\int |(F^2)_y|}. \tag{28}$$

It follows from (28) that $e = 1$ corresponds to a radially-symmetric ground-state, and $e < 1$ and $e > 1$ correspond to a ground-state that is relatively wider along the x and y axes, respectively. In other words, $e \approx L_y/L_x$, where L_x and L_y are the full-widths at half-max of the function.

Fig. 4(a) and (b) shows the on-axes amplitudes of the ground-state for $\rho = 0$ (i.e., the radially-symmetric R profile); $(\nu, \rho) = (0.5, -1)$; and $(\nu, \rho) = (0.5, 1)$. The contour plots in Fig. 4(c) and (d) correspond to the $\rho = -1$ and $\rho = 1$ cases, respectively. These plots clearly show that the ground-states with $\rho \neq 0$ are astigmatic. In addition, Fig. 5 shows the 3D plots and corresponding contour plots of the ground-state for $(\nu, \rho) = (4, -4)$, which has $e \approx 1.5$. Both $F(x, y)$ and the corresponding mean field $G(x, y)$ are clearly astigmatic. Furthermore, the mean field G is strongly nonlocal (see also Fig. 5d), as can be expected from the Poisson-type Eq. (15b) that is solves.

Fig. 6a shows that (i) the NLS ground-state ($\rho = 0$) is radially-symmetric, (i.e., $e = 1$); (ii) when $\nu = 0.5$ and $\rho < 0$ (water-waves) F is wider along the y-axis (i.e., $e > 1$); and (iii) when $\nu = 0.5$ and $\rho > 0$ (optics) F is wider along the x-axis (i.e., $e < 1$). We note that the parameter space explored in Figs. 1 and 6a is the same. Comparing these two figures, one sees that as ρ is changed from $\rho = 0$ (in either direction), the deviation from the NLS ground state is accompanied by a significant deviation in the critical power, as well as by a deviation from radial-symmetry. Therefore, as $|N_c(\nu, \rho) - N_c(\nu, 0)|$ increases with ρ, so does the astigmatism of the ground-state (along the x or y axes). On the other hand, Figs. 2 and 6b show that the critical power and the astigmatism are only weakly dependent on ν, for either sign of ρ. In addition, Fig. 6a shows that, for the same values of ν, the function F is relatively more astigmatic for $\rho > 0$ (i.e., for optics) than for $\rho < 0$ (i.e., for water waves).

In summary, one has the following *generic picture*:

(1) The ground-state profile in the water-wave case is narrower along the direction of propagation (i.e., $e > 1$), whereas in the nonlinear optics case it is wider along the axis of linear polarization (i.e., $e < 1$).

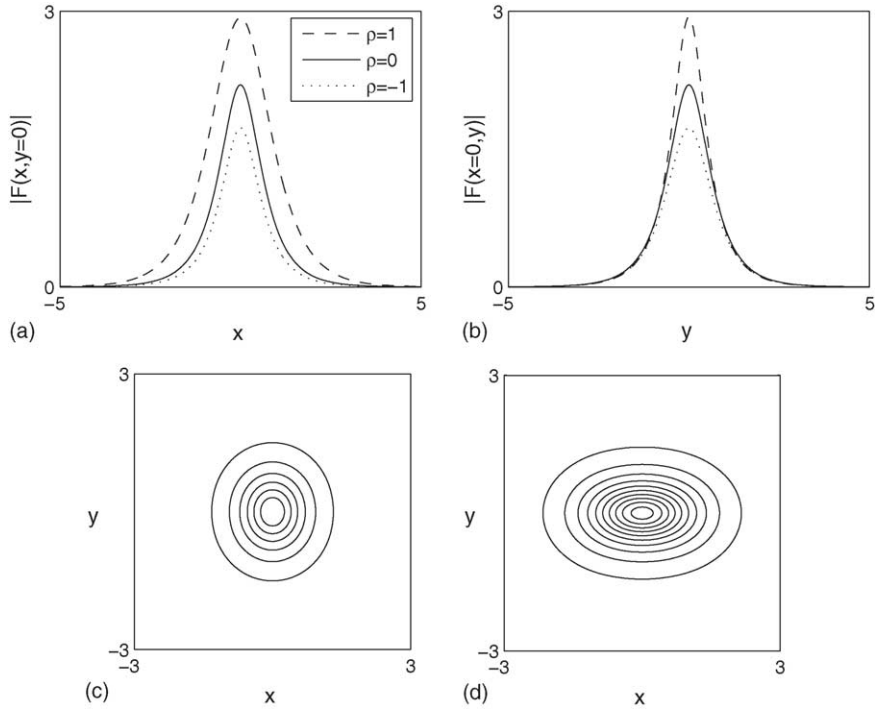

Fig. 4. Top: The on-axes amplitudes of the ground-state (a) along the y-axis and (b) along the x-axis for $(\nu, \rho) = (0.5, 1)$ (dashes), $\rho = 0$ (solid), and $(\nu, \rho) = (0.5, -1)$ (dotted). Bottom: Contour plots of $F(x, y)$ for: (c) $\rho = -1$ (corresponding to dotted above) with astigmatism [i.e., Eq. (28)] $e \approx 1.17$; (d) $\rho = 1$ (corresponding to dashes above) with $e \approx 0.59$.

(2) The ground-state is relatively more astigmatic for nonlinear optics ($\rho > 0$) than for water waves ($\rho < 0$).
(3) Whereas the astigmatism of the ground-state changes significantly with ρ, it depends only weakly on ν.

6. Quasi self-similar astigmatic collapse

Asymptotic analysis and numerical simulations strongly suggest that when collapse occurs in NLS Eq. (1), under quite general conditions, it occurs with a quasi self-similar profile that is a modulation (up to a phase) of the ground-state (cf. [30]), i.e.,

$$|u(x, y, z)| \sim \frac{1}{L(z)} R\left(\frac{r}{L(z)}\right), \tag{29}$$

where (x, y) are in some region surrounding of the collapse point (which typically shrinks during the self-focusing process), $R(r)$ is the NLS ground-state (see Section 3), and $L(z)$ is a modulation function, such that $\lim_{z \to Z_c} L(z) = 0$, where Z_c is the collapse distance (or time). In the NLS case, the ground-state $R(r)$ is radially-symmetric and, to the best of our knowledge, all the NLS-collapse simulations to date have shown that collapse occurs with a radially-symmetric profile. The quasi self-similar collapse has received much theoretical attention since the contribution of Merle and Tsutsumi [25]. However, it is very difficult to justify (29) rigorously. Only very recently did Merle and Raphael [26] provide a sharp result explaining this quasi self-similar behavior in the case of the NLS Eq. (1). Furthermore, on the experimental side, Gaeta and coworkers [24] recently carried out detailed measurements in optical Kerr media showing that the collapse process occurs with a self-similar profile, in consistency with Eq. (29).

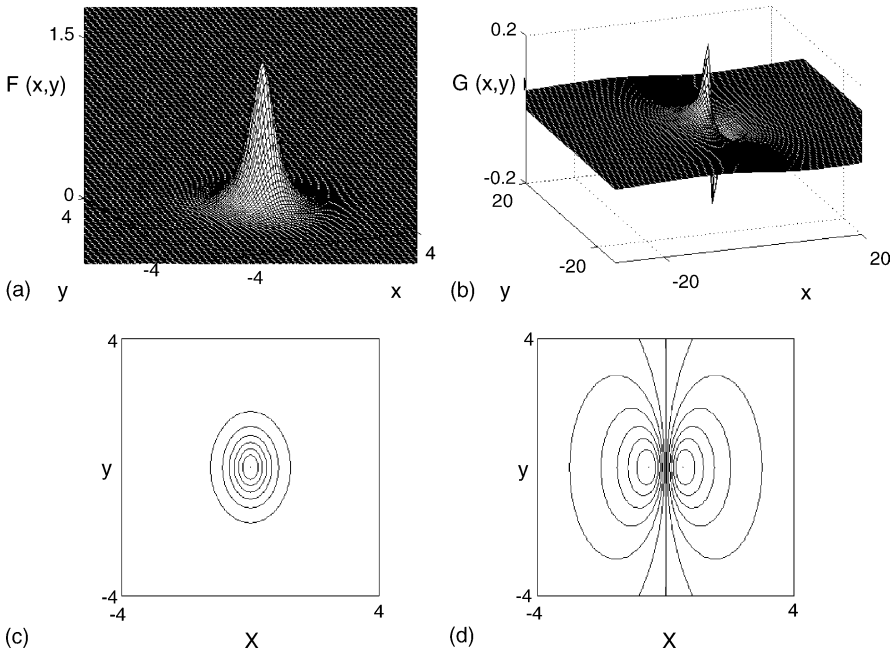

Fig. 5. The ground-state [i.e., solution of System (15)] for $(\nu, \rho) = (4, -4)$. (a) and (b) are 3D plot of $F(x, y)$ and $G(x, y)$, respectively; (c) and (d) are contour plots corresponding to (a) and (b), respectively.

In contrast to the NLS case, when $\rho \neq 0$ and $\nu > 0$ the NLSM System (4) is not rotationally invariant and the stationary solutions of (15) are not radially symmetric. Moreover, with this choice of parameters the stationary solutions cannot be transformed into radially-symmetric functions by any rescaling of x and y. Therefore, the NLSM ground-state, $F(x, y)$, is inherently astigmatic, which makes the analysis and numerical simulations more difficult. The asymptotic analysis of Papanicolaou et al. [28] indicates that, similar to the NLS collapse, NLSM collapse occurs with a modulated profile, i.e.,

$$|u(x, y, z)| \sim \frac{1}{L(z)} P\left(\frac{x}{L(z)}, \frac{y}{L(z)}, b(z)\right), \tag{30}$$

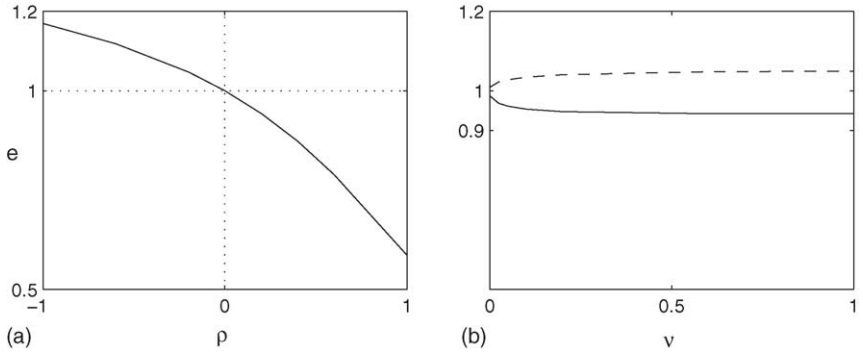

Fig. 6. The astigmatism (28) of the ground-state $F(x, y)$ of System (4) for: (a) $\nu = 0.5$ with $-1 \leq \rho \leq 1$ (i.e., same as Fig. 1); (b) $\rho = -0.2$ (dashes) and $\rho = 0.2$ (solid) with $0 \leq \nu \leq 1$ (i.e., same as Fig. 2a and b, respectively).

for certain functions $P(x, y, z)$, $L(z)$, and $b(z)$, such that as $z \to Z_c$, $L(z)$ and $b(z)$ approach zero and $P(x, y, z)$ asymptotically approaches the corresponding ground-state $F(x, y)$. Numerical simulations of the NLSM using "dynamic rescaling" suggested that, indeed, the collapsing solution approaches a modulated profile. However, in [28] the ground-state itself was not computed. Since it was not computed, it was not shown (numerically) that the asymptotic profile approaches the corresponding ground-state. The numerical results in this section suggest that, down to moderately small values of $L(z)$, the amplitude of the collapsing solution behaves as

$$|u(x, y, z)| \sim \frac{1}{L(z)} F\left(\frac{x}{L(z)}, \frac{y}{L(z)}\right), \tag{31}$$

where $F(x, y)$ is the ground-state of System (4). Therefore, the results of this study strengthen those of [28], because the collapsing wave is directly compared to the corresponding ground-state and is shown to approach a quasi self-similar modulation of the ground-state itself.

To study NLSM collapse numerically, System (4) is solved with the Gaussian initial conditions (19). The self-focusing dynamics are recovered from the simulations using the focusing factor, $|u(0, 0, z)|/u_0(0, 0)$, as a function of the propagation distance z. The astigmatism of the solution is recovered in accordance with (28) as

$$e(z) = \frac{\int |(|u|^2)_x|}{\int |(|u|^2)_y|}. \tag{32}$$

We begin by presenting several numerical simulations of collapse, that also serve to verify some of the results of the previous sections. As noted in Section 3, the Hamiltonian of the NLSM suggests, loosely speaking, that the water-wave case ($\rho < 0$) is "more focusing" than the optics case ($\rho > 0$). Indeed, Fig. 7 shows that when the same initial conditions are used for all cases, collapse with $\rho = -1$ precedes collapse with $\rho = 0$, which, in turn precedes collapse with $\rho = 1$. For this figure, the input power is taken as $1.2N_c(\nu = 0.5, \rho = 1) \approx 12.2$. We note that this value of N_c is approximately twice as large as $N_c(R)$ and approximately 3.3 times larger than $N_c(\nu = 0.5, \rho = -1)$ (see Fig. 1).

Since $\rho < 0$ and $\rho > 0$ correspond water waves and optics, respectively, and since critical power depends on ρ, a more "balanced" comparison between the water-wave and optics cases requires using the same initial conditions with an input power chosen with respect to the corresponding critical power (which is different for water-waves and optics). Therefore, the rest of the simulations below [i.e., Figs. 8–13] use the input power $N = 1.2N_c(\nu, \rho)$, i.e., 20% above the corresponding critical power for collapse. Fig. 8a shows the dynamics of the focusing factor for $\nu = 0.5$ with: $\rho = 0$ (NLS), $\rho = 1$ (optics), and $\rho = -1$ (water waves). Similarly to Fig. 7, the collapse distance with $\rho > 0$ is greater than with $\rho \leq 0$. Surprisingly, the collapse distance in the $\rho = 0$ and $\rho < 0$ cases is almost the

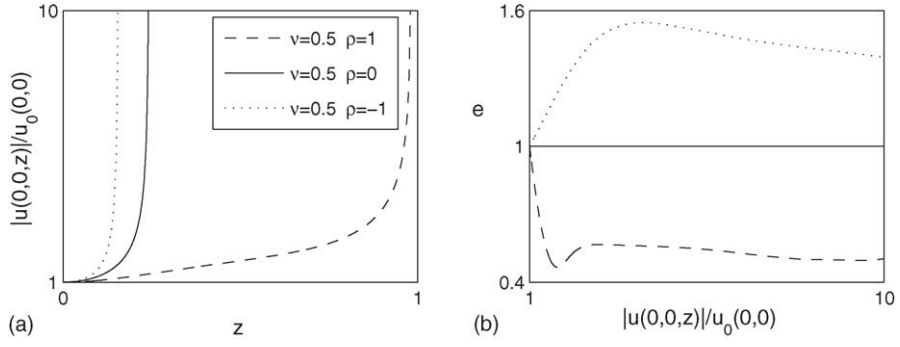

Fig. 7. (a) The focusing factor the NLSM solutions [i.e., System (4)] with $\nu = 0.5$ and three values of ρ (see legend) using the initial conditions (19) with the same input power $N = 1.2N_c(\nu = 0.5, \rho = -1) \approx 12.2$. (b) The corresponding astigmatism (32) of the solution as a function of the focusing factor.

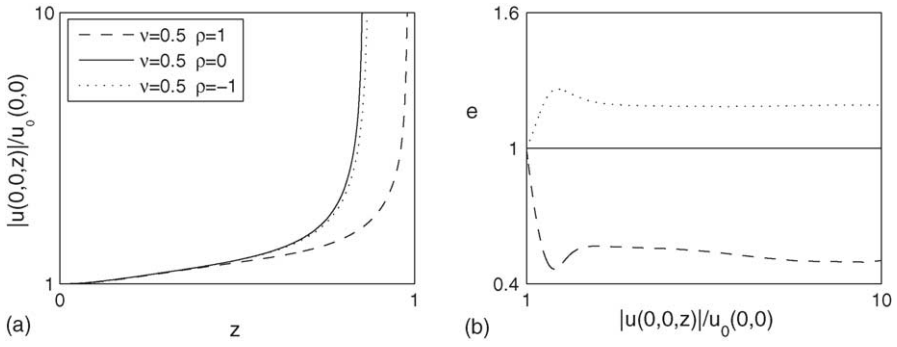

Fig. 8. Same as Fig. 7, but with the input power $N = 1.2N_c(\nu, \rho)$, i.e., 20% above the corresponding critical power.

same. Although one might have expected the collapse with $\rho < 0$ to precede collapse with $\rho = 0$ (as in Fig. 7), this is not the case here, because $N(\rho = -1)$ is approximately 1.6 times smaller than $N(\rho = 0)$ (see Fig. 3). Thus, in Fig. 8 the collapse distances of the $\rho = -1$ and $\rho = 0$ simulations are close, because the input power in the $\rho = 0$ simulation is much larger than the input power in the $\rho = -1$ one.

In addition, Fig. 8b shows the corresponding astigmatism plots. The astigmatism is plotted as a function of the focusing factor (rather than as a function of z) in order to "blow up" the dynamics near the collapse point, where the interesting changes in the astigmatism are expected to occur. While the NLS solution remains radially-symmetric (i.e., $e \equiv 1$), the NLSM solutions become astigmatic during propagation. Furthermore, $\rho < 0$ and $\rho > 0$ correspond

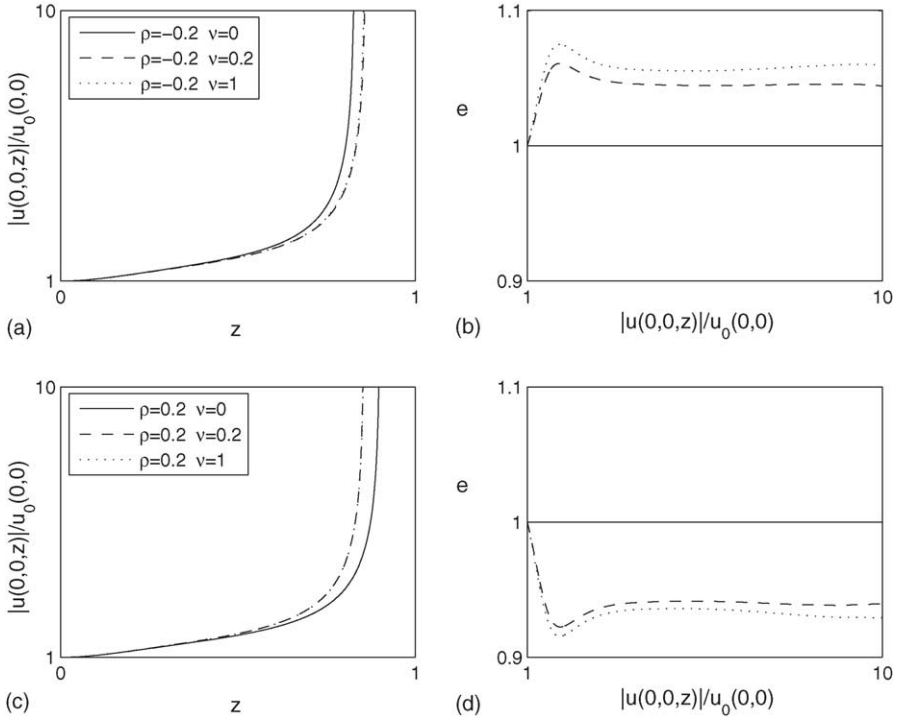

Fig. 9. Same as Fig. 8 with [(a) and (b)] $\rho = -0.2$ and $\nu = 0$ (solid), $\nu = 0.2$ (dashes), and $\nu = 1$ (dotted, on top of the dashes); [(c) and (d)] same as above with $\rho = 0.2$.

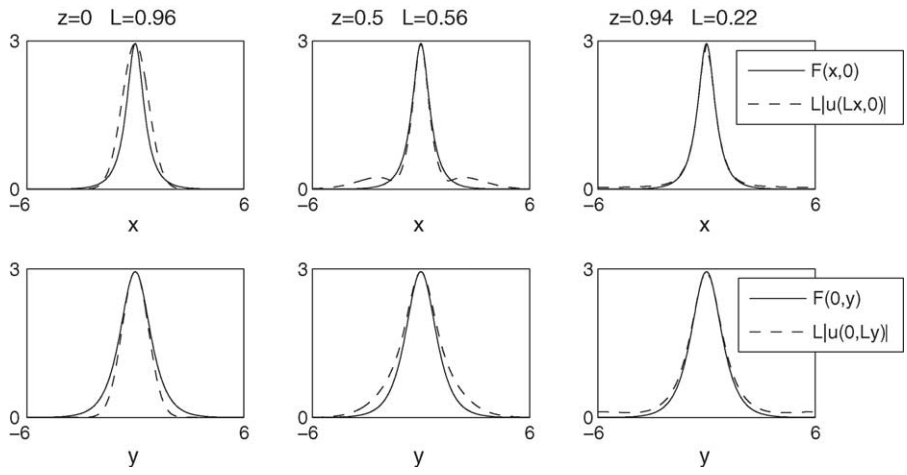

Fig. 10. Convergence of the modulated collapse profile (dashes) to the NLSM ground state (solid) along the x-axis (top) and the y-axis (bottom) with $(\nu, \rho) = (0.5, 1)$. The initial conditions are (19) with $N = 1.2N_c(\nu, \rho)$.

to $e > 1$ and $e < 1$, respectively, which is consistent with in Figs. 4 and 6. As can be seen from this figure, at the initial stage of the propagation the astigmatism of the NLSM solutions becomes large, in a direction that depends on ρ. Based on these simulations it appears that the astigmatism approaches a (more or less) constant value at the collapse point, a value that depends on ν and ρ (such that $e \neq 1$). This is consistent with the results in [28], as well as with the results presented below.

Figs. 7–9 indicate that NLSM collapse is astigmatic, however, they do not show that the collapse process is quasi self-similar. In order to study the self-similarity of the collapse process, in accordance with Eq. (31), the modulation function is recovered from the solution as

$$L(z) = \frac{F(0,0)}{|u(0,0,z)|},$$

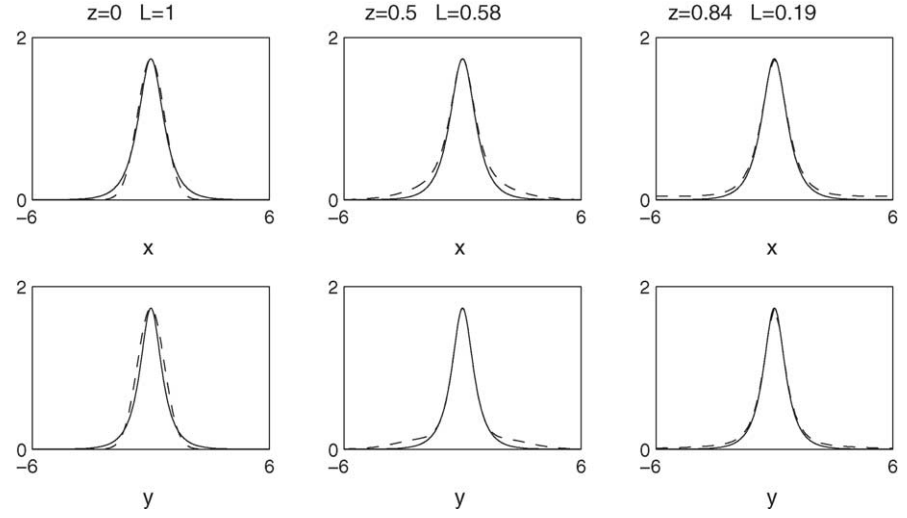

Fig. 11. Same as Fig. 10 with $(\nu, \rho) = (0.5, -1)$.

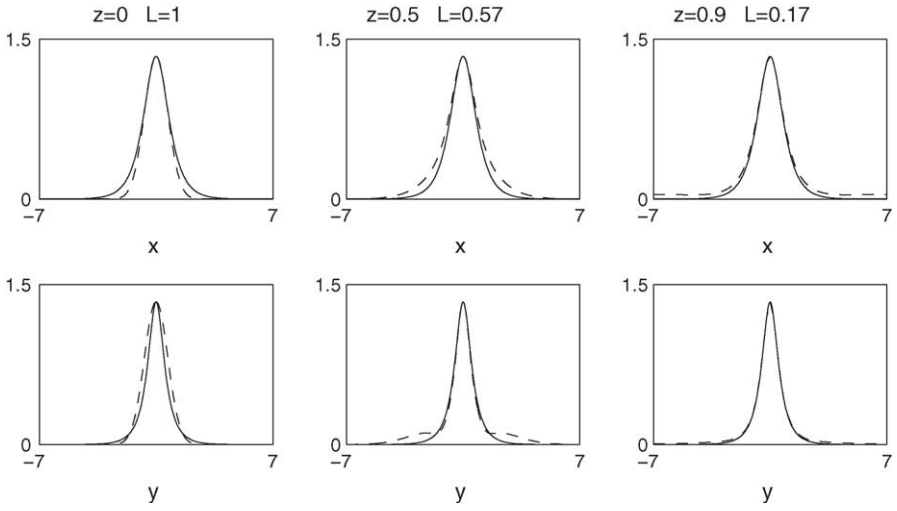

Fig. 12. Same as Fig. 10 with $(\nu, \rho) = (4, -4)$.

where $F(x, y)$ is the corresponding ground-state. The rescaled amplitude of the solution of the NLSM, i.e., $L|u(L\tilde{x}, L\tilde{y}, z)|$, is compared with $F(\tilde{x}, \tilde{y})$, where $F(\tilde{x}, \tilde{y})$ is the ground-state and $(\tilde{x}, \tilde{y}) = (\frac{x}{L}, \frac{y}{L})$. In order to show that the collapse process is, indeed, quasi self-similar with the corresponding ground-state, the rescaled amplitude is shown to converge pointwise to F near the origin as $z \to Z_c$ (i.e., near the collapse point).

Fig. 10 shows that the NLSM collapse is indeed self-similar with the ground-state for $\nu = 0.5$ and $\rho = 1$. The rescaled on-axis amplitude is compared separately on the x and y axes (top and bottom plots, respectively). One can see that, as the solution is undergoing self-focusing [i.e., as $L(z)$ approached zero], its rescaled profile approaches that of the astigmatic ground-state near the origin.

Fig. 11 shows the same picture with $\rho = -1$, whose ground-state is somewhat less astigmatic than with $\rho = 1$ (as mentioned above). In order to observe self-similar collapse with $\rho < 0$ and a more astigmatic profile, Fig. 12

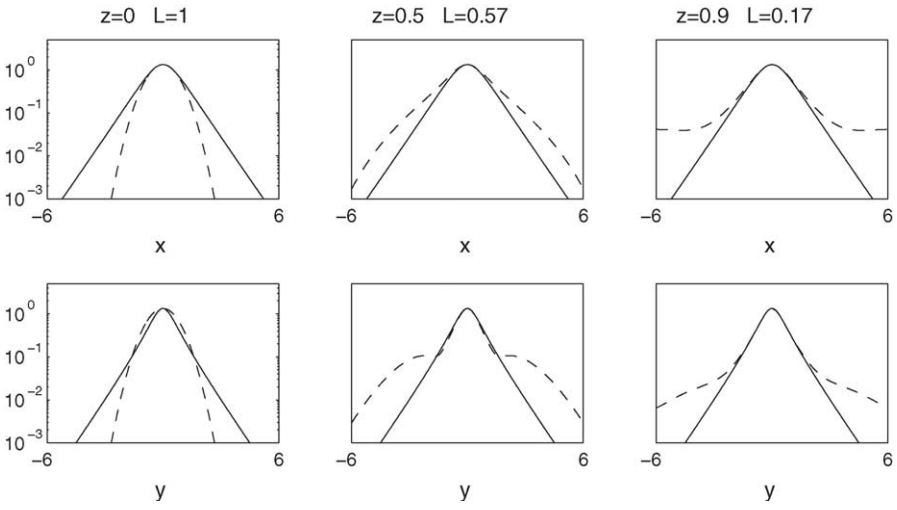

Fig. 13. Same as Fig. 12 on a semi-log plot.

compares the solution and the ground-state with $\nu = 4$ and $\rho = -4$. The ground-state in this latter case is clearly astigmatic and, in turn, the collapse process is quasi self-similar with the ground-state. Fig. 13 further demonstrates the local nature of the self-similar collapse process. While the spatial region in the vicinity of the collapse point is self-similar to the ground-state, the outer "wings" of the solution do not approach the ground-state. This phenomenon is well-known in the NLS case as well [30], and can be understood as follows: in accordance with Eq. (31), exactly one critical power enters the collapse region. More precisely, as $z \to Z_c$, the power of $u(x, y, z)$ contained in a "ball" of radius $L(z)$ around the collapse point is just slightly above N_c (cf. [25]). Since the input power is 20% above N_c, the residual 20% radiates into the outer wings in a process that is not self-similar with the ground-state.

7. Collapse arrest

As mentioned in Section 2.2, within the context of nonlinear optics, the self-focusing mechanism in the NLSM is due to a quadratic effect [1,2]. However, it is well-known that collapse with an infinite amplitude does not occur in physical situations. In reality, there are always physical mechanisms that arrests the collapse. Such mechanisms have been studied extensively in nonlinear optics, e.g., nonlinear saturation [11,33], beam nonparaxiality [15], and vectorial effects [18]. In order to investigate the arrest of collapse in NLSM in the optics case, we consider the NLSM with a small nonlinear saturation of the cubic nonlinearity as

$$\mathrm{i}u_z + \frac{1}{2}\Delta u + \frac{|u|^2 u - \rho u \phi_x}{1 + \varepsilon |u|^2} = 0, \tag{33a}$$

$$\phi_{xx} + \nu \phi_{yy} = (|u|^2)_x, \tag{33b}$$

where ε is the small nonlinear-saturation parameter.

When $\rho \ll 1$ and $\varepsilon \ll 1$ System (33) is a small perturbation of the NLS Eq. (1). In that case, the asymptotic analysis of Fibich and Papanicolaou [19] for the perturbed NLS can be used. Their analysis is based on the asymptotic and numerical observations that the collapsing solution in the NLS case is self-similar with the ground-state (Townes profile), i.e., as in Eq. (29). The asymptotic analysis predicts that, to leading order, the dynamics of the focusing factor in the solution of System (33) is given by the following ODE (see [19, 5.3–5.4])

$$(w_z)^2 = -\frac{4H_0}{M}\frac{(w_M - w)(w - w_m)}{w}, \tag{34}$$

where $w(z) = L^2(z)$, $L(z)$ is the focusing-factor in Eq. (29), $M \approx 0.55$, and H_0, w_M, and w_m are constants that depend only on ε and the initial conditions, such that $w_M > w_m$. It follows from this nonlinear-oscillator-type equation that for generic initial conditions the intensity of the solution initially focuses [i.e., $L(z)$ decreases] until $L \sim \sqrt{w_m} = \mathrm{O}(\sqrt{\varepsilon})$, then defocuses [i.e., $L(z)$ increases] until $L \sim \sqrt{w_M}$, followed by focusing–defocusing oscillations, such that $\sqrt{w_m} \le L(z) \le \sqrt{w_M}$.

Fig. 14 shows the on-axis amplitude of the numerical solution of System (33) for $\rho = 0.5$, $\nu = 1$, $\varepsilon = 0.0025$, and the initial conditions (19) with $N = 1.5N_c$, where N_c is the critical power corresponding to $\varepsilon = 0$. The numerical solution of System (33) agrees qualitatively with the predictions based on Eq. (34). Indeed, one sees that collapse is arrested by the small nonlinear saturation, followed by a series of focusing–defocusing oscillations.

It should be mentioned that the physical mechanisms that arrest the collapse in water waves are not understood to the same level as in optics, in part because of the scarce experimental results on water waves with large surface tension.

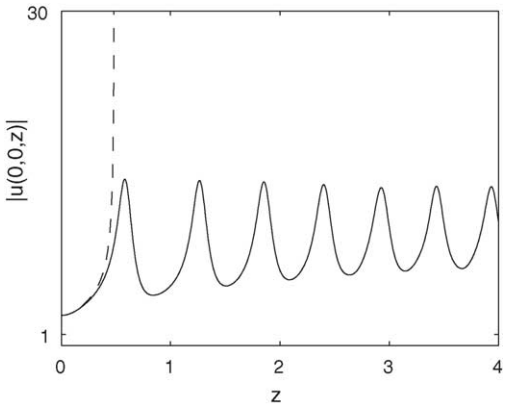

Fig. 14. Collapse in the NLSM [i.e., System (4) with $(\nu, \rho) = (1, 0.5)$, dashes] is arrested by small nonlinear saturation [i.e., System (33) with $(\nu, \rho) = (1, 0.5)$ and $\varepsilon = 0.0025$, solid] leading instead to focusing–defocusing oscillations.

8. Summary and final remarks

The results of this study show that nonlinear-wave systems that admit a quadratic–cubic type interaction, such as in nonlinear optics and in nonlinear free-surface water waves, lead to the NLSM System (4). The NLSM can admit finite-distance collapse in a certain parameter regime. The regions of collapse and global-existence is explored in a relevant parameter space and the consistency between global existence theory, the Virial Theorem, and numerical simulations the NLSM System (4) is established. Furthermore, numerical simulations of the NLSM show that the collapse process occurs with a quasi self-similar profile, which is a modulation of the ground-state profile. The ground-state profile is found using a numerical algorithm that was recently used in dispersion-managed NLS theory. Generically, the ground-state profile is astigmatic and, therefore, the collapse profile is astigmatic as well.

These results are in the same spirit as for the NLS Eq. (1). However, NLSM theory is more difficult and not as advanced as NLS theory. There are several remaining questions and problems. For example, it remains an open problem to extend the sharp theoretical results on the self-similar nature of the singularity to the NLSM case. From the numerical perspective, while our simulations indicate that NLSM collapse occurs with a self-similar ground-state, we only resolve moderate focusing factors [i.e., O(10)] near the collapse point. Using more specialized numerical methods (cf. [28,20]), much larger focusing factors (e.g., greater than 10^4) could furnish more convincing evidence of this self-similar collapse. From the experimental perspective, self-similar collapse in quadratic–cubic type media remains to be demonstrated in either free-surface water waves or nonlinear optics.

Acknowledgments

This research was partially supported by the U.S. Air Force Office of Scientific Research, under grant 1-49620-03-1-0250 and by the National Science Foundation, under grant DMS-0303756.

Appendix A. Proof of Proposition 3.2

Following Weinstein [35], if one substitutes the stationary solution (15) into the Virial Theorem (14), one finds that the variance, i.e., the integral on left-hand side, is independent of z. Therefore, its second-z derivative is zero, which implies that the right-hand side, i.e., the Hamiltonian of the stationary solution (15), is zero as well. □

Below an alternative constructive proof is given. Multiplying Eq. (15a) by F and Eq. (15b) by G and integrating gives

$$-\lambda\int F^2+\frac{1}{2}\int(FF_{xx}+FF_{yy})+\int F^4-\rho\int F^2G_x=0, \tag{A.1a}$$

$$\int(GG_{xx}+\nu GG_{yy})=\int(F^2)_xG. \tag{A.1b}$$

Using integration by-parts (IBP) on (A.1b) gives

$$\int F^2G_x=\int(\nabla_\nu G)^2, \tag{A.2}$$

where $(\nabla_\nu G)^2\equiv G_x^2+\nu G_y^2$. Combining (A.1b) and (A.1a) leads to

$$\lambda\int F^2+\frac{1}{2}\int(\nabla F)^2-\int F^4+\rho\int(\nabla_\nu G)^2=0\,. \tag{A.3}$$

On the other hand, multiplying Eq. (15a) by (xF_x+yF_y) gives that

$$\begin{aligned}&-\frac{\lambda}{2}\int[x(F^2)_x+y(F^2)_y]+\frac{1}{4}\int[x(F_x^2)_x+y(F_y^2)_y]+\frac{1}{2}\int(xF_{yy}F_x+yF_{xx}F_y)\\&\quad+\frac{1}{4}\int[x(F^4)_x+y(F^4)_y]-\frac{\rho}{2}\int[x(F^2)_xG_x+y(F^2)_yG_x]=0.\end{aligned}$$

Using IBP several times on the first four terms we arrive at

$$\lambda\int F^2-\frac{1}{2}\int F^4-\frac{\rho}{2}\int[x(F^2)_xG_x+y(F^2)_yG_x]=0. \tag{A.4}$$

Similarly, multiplying Eq. (A.1b) by (xG_x+yG_y) and using IBP leads to

$$\int[x(F^2)_xG_x+y(F^2)_xG_y]=0.$$

Using IBP and Eq. (A.2) gives

$$\int[x(F^2)_xG_x+y(F^2)_yG_x]=-\int F^2G_x=-\int(\nabla_\nu G)^2. \tag{A.5}$$

Substituting (A.5) into (A.4) we obtain that

$$\lambda\int F^2-\frac{1}{2}\int F^4+\frac{\rho}{2}\int(\nabla_\nu G)^2=0.$$

Subtracting from Eq. (A.3) gives Eq. (18). □

Appendix B. Derivation of the Hamiltonians (20) and (24)

The derivation of Eq. (24) is outlined below. Substituting the astigmatic Gaussian initial conditions (23) into the first two terms of the Hamiltonian (13) gives

$$\frac{1}{2}\int|\nabla u_0|^2-\frac{1}{2}\int|u_0|^4=\frac{(1+E^2)N}{2}-\frac{EN^2}{2\pi}. \tag{B.1}$$

It remains to calculate the third term in Eq. (13). To do that it is convenient to use the Fourier Transform. Below we denote

$$\hat{f}(k_x, k_y) = \mathcal{F}[f] \equiv \int f(x, y)\, \mathrm{e}^{-\mathrm{i}k_x x - \mathrm{i}k_y}, \quad f(x, y) = \mathcal{F}^{-1}[\hat{f}] \equiv \frac{1}{(2\pi)^2} \int \hat{f}(k_x, k_y) \mathrm{e}^{\mathrm{i}k_x x + \mathrm{i}k_y y},$$

as the direct and inverse 2D Fourier Transforms, respectively, where (k_x, k_y) are the Fourier frequencies in (x, y) directions and the integrations are carried over the (x, y) and (k_x, k_y) planes, respectively. Therefore, it follows from Eq. (4b) that

$$\hat{\phi}_0 \equiv \mathcal{F}[\phi(x, y, 0)] = -\frac{\mathrm{i}k_x}{k_x^2 + \nu k_y^2} \widehat{u_0^2}.$$

Using Parseval's identity and substituting the Gaussian initial conditions (19) leads to

$$\int (\phi_x^2 + \nu \phi_y^2) = \frac{1}{4\pi^2} \int \frac{k_x^2 (\widehat{u_0^2})^2}{k_x^2 + \nu k_y^2} = \frac{N^2}{4\pi^2} \int \frac{k_x^2\, \mathrm{e}^{-(k_x^2 + E^2 k_y^2)/(4E^2)}}{k_x^2 + \nu k_y^2}.$$

Transforming to the cylindrical coordinates defined by $(k_x, k_y) = (r \cos\theta, E^{-1} r \sin\theta)$ yields

$$\frac{\rho}{2} \int (\phi_x^2 + \nu \phi_y^2) = \frac{\rho N^2}{8\pi^2 E} \int_0^\infty \mathrm{e}^{-r^2/4E^2} r\, \mathrm{d}r \int_0^{2\pi} \frac{\mathrm{d}\theta}{1 + (\nu/E^2)\cot^2\theta} = \frac{\rho N^2 E}{4\pi^2} \frac{2\pi}{1 + \sqrt{\nu}/E}.$$

Combining with Eq. (B.1) and the Hamiltonian (13) yields Eq. (24). Note that Eq. (20) is a special case of Eq. (24) with $E = 1$.

Appendix C. Calculating the ground state

The NLSM ground state is obtained in this study using a fixed-point numerical procedure similar to that recently used in dispersion-managed soliton theory (cf. [5,29]).

Below we use the following formulation. Let $u(x, y, z)$ and $v(x, y, z)$ be solutions of the system

$$\mathrm{i}u_z + \tfrac{1}{2}(u_{xx} + u_{yy}) + |u|^2 u - \rho u v = 0, \tag{C.1a}$$

$$v_{xx} + \nu v_{yy} = (|u|^2)_{xx}. \tag{C.1b}$$

We note that Systems (4) and (C.1) are mathematically equivalent under the transformation $v \equiv \phi_x$. A stationary solution of system (C.1) has the form $u(x, y, z) = \mathrm{e}^{\mathrm{i}\lambda z} F(x, y)$ and $v(x, y, z) = V(x, y)$, where F and V are real functions and λ is an arbitrary real number. Substituting this ansatz into system (C.1) gives

$$-\lambda F + \tfrac{1}{2}(F_{xx} + F_{yy}) + F^3 - \rho F V = 0, \tag{C.2a}$$

$$V_{xx} + \nu V_{yy} = (F^2)_{xx}. \tag{C.2b}$$

When the stationary solutions are known to be radially-symmetric, e.g., when $\rho = 0$ or $\nu = 0$, one can write this system as a single ODE in the radial variable. In that case, one can solve the ODE using a "shooting" method. This technique, however, does not work well for a "true" PDE, i.e., when F and G are not radially-symmetric, which is the case in this study when both ρ and ν are nonzero. Therefore, in order to solve this system we use a fixed-point method as explained below.

Taking the Fourier Transform (see Appendix B) of System (C.2) gives

$$-\lambda\hat{F} - \frac{|k|^2}{2}\hat{F} + \mathcal{F}[F^3 - \rho FV] = 0, (k_x^2 + \nu k_y^2)\hat{V} = k_x^2\mathcal{F}[F^2],$$

where $\hat{F}(k_x, k_y)$ and $\hat{V}(k_x, k_y)$ are the Fourier transforms of $F(x, y)$ and $V(x, y)$, respectively, and $|k|^2 = k_x^2 + k_y^2$. This system can be re-written as

$$\hat{F} = \frac{1}{\lambda + |k|^2/2}\mathcal{F}[F^3 - \rho FV], \tag{C.3a}$$

$$\hat{V} = \frac{k_x^2}{k_x^2 + \nu k_y^2}\mathcal{F}[F^2]. \tag{C.3b}$$

The idea is to use the fixed-point iterative method

$$\hat{F}^{(n+1)} = \frac{1}{\lambda + |k|^2/2}\,\mathcal{F}[F^3 - \rho FV]^{(n)},$$

where the right-hand side is evaluated using $V^{(n)}$ found using Eq. (C.3b). This procedure is then supplemented with an initial guess $F^{(0)}(x, y) = f_0(x, y)$, which is typically chosen to be a Gaussian, i.e., $f_0(x, y) = \mathrm{e}^{-x^2-y^2}$. However, this approach fails, because the right-hand side of Eq. (C.2) is nonlinear and, as a result, the iterations either converge to the trivial solution or diverge to infinity. To rectify this problem, one can "homogenize" the right-hand side of Eq. (C.3) as follows. Multiplying (C.3a) by $\hat{F}^*$ and integrating over the (k_x, k_y) plane yields the equation SL = SR, where

$$\mathrm{SL} \equiv \int |\hat{F}|^2, \quad \mathrm{SR} \equiv \int \frac{1}{\lambda + |k|^2/2}\mathcal{F}[F^3 - \rho FV]\hat{F}^*.$$

Here SL and SR are two scalar quantities that can be efficiently calculated using Fast-Fourier Transforms. Since SL = SR when F and V are solutions of (C.2), one can use instead the modified iterative method

$$\hat{F}^{(n+1)} = \frac{1}{\lambda + |k|^2/2}\left(\frac{\mathrm{SL}}{\mathrm{SR}}\right)^{\alpha}\mathcal{F}[F^3 - \rho FV]^{(n)}, \tag{C.4}$$

where SL and SR are calculated using F and V at step n and $V^{(n)}$ is found using Eq. (C.3b). Here α is an arbitrary constant that is chosen to make the right-hand side of (C.4) have homogeneity zero with respect to F, which is to be expected to prevent the aforementioned divergence. In our case the right-hand side of (C.4) scales like $(\mathrm{SL}/\mathrm{SR})^{\alpha}F^3 = F^{3-2\alpha}$. This observation suggests using $\alpha = 3/2$, which, indeed, allows the fixed-point method (C.4) to converge. The convergence can be monitored using error := $|(\mathrm{SL}/\mathrm{SR}) - 1|$, which should approach zero. Typically, 20–40 steps suffice for obtaining error $< 10^{-8}$. In addition, when the solution obtained by this method is substituted for the initial conditions of the NLSM System (4), the NLSM solution is confirmed to be stationary, i.e., its amplitude remains (approximately) constant for a propagation distance of $z = \mathrm{O}(10)$.

References

[1] M.J. Ablowitz, G. Biondini, S. Blair, Multi-dimensional pulse propagation in resonant materials $\chi^{(2)}$ materials, Phys. Lett. A 236 (1997) 520.

[2] M.J. Ablowitz, G. Biondini, S. Blair, Nonlinear Schrödinger equations with mean terms in nonresonant multidimensional quadratic materials, Phys. Rev. E 63 (2001) 605.

[3] M.J. Ablowitz, P.A. Clarkson, Solitons, Nonlinear Evolution Equations and Inverse Scattering, Cambridge University Press, Cambridge, 1991.
[4] M.J. Ablowitz, R. Haberman, Nonlinear evolution equations—two three dimensions, Phys. Rev. Lett. 35 (1975) 1185.
[5] M.J. Ablowitz, Z. Musslimani, Dark and gray strongly-dispersion managed solitons, Phys. Rev. E 67 (2003) 025601(R).
[6] M.J. Ablowitz, H. Segur, On the evolution of packets of water waves, J. Fluid Mech. 92 (1979) 691.
[7] M.J. Ablowitz, H. Segur, Solitons and the Inverse Scattering Transform, SIAM, Philadelphia, 1981.
[8] D.J. Benney, G.J. Roskes, Wave instabilities, Stud. Appl. Math. 48 (1969) 377.
[9] R.Y. Chiao, E. Garmire, C.H. Townes, Self-trapping of optical beams, Phys. Rev. Lett. 13 (1964) 479.
[10] R. Cipolatti, On the existence of standing waves for the Davey–Stewartson system, Commun. Part. Diff. Eq. (1992) 967.
[11] B.I. Cohen, B.F. Lasinski, A.B. Langdon, J.C. Cummings, Dynamics of ponderomotive self-focusing in plasmas, Phys. Fluids B-Plasma Phys. 3 (1992) 766.
[12] L.C. Cravosan, J.P. Torres, D. Mihalache, L. Torner, Arresting wave collapse by self-rectification, Phys. Rev. Lett. 91 (2003) 063904.
[13] A. Davey, K. Stewartson, On three-dimensional packets of surface waves, Proc. R. Soc. Lond. A 338 (1974) 101.
[14] V.D. Djordevic, L.G. Reddekopp, On two-dimensional packets of capillary gravity waves, J. Fluid Mech. 79 (1977) 703.
[15] G. Fibich, Small beam nonparaxiality arrests self-focusing of optical beams, Phys. Rev. Lett. 76 (1996) 4356.
[16] G. Fibich, A.L. Gaeta, Critical power for self-focusing in bulk media and in hollow waveguides, Opt. Lett. 25 (2000) 335.
[17] G. Fibich, B. Ilan, Self-focusing of elliptic beams: an example for the failure of the aberrationless approximation, J. Opt. Soc. Am. B 17 (2000) 1749.
[18] G. Fibich, B. Ilan, Vectorial and random effects in self-focusing and in multiple filamentation, Physica D 157 (2001) 113.
[19] G. Fibich, G.C. Papanicolaou, Self-focusing in the perturbed and unperturbed nonlinear Schrödinger equation in critical dimension, SIAM J. Appl. Math. 60 (1999) 183.
[20] G. Fibich, W. Ren, X.P. Wang, Numerical simulations of self-focusing of ultrafast laser pulses, Phys. Rev. E 67 (2003) 056603.
[21] A.S. Fokas, M.J. Ablowitz, On a method of solution for a class of multidimensional nonlinear evolution equations, Phys. Rev. Lett. 51 (1983) 7.
[22] J.M. Ghidaglia, J.C. Saut, On the initial value problem for the Davey–Stewartson systems, Nonlinearity 3 (1990) 475.
[23] P.L. Kelley, Self focusing of optical beams, Phys. Rev. Lett. 15 (1965) 1005.
[24] K.D. Moll, A.L. Gaeta, G. Fibich, Self-similar optical wave collapse: observation of the Townes profile, Phys. Rev. Lett. 90 (2003) 203902.
[25] F. Merle, Y. Tsutsumi, L^2 concentration of blow-up solutions for the nonlinear Schrödinger equation with critical power nonlinearity, J. Diff. Eq. 84 (1990) 205.
[26] F. Merle, P. Raphael, On the universality of blow-up profile for L^2 critical nonlinear Schrödinger equation, Inventiones Mathematicae 156 (2004) 565.
[27] G.C. Papanicolaou, D. McLaughlin, M. Weinstein, Focusing singularity for the nonlinear Schrödinger equation, Lec. No. Numer. Appl. Anal. 5 (1982) 253.
[28] G.C. Papanicolaou, C. Sulem, P.L. Sulem, X.P. Wang, The focusing singularity of the Davey–Stewartson equations for gravity-capillary surface waves, Physica D 72 (1994) 61.
[29] V.I. Petviashvili, Equation of an extraordinary soliton, Sov. J. Plasma Phys. 2 (1976) 257.
[30] C. Sulem, P.L. Sulem, The Nonlinear Schrödinger Equation, Springer-Verlag, New York, 1999.
[31] V.I. Talanov, Self focusing of wave beams in nonlinear media, Sov. Phys. JETP Lett. 2 (1965) 138.
[32] J.P. Torres, L. Torner, I. Biaggio, M. Segev, Tunable self-action of light in optical rectification, Opt. Commun. 213 (2002) 351.
[33] F. Vidal, T.W. Johnston, Electromagnetic beam breakup: Multiple filaments, single beam equilibria, and radiation, Phys. Rev. Lett. 77 (1996) 1282.
[34] S. Vlasov, V. Petrishchev, V. Talanov, Averaged description of wave beams in linear and nonlinear media, Radiophys. Quant. Elec. 14 (1971) 1062 (1070 in English).
[35] M.I. Weinstein, Nonlinear Schrödinger equations and sharp interpolation estimates, Commun. Math. Phys. 87 (1983) 567.
[36] G.B. Whitham, Linear and Nonlinear Waves, Wiley, New York, 1974.

Noise-induced linewidth in frequency combs

Mark J. Ablowitz

Department of Applied Mathematics, University of Colorado, Boulder, Colorado 80309-0526

Boaz Ilan

School of Natural Sciences, University of California, Merced, P.O. Box 2039, Merced, California 95344

Steven T. Cundiff

JILA, National Institute of Standards and Technology and the University of Colorado, Boulder, Colorado 80309-0440

Received January 26, 2006; revised March 16, 2006; accepted April 3, 2006; posted April 7, 2006 (Doc. ID 67456)

Frequency combs generated by trains of pulses emitted from mode-locked lasers are analyzed when the center time and phase of the pulses undergo noise-induced random walk, which broadens the comb lines. Asymptotic analysis and computation reveal that, when the standard deviation of the center-time jitter of the nth pulse scales as $n^{p/2}$, where p is a jitter exponent, the linewidth of the kth comb line scales as $k^{2/p}$. The linear-dispersionless ($p=1$) and pure-soliton ($p=3$) dynamics in lasers are derived as special cases of this time-frequency duality relation. In addition, the linewidth induced by phase jitter decreases with power P_{out}, as $(P_{\text{out}})^{-1/p}$. © 2006 Optical Society of America

OCIS codes: 190.5530, 140.4050.

Frequency combs are a ubiquitous tool in time and frequency metrology. They are generated by trains of evenly spaced pulses, whose spectrum consists of a comb of oscillators with evenly spaced frequencies, or comb lines. Advanced ultrafast mode-locked lasers can generate broad optical frequency combs with unprecedented stability. This breakthrough has revolutionized the field of frequency metrology, since it allows for bidirectional conversion between high (optical) and low (radio, microwave) frequencies.[1,2] However, noise sources in the lasing medium broaden the comb lines.[3,4] Schawlow and Townes (S–T) derived a formula for the linewidth of cw lasers.[5] With the advent of pulsed mode-locked lasers, quantum-noise theory developed by Haus and collaborators has been useful for studying the stability of the ensuing modes.[6] Many theoretical studies have since been devoted to the understanding of the pulse dynamics (see Ref. 4 and references therein). It is known that many physical mechanisms can broaden the comb lines; see, for example, Takushima *et al.*[3] and Kärtner *et al.*,[4] who recently studied the linewidth experimentally and theoretically in passively and actively mode-locked lasers. In this Letter, the pulse's jitter is treated as a generalized random walk, from which the induced linewidth is derived. Asymptotic analysis reveals that, when the standard deviation of the nth pulse's time-jitter scales $n^{p/2}$, where p is a jitter exponent, the linewidth of the kth comb line scales like $k^{2/p}$. The S–T (linear-dispersionless) and pure-soliton (nonlinear-dispersive) dynamics are derived as two special cases of this scaling law. These results have potential implications for current research in ultrafast spectroscopy.[1,2,7]

A mode-locked laser emits an ultrashort pulse each time the intracavity pulse arrives at the output coupler. The spectrum of N successively emitted pulses is

$$\mathcal{F}\left\{\sum_{n=1}^{N} E(t-T_n)e^{i\phi_n}e^{-i\omega_c t}+\text{c.c.}\right\}=\hat{E}(\tilde{\omega})\hat{S}(\tilde{\omega})+\text{c.c.}, \tag{1}$$

where $E(t-T_n)e^{i\phi_n}$ is the complex, slowly varying electric-field envelope of the nth pulse, where T_n and ϕ_n are the arrival time and overall phase of the nth pulse, respectively, and ω_c is the carrier frequency; we define $\tilde{\omega}\equiv\omega-\omega_c$, c.c. stands for the complex conjugate, $\hat{u}=\mathcal{F}[u]=\int u(t)e^{i\omega t}dt$ denotes the Fourier transform, $\hat{E}(\tilde{\omega})$ is the single-pulse spectrum, and the comb function is

$$\hat{S}(\tilde{\omega})=\sum_{n=1}^{N} e^{i\tilde{\omega}T_n+i\phi_n}. \tag{2}$$

In the absence of noise, the time between successive pulses is $T_{\text{rep}}=T_{n+1}-T_n$; the repetition frequency is $\omega_{\text{rep}}=2\pi/T_{\text{rep}}$; and the pulse-to-pulse (overall) phase change is $\Delta\phi=\phi_{n+1}-\phi_n$, which is related to the carrier-envelope phase change, $\Delta\phi_{\text{CE}}$, as $\Delta\phi=\Delta\phi_{\text{CE}}+\omega_c T_{\text{rep}}$. Therefore apart from absolute time and phase offsets, $T_n=nT_{\text{rep}}$, $\phi_n=n\Delta\phi$, and the measurement time is NT_{rep}. In the limit of an infinite number of pulses, the comb function approaches the ideal frequency comb (see Fig. 1), i.e., $|\hat{S}(\tilde{\omega})|\to\Sigma_{k=-\infty}^{\infty}\delta(\tilde{\omega}-\tilde{\omega}_k)$ as $N\to\infty$, where $\delta(\omega)$ is the Dirac delta function, and the kth comb line's frequency is given by

$$\tilde{\omega}_k=k\omega_{\text{rep}}+\tilde{\omega}_{\text{o}},\quad \tilde{\omega}_{\text{o}}=-\frac{\Delta\phi}{2\pi}\omega_{\text{rep}}, \tag{3}$$

where $\tilde{\omega}_{\text{o}}$ is the offset frequency and, for convenience, the comb lines are enumerated around ω_c.

When noise is considered, let $T_n=nT_{\text{rep}}+x$ and $\phi_n=n\Delta\phi+y$ be the center time and phase of the nth

0146-9592/06/121875-3/$15.00

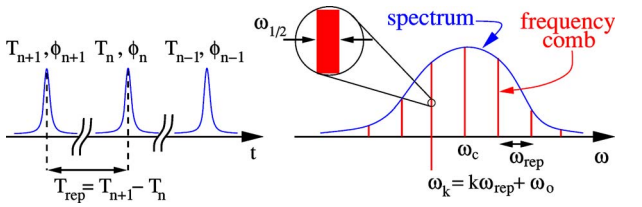

Fig. 1. (Color online) Schematic of a pulse train (left) and its spectrum (right). In the absence of noise, the pulse's spectrum determines the bandwidth, while the repetition time, $T_{\mathrm{rep}}=T_{n+1}-T_n$, and overall phase change, $\Delta\phi=\phi_{n+1}-\phi_n$, determine the comb function [Eqs. (1)–(3)]. The frequency of the kth comb line (enumerated around ω_c) is $\tilde{\omega}_k = k\omega_{\mathrm{rep}}+\tilde{\omega}_o$, where ω_{rep} and $\tilde{\omega}_o$ are the repetition and offset frequencies. Noise induces a random jitter in the center time and phase, T_n and ϕ_n, which broadens the comb lines. The linewidth ($\omega_{1/2}$ in the inset) is the FWHM of the comb function [Eq. (2)] around a comb frequency [Eq. (7)].

pulse, respectively, where T_{rep} and $\Delta\phi$ are the average repetition time and phase change, and $x=\Delta T_n$ and $y=\Delta\phi_n$ correspond to zero-mean random jitter. The probability density of the nth center-time and phase jitter is assumed to be joint Gaussian[8]:

$$g_n(x,y) = Ae^{-[1/2(1-r^2)][(x/\sigma_x)^2-(2r^2xy/C_{x,y})+(y/\sigma_y)^2]}, \quad (4)$$

where σ_x and σ_y are the standard deviations of the center-time and phase jitter, respectively; the covariance is $C_{x,y}=\langle\Delta T_n\Delta\phi_n\rangle=r\sigma_x\sigma_y$, where r is the correlation coefficient; and $A=(2\pi\sigma_x\sigma_y\sqrt{1-r^2})^{-1}$. We consider pulses that undergo generalized random walks; i.e., their center-time and phase jitter satisfy

$$\sigma_x^2 = c_x(\sigma\tau)^2 n^p, \quad C_{x,y} = c_{xy}\sigma\tau n^p, \quad \sigma_y^2 = c_y\sigma^2 n^p, \quad (5)$$

where c_x, c_y, c_{xy} are $O(1)$ constants, σ is nondimensional noise strength, τ is the pulse temporal FWHM, and p is the jitter exponent. Our analysis holds for all $p\geqslant 1$; however, we focus on two physically special cases:

Linear-dispersionless dynamics ($p=1$). This corresponds to cw laser beams, whose dynamics are governed by a linear-dispersionless wave equation. Spontaneous emission leads to a random jitter of the phase of the carrier wave, which, in turn, broadens the spectrum.[5] It can be shown that the phase jitter is a first integral of the noise along the intracavity propagation distance, z, which leads to a (standard) random walk of the phase. Therefore considering a wave train that is emitted from the laser cavity at every $z_n=nL$, for cavity length L, the standard deviation of the phase of the nth wave packet scales as $\sigma_y\sim\sqrt{z_n}\sim\sqrt{n}$; i.e., Eq. (5) with $p=1$. We note that this scaling law has also been found to describe center-time jitter of certain mode-locked lasers.[3,4]

Pure-soliton dynamics ($p=3$). Pulse propagation in mode-locked lasers is described by the master equation; i.e., a nonlinear Schrödinger equation for the electric field in the laser cavity that takes gain and loss mechanisms into account.[6] In many types of mode-locked lasers, the dispersion and nonlinear coefficients vary along z, generating dispersion and nonlinear managed solitons.[9,10] SE occurs in the gain medium, e.g., a Ti:sapphire crystal. These models resemble soliton propagation in amplified telecommunication fibers, which have been studied extensively. Based on such models, Gordon and Haus[11] and Gordon and Mollenauer[12] showed that the center-time and phase jitter of solitons scale as $z^{3/2}$; i.e., Eq. (5) with $p=3$. This is because the frequency jitter is a first integral (along z) of the noise, and, therefore, a standard random walk, whereas nonlinearity and dispersion cause the center-time and phase jitter to be integrals of the frequency jitter.

Taking the average of the comb function Eq. (2) as $\bar{S}(\tilde{\omega})=\int\int\hat{S}(\tilde{\omega})g_n(x,y)\mathrm{d}x\mathrm{d}y$, and using Eqs. (4) and (5), yields the averaged comb function as

$$\bar{S}(\tilde{\omega}) = \sum_{n=1}^{N} \underbrace{e^{i(\tilde{\omega}T_{\mathrm{rep}}+\Delta\phi)n}}_{\text{deterministic}} \underbrace{e^{-(1/2)\epsilon(\tilde{\omega})n^p}}_{\text{averaged noise}},$$
$$\epsilon(\tilde{\omega}) = (c_x\tau^2\tilde{\omega}^2 + 2c_{xy}\tau\tilde{\omega} + c_y)\sigma^2, \quad (6)$$

where $\epsilon(\tilde{\omega})$ is dimensionless.

Our goal is to find the linewidth of the kth comb line, defined as the FWHM of $|\bar{S}(\tilde{\omega})|^2$ around $\tilde{\omega}_k$. It is convenient to normalize this linewidth with respect to ω_{rep}, in which case the normalized $\delta\omega_{1/2}(k)$ satisfies

$$\left|\bar{S}\left(\tilde{\omega}_k+\frac{1}{2}\omega_{\mathrm{rep}}\delta\omega_{1/2}\right)\right|^2 = \frac{1}{2}|\bar{S}(\tilde{\omega}_k)|^2. \quad (7)$$

We first analyze the broadening induced solely by center-time jitter; i.e., when $c_{xy}=c_y=0$, $c_x=1$, and $\epsilon(\tilde{\omega})=(\sigma\tau\tilde{\omega})^2$. Recalling that $\tilde{\omega}=\omega-\omega_c$, the averaged comb function [Eq. (6)] admits the following frequency regimes. Near the carrier frequency, i.e., for $|\omega-\omega_c|\ll(\sigma\tau N^{p/2})^{-1}$ [or $N^p\epsilon(\tilde{\omega})\ll 1$], the broadening is due only to the finite number of pulses. This gives the time-measurement-limited (TML) linewidth that scales like the inverse of the measurement time; i.e., $\delta\omega_{1/2}\sim(NT_{\mathrm{rep}})^{-1}$ (see Fig. 2A). On the other hand, for $|\omega-\omega_c|\gg(\sigma\tau)^{-1}$, the noise-induced exponent in Eq. (6) is so large that the noise smears out the comb lines. In between there is an asymptotic frequency regime, which is characterized by weak noise, i.e., $\epsilon(\tilde{\omega})=(\sigma\tau\tilde{\omega})^2\ll 1$, and many pulses (or long measurement time); i.e., $N^p\epsilon(\tilde{\omega})\gg 1$. These asymptotic conditions bound the frequency as

$$\frac{1}{\sigma\tau N^{p/2}} \ll |\omega-\omega_c| \ll \frac{1}{\sigma\tau}. \quad (8)$$

Within this range, careful asymptotic analysis of Eq. (6) reveals that the linewidth scales as $\delta\omega_{1/2}\sim\epsilon^{1/p}(\tilde{\omega})$. Since $\tilde{\omega}_k\sim k\omega_{\mathrm{rep}}$, it follows that the fundamental relation between center-time jitter and linewidth is given by

$$\sigma_x\sim\sigma\tau n^{p/2} \Rightarrow \delta\omega_{1/2}\sim(\sigma\tau\omega_{\mathrm{rep}})^{2/p}k^{2/p}, \quad (9)$$

where n is pulse number and k is comb-line number. Equation (9) shows that the standard deviation of center-time jitter and the broadening of the comb lines have reciprocal exponents. Since k is enumerated with respect to ω_c, the broadening Eq. (9) is the

largest at the outer edges of the spectrum. Of particular interest are the linear-dispersionless ($p=1$) and pure-soliton ($p=3$) dynamics, which yield $\delta\omega_{1/2}^{\text{linear}} \sim k^2$ and $\delta\omega_{1/2}^{\text{soliton}} \sim k^{2/3}$, respectively (see Fig. 2A). To generate Fig. 2, the averaged comb function [Eq. (6)] is summed in the vicinity of a given comb line [Eq. (3)], and the FWHM [Eq. (7)] of the resulting function is calculated to obtain the linewidth of that comb line. This is repeated for many comb lines to generate the graphs. It follows that the linear-dispersionless linewidth increases parabolically around ω_c, whereas the soliton linewidth increases as $(\omega-\omega_c)^{2/3}$ (see Fig. 2B). We note that Eq. (9) gives the limiting value of the linewidth for long measurement time; i.e., after $N(\omega) \gg |\sigma\tau(\omega-\omega_c)|^{-2/p}$ pulses. All subsequent pulses have a negligible effect on the linewidth. Indeed, we verified that the asymptotic linewidth in Fig. 2 is almost the same with 10^3 and 10^4 pulses.

Returning to the averaged comb function [Eq. (6)], for pure phase jitter, $c_x=c_{xy}=0$, and $\epsilon=c_y\sigma^2$ is independent of ω. Thus phase jitter causes all the comb lines to drift together, maintaining their relative spacing. Using similar analysis as above yields $\delta\omega_{1/2} \sim \sigma^{2/p}$, when $N^{-p/2} \ll \sigma \ll 1$. Since σ^2 scales as the ratio of lasing-threshold power, P_{th}, to mode power, P_{out}, the fundamental relation between phase jitter and linewidth is given by

$$\sigma_y^2 \sim \frac{P_{\text{th}}}{P_{\text{out}}} n^p \Rightarrow \delta\omega_{1/2} \sim \left(\frac{P_{\text{th}}}{P_{\text{out}}}\right)^{1/p}. \qquad (10)$$

For $p=1$ the well-known S–T scaling law is recovered, i.e., $\delta\omega_{1/2}^{\text{S–T}} \sim (P_{\text{out}})^{-1}$, whereas for solitons we obtain that $\delta\omega_{1/2}^{\text{soliton}} \sim (P_{\text{out}})^{-1/3}$. Since $P_{\text{out}} \gg P_{\text{th}}$, this suggests that phase-jitter broadening is more sensitive to power changes with soliton dynamics than with linear-dispersionless dynamics.

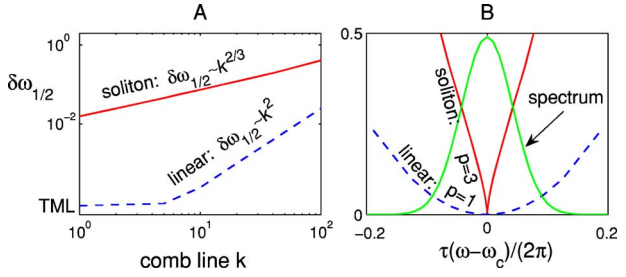

Fig. 2. (Color online) Relative linewidth [i.e., Eq. (7)] induced solely by center-time jitter [i.e., Eq. (6) with $c_{xy}=c_y=0$ and $c_x=1$] with $\omega_{\text{rep}}=2\pi$[GHz], $\tilde{\omega}_o=0$, pulse width $\tau=100$ fs, $N=10^4$ pulses, and noise strength $\sigma=1$. A, Log-log plot, where $k=0$ corresponds to ω_c. Within the asymptotic regime [Eq. (8)], the linewidths computed for the linear dispersionless ($p=1$, dashes) and pure-soliton ($p=3$, solid) dynamics obey the scaling law [Eq. (9)]; i.e., they fit the power laws $\delta\omega_{1/2}^{\text{linear}} \sim k^{2.0}$ and $\delta\omega_{1/2}^{\text{soliton}} \sim k^{0.67}$, respectively. Near the center frequency for $p=1$, the TML linewidth scales as $1/N$. B, Same as A using normalized absolute frequency. The linear-dispersionless and soliton linewidths increase as $(\omega-\omega_c)^2$ and $(\omega-\omega_c)^{2/3}$, respectively. For reference, a single-pulse spectrum with a dimensional FWHM of $1/(10\tau)$ is depicted.

When both center-time and phase jitter are considered, it follows from the comb function [Eq. (6)] that the contribution from center-time jitter dominates at the outer edges of the spectrum, i.e., when $|\omega-\omega_c| \gg 1/\tau$; the phase-jitter contribution dominates near ω_c, i.e., when $|\omega-\omega_c| \ll 1/\tau$; while center-time, phase, and cross-correlation jitter can have comparable effects when $|\omega-\omega_c| \approx 1/\tau$.

In summary, the broadening induced by center-time jitter of linear-dispersionless waves increases parabolically around the center frequency, whereas for solitons, it grows as $(\omega-\omega_c)^{2/3}$. In general, the center-time jitter and linewidth have reciprocal exponents. This result can be understood as a noise-induced manifestation of time-frequency duality. In addition, phase jitter induces a linewidth that scales like $P_{\text{out}}^{-1/p}$, which yields a $P_{\text{out}}^{-1/3}$ scaling law for solitons. We remark that due to the wide range of operating regimes of mode-locked lasers,[3,4,6] one should not rule out any value of the jitter exponent from consideration. In addition, technical noise could change the carrier-envelope phase (instead of the overall phase), which would call for a different choice of random variables.

The authors acknowledge useful conversations with C. R. Menyuk. This research was partially supported by the U.S. Air Force Office of Scientific Research under grant F-49620-03-1-0250 and by the National Science Foundation under grant DMS-0505352. B. Ilan's e-mail address is bilan@ucmerced.edu.

References

1. Th. Udem, R. Holzwarth, and T. W. Hänsch, Nature **416**, 233 (2002).
2. S. T. Cundiff and J. Ye, eds. *Femtosecond Optical Frequency Comb Technology* (Springer, 2005).
3. Y. Takushima, H. Sotobayashi, M. E. Grein, E. P. Ippen, and H. A. Haus, in Proc. SPIE **5595**, 213 (2004).
4. F. X. Kärtner, U. Morgner, T. Schibli, R. Ell, H. A. Haus, J. G. Fujimoto, and E. P. Ippen, Vol. 95 of *Topics in Applied Physics XIV* (Springer-Verlag, 2004), p. 73.
5. A. L. Schawlow and C. H. Townes, Phys. Rev. **112**, 1940 (1958).
6. H. A. Haus and A. Mecozzi, IEEE J. Quantum Electron. **29**, 983 (1993).
7. A. Marian, M. C. Stowe, D. Felinto, and J. Ye, Phys. Rev. Lett. **95**, 023001 (2005).
8. A. Papoulis and S. Unnikrishna Pillai, *Probability, Random Variables and Stochastic Processes* (McGraw-Hill, 2001).
9. Y. Chen, F. X. Kärtner, U. Morgner, S. H. Cho, H. A. Haus, E. P. Ippen, and J. G. Fujimoto, J. Opt. Soc. Am. B **16**, 1999 (1999).
10. Q. Quraishi, S. T. Cundiff, B. Ilan, and M. J. Ablowitz, Phys. Rev. Lett. **94**, 243904 (2005).
11. J. P. Gordon and H. A. Haus, Opt. Lett. **11**, 665 (1986).
12. J. P. Gordon and L. F. Mollenauer, Opt. Lett. **15**, 1351 (1990).

Solitons in two-dimensional lattices possessing defects, dislocations and quasicrystal structures

Mark J. Ablowitz[1], Boaz Ilan[2], Ethan Schonbrun[3], and Rafael Piestun[3]
[1]*Department of Applied Mathematics, University of Colorado, Boulder, Colorado 80309-0526, USA*
[2]*School of Natural Sciences, University of California, Merced, P.O. Box 2039, Merced, California 95344, USA and*
[3]*Department of Electrical and Computer Engineering,*
University of Colorado, Boulder, Colorado 80309-0425, USA
(Dated: August 29, 2006)

Localized nonlinear modes, or solitons, are obtained for the two-dimensional nonlinear Schrödinger equation with various external potentials that possess large variations from periodicity, i.e., vacancy defects, edge dislocations, and quasicrystal structure. The solitons are obtained by employing a spectral fixed-point computational scheme. Investigation of soliton evolution by direct numerical simulations shows that irregular-lattice solitons can be stable, unstable or undergo collapse.

PACS numbers: 05.45.Yv: Solitons; 63.20.Pw: Localized modes in Lattices; 61.44.Br: Quasicrsytals; 42.65.Tg: Optical solitons; nonlinear guided waves

Solitons are localized nonlinear waves that occur in many branches of physics and their properties have provided a deep and fundamental understanding of complex nonlinear systems. In recent years there has been considerable interest in the study of solitons in systems with periodic potentials or lattices, in particular those that can be generated in nonlinear optical materials. [1–5] In periodic lattices, solitons can form when their propagation constant, or eigenvalue, lies within certain regions, often called gaps, a concept that is borrowed from Floquet-Bloch theory for linear propagation. However, the external potential of complex systems can be much more general and physically richer than a periodic lattice. For example, atomic crystals can possess various irregularities, such as defects and edge dislocations, as well as quasicrystal structures, which have long-range orientational order but no translational symmetry [6, 7]. In general, when the lattice's periodicity is slightly perturbed, the band-gap structure and soliton properties become slightly perturbed as well, but otherwise solitons are expected to exist in much the same way as in the perfectly periodic case [8, 9]. However, the existence and properties of multidimensional solitons when the external potential possesses *large variations from periodicity* has remained largely unexplored.

In this Letter, we find two-dimensional (**2D**) solitons in lattices possessing vacancy defects, edge-dislocations, and quasicrystal structures. This is achieved using a fixed-point spectral method for computing the ground-states of the underlying Nonlinear Schrödinger (**NLS**) equation. A comparative study of the power-eigenvalue dependence leads to important observations regarding soliton power, gap edge and stability properties. Evolution is investigated by direct numerical simulations, showing that slightly-perturbed solitary waves in irregular lattices can either undergo small or large amplitude oscillations or collapse. We note that the physical properties of optically generated quasicrystal potentials have generated significant interest and that vortex waves have recently been employed in the generation of localized defects within optical lattices [10, 11]. Our results also have application to photonic band-gap systems, wherein novel experimental techniques have recently been used to fabricate irregular lattice structures [11–14].

We study the nonlinear system governed by the focusing (2+1)D NLS equation (in nondimensional units) with an external potential,

$$iu_z + \Delta u + |u|^2 u - V(x,y)u = 0\,. \tag{1}$$

In optics, $u(x,y,z)$ corresponds to a complex-valued slowly-varying amplitude of the electric field in the (x,y) plane that is propagating along the z direction, $\Delta u \equiv u_{xx} + u_{yy}$ corresponds to diffraction, the cubic term in u originates from the nonlinear (Kerr) change in the refractive index, and the potential $V(x,y)$ corresponds to a modulation of the linear refractive index of the medium. Equation (1) also governs the dynamics of certain Bose-Einstein Condensates (**BEC**), where $u(x,y,z)$ represents the wave function of the mean-field atomic condensate that is trapped in a potential [15].

We look for localized solutions of Eq. (1) in the form $u(x,y,z) = f(x,y)\,e^{-i\mu z}$, where μ is the propagation constant (or eigenvalue) and $f(x,y)$ is a real-valued localized function that, following Eq. (1), satisfies the nonlinear eigenequation

$$\Delta f + \left[\mu + |f|^2 - V(x,y)\right] f = 0\,. \tag{2}$$

In this study we consider potentials that can be written as the intensity of a sum of N phase-modulated plane waves, i.e.,

$$V(x,y) = \frac{V_0}{N^2}\left|\sum_{n=0}^{N-1} e^{i\vec{\mathbf{k}}_n\cdot\vec{\mathbf{r}}+i\theta_n(x,y)}\right|^2\,, \tag{3}$$

where $V_0 > 0$ is constant, $\vec{\mathbf{r}} = (x,y)$, $\vec{\mathbf{k}}_n$ is a wavevector, $\theta_n(x,y)$ is a phase function through which irregularities are introduced, and the normalization by N^2 gives that V_0 is the potential's peak-depth, i.e., $V_0 = \max_{x,y} V(x,y)$. Such 2D potentials can be physically realized in optics by interference of plane waves and phase functions [11]. In some situations, they are invariant in the third dimension [16]. For example, these phase functions can be composed from different configurations of vortices [17], which, in turn, can be created using computer-generated holograms [11].

In order to solve Eq. (2), we use a fixed point spectral computational method [18], as explained below. Applying the

Fourier transform of to Eq. (2) and adding and subtracting a term $r\hat{u}$, where $r > 0$ is constant, leads to

$$\hat{f}(\nu) = \hat{R}[\hat{f}] \equiv \frac{(r+\mu)\hat{f} + \mathcal{F}\left\{[|f|^2 - V(x,y)]f\right\}}{r + |\nu|^2} ,$$

where $\nu = (\nu_x, \nu_y)$ are the Fourier variables, $\mathcal{F}$ stands for the Fourier transform, and the role of the constant r is to avoid a singularity in the denominator (we use $r = 5$). A new field variable is introduced as $f(x,y) = \lambda w(x,y)$, where $\lambda \neq 0$ is a constant to be determined. The iteration method takes the form $\hat{w}_{m+1} = \lambda_m^{-1}\hat{R}[\lambda_m \hat{w}_m], m = 0, 1, 2, \dots$, where λ_m satisfies the associated *algebraic condition*

$$\iint_{-\infty}^{+\infty} |\hat{w}_m(\nu)|^2 \, d\nu = \lambda_m^{-1} \iint_{-\infty}^{+\infty} \hat{R}[\lambda_m \hat{w}_m]\hat{w}_m^*(\nu) \, d\nu .$$

It has been found that this method prevents the numerical scheme from diverging. Thus, the soliton is obtained from a convergent iterative scheme (see also [19] for an alternative procedure in case there is a well-defined homogeneity). The initial "starting point", $w_0(x,y)$, is typically chosen to be a Gaussian. The iterations are stopped when the relative convergence factor, $\delta = \left|\frac{\lambda_{m+1}}{\lambda_m} - 1\right|$, reaches 10^{-10}. We note that convergence is reached quickly, but slows down as the mode becomes more extended, i.e., as μ approaches the (nonlinear) gap edge. We also note that the convergence of a similar method has been proven under suitable assumptions on the potential. [20]

The first case of the potential (3) we study is an irregular 2D square lattice with a *vacancy defect* [see Figure 1(a)], i.e.,

$$V(x,y) = \frac{V_0}{25}\left|2\cos(k_x x) + 2\cos(k_y y) + e^{i\theta(x,y)}\right|^2 , \quad (4)$$

where the phase function $\theta(x,y)$ is given by

$$\theta(x,y) = \tan^{-1}\left(\frac{y-y_0}{x}\right) - \tan^{-1}\left(\frac{y+y_0}{x}\right).$$

Physically, $\theta(x,y)$ corresponds to two first-order phase dislocations displaced in the y-direction by a distance of $2y_0$. A vacancy defect can thus be obtained using $y_0 = \pi/K$, where $K = k_x = k_y$. Note that the "vacancy" in the origin is created from a continuous function and that far from the origin the potential (4) is locally a square lattice with period $2\pi/K$. Using the computational method outlined above, localized modes (solitons) of Eqs. (2) and (4) are found, centered around the vacancy as shown in Fig. 1(b). In certain respects, they resemble solitons centered around a minimum of a periodic square lattice. In further investigations, it is found that as the soliton's center is moved farther from the vacancy, its profile and band-gap structure converge to those of the corresponding periodic lattice [i.e., Eq. (4) with $\theta(x,y) \equiv 0$].

In a similar manner, a lattice with an *edge dislocation*, analogous to those that can be found in atomic crystals [7, 11], can be obtained from Eq. (3) using

$$V(x,y) = \frac{V_0}{25}\{2\cos[k_x x + \theta(x,y)] + 2\cos(k_y y) + 1\}^2 \quad (5)$$

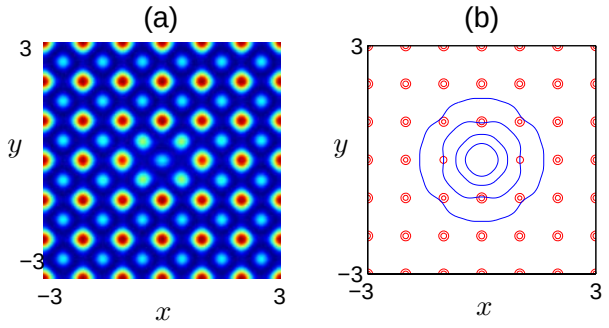

FIG. 1: (Color online) (a) Contour image of a lattice with a vacancy defect, i.e., Eq. (4) with $K = k_x = k_y = 2\pi$ and $V_0 = 12.5$. Spots correspond to local maxima. (b) Contour plot of the soliton with $\mu = 0.5$ superimposed on the lattice. For visibility, only a small portion of the $[-10, 10]^2$ computational domain is presented.

with the phase-dislocation function $\theta(x,y) = \frac{3\pi}{2} - \tan^{-1}\left(\frac{y}{x}\right)$. Figure 2(a) shows that this dislocation is unlike a point defect, insofar as the density of lattice sites changes vertically across the lattice. Despite this strong irregularity, solitons are found to exist in the vicinity of the phase dislocation. Figure 2(b) shows that the soliton has an asymmetric shape. The soliton's center is situated above the phase dislocation, in between neighboring local maxima of the lattice. In this respect, it is like a soliton on a lattice minimum. It should be noted that the starting point of the computational method is around the origin and, during the iterations, the solution moves upward along the y axis, until convergence is reached.

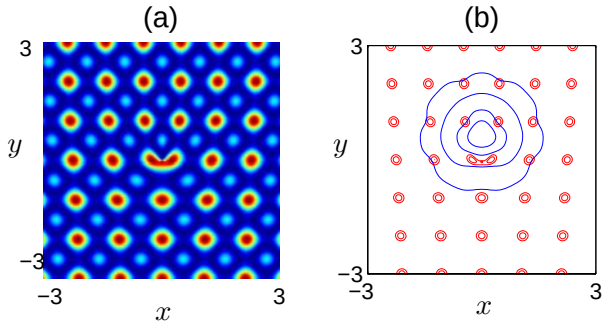

FIG. 2: (Color online) Same as Fig. 1 for a lattice with an edge dislocation [Eq. (5)], using the same lattice parameters and $\mu = 0.5$ as in Fig. 1. The soliton's peak is located at $(0, 0.68)$.

Next we investigate solitons on *quasicrystal lattices*. Such lattices appear naturally in certain molecules [6, 7], have been investigated in optics [21–23], and studied in BEC [24]. Importantly, Freedman *et al.* recently predicted and observed solitons in Penrose quasicrystals, which were generated using the method of optical induction [25]. In this study, the optical potential is formed by the far-field diffraction pattern of a mask with point-apertures that are located on the N vertices

of a regular polygon. The corresponding potential is given by

$$V(x,y) = \frac{V_0}{N^2}\left|\sum_{n=0}^{N-1} e^{i(k_x x + k_y y)}\right|^2, \qquad (6)$$

where $(k_x, k_y) = (K\cos(2\pi n/N), K\sin(2\pi n/N))$. The potential (6) with $N = 2, 3, 4, 6$ yields periodic lattices, which correspond to the standard 2D crystal structures. All other values of N correspond to quasicrystals, which have a local symmetry around the origin and long-range order, but, unlike periodic crystals, are not invariant under spatial translation [26]. Below we focus on the case $N = 5$ [see Fig. 3(a)], whose lattice is often referred to as a Penrose quasicrystal.

We find solitons on the Penrose lattice [see Fig. 3(b)], centered around the origin, which is the global maximum of the lattice potential. Similar to solitons centered at the maximum of a periodic square lattice, these Penrose solitons have a dimple (see Fig. 4). Further investigations reveal that Penrose solitons centered around local minima do not have a dimple, similar to their periodic-lattice counterparts.

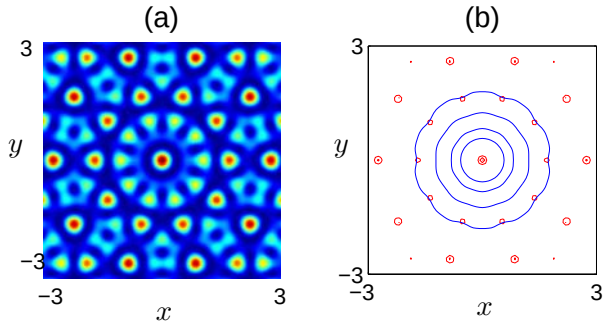

FIG. 3: (Color online) Same as Fig. 1 for a Penrose lattice [Eq. (6) with $N = 5$] and corresponding soliton centered around the center (maximum), using the same lattice parameters and $\mu = 0.5$ as in Fig. 1.

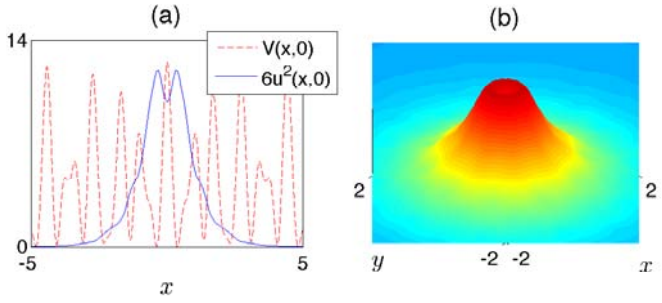

FIG. 4: (Color online) Similar to solitons on the maxima of periodic lattices, Penrose solitons can have a dimple, which becomes more pronounced for large values of μ, i.e., near the gap edge. (A) Cross-section along the y axis of a Penrose soliton ($6u^2(x,0)$, solid) with $\mu = 2$, superimposed on the underlying lattice (dashes). (B) 3D view of a soliton's intensity showing the dimple.

It is noteworthy that in the limit of waves impinging from all directions (i.e., $N \to \infty$) the quasicrystal lattice (6) approaches the Bessel lattice, i.e., $\lim_{N\to\infty} V_(x,y;N) = V_0 J_0^2(Kr)$, in which solitons have recently been studied (cf. [27]). In fact, as N increases, at any given radius the angular distance between the lattice maxima (and minima) decreases and the limiting Bessel lattice has continuous rings of maxima.

We note that some of the previous studies of Penrose lattices considered a different definition of the lattice, whereby cylinders of Kerr material were located at vertices of a (virtual) Penrose tile surrounded by air [21–23, 28, 29]. In contrast, the medium considered here is homogeneous, with a constant Kerr coefficient and continuous modulation of the linear refractive index (6).

To compare the different lattice solitons, in Fig. 5 we plot the soliton power, $P = \int |u|^2\, dxdy$, as a function of eigenvalue μ, for all the lattices studied above as well as for the corresponding periodic square-lattice [i.e., Eq. (4) with $\theta(x,y) \equiv 0$] centered around either local minima and maxima. We remark that all the above lattices share a common peak-depth, $V_0 = 12.5$, as well as periodicity far from the irregularity, $K = 2\pi$, where, for the Penrose lattice, K can be thought of as a "local" wavenumber [see Eq. (6)].

We define the first nonlinear gap edge, $\mu_{\max}$, as the minimal eigenvalue beyond which the numerical method does not converge to a localized state. The comparison shows that all the lattices above have a semi-infinite gap, i.e., the numerical method converges to a localized state when $\mu < \mu_{\max}$, for some lattice-dependent $\mu_{\max}$. When the eigenvalue exceeds $\mu_{\max}$, the numerical method typically converges to an extended state (but see below for exceptions). In addition, the comparison reveals that (see Fig. 5): (*i*) The power of vacancy-defect, edge-dislocation, and Penrose-quasicrystal lattice solitons is lower than their periodic counterparts for a considerable range of eigenvalues. In particular, of all the lattices studied here, the lowest power is obtained for vacancy and edge dislocation solitons. (*ii*) A vacancy defect has little effect on the gap size ($\mu_{\max} \approx 2$), but it significantly reduces the power threshold, i.e., the minimal soliton power throughout the gap. However, it is noteworthy that the power threshold is positive for all these potentials, i.e., the irregularities do not allow the formation of linear (zero-power) modes within the gap. (*iii*) An edge-dislocation reduces the gap size (note: $\mu_{\max} \approx 0.95$), whereas, (*iv*) a Penrose soliton has a slightly larger gap size ($\mu_{\max} \approx 2.2$) compared to a solitons on a periodic square lattice. However, solitons on the maxima of periodic-square and Penrose lattices have a similar power behavior, which is a somewhat unexpected result, since these lattices have a very different structure.

A striking observation in Fig. 5 is that the gap edge with an edge-dislocation occurs at $0.9 < \mu_{\max} < 0.95$, which is considerably smaller than for the other lattices. In fact, during the computation, an interesting phenomenon occurs as μ is increased. When $\mu = 0.9$, a reliable convergence ($\delta = 10^{-10}$) is reached and, in this case, the solution is between the local maxima shown in Fig. 2(b). When $\mu = 0.95$, the solution initially converges at the same location (with $\delta = 10^{-5}$). However, this "convergence" is misleading, since with further iterations the solution moves upward along the y axis, "slid-

ing" up in between two local maxima and eventually converging (with $\delta = 10^{-10}$) in between the four local maxima that are one lattice cell above the edge dislocation. The resulting soliton is therefore similar to one on a periodic square lattice, insofar as the nearest four lattice maxima are approximately symmetric and equi-spaced. In fact, further investigations reveal that for $0.95 < \mu < 2$ the soliton remains one lattice cell above the dislocation and its power-eigenvalue dependence is very similar to that of on a periodic lattice. Thus, the edge-dislocation clearly shrinks the size of the nonlinear gap.

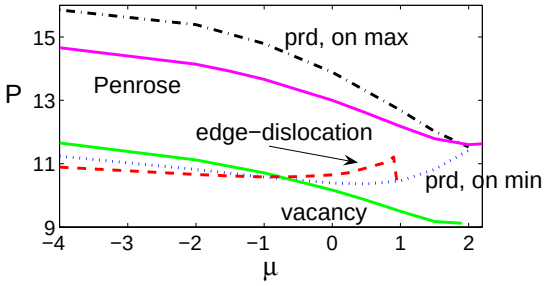

FIG. 5: (Color online) Soliton power as a function of eigenvalue within the semi-infinite band-gap, for the same lattices as in the previous figures, as well as solitons on the maximum and minimum of a periodic ("prd") square lattice. All lattices share a common peak depth, $V_0 = 12.5$, and background periodicity, $K = 2\pi$.

The question of soliton evolution under perturbations is important for applications. To study this, we perform direct computations of Eq. (1) using the various potentials, where the initial conditions are the soliton with 1% random noise in amplitude and phase. Generically, it is found that: (*i*) solitons centered around lattice minima (e.g., of periodic, vacancy, edge-dislocation and quasicrystal lattices) undergo small-amplitude oscillations when $dP/d\mu < 0$ and large-amplitude oscillations when $dP/d\mu > 0$; (*ii*) solitons centered around lattice maxima (e.g., of periodic and quasicrystal lattices) can undergo collapse after finite propagation distance.

In conclusion, the existence of stable 2D solitons is demonstrated in self-focusing media with irregular lattice potentials possessing vacancy defects, dislocations, and quasicrystal structures. Fig. 5 shows that these Penrose solitons are similar to solitons on periodic-lattice maxima; whereas, there are significant differences between vacancy and edge-dislocations solitons as compared to their periodic-lattice counterparts.

This work was partially supported by US Air Force under grant F-49620-03-1-0250.

[1] D. N. Christodoulides, F. Lederer, and Y. Silberberg, Nature **424**, 817 (2003).
[2] A. A. Sukhorukov, Y. S. Kivshar, H. S. Eisenberg, and Y. Silberberg, IEEE J. Quant. Elec. **39**, 31 (2003).
[3] N. K. Efremidis, J. Hudock, D. N. Christodoulides, J. W. Fleischer, O. Cohen, and M. Segev, Phys. Rev. Lett. **91**, 213906 (2003).
[4] J. W. Fleischer, M. Segev, N. K. Efremidis, and D. N. Christodoulides, Nature **422**, 147 (2003).
[5] D. Neshev, Y. S. Kivshar, H. Martin and Z. Chen, Opt. Lett. **29**, 486 (2004).
[6] D. Shechtman, I. Blech, D. Gratias, and J. W. Cahn, Phys. Rev. Lett. **53**, 1951 (1984).
[7] M. P. Marder, *Condensed Matter Physics* (Wiley-Interscience, New-York, 2001).
[8] F. Fedele, J. Yang, and Z. Chen, Stud. Appl. Math. **115**, 279 (2005).
[9] H. Buljan, G. Bartal, O. Cohen, T. Schwartz, O. Manela, M. Segev, T. Carmon, J. W. Fleischer, and D. N. Christodoulides, Stud. Appl. Math. **115**, 173 (2005).
[10] L. Guidoni, C. Triché, P. Verkerk, and G. Grynberg, Phys. Rev. Lett. **79**, 3363 (1997).
[11] E. Schonbrun and R. Piestun, Opt. Eng. **45**, 028001 (2006).
[12] T. Pertsch, U. Peschel, F. Lederer, J. Burghoff, M. Will, S. Nolte, and A. Tünnermann, Opt. Lett. **29**, 468 (2004).
[13] M. Qi, E. Lidorikis, P. T. Rakich, S. G. Johnson, J. D. Joannopoulos, E. P. Ippen, and H. I. Smith, Nature **429**, 538 (2004).
[14] W. Cai and R. Piestun, Appl. Phys. Lett. **88**, 111112 (2006).
[15] C. J. Pethick and H. Smith, *Bose-Einstein Condensation in Dilute Gases* (Cambridge University Press, 2001).
[16] R. Piestun and J. Shamir, J. Opt. Soc. Am. A **15**, 3039 (1998).
[17] J. F. Nye and M. V. Berry, Proc. Royal Soc. London **336**, 165 (1974).
[18] M. J. Ablowitz and Z. H. Musslimani, Opt. Lett. **30**, 2140 (2005).
[19] Z. H. Musslimani and J. Yang, J. Opt. Soc. Am. B **21**, 973 (2004).
[20] D. E. Pelinovsky and Y. A. Stepanyants, SIAM J. Appl. Math. **42**, 1110 (2004).
[21] R. T. Bratfalean, A. C. Peacock, N. G. R. Broderick, K. Gallo, and R. Lewen, Opt. Lett. **30**, 424 (2004).
[22] R. Lifshitz, A. Arie, and A. Bahabad, Phys. Rev. Lett. **95**, 133901 (2005).
[23] W. Man, M. Megens, P. J. Steinhardt, and P. M. Chaikin, Nature **436**, 993 (2005).
[24] L. Sanchez-Palencia and L. Santos, PRA **72**, 053607 (2005).
[25] B. Freedman, G. Bartal, M. Segev, R. Lifshitz, D. N. Christodoulides, and J. W. Fleischer, Nature **440**, 1166 (2006).
[26] M. Senechal, *Quasicrystals and Geometry* (Cambridge University Press, 1995).
[27] Y. V. Kartashov, V. A. Vysloukh, and L. Torner, Phys. Rev. Lett. **93**, 093904 (2004).
[28] P. Xie, Z.-Q. Zhang, and X. Zhang, Phys. Rev. E **67**, 026607 (2003).
[29] A. Della Villa, S. Enoch, G. Tayeb, V. Pierro, V. Galdi, and F. Capolino, Phys. Rev. Lett. **94**, 183903 (2005).

DISCRETE SCALAR AND VECTOR DIFFRACTION-MANAGED NONLINEAR SCHRÖDINGER EQUATION

MARK J. ABLOWITZ AND ZIAD H. MUSSLIMANI

Department of Applied Mathematics, University of Colorado at Boulder
Campus Box 526, Boulder, CO 80309-0526, USA

In this paper, an asymptotic equation is derived from first principles which governs the propagation of electromagnetic waves in a waveguide array in the presence of both normal and anomalous diffraction. This is termed diffraction management. The theory is then extended to the vector case of coupled polarization modes.

1. Introduction

Dynamics of discrete nonlinear systems dates back to the mid fifties when Fermi, Pasta and Ulam (FPU) studied dynamics of nonlinear springs [1]. Apart from the fact that the work of FPU motivated the discovery of solitons, it also stimulated considerable interest in the study of discrete nonlinear media which possesses self-confined structures (discrete solitary waves). Such waves are localized modes of nonlinear lattices that form when "discrete diffraction" is balanced by nonlinearity. In physics a soliton usually denotes a stable localized wave structure, i.e., solitary wave. We shall use the term soliton in this broader sense (i.e., they do not necessarily interact elastically). Discrete solitons have been demonstrated to exist in a wide range of physical systems [2−5]. For example, atomic chains [6,7] (discrete lattices) with on-site cubic nonlinearities, molecular crystals [8], biophysical systems [9], electrical lattices [10], and recently in arrays of coupled nonlinear optical waveguides [11,12]. An array of coupled optical waveguides is a setting that represents a convenient laboratory for experimental observations.

The first theoretical prediction of discrete solitons in an optical waveguide array was reported by Christodoulides and Joseph [13]. Later, many theoretical studies of discrete solitons in a waveguide array reported switching, steering and other collision properties of these solitons [14−19] (see also the review papers [20,21]). In all of the above cases, the localized modes are solutions of the well known discrete nonlinear Schrödinger (DNLS) equa-

tion which describes beam propagation in Kerr nonlinear media (according to coupled mode theory). Discrete bright and dark solitons have also been found in quadratic media [22], in some cases, their properties differ from their Kerr counterparts [23].

In fact, the DNLS equation (and its "cousins" such as diffraction managed DNLS or DNLS with a potential such as discrete BEC) is "asymptotically universal". Namely it is the discrete equation which emerges from either a weakly nonlinear Helmholtz equation with a suitable "potential" or a weakly nonlinear continuous NLS equation with a suitable potential where the following terms are in balance:

i) slow variation in either distance (waveguide array) or time (for BEC);
ii) linear terms induced by a potential which can be viewed as asymptotically separated localized potentials (sometimes called the "tight binding approximation");
iii) nonlinearity.

It took almost a decade until self-trapping of light in discrete nonlinear waveguide array was experimentally observed (Eisenberg et. al. [11,12]). When a low intensity beam is injected into one or a few waveguides, the propagating field spreads over the adjacent waveguides hence experiencing discrete diffraction. However, at sufficiently high power, the beam self-traps to form a localized state (a soliton) in the center waveguides. Subsequently, many interesting properties of nonlinear lattices and discrete solitons were reported. For example the experimental observation of linear and nonlinear Bloch oscillations in: AlGaAs waveguides [24], polymer waveguides [25] and in an array of curved optical waveguides [26]. Discrete systems have unique properties that are absent in continuous media such as the possibility of producing *anomalous* diffraction [27]. Hence, self-focusing and defocusing processes can be achieved in the same medium (structure) and wavelength. This also leads to the possibility of observing discrete dark solitons in self-focusing Kerr media [28]. The recent experimental observations of discrete solitons [11] and diffraction management [27] have motivated further interest in discrete solitons in nonlinear lattices. This includes the newly proposed model of discrete diffraction managed nonlinear Schrödinger equation [29,30] whose width and peak amplitude vary periodically; optical spatial solitons in nonlinear photonic crystals [31−33] and the possibility of creating discrete solitons in Bose-Einstein condensation [34]. Also, recently, it was shown that discrete solitons in two-dimensional networks of nonlinear waveguides can be used to realize intelligent functional operations such as blocking,

routing, logic functions and time gating [35−38]. In addition, spatiotemporal discrete solitons have been recently suggested in nonlinear chains of coupled microcavities embedded in photonic crystal structures [39]. Additional useful references could be found in [40−56].

In this paper, an asymptotic equation is derived from first principles which governs the propagation of electromagnetic waves in a waveguide array in the presence of both normal and anomalous diffraction. This is related to the second model discussed above, i.e., diffraction managed DNLS equation. The theory is then extended to the vector case of coupled polarization modes.

2. Linear and Nonlinear Propagation

If the full width at half maximum (FWHM), τ, of the optical field is small compared to the distance, d, between adjacent waveguides, then the propagating beams across each single waveguide do not "feel" each other. Therefore, the amplitude of each beam evolves independently according to the linear wave equation:

$$\frac{d^2\psi_0}{dx^2} + \left[k_0^2 f_0^2(x) - \lambda_0^2\right]\psi_0 = 0 \,, \tag{2.1}$$

where k_0 is the wavenumber of the optical field in vacuum; f_0^2 is the refractive index of a single waveguide and λ_0 is the lowest eigenvalue (propagation constant) that corresponds to the ground state ψ_0 (a bell shape eigenfunction). In this respect we have assumed that a single waveguide supports only a single mode. The more intricate situation of multimode waveguide is also possible in which case $\lambda_0 \to \lambda_j$ and $\psi_0 \to \psi_j$ where j is the number of modes occupied by a single waveguide. On the other hand when τ is on the order of d or larger, then there is significant overlap between modes of adjacent waveguides. In either case, the beam's amplitude is not constant in z anymore. Moreover, when the intensity of the incident beam is sufficiently high then the refractive index of the medium will depend on the intensity, which for Kerr media is proportional to the intensity. In this case, the evolution of the total field's amplitude Ψ follows from Maxwell equations

$$\left(\frac{\partial^2}{\partial z^2} + \frac{\partial^2}{\partial x^2}\right)\Psi + \left(k_0^2 f^2(x) + \delta|\Psi|^2\right)\Psi = 0 \,, \tag{2.2}$$

where $f^2(x)$ represents the refractive index of the entire structure and δ is a small parameter to be determined later. If the overlap between adjacent modes is "small", which is valid in the regime $\mu \equiv \tau/d \ll 1$, we expect

the power exchange to be slow. By introducing a slow scale $Z = \varepsilon z$ (ε is a small parameter to be determined later) we approximate the solution to Eq. (2.2) as a multiscale perturbation series:

$$\Psi = \sum_{m=-\infty}^{+\infty} E_m(Z)\psi_m(x)\exp(-i\lambda_0 z) \; . \tag{2.3}$$

In this notation, $\psi_m(x) = \psi_0(x - md)$ and $f_m^2(x) = f_0^2(x - md)$. Substituting the ansatz (2.3) into Eq. (2.2), we find

$$\sum_{m=-\infty}^{+\infty}\Bigg[-2i\varepsilon\lambda_0\psi_m\frac{\partial E_m}{\partial Z} + \varepsilon^2\psi_m\frac{\partial^2 E_m}{\partial Z^2} + \left(\frac{d^2\psi_m}{dx^2} + k_0^2 f^2\psi_m - \lambda_0^2\psi_m\right)E_m + \delta\sum_{m',m''} E_m E_{m'} E^*_{m''}\psi_m\psi_{m'}\psi^*_{m''}\Bigg] e^{-i\lambda_0 z} = 0 \; . \tag{2.4}$$

Using Eq. (2.1) in the above equation, multiplying Eq. (2.4) by $\psi_n^* \exp(i\lambda_0 z)$ and integrating over x yields the following

$$\sum_{m=-\infty}^{+\infty}\Bigg[\left(-2i\varepsilon\lambda_0\frac{\partial E_m}{\partial Z} + \varepsilon^2\frac{\partial^2 E_m}{\partial Z^2}\right)\int_{-\infty}^{+\infty} dx\psi_m\psi_n^* + k_0^2 E_m\int_{-\infty}^{+\infty} dx\Delta f_m^2\psi_m\psi_n^* + \delta\sum_{m',m''} E_m E_{m'} E^*_{m''}\int_{-\infty}^{+\infty} dx\psi_n^*\psi_m\psi_{m'}\psi^*_{m''}\Bigg] = 0 \; . \tag{2.5}$$

Here, $\Delta f_m^2 \equiv f^2 - f_m^2$ which measures the deviation of the total refractive index from each individual waveguide. As mentioned earlier, the overlap integral between adjacent waveguides is an important measure in determining the dynamic evolution of the modes. With this in mind, we shall *assume* that the overlap integrals appearing in Eq. (2.5) can be approximated by

$$\begin{gathered}\int dx\psi_m\psi^*_{m+N} = a_N\varepsilon^N \; , \quad \int dx\Delta f_m^2|\psi_m|^2 = c_0\varepsilon \; , \\ \int dx\Delta f_m^2\psi_m\psi^*_{m\pm1} = c_1\varepsilon \; .\end{gathered} \tag{2.6}$$

In order to understand the idea behind this scaling, we will assume that the mode at waveguide m can be modeled by

$$\psi_m(x) = \mathrm{sech}\kappa(x - md) \; , \tag{2.7}$$

where $\kappa = 1/\tau$; τ is the FWHM. The reason for this choice is only to simplify the analysis. In fact, the real modes of a step index waveguide has exponential behavior which is close to a sech like mode. Other choices of

eigen-functions with different exponential decay are possible, e.g., $\psi_m(x) = \exp[-(x-md)^2/\tau^2]$ but the basic ordering mechanism remains the same. A straightforward calculation shows that

$$\int_{-\infty}^{+\infty} dx \psi_m \psi_n^* = c e^{-|n-m|/\mu} \ , \tag{2.8}$$

with c being a constant of order one. Since $\mu \ll 1$, then the choice $\varepsilon = \exp(-1/\mu)$ provides a measure for the order of magnitude for the overlap integral. Restricting the sum in Eq. (2.5) to nearest neighbors i.e., $m = n, n \pm 1$ (which contribute to the order ε equation) and assuming that the only order 1 contribution comes from the nonlinear term is when $m = n = m' = m''$ and that

$$\int_{-\infty}^{+\infty} dx |\psi_n|^4 = g_{nl} \ ,$$

we find that to $O(\varepsilon)$ the nonlinear evolution of E_n is given by

$$-2i\lambda_0 a_0 \frac{\partial E_n}{\partial Z} + k_0^2 c_0 E_n + k_0^2 c_1 (E_{n+1} + E_{n-1}) + g_{nl} |E_n|^2 E_n = 0 \ , \tag{2.9}$$

where we have taken $\delta = \varepsilon$ to ensure maximal balance. By defining new variables $\tilde{z} = Z/(2\lambda_0 a_0)$, $k_0^2 c_1 = C$, $E_n = \tilde{E}_n^* \exp(-ik_0^2 c_0 \tilde{z})$ we find that $\tilde{E}_n$ satisfies (dropping the tilde)

$$i\frac{\partial E_n}{\partial z} + C(E_{n+1} + E_{n-1}) + g_{nl} |E_n|^2 E_n = 0 \ . \tag{2.10}$$

To put the DNLS equation in dimensionless form, we define

$$E_n = \sqrt{P_*} \phi_n \exp(2iCz) \ , \qquad z' = z/z_{nl} \tag{2.11}$$

with P_* and z_{nl} being the characteristic power and z_{nl} the nonlinear length scale. Then ϕ_n satisfies

$$i\frac{d\phi_n}{dz} + \frac{1}{h^2}\Big(\phi_{n+1} + \phi_{n-1} - 2\phi_n\Big) + |\phi_n|^2 \phi_n = 0 \ , \tag{2.12}$$

with $z_{nl} C = 1/h^2$ and $z_{nl} = 1/(g_{nl} P_*)$. In the DNLS equation there are two important length scales: the diffraction and nonlinear length scales respectively defined by $L_D \sim 1/C$ and $z_{nl} = 1/(g_{nl} P_*)$. Solitons which are self-confined and invariant structures are expected to form when $L_D \sim z_{nl}$.

3. Asymptotic Theory for Diffraction Management

3.1. *Renormalization*

We have seen in the preceding section how can we build, based on physical heuristic arguments, a model that incorporate both normal and anomalous

diffraction. The key idea in formulating a model of diffraction management, is to use a cascade of different segments of waveguide, each piece being tilted by an angle zero and γ respectively. Here, we give a derivation of the model, in the scalar case, based on asymptotic theory. Two approaches are given. The first is based on perturbation expansion using a renormalized eigen-mode of each single waveguide, whereas in the second we expand around eigenfunction of an untilted waveguide. It is clear that each single waveguide is not stationary. As a result, the evolution of the beam's amplitude in the linear approximation is governed by

$$\left(\frac{\partial^2}{\partial z^2}+\frac{\partial^2}{\partial x^2}\right)\Psi+k_0^2 f^2(X)\Psi=0\;,\qquad X=x-\frac{\alpha}{\varepsilon}\int_0^Z \mathsf{D}(Z')dZ'\;, \quad (3.13)$$

where as before, $Z=\varepsilon z$; α is a small parameter to be determined later and $\mathsf{D}(Z)$ is a *piecewise constant* periodic function that measures the local value of diffraction. When the waveguides are well separated then the dynamics of each mode ψ_m in waveguide f_m^2 is decoupled and is given by

$$\Big(\alpha^2\mathsf{D}^2(Z)+1\Big)\frac{d^2\psi_m}{dX^2}+\Big(k_0^2 f_m^2(X)-\lambda_0^2\Big)\psi_m=0\;. \quad (3.14)$$

However when the waveguides are at close proximity, we approximate the solution to Eq. (3.13) as a multiscale perturbation series:

$$\Psi=\sum_{m=-\infty}^{+\infty}\mathsf{E}_m(Z)\psi_m(X)e^{-i\lambda_0 z}\;. \quad (3.15)$$

Substituting the ansatz (3.15) into Eq. (3.13), we find

$$\begin{aligned}&\sum_{m=-\infty}^{+\infty}\Bigg[-2i\varepsilon\lambda_0\psi_m\frac{\partial\mathsf{E}_m}{\partial Z}+\varepsilon^2\psi_m\frac{\partial^2\mathsf{E}_m}{\partial Z^2}\\&+\left(\Big(\alpha^2\mathsf{D}^2+1\Big)\frac{d^2\psi_m}{dX^2}+k_0^2f^2\psi_m-\lambda_0^2\psi_m\right)\mathsf{E}_m\\&+2i\alpha\lambda_0\mathsf{D}\mathsf{E}_m\frac{d\psi_m}{dX}-2\alpha\varepsilon\mathsf{D}\frac{\partial\mathsf{E}_m}{\partial Z}\frac{d\psi_m}{dX}-\alpha\varepsilon\mathsf{E}_m\frac{d\mathsf{D}}{dZ}\frac{d\psi_m}{dX}\Bigg]e^{-i\lambda_0 z}=0 \quad (3.16)\end{aligned}$$

Using Eq. (3.14) in the above equation, multiplying Eq. (3.16) by $\psi_n^*\exp(i\lambda_0 z)$ and integrating over X yields the following

$$\begin{aligned}&\sum_{m=-\infty}^{+\infty}\Bigg[\left(-2i\varepsilon\lambda_0\frac{\partial\mathsf{E}_m}{\partial Z}+\varepsilon^2\frac{\partial^2\mathsf{E}_m}{\partial Z^2}\right)\int_{-\infty}^{+\infty}dX\psi_m\psi_n^*\\&+k_0^2\mathsf{E}_m\int_{-\infty}^{+\infty}dX\Delta f_m^2\psi_m\psi_n^*+2i\alpha\lambda_0\mathsf{D}\mathsf{E}_m\int_{-\infty}^{+\infty}dX\frac{d\psi_m}{dX}\psi_n^*\\&-\varepsilon\alpha\left(2\mathsf{D}\frac{\partial\mathsf{E}_m}{\partial Z}+\mathsf{E}_m\frac{d\mathsf{D}}{dZ}\right)\int_{-\infty}^{+\infty}dX\frac{d\psi_m}{dX}\psi_n^*\Bigg]=0\;. \quad (3.17)\end{aligned}$$

Similar to the arguments we presented before, we shall assume that the overlap integrals follow the scaling given in Eqs. (2.6) and that $\alpha = O(\mu)$. In close analogy to the calculations given before, we find that for a sech-like mode [Eq. (2.7)] profile we have

$$\int_{-\infty}^{+\infty} dX \frac{d\psi_m}{dX}\psi_n^* = \frac{\beta}{\mu} e^{-|n-m|/\mu} , \tag{3.18}$$

where b is a constant. Restricting the sum in Eq. (3.17) to nearest neighbors i.e., $m = n, n \pm 1$ and by defining $\tilde{z} = Z/(2\lambda_c a_0)$, $k_0^2 c_1 = C_1$, $2\lambda_c b\mathsf{D} = \tilde{\mathsf{D}}$; $\mathsf{E}_n = \tilde{\mathsf{E}}_n^* \exp(-ik_0^2 c_0 \tilde{z})$ we find that E_n satisfies (dropping the tilde)

$$i\frac{\partial \mathsf{E}_n}{\partial z} + C_1\Big(\mathsf{E}_{n+1} + \mathsf{E}_{n-1}\Big) + i\mathsf{D}(z)\Big(\mathsf{E}_{n+1} - \mathsf{E}_{n-1}\Big) = 0 . \tag{3.19}$$

The constant diffraction case, i.e., Eq. (2.10) is recovered when $\mathsf{D} = 0$. Eq. (3.19) is the general dynamical equation that governs the evolution of optical beam in a diffraction-managed linear waveguide array. However, when the intensity of the incident beam is sufficiently high then the refractive index of the medium will depend on the intensity which for Kerr media is proportional to the intensity. Therefore, by following the same procedure outlined in Sec. 2 we find that the general evolution equation for the optical field in a diffraction-managed nonlinear waveguide array is governed by

$$i\frac{\partial \mathsf{E}_n}{\partial z} + C_1\Big(\mathsf{E}_{n+1} + \mathsf{E}_{n-1}\Big) + i\mathsf{D}(z)\Big(\mathsf{E}_{n+1} - \mathsf{E}_{n-1}\Big) + g_{nl}|\mathsf{E}_n|^2\mathsf{E}_n = 0 . \tag{3.20}$$

In the case of strong diffraction for which $\max|\mathsf{D}(z)| >> |C_1|$ (recall that $\mathsf{D}(z)$ is a piecewise constant function) and by defining $\mathsf{E}_n = E_n \exp(i\pi n/2)$, Eq. (3.20) reduces to

$$i\frac{\partial E_n}{\partial z} + \mathsf{D}(z)\Big(E_{n+1} + E_{n-1}\Big) + g_{nl}|E_n|^2 E_n = 0 . \tag{3.21}$$

3.2. *Direct Approach*

In this section, we give a different approach to derive a model for diffraction management. We approximate the solution to Eq. (3.13) again as a multiscale perturbation series

$$\Psi = \sum_{m=-\infty}^{+\infty} \mathsf{E}_m(Z)\psi_m(X)e^{i[\varphi_m(z) - \lambda_0 z]} , \tag{3.22}$$

where the the phase $\varphi_m(z)$ will be chosen later. Substituting the ansatz (3.22) into Eq. (3.13), we find

$$\sum_{m=-\infty}^{+\infty} e^{i[\varphi_m(z)-\lambda_0 z]} \Bigg[\mathsf{E}_m \frac{d^2\psi_m}{dX^2}\Big(1 + \alpha^2\mathsf{D}^2\Big) + k_0^2 f^2 \mathsf{E}_m \psi_m$$

$$+2i\Big(\frac{d\varphi_m}{dz}-\lambda_0\Big)\Big(\varepsilon\frac{\partial \mathsf{E}_m}{\partial Z}\psi_m-\alpha\mathsf{D}\frac{d\psi_m}{dX}\mathsf{E}_m\Big)-\Big(\frac{d\varphi_m}{dz}-\lambda_0\Big)^2\mathsf{E}_m\psi_m$$
$$-2\alpha\varepsilon\mathsf{D}\frac{\partial \mathsf{E}_m}{\partial Z}\frac{d\psi_m}{dX}-\alpha\varepsilon\mathsf{E}_m\frac{d\mathsf{D}}{dZ}\frac{d\psi_m}{dX}+i\frac{d^2\varphi_m}{dz^2}\mathsf{E}_m\psi_m+\varepsilon^2\frac{\partial \mathsf{E}_m}{\partial Z}\psi_m\Big]=0. \quad (3.23)$$

Using Eq. (2.1) and multiplying Eq. (3.23) by $\psi_n^*\exp[-i\varphi_n(z)]$ and integrating over $-\infty<X<\infty$ yields the following equation (ignoring the order ε^2 term)

$$\sum_{m=-\infty}^{+\infty}e^{i[\varphi_m(z)-\varphi_n(z)]}\Big\{\mathsf{E}_m\int dX\psi_m\psi_n^*$$
$$\times\Big[\alpha^2\mathsf{D}^2(\lambda_0^2-k_0^2f_m^2)+k_0^2\Delta f_m^2-\Big(\frac{d\varphi_m}{dz}\Big)^2+2\lambda_0\frac{d\varphi_m}{dz}+i\frac{d^2\varphi_m}{dz^2}\Big]$$
$$-\alpha\Big[\mathsf{E}_m\Big(2i\Big(\frac{d\varphi_m}{dz}-\lambda_0\Big)\mathsf{D}+\frac{d\mathsf{D}}{dZ}\Big)+2\varepsilon\mathsf{D}\frac{\partial \mathsf{E}_m}{\partial Z}\Big]$$
$$\times\int dX\frac{d\psi_m}{dX}\psi_n^*+2i\varepsilon\Big(\frac{d\varphi_m}{dz}-\lambda_0\Big)\frac{\partial \mathsf{E}_m}{\partial Z}\int dX\psi_m\psi_n^*\Big\}=0\,.$$

Until now the phase factor φ_m is arbitrary. Therefore, we shall choose the phase in such a way that

$$\alpha^2\mathsf{D}^2\int_{-\infty}^{+\infty}dX\Big(\lambda_0^2-k_0^2f_m^2\Big)|\psi_m|^2=\Big[\Big(\frac{d\varphi_m}{dz}\Big)^2-2\lambda_0\frac{d\varphi_m}{dz}\Big]\int_{-\infty}^{+\infty}dX|\psi_m|^2\,. \quad (3.24)$$

Eq. (3.24) implies that

$$\frac{d\varphi_m}{dz}=O(\alpha^2)\,,\qquad\Big(\frac{d\varphi_m}{dz}\Big)^2=O(\alpha^4)\,,\qquad\frac{d^2\varphi_m}{dz^2}=O(\alpha\varepsilon)\,. \quad (3.25)$$

The localized nature of the waveguides indicates that φ_m is independent of m, i.e., it is the same for all waveguides. With this scaling in mind and by taking as before $\alpha=O(\mu)$, we recover Eq. (3.19).

4. Asymptotic Theory for Vector Diffraction Management

In this section we present a derivation of the vector diffraction managed DNLS equation starting from the nonlinear vector Helmholtz equations (which is obtained from Maxwell's equations). The propagation of an intense laser beam in a Kerr medium is described by the vector Helmholtz equations:

$$\left(\frac{\partial^2}{\partial x^2}+\frac{\partial^2}{\partial z^2}\right)\mathbf{E}+\delta\nabla\Big(\nabla\cdot\mathbf{P}_{\rm NL}\Big)+k_0^2f^2(x)\mathbf{E}+\delta\mathbf{P}_{\rm NL}=0\,. \quad (4.26)$$

The nonlinear polarization $\mathbf{P}_{\rm NL}$ can be expressed in terms of the electric field as

$$\mathbf{P}_{\rm NL}=(\mathbf{E}\cdot\mathbf{E}^*)\mathbf{E}+\gamma(\mathbf{E}\cdot\mathbf{E})\mathbf{E}^*\,, \quad (4.27)$$

where γ is a constant related to the third order nonlinear susceptibility [56]. Since we are interested in interaction between two coupled laser beams, we shall assume that each one is initially linearly polarized and mutually orthogonal, i.e.,

$$\mathbf{E}(x,z) = \mathcal{E}_1(x,z)\hat{\mathbf{x}} + \mathcal{E}_2(x,z)\hat{\mathbf{y}} + \mathcal{E}_3(x,z)\hat{\mathbf{z}} \,. \tag{4.28}$$

In this case, the nonlinear polarization takes the form

$$\mathbf{P}_{\rm NL} = P^{(1)}_{\rm NL}\hat{\mathbf{x}} + P^{(2)}_{\rm NL}\hat{\mathbf{y}} + P^{(3)}_{\rm NL}\hat{\mathbf{z}} \,, \tag{4.29}$$

where

$$P^{(1)}_{\rm NL} = \Big((1+\gamma)|\mathcal{E}_1|^2 + |\mathcal{E}_2|^2\Big)\mathcal{E}_1 + \gamma\mathcal{E}_2^2\mathcal{E}_1^* + \gamma\mathcal{E}_3^2\mathcal{E}_1^* \,, \tag{4.30}$$

$$P^{(2)}_{\rm NL} = \Big(|\mathcal{E}_1|^2 + (1+\gamma)|\mathcal{E}_2|^2\Big)\mathcal{E}_2 + \gamma\mathcal{E}_1^2\mathcal{E}_2^* + \gamma\mathcal{E}_3^2\mathcal{E}_2^* \,. \tag{4.31}$$

$$P^{(3)}_{\rm NL} = \Big(|\mathcal{E}_1|^2 + |\mathcal{E}_2|^2 + (1+\gamma)|\mathcal{E}_3|^2\Big)\mathcal{E}_3 + \gamma\mathcal{E}_1^2\mathcal{E}_3^* + \gamma\mathcal{E}_2^2\mathcal{E}_3^* \,. \tag{4.32}$$

Substituting the expression for $\mathbf{E}$ in Eq. (4.26) and taking into account the nonlinear polarization, leads to the coupled system:

$$\left(\frac{\partial^2}{\partial x^2} + \frac{\partial^2}{\partial z^2}\right)\mathcal{E}_1 + \delta\frac{\partial^2 P^{(1)}_{\rm NL}}{\partial x^2} + k_0^2 f^2(x)\mathcal{E}_1 + \delta P^{(1)}_{\rm NL} = 0 \,, \tag{4.33}$$

$$\left(\frac{\partial^2}{\partial x^2} + \frac{\partial^2}{\partial z^2}\right)\mathcal{E}_2 + k_0^2 f^2(x)\mathcal{E}_2 + \delta P^{(2)}_{\rm NL} = 0 \,, \tag{4.34}$$

$$\left(\frac{\partial^2}{\partial x^2} + \frac{\partial^2}{\partial z^2}\right)\mathcal{E}_3 + \delta\frac{\partial^2 P^{(1)}_{\rm NL}}{\partial x\partial z} + \delta\frac{\partial^2 P^{(3)}_{\rm NL}}{\partial z^2} + k_0^2 f^2(x)\mathcal{E}_3 + \delta P^{(3)}_{\rm NL} = 0 \,. \tag{4.35}$$

In this work, we are interested in interaction of two mutually orthogonal beams. However, if we initially assume that $\mathcal{E}_3 = 0$, then the source term $\partial^2 P^{(1)}_{\rm NL}/\partial x\partial z$ appearing in Eq. (4.35) will eventually generate a nonzero $\mathcal{E}_3$ component. In fact, this additional term (due to nonlinear polarization) is of order δ. Hence, we are justified in neglecting $\mathcal{E}_3$ as compared to $\mathcal{E}_1$ and $\mathcal{E}_2$. Next we follow the same expansion as mentioned earlier and let

$$\begin{aligned} \mathcal{E}_1 &= \textstyle\sum_{m=-\infty}^{+\infty} A_m(Z)\psi_m(X)e^{-i\lambda_0 z} \\ \mathcal{E}_2 &= \textstyle\sum_{m=-\infty}^{+\infty} B_m(Z)\psi_m(X)e^{-i\lambda_0 z} \,, \end{aligned} \tag{4.36}$$

where X has been defined in Eq. (3.13). The expansion of the linear terms is already given in (3.19) with the addition of onsite terms $k_{wg}A_n$ and $k_{wg}B_n$. Therefore, we focus the attention below solely on the nonlinear terms and in particular give an estimate on the order of magnitude of $\partial^2 P^{(1)}_{\rm NL}/\partial x^2$. Substituting the ansatz (4.36) into Eqs. (4.33) and (4.34);

multiplying by $\psi_n^* \exp(i\lambda_0 z)$ and integrating over X yields the following result for the nonlinear terms:

$$\int_{-\infty}^{+\infty} dX P_{\rm NL}^{(1)} \psi_n^* e^{i\lambda_0 z} = (1+\gamma) \sum_{m,m',m''} A_m A_{m'} A_{m''}^* \int_{-\infty}^{+\infty} dX \psi_m \psi_{m'} \psi_{m''}^* \psi_n^* + \sum_{j,j',j''} B_j B_{j'}^* A_{j''} \int_{-\infty}^{+\infty} dX \psi_j \psi_{j'} \psi_{j''}^* \psi_n^* + \gamma \sum_{l,l',l''} B_l B_{l'} A_{l''}^* \int_{-\infty}^{+\infty} dX \psi_l \psi_{l'} \psi_{l''}^* \psi_n^* \,. \quad (4.37)$$

$$\int_{-\infty}^{+\infty} dX P_{\rm NL}^{(2)} \psi_n^* e^{i\lambda_0 z} = \sum_{m,m',m''} A_m A_{m'}^* B_{m''} \int_{-\infty}^{+\infty} dX \psi_m \psi_{m'} \psi_{m''}^* \psi_n^* + (1+\gamma) \sum_{j,j',j''} B_j B_{j'} B_{j''}^* \int_{-\infty}^{+\infty} dX \psi_j \psi_{j'} \psi_{j''}^* \psi_n^* + \gamma \sum_{l,l',l''} A_l A_{l'} B_{l''}^* \int_{-\infty}^{+\infty} dX \psi_l \psi_{l'} \psi_{l''}^* \psi_n^* \,. \quad (4.38)$$

Due to the assumption of widely separated waveguides, the only order one contribution comes from the nonlinear term when $m = m' = m'' = n$. We therefore find that to $O(\varepsilon)$ the nonlinear evolution of A_n and B_n is given by (taking $\delta = \varepsilon$)

$$i\frac{\partial A_n}{\partial z} + k_{wg} A_n + \mathcal{C}(z) A_{n+1} + \mathcal{C}^*(z) A_{n-1} + (\tilde{a}_1 |A_n|^2 + \tilde{b}_1 |B_n|^2) A_n + \tilde{\eta}_1 B_n^2 A_n^* = 0 \,, \quad (4.39)$$

$$i\frac{\partial B_n}{\partial z} + k_{wg} B_n + \mathcal{C}(z) B_{n+1} + \mathcal{C}^*(z) B_{n-1} + (\tilde{a}_2 |B_n|^2 + \tilde{b}_2 |A_n|^2) B_n + \tilde{\eta}_2 A_n^2 B_n^* = 0 \,, \quad (4.40)$$

where the coefficients $\tilde{a}_1, \tilde{a}_2, \tilde{b}_1, \tilde{b}_2, \tilde{\eta}_1, \tilde{\eta}_2$ are given by:

$$\tilde{a}_1 = (1+\gamma)\eta_{nl} + \gamma_{nl} \,, \quad \tilde{b}_1 = \eta_{nl} + \gamma_{nl} \,,$$
$$\tilde{a}_2 = (1+\gamma)\eta_{nl} \,, \quad \tilde{b}_2 = \eta_{nl} \,,$$
$$\tilde{\eta}_1 = \gamma\eta_{nl} + \gamma_{nl} \,, \quad \tilde{\eta}_2 = \gamma\eta_{nl} \,,$$

and

$$\int_{-\infty}^{+\infty} dX |\psi_n|^4 = \eta_{nl} \,, \quad \int_{-\infty}^{+\infty} dX \frac{\partial^2}{\partial X^2} \Big(|\psi_n|^2 \psi_n \Big) \psi_n^* = \gamma_{nl} \,.$$

By rescaling the field amplitudes, i.e., $A_n = \tilde{A}_n/\sqrt{\tilde{a}_1}$, $B_n = \tilde{B}_n/\sqrt{\tilde{a}_2}$ we find the system (dropping the tilde):

$$i\frac{\partial A_n}{\partial z}+k_{wg}A_n+\mathcal{C}(z)A_{n+1}+\mathcal{C}^*(z)A_{n-1}+(|A_n|^2+b_1|B_n|^2)A_n+\eta_1 B_n^2 A_n^* = 0\,,$$

$$i\frac{\partial B_n}{\partial z}+k_{wg}B_n+\mathcal{C}(z)B_{n+1}+\mathcal{C}^*(z)B_{n-1}+(|B_n|^2+b_2|A_n|^2)B_n+\eta_2 A_n^2 B_n^* = 0\,,$$

with $b_1 = \tilde{b}_1/\tilde{a}_2, b_2 = \tilde{b}_2/\tilde{a}_1, \eta_1 = \tilde{\eta}_1/\tilde{a}_2, \eta_2 = \tilde{\eta}_2/\tilde{a}_1$ (see also the introduction). Finally, we would like to comment on the FWM term in Eqs. (4.39) and (4.40). In case that $k_{wg} \gg 1$ then by defining new fields $A_n = \mathcal{A}_n \exp(k_{wg}z)$ and $B_n = \mathcal{B}_n \exp(k_{wg}z)$ the FWM term $B_n^2 A_n^*$ becomes $\mathcal{B}_n^2 \mathcal{A}_n \exp(k_{wg}z)$ which averages to zero due to the rapid variation in z. Similar arguments hold for $A_n^2 B_n^*$. However, if k_{wg} is of order one, then it is necessary to study the effect of FWM on the discrete vector solitons.

5. Conclusions

In this paper we have derived and investigated scalar and vector discrete diffraction managed systems. The proposed vector model describes propagation of two polarization modes interacting in a waveguide array with Kerr nonlinearity in the presence of varying diffraction. The coupling of the two fields is described via a cross-phase modulation coefficient.

Acknowledgment

M.J.A. is partially supported by the Air Force Office of Scientific Research, under grant number F49620-03-1-0250, and NSF under grant number DMS-0070792.

References

1. E. Fermi, J. Pasta, and S. Ulam, Studies of nonlinear problems, Los Alamos Rep. LA1940, 1955.
2. O. M. Braun and Y. S. Kivshar, Nonlinear dynamics of the Frenkel-Kontorova model, Phys. Rep. **306**, (1998) 1-108.
3. D. Henning and G. P. Tsironis, Wave transmission in nonlinear lattices, Phys. Rep. **307**, (1999) 333-432.
4. S. Flach and C. R. Willis, Discrete breathers, Phys. Rep. **295**, (1998) 181-264.
5. F. Lederer and J. S. Aitchison, Discrete solitons in nonlinear waveguide arrays, Les Houches Workshop on Optical Solitons, Eds. V. E. Zakharov and S. Wabnitz, Springer-Verlag (1999) 349-365.
6. A. C. Scott and L. Macneil, Binding-energy versus nonlinearity for a small stationary soliton, Phys. Lett. A **98**, (1983) 87-88.

7. A. J. Sievers and S. Takeno, Intrinsic localized modes in anharmonic crystals, Phys. Rev. Lett. **61**, (1988) 970-973.
8. W. P. Su, J. R. Schieffer, and A. J. Heeger, Solitons in polyacetylene, Phys. Rev. Lett. **42**, (1979) 698-1701.
9. A. S. Davydov, Theory of contraction of proteins under their excitation, J. Theor. Biol. **38**, (1973) 559-569.
10. P. Marquii, J. M. Bilbaut, and M. Remoissenet, Observation of nonlinear localized modes in an electrical lattice, Phys. Rev. E **51**, (1995) 6127-6133.
11. H. Eisenberg, Y. Silberberg, R. Morandotti, Discrete spatial optical solitons in waveguide arrays, A. Boyd, and J. Aitchison, Phys. Rev. Lett. **81**, (1998) 3383-3386.
12. R. Morandotti, U. Peschel, J. Aitchison, H. Eisenberg, and Y. Silberberg, Dynamics of discrete solitons in optical waveguide array, Phys. Rev. Lett. **83**, (1999) 2726-2729.
13. D. N. Christodoulides and R. J. Joseph, Discrete self-focusing in nonlinear arrays of coupled wave-guides, Opt. Lett. **13**, (1988) 794-796 .
14. Y. S. Kivshar, Self-localization in arrays of defocusing waveguides, Opt. Lett. **18**, (1993) 1147-1149.
15. W. Krolikowski and Y. S. Kivshar, Soliton-based optical switching in waveguide arrays, J. Opt. Soc. Am. B **13**, (1996) 876-887.
16. A. B. Aceves, C. De Angelis, S. Trillo, and S. Wabnitz, Storage and steering of self-trapped discrete solitons in nonlinear wave-guide arrays, Opt. Lett. **19**, (1994) 332-334.
17. B. Malomed and M. I. Weinsrein, Soliton dynamics in the discrete nonlinear Schrödinger equations, Phys. Lett. A **220**, (1996) 91-96.
18. A. B. Aceves, C. De Angelis, T. Peschel, R. Muschall, F. Lederer, S. Trillo, and S. Wabnitz, Discrete self-trapping, soliton interactions, and beam steering in nonlinear waveguide arrays, Phys. Rev. E **53**, (1996) 1172-1189.
19. A. B. Aceves, C. De Angelis, A. M. Rubenchik, and S. K. Turitsyn, Multidimensional solitons in fiber arrays, Opt. Lett. **19**, (1994) 329-331.
20. F. Lederer, S. Darmanyan, and A. Kobyakov, Discrete solitons, In: *Spatial Solitons*, Eds. S. Trillo and W. Torruellas (Springer-Verlag, Berlin, 2001), 267-290.
21. P.G. Kevrekidis, K.Ø. Rasmussen and A.R. Bishop, The discrete nonlinear Schrödinger equation: A survey of recent results, Int. J. of Mod. Phys. B **15**, (2001) 2833-2900.
22. T. Peschel, U. Peschel, and F. Lederer, Discrete bright solitary waves in quadratically nonlinear media, Phys. Rev. E **57**, (1998) 1127-1133.
23. S. Darmanyan, A. Kobyakov, and F. Lederer, Strongly localized modes in discrete systems with quadratic nonlinearity, Phys. Rev. E **57**, (1998) 2344-2349.
24. R. Morandotti, U. Peschel, J. Aitchison, H. Eisenberg, Experimental observation of linear and nonlinear optical Bloch oscillations, and Y. Silberberg, Phys. Rev. Lett. **83**, (1999) 4756-4759.
25. T. Pertsch, P. Dannberg, W. Elflein, A. Bräuer, and F. Lederer, Optical Bloch oscillations in temperature tuned waveguide arrays, Phys. Rev. Lett. **83**, (1999) 4752-4755 .

26. G. Lenz, I. Talanina, and C. Martijn de Sterke, Bloch oscillations in an array of curved optical waveguides, Phys. Rev. Lett. **83**, (1999) 963-966.
27. H. Eisenberg, Y. Silberberg, R. Morandotti, and J. Aitchison, Diffraction management, Phys. Rev. Lett. **85**, (2000) 1863-1866.
28. R. Morandotti, H. Eisenberg, Y. Silberberg, M. Sorel, and J. Aitchison, Self-focusing and defocusing in waveguide arrays, Phys. Rev. Lett. **86**, (2001) 3296-3299.
29. M. J. Ablowitz and Z. H. Musslimani, Discrete diffraction managed spatial solitons, Phys. Rev. Lett. **87**, (2001) 254102.
30. M. J. Ablowitz and Z. H. Musslimani, Discrete vector spatial solitons in a nonlinear waveguide array, Phys. Rev. E **65**, (2002) 056618.
31. S. F. Mingaleev, and Y. S. Kivshar, Self-trapping and stable localized modes in nonlinear photonic crystals, Phys. Rev. Lett. **86**, (2001) 5474-5477.
32. A. A. Sukhorukov and Y. S. Kivshar, Nonlinear localized waves in a periodic medium, Phys. Rev. Lett. **87**, (2001) 083901.
33. A. A. Sukhorukov and Y. S. Kivshar, Spatial optical solitons in nonlinear photonic crystals, Phys. Rev. E **65** (2002) 036609.
34. A. Trombettoni and A. Smerzi, Discrete solitons and breathers with dilute Bose-Einstein condensates, Phys. Rev. Lett. **86**, (2001) 2353-2356.
35. D. N. Christodoulides and E. D. Eugenieva, Blocking and routing discrete solitons in two-dimensional networks of nonlinear waveguide arrays, Phys. Rev. Lett. **87**, (2001) 233901.
36. D. N. Christodoulides and E. D. Eugenieva, minimizing bending losses in two-dimensional discrete soliton networks, Opt. Lett. **26**, (2001) 1876-1878.
37. E. D. Eugenieva, N. K. Efremidis, and D. N. Christodoulides, Design of switching junctions for two-dimensional discrete soliton, Opt. Lett. **26**, (2001) 1978-1980.
38. E. D. Eugenieva, N. K. Efremidis, and D. N. Christodoulides, *Optics and Photonics News* **12**, 57, (2001).
39. D. N. Christodoulides and N. K. Efremidis, Discrete temporal solitons along a chain of nonlinear coupled microcavities embedded in photonic crystals, Opt. Lett. **27**, (2002) 568-570.
40. M. J. Ablowitz and J. F. Ladik, Nonlinear differential-difference equations and Fourier-analysis J. Math. Phys. **17**, (1976) 1011-1018.
41. M. Peyrard, and M. D. Kruskal, Kink dynamics in the highly discrete sine-Gordon system, Physica D **14**, (1984) 88-102.
42. V. I. Petviashvili, Equation of an extraordinary soliton, Sov. J. Plasma Phys. **2**, 257 (1976).
43. M. J. Ablowitz and G. Biondini, Multiscale pulse dynamics in communication systems with strong dispersion management, Opt. Lett. **23**, (1998) 1668-1670.
44. S. Flach and K. Kladko, Moving discrete breathers? Physica D **127**, (1999) 61-72.
45. S. Flach, Y. Zolotaryuk and K. Kladko, Moving lattice kinks and pulses: An inverse method, Phys. Rev. E **59**, (1999) 6105-6115.
46. S. Aubry and T. Cretegny, Mobility and reactivity of discrete breathers, Physica D **119**, (1998) 34-46.
47. Ch. Claude, Y. S. Kivshar, O. Kluth, and K. H. Spatschek, Moving localized

modes in nonlinear lattices, Phys. Rev. B **47**, (1993) 14228-14232.
48. M. J. Ablowitz, Z. H. Musslimani, and G. Biondini, Methods for discrete solitons in nonlinear lattices, Phys. Rev. E **65**, (2002) 026602.
49. V. I. Karpman, Evolution of solitons described by higher-order nonlinear Schrodinger equations, Phys. Lett. A, **244**, (1998) 397-400.
50. M. Karlsson and A. Höök, Soliton-like pulses governed by fourth order dispersion in optical fibers, Opt. Commun, **104**, (1994) 303-307.
51. H. Feddersen, Lecture Notes in Physics, pp. 159-167 (Springer-Verlag, Berlin, 1991).
52. D. B. Duncan, J. C. Eilbeck, H. Feddersen, and J. A. D. Wattis, Solitons on lattices, Physica D, **68**, (1993) 1-11.
53. S. Darmanyan, A. Kobyakov, E. Schmidt, and F. Lederer, Strongly localized vectorial modes in nonlinear waveguide arrays, Phys. Rev. E **57**, (1998) 3520-3530.
54. S. Somekh, E. Garmire, A. Yariv, H. L. Garvin, and R. G. Hunsperger, Channel optical wavguide directional couplers, Appl. Phys. Lett. **22**, (1973) 46-47.
55. A. Yariv, Optical Electronics, Oxford University Press, Fifth Edition, (1997).
56. R.W. Boyd, Nonlinear Optics, Wily Inc. (1992).

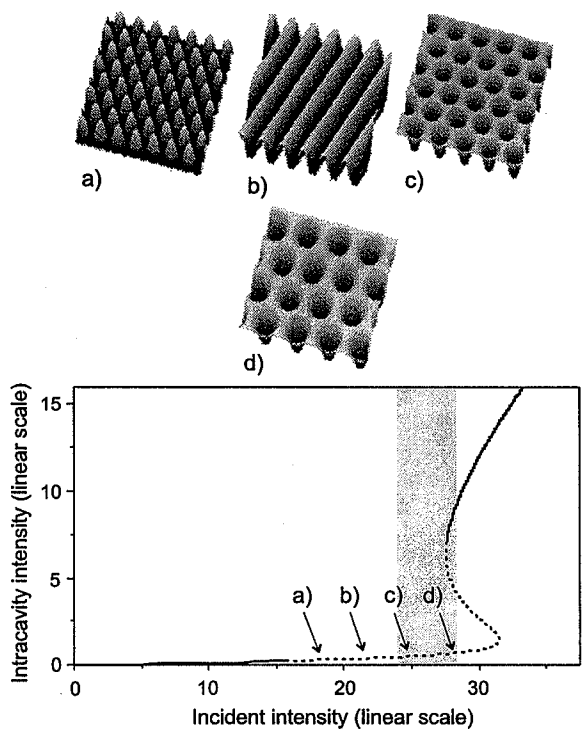

Fig. 57 The steady state bistable plane wave characteristic together with "in-resonator" intensities for various resonator input field intensities

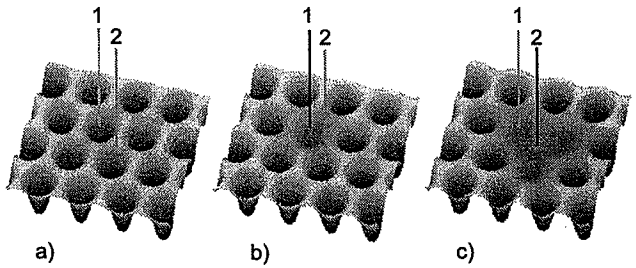

Fig. 58 Model calculation reproduces the switching of Fig. 10. The shown field structures are stable

Chapter 9

Nonlinear Waves and (Interesting) Applications

Mark J. Ablowitz, Toshihiko Hirooka, and Ziad H. Musslimani

Department of Applied Mathematics, University of Colorado at Boulder, Boulder, Colorado 80309-0526, USA

Abstract. This paper consists of three self contained chapters. They are a summary of lectures given by MJA in the conference: Dynamic Summer in Canberra, Australia, January, 2002. The three chapters are:
1. Waves Everywhere
2. Nonlinear Waves in High Bit-Rate Communications
3. Discrete solitons

1 Waves Everywhere

This chapter begins with a discussion of John Scott Russell's remarkable discovery of the "Great Wave of Translation", which many scientists now often refer to as a solitary wave or soliton. Many years after Russell's discovery, Boussinesq and Korteweg-deVries showed that solitary waves could be obtained from the water wave equations. In recent years researchers have been able to effectively study a class of nonlinear evolution equations which admit multi-soliton solutions and a linearization procedure termed the Inverse Scattering Transform (IST). Some of the types of equations for which the IST procedure can be applied are discussed.

1.1 *Introduction*

Waves are of interest to anyone who looks at the sea or even a pond of water. Many of us have sat beside beach watching waves roll in and eventually break as they become "too heavy" to support the relatively smooth hump of water they once were. John Scott Russell (1808-1882), a Scottish Naval architect, was intrigued by waves, and was especially concerned about

whether there were some special wave forms that could help him improve the design of boats and ships. In 1834 he made a remarkable discovery. He described it in his "Report on Waves" in 1844 [1]

"I was observing the motion of a boat which was rapidly drawn along a narrow channel by a pair of horses, when the boat suddenly stopped–not so the mass of water which it had put into motion; it accumulated round the prow of the vessel in a state of violent agitation, then suddenly leaving it behind, rolled forward with great velocity, assuming the form of a large solitary elevation, a rounded, smooth and well-defined heap of water, which continued its course along the channel apparently without change of form or dimuntion of speed. I followed it on horseback, and overtook it still rolling on at a rate of some eight or nine miles an hour, preserving its original figure ... Its height gradually diminished, and after a chase of one or two miles I lost it in the windings of the channel. Such in the month of August 1834, was my first chance interview with that singular and beautiful phenomenon which I have called the Wave of Translation."

In his paper, Russell did experiments on these solitary waves, the main one which he called the Great Wave of Translation. He also called for mathematicians to study this phenomena:

"...it now remained for the mathematician to predict the discovery after it had happened...".

Unfortunately it took many years for this to occur. In 1871 Boussinesq [2] and later in 1895 Korteweg and deVries [3] showed that solitary waves indeed resulted from the known equations of water waves. The work of Korteweg and deVries was devoted to the detailed approximations involving long waves and small amplitude which led them to the equation:

$$\frac{\eta_t}{\sqrt{gh}} + \eta_x + \frac{3}{2h}\eta\eta_x + h^2\eta_{xxx} = 0, \tag{1.1}$$

where η is the elevation of the wave, h is the height of the undisturbed fluid, and g is gravity. Equation (1.1) can be put in dimensionless form by using: $t' = \sqrt{gh}t/6h, x' = (x - \sqrt{gh}t)/h, \eta = 2hu/3$ to find (after dropping primes for convenience),

$$u_t + 6uu_x + u_{xxx} = 0. \tag{1.2}$$

Equation (1.1) or (1.2) is called the Kortweg deVries (KdV) equation It

is straight forward to verify that KdV has the special solitary wave solution,

$$u(x,t) = 2\kappa^2 \mathrm{sech}^2\kappa(x - 4\kappa^2 t - x_0). \tag{1.3}$$

Between 1895 and 1960 virtually all applications of the KdV equation and solitary waves were in the area of water waves. It found application in coastal engineering and from a theoretical point of view held the fascination of mathematical hydrodynamicists. With the development of more sophisticated singular perturbation methods, notably the method of multiple scales, the KdV equation was shown to arise in other important fields; e.g. plasma physics [4], internal waves [5], and as an approximation to lattice dynamics [6]. Indeed the work of Fermi, Pasta, Ulam in lattice dynamics motivated Kruskal and Zabusky to computationally study the KdV equation [7]. From the computations they observed the remarkable fact that solitary waves interacted elastically. Namely their amplitude and speed were asymptotically unchanged from before to after an interaction. Based on this observation they renamed these solitary waves to be solitons. The term soliton has become widely used in science today. Most researchers now use the term to denote any localized, stable structure (i.e a solitary wave). When the interaction of solitary waves possess the remarkable "elastic property" this usually indicates that there is considerably more mathematical structure that underlies the equations of motion. This was found to be the case for the Korteweg-deVries equation; in 1967 Gardner et al [8] showed that the KdV equation could be linearized by using certain inverse scattering methods, developed earlier by Gel'fand and Levitan [9].

It turned out that the KdV equation was no fluke. In 1972 Zakharov and Shabat [10] showed that inverse scattering could be applied to linearize the nonlinear Schrödinger equation

$$iu_t + u_{xx} \pm 2|u|^2 u = 0, \tag{1.4}$$

which had already begun to become a well known nonlinear equation (cf. [11; 12]).

In the 1970's the method was significantly generalized and shown to apply to certain classes of interesting nonlinear evolution equations including the modified KdV equation

$$u_t + 6u^2u_x + u_{xxx} = 0, \tag{1.5}$$

and the sine-Gordon equation

$$u_{xt} = \sin u. \tag{1.6}$$

Central to whether one can apply inverse scattering at all is to show that the nonlinear evolution equation can be written as the compatibility of two (or possibly more) linear operators. One of the linear operators usually plays the role of the scattering problem. From a conceptual point of view the technique was shown to be analogous to the method of Fourier transforms but now applied to certain classes of nonlinear problems where the direct and inverse Fourier transform are replaced by direct and inverse scattering. The solution contains "N-soliton" solutions, which are connected to the discrete spectrum of the scattering problem plus a radiation tail which is due to the continuous spectrum. The method was termed the Inverse Scattering Transform (IST) (cf. [13; 14]). Amongst other results it was shown that the long time asymptotic structure could be obtained (cf. [14]) and this uncovered that there was a deep connection to Painlevé equations (cf. [14; 15]).

Importantly the IST method was applied to other classes of physically important nonlinear evolution equation. In 1976 Ablowitz and Ladik showed that the method extended naturally to semi-difference nonlinear evolution equation. The following integrable semi-discrete NLS equation is one important case:

$$iu_{n,t} + (u_{n+1} + u_{n-1} - 2u_n)/h^2 \pm |u_n|^2 u_n = 0, \tag{1.7}$$

where h is the grid size. Clearly Eq. (1.7) reduces to the continuous NLS equation as h tends to 0 (cf. [14] for a review). It was also found that there were classes of nonlinear partial difference equation to which the IST method applied, including examples of integrable doubly-discrete NLS equation Interestingly, the IST method also applies to certain singular integral evolution equation such as the Benjamin-Ono equation

$$u_t + 6u^2 u_x + (Hu_{xx}) = 0, \tag{1.8}$$

where

$$Hu = \frac{1}{\pi} \int \frac{u(x',t)}{x'-x} dx',$$

($\int$ denotes Cauchy Principal value integral; see [15] for a review of this work). Indeed equations such as the the KdV equation and Benjamin-Ono equation and another equation that "interpolates" between these two, the so called intermediate long wave equation, all describe long stratified internal waves with small amplitude, in different parameter regimes. These equations all have N-soliton solutions, but the Benjamin-Ono equation has algebraic solitons (of "Lorentzian" form).

In 1980 Osborne and Burch [16] reported on their oceanic observations near Indonesia of "giant" internal soliton waves some 300 feet in amplitude and 5000 feet in length. They also showed that the KdV equation was a good approximation to the dynamics. These solitons are formed because of the lunar tides. Subsequently many researchers have reported on similar observations in different ocean locations. Thus solitons are "real, living" everyday creatures!

It turns out that there are multidimensional nonlinear wave equations which too are solvable by IST. The paradigm equation two space-one time (2+1) dimensional equation is the so-called Kadomtsev-Petviashvili equation [17]

$$u_{xt} + (3u^2)_{xx} + u_{xxxx} \pm 3u_{yy} = 0, \tag{1.9}$$

which is derived under similar circumstances as the KdV equation but with the additional proviso that the waves are slowly varying in the transverse (i.e. y) direction. This equation also applies to water waves [18], possesses N-line soliton solutions and, for a choice of sign in (1.9), has lump type solutions (cf. [14; 15]). In [15] other 2+1 equations are also discussed including an integrable 2+1 NLS type equation, often called the Davey-Stewartson equation.

There is also a four dimensional system that fits into the IST framework, called the self dual Yang-Mills (SDYM) system. The SDYM system can be obtained as the compatibility of two linear operators each of which contains two independent variables. Therefore it is natural to consider the SDYM system as an equation in "2+2" dimensions. It is not natural to consider SDYM as an evolution equation The compatibility of SDYM shows that there is significant freedom in the resulting SDYM system. Namely one may choose the underlying group containing the dependent variables in a virtually arbitrary manner. With this enormous flexibility, researchers showed that SDYM could be reduced/related to virtually all the 1+1 (cf. [15]) and 2+1 dimensional [19] PDE's mentioned above plus interesting nonlinear ODE's, including all six classical

Painlevé transcendents [20] and other important nonlinear ODE's which contain unusual singularity structure, such as the Chazy equation (see [15; 21]).

The first two of the Painlevé equation and the Chazy equation are given by:

$$d^2w/dz^2 + 6w^2 + z = 0, \tag{1.10a}$$

$$d^2w/dz^2 - zw - 2w^3 - \alpha = 0, \tag{1.10b}$$

$$d^3w/dz^3 - 2wd^2w/dz^2 + 3(dw/dz)^2 = 0, \tag{1.10c}$$

where α is an arbitrary constant, and z is a complex variable.

Eqs. (1.10a–1.10b) have solutions which are meromorphic in the z-plane; the location of their poles (double and simple respectively) depends on initial conditions. The solution of (1.10c) is analytic in the z-plane apart from a natural boundary of singularities which consists of a circle whose radius depends on initial conditions. In cases (1.10a–1.10b) the solutions can be obtained by a modification of the IST procedure, sometimes referred to as the inverse monodromy transform (cf. [15]). The solutions of (1.10c) can be obtained by an implicit change of variables (cf. [15; 22]).

In the study of integrable systems, the SDYM system plays the role of a master "integrable" system from which most, if not all, integrable systems can be obtained by reduction.

At this time, there are no known physically significant or even reasonably simple nonlinear evolution equation in 3+1 dimensions to which the IST procedure applies. This is a major open problem in the study of the Inverse Scattering Transform.

1.2 *Fully Discrete Waves*

It is extremely interesting that nonlinear waves which are "fully" discrete exist. One well known case is the so called "game of life" developed by J. Conway [23]. In its simplest form one considers 2 discrete spatial dimensions plus discrete "time" with the dependent variable $x(i,j,t)$ taking values in the finite field $GF(2)$; i.e. x has two states 0,1. Usually such finite state systems are referred to as cellular automata (CA). In the game of life one associates 0 with a "dead cell" and 1 with a "live cell". The rule of evolution

depends on the 8 element neighborhood N of $x(i,j,t)$; i.e. $x(i+l,j+k,t)$ where l, k can be 0,1,−1 but not both 0.

The rule is:

A. $x(i,j,t+1) = 1$ if

i. $x(i,j,t) = 0$ and there are exactly 3 living cells in N (i.e we have a "birth" from N)

or

ii. $x(i,j,t) = 1$ and there are 2 or 3 living cells in N (i.e a "living cell remains living")

B. $x(i,j,t+1) = 0$ if $x(i,j,t) = 0$ or 1 and there are less than 2 or more than 3 living cells in N (i.e. "death due to loneliness or overpopulation")

This simple rule is shown to contain a number of localized structures including states which are stationary, have periodic oscillation, and states which move with internal oscillation–i.e solitary waves!

Let us turn our attention to one dimensional cellular automata. The study of one dimensional cellular automata is covered extensively in the book by S. Wolfram [24]. Explicit 1-d rules take the form:

$$x(i,t+1) = F[x(i-r,t),...,x(i,t),...,x(i+r,t)], \tag{1.11}$$

where the "radius" r is given as are the values $x(i+j,t)$ for $j = -r,...r$. Despite the interesting and varied nature of such 1-d explicit cellular automata, none of them appear to yield a soliton type solution. However if we consider a "filter", or implicit, cellular automata then it turns out that there is a soliton CA. More precisely, consider the 1-d "filter" automata

$$x(i,t+1) = F[x(i-r,t+1),...,x(i-1,t),x(i,t),...,x(i+r,t)], \tag{1.12}$$

supplemented with the additional proviso that we assume all values sufficiently far to the left are zero (i.e we assume "compact support to the left) and "sweep" left to right to obtain new values.

One such filter automata, termed the parity rule filter automata, was proposed in [25]. It is:

$$\begin{aligned} x(i,t+1) &= 1 \text{ if } S_i \text{ is even and nonzero,} \\ &= 0 \text{ if } S_i \text{ is odd or zero,} \end{aligned} \tag{1.13}$$

where $S_i = \sum_{j=0}^{r} x(i+j,t) + \sum_{j=1}^{r} x(i-j,t+1)$

This rule is found to have a wide class of particle-like solutions. Some of these particles are found to interact elastically, hence possess the "strict

soliton property". In addition the rule can be rewritten in another way to analytically show "stability" and this particle-soliton property [26], and cf. [15]. However the rule is not reversible! For example the initial states of all zeros or the state of one 1 surrounded by all zeroes both evolve to zero–hence there is no unique predecessor.

Subsequently in [27] it was shown that this rule could be modified to be reversible . The idea is to write the above rule as a difference equation:

$$x(i,t+1) = S_i + \delta(x(i,t))P_i - 1, \qquad (1.14)$$

where $\delta(x(i,t))$ is 1 if $x(i,t)$ =0,mod2, 0 otherwise, and $P_i = \Pi_{j=1}^{r}\delta(x(i+j,t))\delta(x(i-j,t+1))$

Indeed the reversible rule is found to be:

$$x(i,t+1) = S_i + P_i - 1, \qquad (1.15)$$

which clearly is reversible. It possesses a symmetry which says "forward" evolution corresponds to a left to right sweep, while "backward" evolution corresponds to a right to left sweep.

The reversible rule has a large class of particle-like solutions including all previously obtained elastic "reversible" solitons obtained from the parity rule automata plus many others, including the "elementary particle" of 1 followed by r zeros. This rule can be generalized to be "k-state", put on a finite interval and the coefficients of the rule can be easily modified. For example, the term S_i can be taken to be $S_i = \sum_{j=0}^{r} a(i+j,t)x(i+j,t) + \sum_{j=1}^{r} a(i-j,t+1)x(i-j,t+1)$ with $a(i,t) = 1$, the others arbitrary. This allows us to connect the linear part of (1.15) with linear feedback shift registers, which have been heavily studied in the literature. This reversible rule can take data at a given time, transform it via this nonlinear feedback shift register (NLFSR), to another state, and then one can exactly reverse the scenario. This situation has been recently discussed in detail in [28].

1.3 *Conclusions*

In this first chapter, of this three part manuscript, a discussion of a class of nonlinear wave problems was presented. We began with the famous observations of John Scott Russell (1834-44) and mentioned the work of Korteweg and deVries (1895). The "modern" history of the KdV equation was described including the concept of a soliton and the method of solution via the inverse scattering transform. While solitons were originally defined

to have the property of interacting with each other elastically, most scientists today use the term more broadly, and often call a localized, stable wave structure (i.e. a solitary wave) a soliton. In subsequent sections we shall use the term soliton in this latter, more general context.

We also mentioned that there were other classes of nonlinear equations beyond PDE's in 1+1 and 2+1 dimensions to which the inverse scattering transform could be applied. These include certain classes of: semi-difference, partial difference, singular integral evolution equations and nonlinear ODE's such as the Painlevé equations. It was mentioned that the self dual Yang-Mills system occupies a special place in the study of integrable systems. In a sense it is a master system from which many important integrable systems can be derived.

2 Nonlinear Waves in High Bit-Rate Communications

This chapter describes an unexpected encounter of applied mathematics (solitons and nonlinear waves) with a state-of-the-art technology (optical fiber communications). Propagation of optical pulses in fibers in the presence of dispersion and nonlinearity is governed by the nonlinear Schrödinger (NLS) equation – an integrable equation which is mentioned in chapter 1 and has been well studied in applied mathematics. The NLS equation has a special solution called a "soliton". A soliton is a stable localized pulse propagating in a dispersive and nonlinear media without change of shape. This motivates the use of solitons for an information carrier (soliton communications). The most recent transmission systems employ a technique called "dispersion management" to improve system performance. The idea and motivation of dispersion management is discussed, and the analytical tools to study the behavior of dispersion-managed pulses are developed. Based on a unified analytical framework, two different formats of dispersion-managed pulses: "dispersion-managed solitons" where nonlinearity balances dispersion and "quasi-linear pulses" where nonlinearity is managed, are studied.

2.1 *Introduction*

Optical fiber communications have made enormous progress in recent years. Long-haul high-speed transmission over transoceanic distances with total

capacity in excess of tera (10^{12}) bits per second has already been achieved. Behind the success of these achievements, there have been significant technical advances such as the development of optical amplifiers and extensive fundamental studies of signal transmission in optical fibers. Indeed, in such a complex transmission system, signal deformation during propagation due to various properties of optical fibers such as dispersion and nonlinearity becomes one of the major limitations to transmission speed and distance. In order to design a transmission system and optimize system performance, it is crucial to understand the fundamental physical properties of optical fibers and investigate carefully their impact on signal transmission.

2.2 *Dispersion and Nonlinearity in Optical Fibers*

Among the physical properties of optical fibers, group-velocity dispersion (GVD) and nonlinearity are the main source of signal deformation. (Fiber loss, which used to be the major limitation, is now overcome by the use of optical amplifiers.)

GVD is the frequency dependence of the group velocity and originates from the frequency dependence of the refractive index of the fiber. In the presence of GVD, different spectral components of an optical pulse propagate at different group velocities and thus arrive at different times. This leads to pulse broadening, resulting in signal distortion.

Fiber nonlinearity responsible for signal deformation is the Kerr effect, where the refractive index changes in proportion to the intensity of the optical pulse. The Kerr effect brings about an intensity dependent phase shift and results in spectral broadening during propagation. In the presence of GVD and Kerr nonlinearity, the refractive index is expressed as

$$n(\omega, E) = n_0(\omega) + n_2|E|^2 \tag{2.1}$$

where ω and E represent the frequency and the electric field of the lightwave respectively, n_0 corresponds to the linear refractive index, and n_2 (the Kerr coefficient) has a value $\sim 10^{-22}\mathrm{m}^2/\mathrm{W}$. Although fiber nonlinearity is small, the nonlinear effects accumulate over a long distance and can have a significant impact because of low loss and high intensity of the lightwave over a small area of fiber cross section.

2.3 *Nonlinear Schrödinger Equation and Optical Solitons*

When one transmits information using lightwaves as a carrier, the information is usually modulated on the amplitude of the envelope $\mathcal{E}$ of the lightwave, which is a slowly varying function of the distance along the fiber Z and time τ. A modulated lightwave E is written as

$$E(Z,\tau) = \mathcal{E}(Z,\tau)\exp(ik_0Z - i\omega_0\tau) + \text{c.c.}. \tag{2.2}$$

Hasegawa and Tappert [29] derived the equation which describes the evolution of the modulated amplitude $\mathcal{E}$ along the axis of the fiber z. This can be obtained most conveniently from the dispersion relation $k(\omega, E) = (\omega/c)n(\omega, E)$ where c is the speed of light. (A detailed approach to derive it from the Maxwell's equation by means of the multiple scale method can be found in [30].)

A Taylor series expansion of $k(\omega, E)$ around the carrier frequency $\omega = \omega_0$ yields

$$k - k_0 = k'(\omega_0)(\omega - \omega_0) + \frac{k''(\omega_0)}{2}(\omega - \omega_0)^2 + \frac{\omega_0 n_2}{c}|E|^2, \tag{2.3}$$

where the prime represents the derivative with respect to ω. By replacing $k - k_0$ and $\omega - \omega_0$ by the operators $i\partial/\partial Z$ and $-i\partial/\partial\tau$ respectively and letting them operate on $\mathcal{E}$, we have

$$i\left(\frac{\partial\mathcal{E}}{\partial Z} + k_0'\frac{\partial\mathcal{E}}{\partial\tau}\right) - \frac{k_0''}{2}\frac{\partial^2\mathcal{E}}{\partial\tau^2} + \nu|\mathcal{E}|^2\mathcal{E} = 0, \tag{2.4}$$

where $\nu = \omega n_2/cA_{\text{eff}}$ with A_{eff} being the (effective) area of the cross section of the fiber (the factor $1/A_{\text{eff}}$ is required to take into account the variation of the field intensity in the cross section). If we introduce a retarded time coordinate $\tau_{\text{ret}} = \tau - k_0'Z$ moving at the group velocity $1/k_0'$ and normalize the variables by the characteristic parameters (denoted by the subscript $*$) $t = \tau_{\text{ret}}/\tau_*$, $z = Z/Z_*$, $u = \mathcal{E}/\sqrt{P_*}$ such that $Z_* = 1/\nu P_* = \tau_*^2/|k_0''|$, the envelope equation can be written as

$$i\frac{\partial q}{\partial z} - \frac{1}{2}\mathrm{sgn}(k_0'')\frac{\partial^2 q}{\partial t^2} + |q|^2 q = 0. \tag{2.5}$$

This is known as the nonlinear Schrödinger (NLS) equation and is special in the mathematical literature, since the NLS equation can be integrated by the inverse scattering transform (IST). The NLS equation has a special solution called a (bright) soliton for $k_0'' < 0$ [10]. A soliton is a stationary

and stable pulse, where the stationarity originates from the balance between dispersion and nonlinearity, and the stability is attributed to the integrability of the equation (via IST), allowing special interaction properties. In a technical context, solitons preserve their shape during propagation in a fiber even in the presence of dispersion and nonlinearity. Thus using solitons as an information bit allows us to overcome signal distortion due to dispersion and nonlinearity. Interestingly, the NLS equation also frequently appears in a wide variety field of science such as water waves, plasma physics, and magnetics (cf. [14]).

2.4 *All Optical Soliton Transmission Systems*

It took seven years from the theoretical prediction of optical solitons by Hasegawa and Tappert in 1973 until they were observed experimentally in optical fibers [31]. Since then, as a result of technical advances in lightwave systems such as the development of high power semiconductor lasers, fibers with low loss, and optical fiber amplifiers, there have been a large number of theoretical and experimental contributions aimed toward the development of all optical soliton transmission systems. By "all optical" one means that no optical-to-electrical (O-E) or E-O conversion of signals is employed in processing signals such as amplification in the middle of transmission. O-E/E-O conversion requires complicated processes and becomes a major limitation to transmission speed. The development of optical amplifiers, in particular, made a remarkable contribution by increasing the transmission capacity by the use of wavelength division multiplexing (WDM); namely by allowing the transmission of multiple signals having different wavelengths .

One important theoretical discovery is that the averaged dynamics of optical pulses in the presence of periodic perturbations such as weak variation of GVD or non-adiabatic loss and lumped amplification can also be described within the framework of the NLS equation, as long as the periodicity is short enough. In the presence of GVD variation $d(z)$, loss Γ and periodic lumped amplifiers $G(z)$, the NLS equation is modified as

$$i\frac{\partial q}{\partial z} + \frac{d(z)}{2}\frac{\partial^2 q}{\partial t^2} + |q|^2 q = -i\Gamma q + iG(z)q. \tag{2.6}$$

By introducing a new amplitude u through $q(z,t) = A(z)u(z,t)$ where $A(z)$ satisfies $dA/dz = (-\Gamma + G(z))A$, we have the perturbed NLS equation of

the form

$$i\frac{\partial u}{\partial z} + \frac{d(z)}{2}\frac{\partial^2 u}{\partial t^2} + g(z)|u|^2 u = 0, \tag{2.7}$$

where $g(z) = A^2(z)$. Hasegawa and Kodama [32] showed that the perturbed NLS equation with $d(z)$ and $g(z)$ assumed to be $O(1)$ can be reduced to the standard NLS equation in the lowest order by means of a Lie transformation, where the GVD and nonlinear coefficients are replaced by the average of $d(z)$ and $g(z)$ respectively over a period. Thus the perturbed NLS equation (2.7) still supports the NLS equation and soliton solutions at the leading order in a perturbation theory. They referred to this as the guiding center soliton. Hereafter we generally refer to the soliton solution of the NLS equation as a "classical" soliton, when it is either the solution of the original NLS equation or in the perturbed sense of the guiding center soliton.

Soliton based communications also suffers technical difficulties unique to solitons. One of the most serious problems is the phenomenon referred to as the Gordon-Haus effect [33]. Gordon-Haus effect is the fluctuation of the temporal position of the soliton pulse which originates from random modulation of the carrier frequency of the soliton caused by the interaction with amplifier noise. The Gordon-Haus effect crucially limits the available transmission speed and distance in soliton based systems.

The nonlinear interaction between two neighboring solitons in the same time series also leads to fluctuations of their temporal position, where two solitons attract or repel each other during propagation depending on their relative phase [34]. Moreover, in WDM transmission, solitons in different wavelengths also suffer from strong interaction [35; 36; 37]. The situation becomes much worse in the presence of loss and lumped amplification.

Because of these difficulties in soliton transmission, all optical transmission systems in an early stage did not adopt solitons but employed the non-return-to-zero (NRZ) format. In the NRZ format a continuous wave is transmitted over the total time slot of successive "1" digits, whereas in the RZ format including solitons an individual pulse is transmitted for each "1" digit regardless of the sequence. NRZ pulses were popular in those systems because their intensity is allowed to be lowered compared with RZ pulses having the same average power within one bit slot and thus they were considered to suffer less nonlinearity. It should be noted, however, that the peak intensity must be enhanced as the bit rate increases and the pulse

width decreases accordingly, since the average power within one bit slot must be maintained at a certain level so that the signal is not buried by the amplifier noise. Thus NRZ pulses also suffer from nonlinearity especially for high bit-rate transmission.

The effects of dispersion and nonlinearity in NRZ systems can also be analyzed in the framework of the perturbed NLS equation (2.7) [38]. The NLS equation (2.5) or (2.7) is now widely recognized as a fundamental equation to describe the evolution of optical pulses regardless of the transmission format. Indeed commercial software packages developed recently to simulate optical signal transmission are, in principle, based on the numerical calculations of the NLS equation. It is not feasible to numerically simulate Maxwell's equations over distances over thousands of kilometers.

2.5 *Dispersion Management*

After numerous of attempts to overcome the limitations mentioned above, a significant breakthrough for both soliton and non-soliton systems has come about. It is referred to as dispersion management. In a dispersion-managed system, the fiber is made up of alternating sections of positive and negative GVD in such a manner as to create a transmission line with high local GVD and low average GVD.

Dispersion management was originally proposed as a way to suppress nonlinear effects in non-soliton transmission. Since the local GVD is made large, the pulse experiences large broadening. This helps suppress certain nonlinear effects because of reduced peak intensity associated with large pulse broadening. At the same time, since the average GVD is close to zero, the pulse recovers its original shape periodically. Such observations led to recent successful experimental demonstrations of dense WDM transmission over transoceanic distances [39]. In dispersion-managed systems, however, nonlinearity is still not entirely avoided, and indeed residual nonlinearity can lead to serious penalties due to nonlinear interactions between neighboring pulses which are strongly overlapped locally as a result of their large pulse width broadening. For this reason, such a system is commonly referred to as "quasi-linear". Quasi-linear systems and their penalties are analytically studied in Sections 8 and 9.

Dispersion management is also found to be a powerful scheme for soliton systems but in a different context. Suzuki et al. [40] proposed the employment of dispersion management in soliton transmission in order to overcome

the Gordon-Haus effect. Their motivation was to reduce the Gordon-Haus effect by compensating for the GVD accumulation periodically by alternating the sign of GVD. Since the Gordon-Haus effect is proportional to the accumulated GVD, they expected the Gordon-Haus effect to be reduced by lowering the average GVD, and indeed demonstrated it experimentally.

It should be noted that an ideal soliton solution does not exist in a dispersion-managed fiber because of the large variation of GVD. However, Smith et al. [41] showed numerically that there exists a nonlinear stationary solution in a dispersion-managed system whose shape is close to Gaussian rather than hyperbolic secant for classical solitons. Whereas the pulse width changes locally because of the periodic variation of GVD, their original shape is recovered exactly at every period even in the presence of nonlinearity. For this reason, this nonlinear pulse, which is, on average, stationary, is referred to as a dispersion-managed (DM) soliton.

The DM soliton is found to have enhanced energy compared with the energy of the classical soliton in a fiber with constant GVD equal to the average GVD of the dispersion-managed line. The energy enhancement is a particularly important property, since it allows the suppression of the Gordon-Haus effect by reducing the average GVD without sacrificing the degradation of the signal-to-noise ratio (SNR). In classical solitons, on the other hand, when the GVD is reduced the peak power must be lowered accordingly in order to maintain the balance between GVD and nonlinearity, which leads to the degradation of the SNR. DM solitons and their properties are analytically studied in Section 7.

2.6 *Dispersion Managed Nonlinear Schrödinger Equation*

The evolution of optical pulses in dispersion managed systems is also governed by the perturbed NLS equation (2.7), where $d(z)$ is now given by a *large*, rapidly varying function whose sign is alternating periodically. Because of the large perturbation, the pulse dynamics in dispersion-managed systems is expected to be completely different from that of the NLS equation. In this section, we derive a reduced model which describes long scale pulse dynamics in strongly dispersion-managed systems from the perturbed NLS equation by introducing multiple scales and thus eliminating fast dynamics due to the large and periodically varying GVD [42]. The obtained equation, referred to as the dispersion managed NLS (DMNLS) equation, elucidates the role of nonlinearity in dispersion-managed transmission, in-

dependently of the transmission format (DM soliton or quasi-linear).

In order to model strong dispersion management, we decompose the GVD $d(z)$ into two parts: a path-average constant δ_a and the rapidly varying function Δ corresponding to local GVD:

$$d(z) = \delta_a + \frac{1}{z_a}\Delta(z/z_a), \tag{2.8}$$

where $z_a(\ll 1)$ is the map period. Note that Δ/z_a represents a large variation about the average due to strong dispersion management and thus the proportionality factor $1/z_a$ is required in front of $\Delta(z/z_a)$ so that both δ_a and Δ are quantities of order one. Since the perturbed NLS equation with $d(z)$ given by (2.8) contains both slowly and rapidly varying terms, it is convenient to introduce the fast and slow scales as $\zeta = z/z_a$ and z respectively. We also expand the field u in powers of z_a:

$$u(\zeta, z, t) = u^{(0)}(\zeta, z, t) + z_a u^{(1)}(\zeta, z, t) + \cdots. \tag{2.9}$$

The perturbed NLS equation is now broken into a series of equations corresponding to the different powers of z_a. At the leading order in the expansion $O(1/z_a)$, we have

$$i\frac{\partial u^{(0)}}{\partial \zeta} + \frac{\Delta(\zeta)}{2}\frac{\partial^2 u^{(0)}}{\partial t^2} = 0, \tag{2.10}$$

namely the evolution of the pulse is determined solely by the large variations of $d(z)$ about the average, and nonlinearity and residual dispersion represent only a small perturbation to the linear solution. Eq. (2.10) can be solved by the Fourier transform

$$\hat{u}^{(0)}(\zeta, z, \omega) = \mathcal{F}[u^{(0)}] = \int_{-\infty}^{\infty} u^{(0)}(\zeta, z, t)\exp(-i\omega t)dt,$$

and the solution is given by

$$\hat{u}^{(0)}(\zeta, z, \omega) = \hat{U}(z, \omega)\exp[-iC(\zeta)\omega^2/2], \quad C(\zeta) = \int_0^{\zeta} \Delta(\zeta')d\zeta', \tag{2.11}$$

where $\hat{U}(z, \omega)$ is the integration constant in terms of ζ and represents the slowly evolving amplitude of $\hat{u}^{(0)}$, whose exact form is determined from the higher order in the expansion.

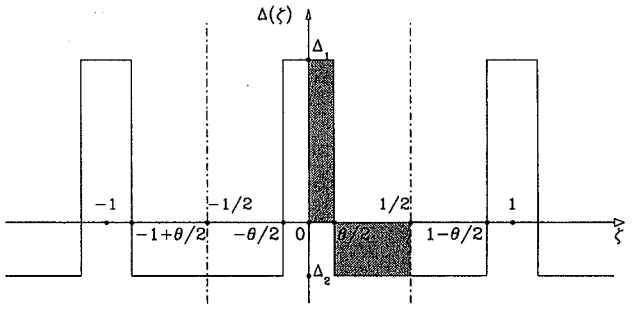

Fig. 1 Schematic diagram of a two-step dispersion map.

At the next order in the expansion $O(1)$, we have (in the frequency domain)

$$i\frac{\partial \hat{u}^{(1)}}{\partial \zeta} - \frac{\Delta(\zeta)}{2}\omega^2\hat{u}^{(1)} = -P^{(1)}, \quad P^{(1)} = i\frac{\partial \hat{u}^{(0)}}{\partial z} - \frac{\delta_a}{2}\omega^2\hat{u}^{(0)} + g(z)\mathcal{F}[|u^{(0)}|^2 u^{(0)}], \tag{2.12}$$

which is written in a more convenient form as

$$i\frac{\partial}{\partial \zeta}\left[\hat{u}^{(1)}\exp(iC\omega^2/2)\right] = -P^{(1)}\exp(iC\omega^2/2). \tag{2.13}$$

In order to remove secularities, namely to avoid resonant growth of $u^{(1)}$ so that the expansion of u in powers of z_a in (2.9) is remained to be well ordered, we require the following condition:

$$\int_0^1 P^{(1)}\exp(iC\omega^2/2)d\zeta = 0. \tag{2.14}$$

This condition yields the following equation for $\hat{U}$:

$$i\frac{\partial \hat{U}}{\partial z} - \frac{\delta_a}{2}\omega^2\hat{U} + \int_{-\infty}^{\infty}\int_{-\infty}^{\infty} r(\omega_1\omega_2)\hat{U}(z, \omega+\omega_1)\hat{U}(z, \omega+\omega_2)\hat{U}^*(z, \omega+\omega_1+\omega_2)d\omega_1 d\omega_2 = 0, \tag{2.15}$$

where the kernel $r(x) = (1/(2\pi)^2)\int_0^1 g(\zeta)\exp(iC(\zeta)x)d\zeta$ represents the structure of GVD profile.

Let us consider two special cases. First, when there is no loss and amplification ($g(z) = 1$), the kernel $r(x)$ of a piecewise constant dispersion map (see Fig. 1) is given by $r(x) = (1/(2\pi)^2) \sin sx/sx$, where $s = [\theta\Delta_1 - (1-\theta)\Delta_2]/4$ is a measure of dispersion map strength. Secondly, if the dispersion has no periodic variations ($\Delta = 0$ and thus $s = 0$), then $r(x) = 1/(2\pi)^2$ and the DMNLS equation reduces to the standard NLS equation, which was obtained via the guiding center soliton theory [32] when $d(z)$ is assumed $O(1)$.

2.7 *Dispersion Managed Solitons*

Special stationary solutions of the DMNLS equation are obtained by looking for solutions of the form $\hat{U}(z,\omega) = F(\omega)\exp(i\lambda^2 z/2)$ which yields the following nonlinear integral equation for $F(\omega)$:

$$(\lambda^2+\delta_a\omega^2)F(\omega) = 2\int_{-\infty}^{\infty}\int_{-\infty}^{\infty} r(\omega_1\omega_2)F(\omega+\omega_1)F(\omega+\omega_2)F^*(\omega+\omega_1+\omega_2)d\omega_1 d\omega_2. \tag{2.16}$$

A rapidly convergent procedure to solve this numerically is described in [43]. The obtained solution is the stationary DM soliton pulses. Some typical pulses are depicted in Fig. 2. We note that (2.16) contains a parameter λ which characterizes the mode, corresponding to the energy. The main features of the DM solitons for large s are a Gaussian like center with exponentially decaying and oscillating tails. For small s, the mode approaches the classical soliton profile. DM solitons have also been found to exist when the average GVD is zero or even positive, where no (bright) solitons exist for the standard NLS equation.

The fast scale evolution (i.e., with respect to ζ) can be reconstructed by multiplying $\exp(-iC\omega^2/2)$ with the slowly varying Fourier amplitude $\hat{U}$. When observed in this scale the pulse shape is changing periodically because of the local GVD variation, whereas the pulse propagates without changing its shape on a slow scale which is characterized by nonlinearity and the average dispersion. Thus DM soliton is considered to be a stationary pulse where nonlinearity balances the average dispersion.

2.8 *Quasi-Linear Pulses*

The evolution of pulses in the quasi-linear regime ($s \gg 1$) can also be studied based on the DMNLS equation [44]. To analyze the behavior of

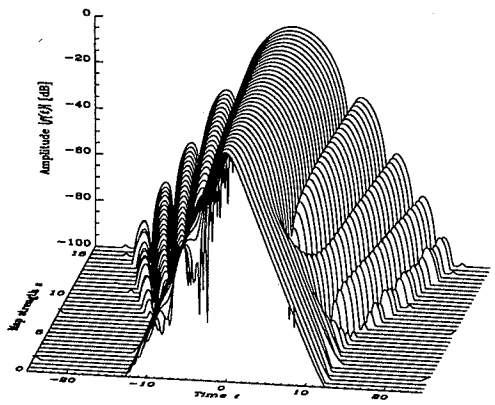

Fig. 2 The shape of the stationary pulses for $\delta_a = 1$, $\lambda = 1$ and various values of s.

quasi-linear pulses, we assume that $\hat{U}(z,\omega)$ depends only weakly on s and compute an asymptotic expansion of the nonlinear nonlocal term in (2.16) for $s \gg 1$.

When $g(z) = 1$ (i.e., in a lossless system), we have

$$i\frac{\partial\hat{U}}{\partial z} - \frac{\delta_a}{2}\omega^2\hat{U} + \Psi[|\hat{U}|^2]\hat{U} = 0, \tag{2.17}$$

$$\Psi[|\hat{U}|^2] = \frac{1}{2\pi s}\left[(\log s - \gamma)|\hat{U}(z,\omega)|^2 - \int_{-\infty}^{\infty}|\hat{U}(z,\omega')|^2 f(\omega'-\omega)\right], \tag{2.18}$$

where $\gamma = 0.57722$ is Euler's constant and $f(\omega) = (1/\pi)\int_{-\infty}^{\infty}\log|t|\exp(i\omega t)dt$. Eq. (2.18) can be solved explicitly as

$$\hat{U}(z,\omega) = \hat{U}(0,\omega)\exp[-i\delta_a\omega^2 z/2 + i\Psi[|\hat{U}(0,\omega)|^2]z]. \tag{2.19}$$

From these results, we note the following important observations in terms of pulse dynamics in the quasi-linear regime. First, nonlinearity is mitigated by $O(\log s/s)$ and vanishes in the limit $s \to \infty$. In other words, the quasi-linear system is in the regime where nonlinearity is managed. Secondly, nonlinearity is responsible only for phase shift $\phi_{\rm NL}(z,\omega) = \Psi[|\hat{U}(0,\omega)|^2]z$ in frequency domain, and thus the spectral intensity $|\hat{U}(z,\omega)|$ is preserved during propagation, as opposed to the self-phase modulation in standard

fibers. Finally we also note that the quasi-linear pulse can be viewed as degenerate limit of a DM soliton. The DM soliton satisfies the DMNLS equation with $\hat{U}(z,\omega) = F(\omega)\exp(i\lambda^2 z/2)$, where $F(\omega)$ is the solution of (2.17) and can be approximated by a Gaussian $F(\omega) \sim \alpha(\lambda)\exp(-\beta(\lambda)\omega^2/2)$. A quasi-linear Gaussian pulse has the same structure but is independent of the "eigenvalue" λ. The quasi-linear pulse can thus be looked at as a limit $\lambda \to 0$ in DM solitons. Importantly, both types of transmission format can be described with the same analytical framework.

When $g(z) \neq 1$ (i.e., in the presence of loss and amplification), the kernel $r(x)$ depends not only on s but also on the relative location of the amplifier within one dispersion map period, and the asymptotic analysis must be modified accordingly [45]. In all cases, the nonlinearity is again mitigated by $O(\log s/s)$. However, the spectral characteristics of the pulse evolution depends strongly on the amplifier locations. When the amplifiers are placed at the locations where the sign of GVD changes, the spectral intensity is found to be still preserved in the evolution. Otherwise, the spectral intensity varies as $O(1/s)$ and spectral compression or broadening is observed.

2.9 *Transmission Penalties in Quasi-Linear Systems*

We have seen in Section 8 that nonlinearity is mitigated by the factor $O(\log s/s)$ in the quasi-linear regime. This suggests the employment of strong dispersion management with large map strength s. Indeed dispersion management with large s is found to be effective in suppressing certain nonlinear interactions between pulses in different wavelength in WDM transmission (cf. [46]).

As s increases, however, different forms of nonlinear interactions take place and result in the main source of signal deformation [47]. In a strongly dispersion managed system, quasi-linear pulses in neighboring bit slots interact with each other because of their large overlap which is as a result of large pulse width broadening associated with high local GVD. This overlap induces nonlinear mixing (crosstalk) between pulses such as their frequency modulation and energy exchange, and leads to the fluctuation of the temporal position and amplitude of the pulses in "1"bits and the generation of "ghost" pulses in "0" bits [48; 49; 50]. The timing and amplitude jitter and the ghost pulse growth impose a major limitation to system performance in the quasi-linear regime with large s.

Let us analyze the growth of a ghost pulse q generated at the 0th bit slot by the interplay between the signals u_l, u_m, and u_n, where u_k, $k = l, m, n$ is the signal at the k-th bit [48]. Assuming that u in the perturbed NLS equation (2.7) is written as the sum of the signals and the ghost pulses $u = u_l + u_m + u_n + q$ and linearizing the equation, we have

$$i\frac{\partial q}{\partial z} + \frac{d(z)}{2}\frac{\partial^2 q}{\partial t^2} = -g(z)\sum_{l,m,n} u_l^* u_m u_n. \tag{2.20}$$

We note that the signals which contribute to the growth of ghost pulse at the 0th bit slot must satisfy the condition $-l + m + n = 0$; so the sum in (2.21) is taken for all the possible integers satisfying $l = m+n$ (e.g. $l = -1$, $m = -2$, $n = 1$, if there are "1" bits in -2, -1, and 1st slots). We solve (2.21) by the Fourier transform. After some manipulation [48], we find

$$\hat{q}(z,\omega)\exp(iC\omega^2/2) = P_0(\omega)z + (\text{periodic}), \tag{2.21}$$

where $P_0 = (1/z_a)\int_0^{z_a} i\mathcal{F}[\sum u_l^* u_m u_n]g(z)\exp(iC\omega^2/2)dz$. The first term on the right-hand side is the dominant cause of the resonant growth of the ghost pulse. The energy of the ghost pulse increases in proportion to z^2: $W(z) = (z^2/2\pi)\int_{-\infty}^{\infty}|P_0(\omega)|^2 d\omega$.

It should be noted that nonlinear pulse interactions in optical fibers are analogous to the so called quartet interactions which are responsible for energy changes between wavetrains in water waves, except for the interchange between time and distance. The condition $l = m+n$ necessary for the ghost pulse to grow resonantly corresponds to the wave number matching condition of the quartet interaction in water waves. The condition that the amplifier period equals the period of dispersion management corresponds to the frequency matching condition in quartet resonance.

2.10 *Conclusion*

We briefly reviewed the history and recent progress in the development of the mathematical theory of pulse propagation in optical fibers, including classical solitons, dispersion-managed solitons, and quasi-linear pulse transmission. Nonlinearity plays a crucial role in pulse dynamics of high-bit rate optical communication systems. The fundamental equation governing pulse propagation is the perturbed NLS equation. Solitons were originally proposed as a way to combat dispersion by the balance with nonlinearity, but

today in dispersion-managed systems, dispersion is positively utilized to manage nonlinearity.

Because of its rich applications and underlying mathematics, engineers, physicists and applied mathematicians have contributed to the development of modeling and analysis of high-bit rate optical fiber communications. We hope this stimulates students and researchers with a wide variety of backgrounds to study this exciting and interesting scientific field.

3 Discrete Solitons

Localized, stable nonlinear waves, often referred to as solitons, are of broad interest in mathematics and physics. They are found in both continuous and discrete media. In this section a unified method is presented which is used to obtain soliton solutions to both discrete and continuous problems. In recent experiments discrete solitons were observed in an optical waveguide array. The fundamental governing system is the discrete nonlinear Schrödinger equation. A suitable modification of this system describes diffraction managed solitons. Mathematically speaking, in the continuous limit these solitons reduce to the dispersion managed solitons described in chapter 2 of this paper.

3.1 *Introduction*

In physics and applied mathematics certain fundamental equations arise frequently. One such set of equations are the nonlinear Schrödinger (NLS) systems-continuous and discrete. NLS equations in continuous media have been studied since the 1960's. In 1967[11] it was shown that the NLS equation (see eq. (2.5)) governs the slowly varying wave amplitude of a carrier wave in dispersive weakly nonlinear media. In 1972 Zakharov and Shabat[10] showed that the NLS equation was solvable by the inverse scattering transform (IST). As such they showed that it possesses soliton solutions which have special elastic interaction properties (see also Ref.[14]). Shortly thereafter, and as mentioned in ch. 2, Hasegawa and Tappert [29] showed that the NLS equation governs long distance pulse propagation of nonlinear waves in optical fibers. In 1974 Manakov [51] showed that a vector extension of the NLS equation was also solvable by IST.

Two well known discretizations of the NLS equation are:

$$i\frac{du_n(z)}{dz} + \frac{1}{h^2}(u_{n+1} + u_{n-1} - 2u_n) + |u_n|^2 u_n = 0\,, \tag{3.1}$$

$$i\frac{du_n(z)}{dz} + \frac{1}{h^2}(u_{n+1} + u_{n-1} - 2u_n) + |u_n|^2 (u_{n+1} + u_{n-1})/2 = 0\,, \tag{3.2}$$

Eq. (3.1) is often called the discrete nonlinear Schrödinger (DNLS) equation. It has been found to be a useful model in many applications (eg biophysics [56], discrete self trapping [57], optical waveguide array [64; 65]). On the other hand eq. (3.2), has been shown to be integrable by the inverse scattering transform method properly extended to discrete problems [75]. It too has been useful in the study of physical problems. Like the continuous problem there is a useful integrable vector extension of eq. (3.2) [84].

In this section we will concentrate on eq. (3.1) above. The physical context we shall describe herein is that of coupled optical waveguides which also is a convenient setting for laboratory experiments.

The first theoretical prediction of discrete solitons in an optical waveguide array was reported by Christodoulides and Joseph[58]. Later on, many theoretical studies of discrete solitons in a waveguide array reported switching, steering and other collision properties of these solitons[59; 60] (see also the review paper[61]). In all of the above cases, the localized modes are solutions of the discrete nonlinear Schrödinger (DNLS) equation which describes beam propagation in Kerr nonlinear media (according to coupled mode theory). Discrete bright and dark solitons have also been found in quadratic media[62]. In some cases, their properties differ from their Kerr counterparts[63].

It took almost a decade until self-trapping of light in discrete nonlinear waveguide array was first experimentally observed by Eisenberg et. al.[64; 65]. When a low intensity beam is injected into one or a few waveguides, the propagating field spreads over the adjacent waveguides hence experiencing discrete diffraction. However, at sufficiently high power, the beam self-traps to form a localized state (a soliton) in the center waveguides. Subsequently, many interesting properties of nonlinear lattices and discrete solitons were reported. For example the experimental observation of linear and nonlinear Bloch oscillations in: AlGaAs waveguides[66], polymer waveguides[67] and in an array of curved optical waveguides[68]. Discrete systems have unique

properties that are absent in continuous media such as the possibility of producing *anomalous* diffraction[69]. Hence, self-focusing and defocusing processes can be achieved in the same medium (structure) and wavelength. This also leads to the possibility of observing discrete dark solitons in self-focusing Kerr media[70].

The recent experimental observations of discrete solitons[64] and diffraction management[69] have motivated further interests in discrete solitons in nonlinear lattices. This includes the newly proposed model of discrete diffraction managed nonlinear Schrödinger equation[71] whose width and peak amplitude vary periodically; optical spatial solitons in nonlinear photonic crystals[72] and the possibility of creating discrete solitons in Bose-Einstein condensation[73]. Also, very recently, it was shown, for the first time, that discrete solitons in two-dimensional networks of nonlinear waveguides can be used to realize intellegent functional operations such as blocking, routing, logic functions and time gating[74].

In this section, we introduce the Fourier transform method to analyze stationary solitons in nonlinear lattices. The essence of the method is to transform the DNLS equation governing the solitary wave into Fourier space, where the wave function is smooth, and then deal with a nonlinear nonlocal integral equation for which we employ a rapidly convergent numerical scheme to find solutions. A key advantage of the method is to transform a differential-delay equation into an integral equation for which computational methods are effective. Mathematically, the method also provides a foundation upon which an analytic theory describing solitons in nonlinear lattices can be constructed. We shall consider in this chapter two important models: the discrete nonlinear Schrödinger (DNLS) equation and the diffraction-managed discrete nonlinear Schrödinger (DM-DNLS) equation. Applying this method to the first model, shows that stationary solitons can readily be constructed. For the second model, we derive in the limit of strong diffraction, averaged equations governing the slow dynamics of the beam's amplitudes. Stationary solutions (in the form of bright-bright vector bound state) are obtained.

3.2 *Waveguide Array*

As mentioned above, an array of coupled optical waveguides is a setting that represents a convenient laboratory for experimental observations and theoretical predictions. Such system (see Fig. 3) is typically composed of

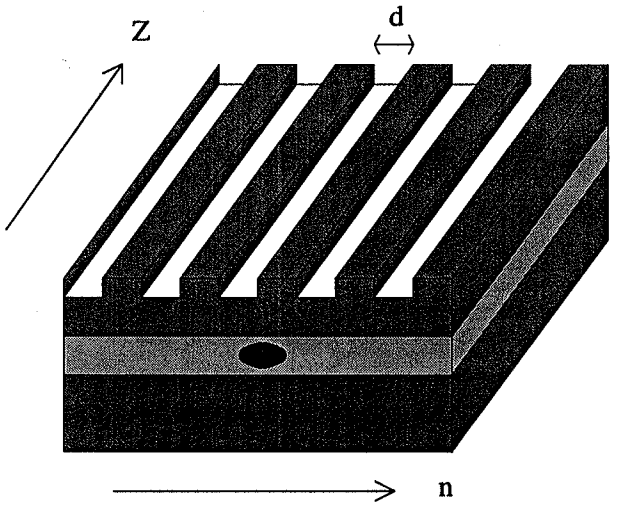

Fig. 3 AlGaAs waveguide structure. It is composed of three layers of AlGaAs material: a substrate with refractive index n_0, a core with higher index (n_1) and surface with index n_0. By etching the surface of the waveguide, one forms a periodic structure which is called a waveguide array.

three layers of AlGaAs material: a substrate with refractive index n_0, a core with higher index (n_1) and surface with index n_0. By etching the surface of the waveguide, one forms a periodic structure which is called a waveguide array. Self-traping of light in the "y" (i.e., vertical) direction is possible (even in the linear regime) by virtue of the principle of total internal reflection. On the other hand, the beam can diffract in the "x" direction unless it is balanced by nonlinearity. In the following we describe the propagation of light in such a periodic structure both in the linear and nonlinear regime.

3.3 *Linear Propagation: Anomalous Diffraction*

If the distance, d, between the waveguides is "large" then the propagating beams across each single waveguide do not "feel" each other. Therefore, the amplitude of each beam evolves independently. On the other hand when d is small then there is an overlap between modes in adjacent waveguides. As a result, the beam's amplitude is *not* constant anymore (see Fig. 4).

Assuming linear coupling between nearest neighbors, the dynamics of the beam's amplitude $E_n(z)$ at waveguide number n follows from coupled-

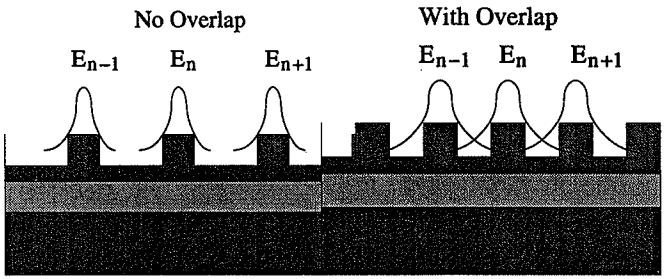

Fig. 4 Cross section of the waveguide array and mode overlap.

mode theory

$$i\frac{\partial E_n}{\partial z} + C(E_{n+1} + E_{n-1}) = 0\,, \tag{3.3}$$

where C is the coupling constant between adjacent waveguides which is given by an overlap integral of the two modes in such waveguides; z is the propagation distance. To facilitate understanding, we first recall basic properties of discrete diffraction of a *linear* array. When a mode of the form

$$E_n(z) = A\exp[i(k_z z - nk_x d)]\,, \tag{3.4}$$

is inserted into Eq. (3.3) it yields the following diffraction relation

$$k_z = 2C\cos(k_x d)\,. \tag{3.5}$$

In close analogy to the definition of dispersion, discrete diffraction is given by $k_z'' = -2Cd^2\cos(k_x d)$. We consider $|k_x d| \le \pi$. In that region, the diffraction is *normal* for wavenumbers k_x satisfying $-\pi/2 < k_x d \le \pi/2$ ($k_z'' < 0$) and is *anomalous* in the range $\pi/2 < |k_x d| \le \pi$. Moreover, contrary to the bulk case, diffraction can even vanish when $k_x d = \pm\pi/2$. In practice, the sign and value of the diffraction can be controlled and manipulated by launching light at a particular angle or equivalently by tilting the waveguide array. This in turn allows the possibility of achieving a "self-defocusing" (with *positive* Kerr coefficient) regime which leads to the formation of discrete dark solitons[70]. To understand more about diffraction management we consider three typical cases for which light enters the central waveguide array at different angles, say, $k_x d = 0, \pi/2$ and π. When $k_x d = 0$ then light tunnels between adjacent waveguides giving rise to discrete diffraction. The phase front in this case has a concave (negative) curvature. On the other hand, if $k_x d = \pi$, then diffusion of light still occurs but this time the phase

front has convex (positive) curvature. Finally, at $k_x d = \pi/2$, diffraction vanishes (even though light can couple to different waveguides) and in the absence of any higher order diffraction the phase front looks almost flat (see Fig. 5).

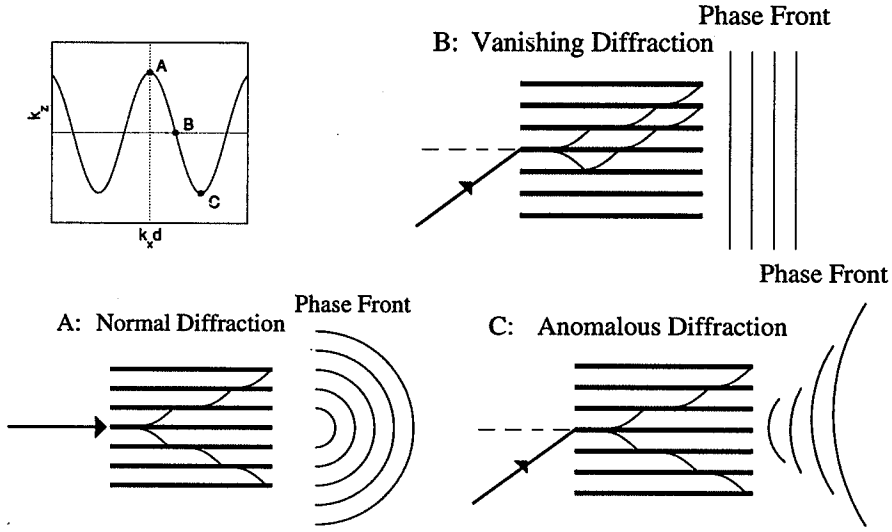

Fig. 5 Diffraction relation (top left) showing three typical examples of diffraction: (A) Normal in which the phase front is concave, (B) vanishing diffraction in which the phase front is flat, (C) anomalous diffraction with convex phase front.

3.4 *The Discrete Nonlinear Schrödinger Equation*

In the preceding section, we addressed the physical manifestation of propagation of light in a discrete linear medium. However, when the intensity of the incident beam is suffeciently high then the refractive index of the medium will depend on the intensity. The equation which governs the evolution of the electric field E_n, according to nonlinear coupled mode theory is given by

$$i\frac{\partial E_n}{\partial z} + C(E_{n+1} + E_{n-1}) + \kappa|E_n|^2 E_n = 0\,, \tag{3.6}$$

where C is the coupling constant between adjacent waveguides, κ is a constant describing the nonlinear index change, z is the propagation distance. First we put the NLS equation in a dimensionless form. To do so, we define

$$E_n = \sqrt{P_*}\phi_n \exp(2iCz)\,, \qquad z' = z/z_{\rm nl} \tag{3.7}$$

with P_* and $z_{\rm nl}$ being the characteristic power and $z_{\rm nl}$ the nonlinear length scale. Then ϕ_n satisfies

$$i\frac{d\phi_n}{dz} + \frac{1}{h^2}\left(\phi_{n+1} + \phi_{n-1} - 2\phi_n\right) + |\phi_n|^2\phi_n = 0\,, \tag{3.8}$$

with $z_{\rm nl}C = 1/h^2$ and $z_{\rm nl} = 1/(\kappa P_*)$. In the NLS equation there are two important length scales: the diffraction and nonlinear length scales respectively defined by $L_D \sim 1/C$ and $z_{\rm nl} = 1/(\kappa P_*)$. Solitons which are self-confined and invariant structures are expected to form when $L_D \sim z_{\rm nl}$.

3.5 *Stationary Solitons: Fourier Transform Method*

In this section, we introduce a new method to obtain stationary solitons for the DNLS equation. The essence of the method is to transform the DNLS equation governing the solitary wave into Fourier space, where the wave function is smooth, and then deal with a nonlinear nonlocal integral equation for which we employ a rapidly convergent numerical scheme to find solutions. A key advantage of the method is to transform a differential-delay equation into an integral equation for which computational methods are effective (see also refs.[80; 42]). Mathematically, the method also provides a foundation upon which an analytic theory describing solitons in nonlinear lattices can be constructed.

3.6 *Stationary Solutions*

We look for a stationary solution to Eq. (3.8) in the form

$$\phi_n = F_n \exp(i\omega z)\,, \tag{3.9}$$

with F_n being real valued function and ω is a real eigenvalue. Then F_n satisfies

$$-\omega F_n + \frac{1}{h^2}\left(F_{n+1} + F_{n-1} - 2F_n\right) + F_n^3 = 0\,. \tag{3.10}$$

Equation (3.10) can be solved using Newton iteration scheme by which one gives initial value for F_0 and F_1 and then iterate. However, our aim here is to provide a different approach based on Fourier transform method. We introduce the discrete Fourier transform

$$\hat{F}(q) = \sum_{m=-\infty}^{+\infty} F_m e^{-iqmh}\,, \qquad F_m = \frac{h}{2\pi}\int_{-\pi/h}^{\pi/h} \hat{F}(q)e^{iqmh}dq\,. \tag{3.11}$$

Then, the above equation, transforms into the following nonlinear integral equation

$$\hat{F}(q) = \frac{h^2}{4\pi^2\Omega(q)}\int dq_1 dq_2 \hat{F}(q_1)\hat{F}(q_2)\hat{F}(q-q_1-q_2) \equiv \mathcal{K}_\omega[\hat{F}(q)]\,, \tag{3.12}$$

where $\Omega(q) = \omega + 2(1-\cos(hq))/h^2$. The important conclusion is that soliton can be viewed as a fixed point of an infinite dimensional nonlinear functional. To numerically find the fixed point, we employ a modified Neumann iteration scheme and write

$$\hat{F}_{n+1}(q) = \left(\frac{\alpha(\hat{F}_n)}{\beta(\hat{F}_n)}\right)^{3/2} \mathcal{K}_\omega[\hat{F}_n(q)]\,, \quad n \geq 0\,, \tag{3.13}$$

with α and β defined by

$$\alpha = \int \hat{F}_n^2(q)dq\,; \quad \beta = \int \hat{F}_n(q)\mathcal{K}_\omega[\hat{F}_n(q)]dq \tag{3.14}$$

The factor 3/2 is chosen to make the right hand side of Eq. (3.13) of degree zero which yields convergence of the scheme[80; 42]. When F_m is real and even, it implies that $\hat{F}(q)$ is also real. Clearly when $\hat{F}_n(q) \to \hat{F}_s(q)$ as $n \to \infty$ then $\alpha/\beta \to 1$ and in turn $\hat{F}_s(q)$ will be the solution to Eq. (3.12). The factors α and β are introduced to stabilize an otherwise divergent simple Neumann iteration scheme. Note that when we apply the continuous Fourier transform on Eq. (3.10) (to find stationary solution), then the numerical scheme based on (3.13) does not converge which indicates that a *continuous* stationary solution to the DNLS may not exist. Fig. 6 shows a typical solution to (3.12) both in the Fourier domain (Fig. 6a) and in physical space (Fig. 6b) for different values of lattice spacing h. Importantly, with suitable modification of Eq. (3.13) this method yields new breathing localized modes: "discrete diffraction managed solitons"[71].

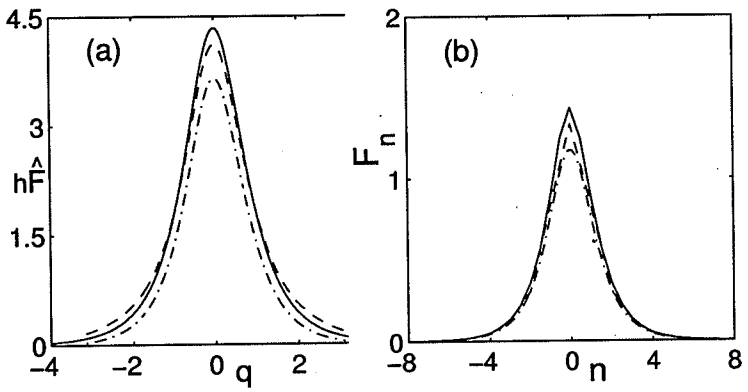

Fig. 6 Mode profiles obtained with $\omega_s = 1$ in Fourier space (a), for $h = 0.5$ (solid), $h = 1$ (dashed) and $h = 1$ (dashed-dotted) for the integrable case. (b) Soliton shape in physical space for $h = 0.5$ (solid), $h = 1$ (dashed) and for the integrable case at $h = 1$ (dashed-dotted).

3.7 *Nonlinear Diffraction Management*

We begin our analysis by considering again an infinite array of weakly coupled optical waveguides with equal separation d. The equation which governs the evolution of the electric field E_n, according to nonlinear coupled mode theory[58; 79; 64], is given by

$$\frac{\partial E_n}{\partial z} = iC(E_{n+1} + E_{n-1}) + ik_w E_n + i\kappa |E_n|^2 E_n \,, \tag{3.15}$$

where C is the coupling constant between adjacent waveguides which is given by an overlap integral of the two modes of such waveguides; κ is a constant describing the nonlinear index change, z is the propagation distance and k_w is the propagation constant of the waveguides. Similar to[69], we use a cascade of different segments of waveguide, each piece being tilted by an angle zero and γ respectively. The actual physical angle γ (the waveguide tilt angle) is related to the wavenumber k_x by the relation[69] $\sin\gamma = k_x/k$ where $k = 2\pi n_0/\lambda_0$ ($\lambda_0 = 1.53$ μm is the central wavelength in vacuum and $n_0 = 3.3$ is the linear refractive index). In this way, we generate a waveguide array with alternating diffraction. To model such a system, we define $E_n = \sqrt{P_*}\phi_n e^{i(k_w+2C)z}$ and $z' = z/z_*$ with P_* and z_* being the characteristic power and nonlinear length scale respectively. Substituting these quantities into Eq. (3.15) yields the following (dropping the prime)

diffraction-managed discrete nonlinear Schrödinger (DM-DNLS) equation

$$\frac{d\phi_n}{dz} = i\frac{D(z/z_w)}{2h^2}(\phi_{n+1} + \phi_{n-1} - 2\phi_n) + i|\phi_n|^2\phi_n \tag{3.16}$$

with $z_* = 1/(\kappa P_*)$ and $z_* C\cos(k_x d) = D(z/z_w)/(2h^2)$ where $D(z/z_w)$ is a piecewise constant periodic function that measures the local value of diffraction. Here, $z_w \equiv 2L/z_*$ with L being the actual length of each waveguide segment (see Fig. 7(a) for schematic representation). Eq. (3.16) describes the dynamical evolution of a laser beam in a Kerr medium with varying diffraction. When the "effective" nonlinearity balances the average diffraction then bright discrete solitons can form.

The coupling constants that correspond to the experimental data reported in[69] (for 2.5 μm waveguide separation and width) are found to be $C = 2.27\ \mathrm{mm}^{-1}$[77], $\kappa = 3.6\ \mathrm{m}^{-1}\mathrm{W}^{-1}$. For typical power $P_* \approx 300$ W and waveguide length $L \approx 100$ μm we find $z_* \approx 1$ mm and $z_w \approx 0.2$. Hence, it is natural to construct an asymptotic theory based on small z_w. It is in this parameter regim that diffraction managed spatial solitons can be experimentally observed. To this end, we consider the case in which the diffraction takes the form

$$D(z/z_w) = \delta_a + \frac{1}{z_w}\Delta(z/z_w)\,, \tag{3.17}$$

where δ_a is the average diffraction (taken to be positive) and $\Delta(z/z_w)$ is a periodic function. Since in this case, Eq. (3.16) contains both slowly and rapidly varying terms, we introduce new fast and slow scales as $\zeta = z/z_w$ and $Z = z$ respectively and expand ϕ_n in powers of z_w

$$\phi_n = \phi_n^{(0)}(\zeta, Z) + z_w\phi_n^{(1)}(\zeta, Z) + O(z_w^2)\,. \tag{3.18}$$

Substituting Eqs. (3.18) and (3.17) into Eq. (3.16) we find that the leading order in $1/z_w$ and the order 1 equations are respectively given by

$$\mathcal{J}(\phi_n^{(0)}) = 0\,, \quad \mathcal{J}(\phi_n^{(1)}) = -\mathcal{F}_n\,, \tag{3.19}$$

where

$$\mathcal{J}(A_n) \equiv i\frac{\partial A_n}{\partial\zeta} + \frac{\Delta(\zeta)}{2h^2}(A_{n+1} + A_{n-1} - 2A_n)\,,$$
$$\mathcal{F}_n = i\frac{\partial\phi_n^{(0)}}{\partial Z} + \frac{\delta_a}{2h^2}\left(\phi_{n+1}^{(0)} + \phi_{n-1}^{(0)} - 2\phi_n^{(0)}\right) + |\phi_n^{(0)}|^2\phi_n^{(0)}\,.$$

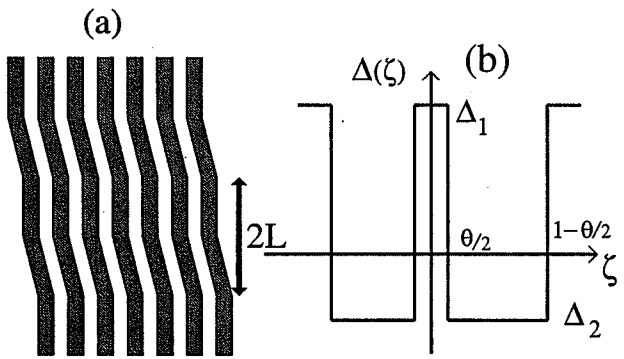

Fig. 7 Schematic presentation of the waveguide array (a) and of the diffraction map (b).

To solve at order $1/z_w$ (see Eq. (3.19)), we introduce the discrete Fourier transform

$$\hat{\phi}_0(q,\zeta,Z) = \sum_{n=-\infty}^{+\infty} \phi_n^{(0)}(\zeta,Z)e^{-iqnh}\,,$$
$$\phi_n^{(0)}(\zeta,Z) = \frac{h}{2\pi}\int_{-\pi/h}^{\pi/h} \hat{\phi}_0(q,\zeta,Z)e^{iqnh}dq\,. \tag{3.20}$$

The solution is therefore given in the Fourier representation by

$$\hat{\phi}_0(q,\zeta,Z) = \hat{\psi}(Z,q)\exp[-i\Omega(q)C(\zeta)]\,, \tag{3.21}$$

with $\Omega(q) = (1-\cos(qh))/h^2$ and $C(\zeta) = \int_0^\zeta \Delta(\zeta')d\zeta'$. The amplitude $\hat{\psi}(Z,q)$ is an arbitrary function whose dynamical evolution will be determined by a secularity condition associated with Eq. (3.19). In other words, the condition of the orthogonality of $\mathcal{F}_n$ to all eigenfunctions Φ_n of the adjoint linear problem which, when written in the Fourier domain, takes the form

$$\int_0^1 d\zeta\hat{\mathcal{F}}(q,\zeta,Z)\hat{\Phi}(q,\zeta,Z) = 0\,, \tag{3.22}$$

where $\hat{\mathcal{F}}$, $\hat{\Phi}$ are the Fourier transform of $\mathcal{F}_n$, Φ_n respectively. Here, $\hat{\mathcal{J}}^\dagger\hat{\Phi} = 0$ with $\hat{\mathcal{J}}^\dagger$ being the adjoint operator to $\hat{\mathcal{J}} \equiv id/d\zeta - \Delta(\zeta)\Omega(q)$. Substituting (3.21) into $\hat{\mathcal{F}}$ and performing the integration in condition (3.22) yields the

following nonlinear evolution equation for $\hat{\psi}(Z,q)$:

$$i\frac{d\hat{\psi}(Z,q)}{dZ} = \delta_a\Omega(q)\hat{\psi}(Z,q) - \mathcal{R}[\hat{\psi}(Z,q)]\,,$$
$$\mathcal{R} \equiv \int d\mathbf{q}\mathcal{K}(q,q_1,q_2)\hat{\psi}(q_1)\hat{\psi}(q_2)\hat{\psi}^*(q_1+q_2-q), \tag{3.23}$$

where $d\mathbf{q} \equiv dq_1dq_2$ and the kernel $\mathcal{K}$ is defined by

$$\mathcal{K}(q,q_1,q_2) = \frac{h^2}{4\pi^2}\int_0^1 d\zeta\exp[iC(\zeta)\chi(q,q_1,q_2)]\,,$$
$$\chi = \frac{4}{h^2}\cos\left(\frac{h(q_1+q_2)}{2}\right)\prod_{j=1}^{2}\sin\left(\frac{h(q_j-q)}{2}\right)\,.$$

Equation (3.23) governs the evolution in Fourier space of an optical beam in a coupled nonlinear waveguide array in the regime of strong diffraction. In the special case of two-step diffraction map shown in Fig. 7(b), i.e., when two waveguide segments are tilted by angle zero and γ alternatively, we have $\Delta(\zeta) = \Delta_1$ for $0 \le |\zeta| < \theta/2$ and Δ_2 in the region $\theta/2 < |\zeta| < 1/2$ where θ is the fraction of the map with diffraction Δ_1. In this case, the kernel $\mathcal{K}$ takes the simple form $\mathcal{K} = h^2\sin(s\chi)/(4\pi^2 s\chi)$ with $s = [\theta\Delta_1 - (1-\theta)\Delta_2]/4$. Importantly, these parameters can be related to the experiments reported in[69]. To achieve a waveguide configuration with alternate diffraction, we use two values of $k_x d = 0$ and $2\pi/3$ ($h = 1$) which corresponds to waveguide tilt angles $\gamma = 0$ and 3.43°. In this case we find, for $\theta = 0.5$, $\Delta_1 = -\Delta_2 = 0.681$, $\delta_a = 1.135$ and $s = 0.17$. Different sets of parameters with a smaller angle γ are also realizable. Next, we look for a stationary solution for Eq. (3.23) (for the particular kernel given above) in the form $\hat{\psi}(Z,q) = \hat{\psi}_s(q)\exp(i\omega_s Z)$. Inserting this ansatz into (3.23) leads to

$$\hat{\psi}_s(q) = \frac{1}{\delta_a\Omega(q)+\omega_s}\mathcal{R}[\hat{\psi}_s(q)] \equiv \mathcal{M}[\hat{\psi}_s(q)]\,, \tag{3.24}$$

which implies that the mode $\hat{\psi}_s(q)$ is a fixed point of the nonlinear functional $\mathcal{M}$. To numerically find the fixed point, we employ a modified Neu-

mann iteration scheme[80; 81; 82] and write Eq. (3.24) in the form

$$\hat{\psi}_s^{(m+1)}(q) = \left(\frac{\alpha(\hat{\psi}_s^{(m)})}{\beta(\hat{\psi}_s^{(m)})}\right)^{3/2} \mathcal{M}[\hat{\psi}_s^{(m)}(q)]\,, \quad m \geq 0\,,$$
$$\alpha = \int |\hat{\psi}_s^{(m)}(q)|^2 dq\,; \quad \beta = \int \hat{\psi}_s^{(m)}(q)\mathcal{M}[\hat{\psi}_s^{(m)}(q)]dq\,.$$

The factors α and β are introduced to stabilize an otherwise divergent Neumann iteration scheme. This method is used to find stationary soliton solutions to the integral equation (3.23) which in turn provides an asymptotic description of the diffraction-managed DNLS Eq. (3.16). It should be also noted that we can obtain periodic diffraction-compensated soliton solutions directly from Eq. (3.16). The technique is similar to that originally proposed for finding periodic dispersion-managed solitons in communications problems[85; 86; 87]. The averaging procedure does not require that the map period, z_w, be small. To implement the method, initially we start with a guess, say $\phi_n^{(0)} = \mathrm{sech}(nh)$ with $\mathcal{E}_0 = \sum_{n=-\infty}^{\infty} \mathrm{sech}^2(nh)$. Over one period this initial ansatz will evolve to $\phi_n^{(0)'}$ which in general will have a chirp[88]. We then define an average: $\phi_n^{(0)''} = (\phi_n^{(0)} + \phi_n^{(0)'} e^{-i\Theta_n})/2$ where $\phi_n^{(0)'} = |\phi_n^{(0)'}| \exp(i\Theta_n)$ which has power $\mathcal{E}_0''$. Then $\phi_n^{(1)} = \phi_n^{(0)''}\sqrt{\mathcal{E}_0/\mathcal{E}_0''}$ is the new guess and in general the m^{th} iteration takes the form

$$\phi_n^{(m+1)} = \sqrt{\mathcal{E}_0/\mathcal{E}_m''}\phi_n^{(m)''}, \quad \mathcal{E}_m'' = \sum_{n=-\infty}^{\infty} |\phi_n^{(m)''}|^2\,. \tag{3.25}$$

In Fig. 8 the mode profiles associated with a stationary solution are depicted for two typical parameter values. The profiles are obtained by using both the integral equation approach as well as the averaged method. The evolution of these discrete diffraction managed solitons are illustrated in Figs. 9 and 10 for the same two set of parameter values as in Fig. 8 respectively. We note that initially the beam has zero chirp[88]. During propagation a chirp develops and the peak amplitude of the beam begins to decrease and, as a result, the beam becomes wider (due to conservation of power). A full recovery of the soliton's initial amplitude and width is achieved at the end of the map period. This breathing behavior is shown in Figs. 9 and 10 for both strongly and moderately confined beams respectively.

To establish the relation between the two approaches and to highlight the periodic nature of these new solitons, we calculate the nonlinear chirp by both the integral equation approach and the averaging method. It is

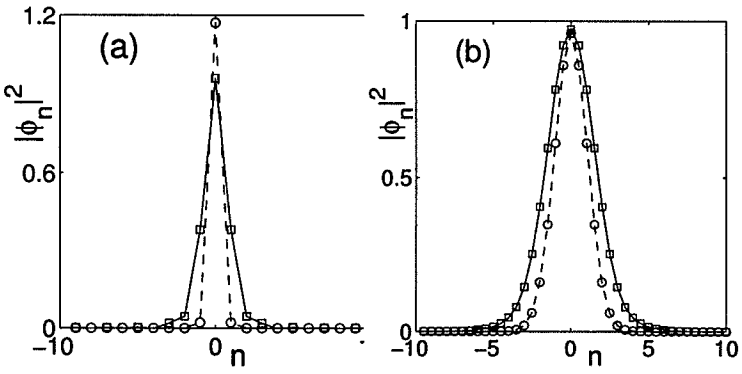

Fig. 8 Mode profile in physical space obtained from Eq. (3.24) (solid line) and from the average method (dashed line). Parameters are: (a) $\omega_s = 1$, $h = 1$, $s = 0.17$, $\Delta_1 = -\Delta_2 = 0.681$, $\delta_a = 1.135$ and $z_w = 0.2$; (b) $\omega_s = 1$, $h = 0.5$, $s = 1$, $\Delta_1 = -\Delta_2 = 4$, $\delta_a = 1$ and $z_w = 0.2$.

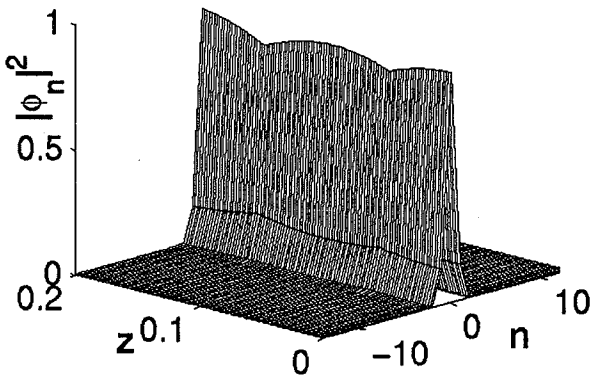

Fig. 9 Beam propagation over one period using Eq. (3.21) as initial condition obtained by a direct numerical simulation of Eq. (3.16). Parameters are the same as used in Fig. 8(a).

clear that for small values of the map period, z_w, the asymptotic analysis is in good agreement with the averaging method, as shown in Fig. 11.

We also mention briefly that the method of analysis associated with Eq. (3.16) can be modified to account for situations where the average diffraction is small, i.e., $\delta_a \ll 1$. In such a situation we write $\delta_a = \epsilon D_a$,

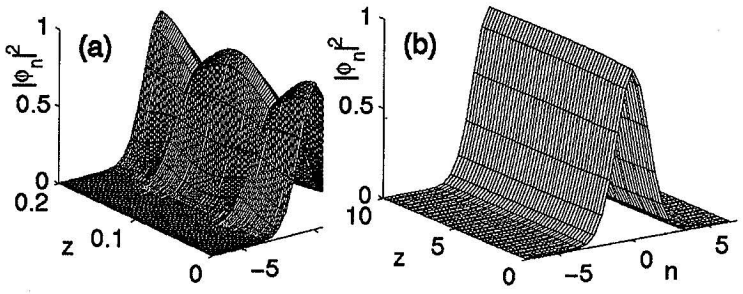

Fig. 10 Beam propagation over one period (a) and stationary evolution (b) obtained by a direct numerical simulation of Eq. (3.16) evaluated at end map period. Parameters are the same as used in Fig. 8(b).

$D = \epsilon D_a + \Delta(z)$, $z = \xi/\epsilon$, and $\phi_n = \sqrt{\epsilon}\Psi_n$. Then it is found that Ψ_n satisfies:

$$\frac{d\Psi_n}{d\xi} = i\frac{\mathcal{D}(\xi/\epsilon)}{2h^2}\left(\Psi_{n+1} + \Psi_{n-1} - 2\Psi_n\right) + i|\Psi_n|^2\Psi_n\,, \tag{3.26}$$

where $\mathcal{D}(\xi/\epsilon) = D_a + \frac{1}{\epsilon}\Delta(\xi/\epsilon)$. The model (3.26) is valid in parameter regimes which applies to physical situation where the average diffraction is small.

3.8 *Conclusion*

A discrete nonlinear wave equation has been investigated by the discrete Fourier transform. We have constructed a discrete equation governing the evolution of an optical beam in a waveguide array with varying diffraction. This equation has a novel type of discrete spatial soliton solution which breathes under propagation and, as a result, gains a nonlinear chirp. A full recovery of the soliton initial power is achieved at the end of each diffraction map. This open the possibility of fabricating a customized waveguide array which admits spechialized diffraction managed spatially confined solitary waves. A nonlocal integral equation governing the slow evolution of the soliton amplitude is derived and its stationary solutions are obtained.

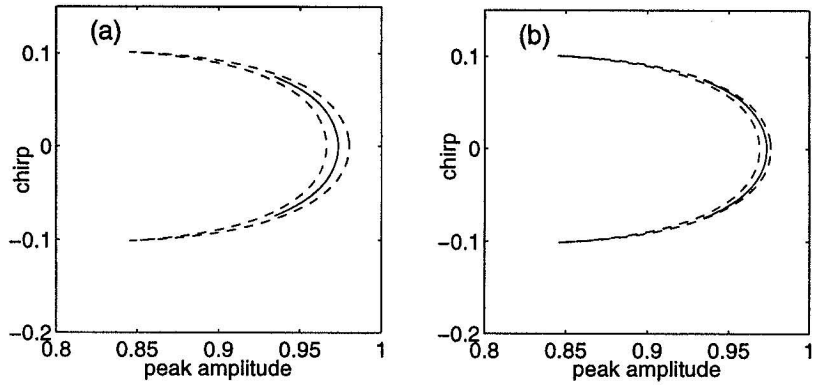

Fig. 11 Periodic evolution of the beam chirp versus maximum peak power. Solid line represents the leading order approximation, i.e., Eq. (3.21); dashed line represents numerical solution of the DM-DNLS. Parameters are the same as used in Fig. 8(b) with $z_w = 0.2$ (a) and 0.1 (b).

Acknowledgement

M.J.A. is partially supported by the Air Force Office of Scientific research, under grant number F49620-03-1-0250, NSF under grant numbers ECS-9800152, DMS-0070792.

References

J. Scott Russell, "Report on waves", Report of the 14th Meeting of the British Association for the Advancement of Science, Liverpool, pp. 417-496, 1844.

J. Boussinesq, "Theorie de l'intumescence liquid appelée onde solitaire ou de translation, se propagente dans un canal rectangulaire," *Compte Rendus Acad. Sci. Paris* **72**, 755-759, 1871.

D. J. Kortegweg and G. deVries, "On the change of form of long waves advancing in a rectngular canal, and on a new type of long stationary waves," *Philos. Mag. Ser.* 5, 39, 1039-1049, 1895.

C. S. Gardner and G. K. Morikawa, "Similarity in the asymptotic behavior of collision free hydromagnetic waves and water waves," Courant Inst. Math. Sci. Res. Rep. NYO-9082, New York University, New York (1960).

D. J. Benney, "Long nonlinear waves in fluid flows," *J. Math. Phys.*, (*Stud. on Appl. Math*), **45**, 52-63, 1966.

M. D. Kruskal, in Proc. IBM Scientific Computing Symposium on Large-Scale Problems in Physics, IBM Data Processing Division, White Plains, NY;

Thomas J. Watson Research Center, Yorktown Heights, NY (1965).
N. J. Zabusky and M. D. Kruskal, "Interaction of solitons in a collisioinless plasma and the recurrence of initial states," *Phys. Rev. Lett.* **15**, 240-243, 1965.
C. S. Gardner, J. M. Greene, M. D. Kruskal, and R. M. Miura, "Method for solving the Korteweg-de Vries equatoin," *Phys. Rev. Lett.* **19**, 1095-1097 (1967).
I. M. Gel'fand and B. M. Levitan, "On the determination of a differential equation from its spectral function," *Amer. Math. Sci. Transl.*, Ser 2, **1**, 259-309, 1955.
V. E. Zakharov and A. B. Shabat, "Exact theory of two-dimensional self-focusing and one-dimensional of waves in nonlinear media," *Sov. Phys. JETP* **34**, 62-69 (1972).
D. J. Benney and A. C. Newell, "The propagation of nonlinear wave envelopes," *J. Math. Phys.*, (*Stud. on Appl. Math*), **46**, 133-139, 1967.
V. E. Zakharov, "Stability of periodic waves of finite amplitude on the surface of a deep fluid," *Sov. Phys. J. Appl. Mech. Tech. Phys.* **4**, 190-194 (1968).
M. J. Ablowitz, D. J. Kaup, A. C. Newell and H. Segur, "The Inverse Scattering Transform – Fourier Analysis for Nonlinear Problems," *Stud. Appl. Math.*, **53**, 249-315 (1974).
M. J. Ablowitz and H. Segur, Solitons and the Inverse Scattering Transform, SIAM Studies in Applied Mathematics, 425 pages, SIAM, Philadelphia, PA, 1981.
M. J. Ablowitz and P. A. Clarkson, "Solitons, Nonlinear Evolution Equations and Inverse Scattering," London Mathematical Society Lecture Notes Series #149, 516 pages, Cambridge University Press, Cambridge, UK, 1991.
A. R. Osborne and T. L. Burch, "Internal solitons in the Andaman Sea," *Science* **258**, 451-460 (1980).
B. B. Kadomstsev and V. I. Petviashvili, "On the stability of solitary waves in weakly dispersing media," *Sov. Phys. Doklady* **15**, 539-541, 1970.
M. J. Ablowitz, and H. Segur, "On the Evolution of Packets of Water Waves," *J. Fluid Mech.*, **92**, 691-715 (1979).
M. J. Ablowitz, S. Chakravarty and L. A. Takhtajan, "A Self-Dual Yang-Mills Hierarchy and its Reductions to Integrable Systems in $1+1$ and $2+1$ Dimensions," *Commun. Math. Phys.*, **158**, 289-314 (1993).
L. J. Mason and N. M. J. Woodhouse, Integrability, Self-Duality, and Twistor Theory, Oxford University Press, LMS Monograph, New Series 15, Oxford, Oxford, 1996.
M. J. Ablowitz, S. Chakravarty and R. Halburd, "The Generalized Chazy Equation from the Self-duality Equations, *Stud. Appl. Math.* **103**, 75-88 (1999).
M. J. Ablowitz and A. S. Fokas, Complex Variables: Introduction and Applications, Cambridge University Press, Cambridge, UK, 1997.
E. R. Berlekamp, J. H. Conway, and R. K. Guy, Winning Ways, Academic Press, New York, 1982.
S. Wolfram, Theory and Applications of Cellular AUtomata, World Scientific,

Singapore, 1986.
J. H. H. Park, K. Steiglitz, and W. Thurston, "Soliton-like behavior in automata," *Physica* **19D**, 423-342 (1986).
T. S. Papatheodorou, M. J. Ablowitz and Y. G. Saridakis, "A Rule for Fast Computation and Analysis of SolitonAutomata, *Stud. in Appl. Math.* **79**, 173-184 (1988).
M. J. Ablowitz, J. M. Keiser and L. A. Takhtajan, "A Class of Stable Multistate Time-Reversible Cellular Automata with Rich Particle Content," *Phys. Rev. A* **44**, 6909-6912 (1991).
M. J. Ablowitz, "Nonlinear Feedback Shift Registers Via Nonlinear Evolution," *Stud. in Appl. Math* **107**, 127-136 (2001).
A. Hasegawa and F. Tappert, "Transmission of stationary nonlinear optical pulses in dispersive dielectric fibers. I. Anomalous dispersion," *Appl. Phys. Lett.* **23**, 142 (1973).
Y. Kodama and A. Hasegawa, "Nonlinear pulse propagation in a monomode dielectric guide," *IEEE J. Quantum Electron.* **23**, 510 (1987).
L. F. Mollenauer, R. H. Stolen, and J. P. Gordon, "Experimental-observation of picosecond pulse narrowing and solitons in optical fibers," *Phys. Rev. Lett.* **45**, 1095 (1980).
A. Hasegawa and Y. Kodama, "Guiding-center soliton," *Phys. Rev. Lett.* **66**, 161 (1991).
J. P. Gordon and H. A. Haus, "Random walk of coherently amplified solitons in optical fiber transmission," *Opt. Lett.* **11**, 665 (1986).
P. L. Chu and C. Desem, "Mutual interaction between solitons of unequal amplitudes in optical fibre," *Electron. Lett.* **21**, 1133 (1985).
L. F. Mollenauer, S. G. Evangelides, Jr. and J. P. Gordon, "Wavelength division multiplexing with solitons in ultra-long distance transmission using lumped amplifiers," *J. Lightwave Technol.* **9**, 362 (1991).
P. V. Mamyshev and L. F. Mollenauer, "Pseudo-phase-matched four-wave mixing in soliton wavelength-division multiplexing transmission," *Opt. Lett.* **21**, 396 (1996).
M. J. Ablowitz, G. Biondini, S. Chakravarty, R. B. Jenkins, and J. R. Sauer, "Four-wave mixing in wavelength-division-mulplexed soliton systems: damping and amplification," *Opt. Lett.* **20**, 1646 (1996).
Y. Kodama and S. Wabnitz, "Analytical theory of guiding-center nonreturn-to-zero and return-to-zero signal transmission in normally dispersive nonlinear-optical fibers," *Opt. Lett.* **20**, 2291 (1995).
N. S. Bergano, C. R. Davidson, M. Ma, A. Pillipetskii, S. G. Evangelides, H. D. Kidorf, J. M. Darcie, E. Golovchenko, K. Rottwitt, P. C. Corbett, R. Menges, M. A. Mills, B. Pedersen, D. Peckham, A. A. Abramov, and A. M. Vengsarkar, in *Digest of Optical Fiber Communication Conference* (Optical Society of America, Washington, D.C., 1998), postdeadline paper PD12.
M. Suzuki, I. Morita, N. Edagawa, S. Yamamoto, H. Taga, and S. Akiba, "Reduction of Gordon-Haus timing jitter by periodic dispersion compensation

in soliton transmission," *Electron. Lett.* **31**, 2027 (1995).
N. J. Smith, F. M. Knox, N. J. Doran, K. J. Blow, and I. Bennion, "Enhanced power solitons in optical fibres with periodic dispersion management," *Electron. Lett.* **32**, 54 (1996).
M. J. Ablowitz and G. Biondini, "Multiscale pulse dynamics in communication systems with dispersion management," *Opt. Lett.* **23**, 1668 (1998).
M. J. Ablowitz, G. Biondini, and E. Olson, "On the evolution and interaction of dispersion-managed solitons," in *Massive WDM and TDM Soliton Transmission Systems*, Ed. A. Hasegawa (Kluwer, Dordrecht, 2000).
M. J. Ablowitz, T. Hirooka, and G. Biondini, "Quasi-linear optical pulses in strongly dispersion-managed transmission systems," *Opt. Lett.* **26**, 459 (2001).
M. J. Ablowitz and T. Hirooka, "Nonlinear effects in quasi-linear dispersion-managed pulse transmission," *IEEE Photon. Technol. Lett.* **13**, 1082 (2001).
R. Horne, "Collision induced timing jitter and four-wave mixingin wavelength division multiplexing soliton systems," Ph. D dissertation, Department of Applied Mathematics, University of Colorado at Boulder (2001).
P. V. Mamyshev and N. A. Mamysheva, "Pulse-overlapped dispersion-managed data transmission and intrachannel four-wave mixing," *Opt. Lett.* **24**, 1454 (1999).
M. J. Ablowitz and T. Hirooka, "Resonant nonlinear intra-channel interactions in strongly dispersion-managed transmission systems" *Opt. Lett.* **25**, 1750 (2000).
M. J. Ablowitz and T. Hirooka, "Intra-channel pulse interactions in dispersion-managed transmission systems: timing shifts," *Opt. Lett.* **26**, 1846 (2001).
M. J. Ablowitz and T. Hirooka, "Intra-channel pulse interactions in dispersion-managed transmission systems: energy transfer," *Opt. Lett.* **27**, 203 (2002).
S. V. Manakov, "On the theory of two-dimensional stationary self-focusing of electromagnetic waves," Sov. Phys. JETP **38**, 248 (1974).
D. Henning and G. P. Tsironis, Phys. Rep. **307**, 333 (1999); O. M. Braun and Y. S. Kivshar, Phys. Rep. **306**, 1 (1998); S. Flach and C. R. Willis, Phys. Rep. **295**, 181 (1998); F. Lederer and J. S. Aitchison, Les Houches Workshop on Optical Solitons, Eds. V. E. Zakharov and S. Wabnitz, Springer-Verlag (1999).
A. C. Scott and L. Macneil, Phys. Lett. **98A**, 87 (1983).
A. J. Sievers and S. Takeno, Phys. Rev. Lett. **61**, 970 (1988).
W. P. Su, J. R. Schieffer, and A. J. Heeger, Phys. Rev. Lett. **42**, 1698 (1979).
A. S. Davydov, J. Theor. Biol. **38**, 559 (1973).
P. Marquii, J. M. Bilbaut, and M. Remoissenet, Phys. Rev. E **51**, 6127 (1995).
D. N. Christodoulides and R. J. Joseph, Opt. Lett. **13**, 794 (1988).
Y. S. Kivshar, Opt. Lett. **18**, 1147 (1993); W. Krolikowski and Y. S. Kivshar, J. Opt. Soc. Am. B **13**, 876 (1996).
A. B. Aceves, C. De Angelis, S. Trillo, and S. Wabnitz, Opt. Lett. **19**, 332 (1994); A. B. Aceves, C. De Angelis, T. Peschel, R. Muschall, F. Lederer, S. Trillo, and S. Wabnitz, Phys. Rev. E **53**, 1172 (1996); A. B. Aceves, C. De Angelis, A. M. Rubenchik, and S. K. Turitsyn, Opt. Lett. **19**, 329 (1994).
F. Lederer, S. Darmanyan, and A. Kobyakov, "*Discrete Solitons*", In: *Spatial Solitons*, Eds. S. Trillo and W. Torruellas (Springer-Verlag, Berlin, 2001), pp. 267-290.
T. Peschel, U. Peschel, and F. Lederer, Phys. Rev. E **57**, 1127 (1998);
S. Darmanyan, A. Kobyakov, and F. Lederer, Phys. Rev. E **57**, 2344 (1998).
H. Eisenberg, Y. Silberberg, R. Morandotti, A. Boyd, and J. Aitchison, Phys. Rev. Lett. **81**, 3383 (1998).
R. Morandotti, U. Peschel, J. Aitchison, H. Eisenberg, and Y. Silberberg, Phys. Rev. Lett. **83**, 2726 (1999).
R. Morandotti, U. Peschel, J. Aitchison, H. Eisenberg, and Y. Silberberg, Phys. Rev. Lett. **83**, 4756 (1999).
T. Pertsch, P. Dannberg, W. Elflein, A Bräuer, and F. Lederer, Phys. Rev. Lett. **83**, 4752 (1999).
G. Lenz, I. Talanina, and C. Martijn de Sterke, Phys. Rev. Lett. **83**, 963 (1999).
H. Eisenberg, Y. Silberberg, R. Morandotti, and J. Aitchison, Phys. Rev. Lett. **85**, 1863 (2000).
R. Morandotti, H. Eisenberg, Y. Silberberg, M. Sorel, and J. Aitchison, Phys. Rev. Lett. **86**, 3296 (2001).
M. J. Ablowitz and Z. H. Musslimani, Phys. Rev. Lett. **87** 254102, (2001).
S. F. Mingaleev, and Y. S. Kivshar, Phys. Rev. Lett. **86**, 5474 (2001); A. A. Sukhorukov and Y. S. Kivshar Phys. Rev. Lett. **87**, 083901 (2001); Phys. Rev. E (to be published).
A. Trombettoni and A. Smerzi, Phys. Rev. Lett. **86**, 2353 (2001).
D. N. Christodoulides and E. D. Eugenieva, Phys. Rev. Lett. **87**, 233901 (2001); Opt. Lett. **26**, 1876 (2001); E. D. Eugenieva, N. K. Efremidis, and D. N. Christodoulides, Opt. Lett. **26**, 1978 (2001); *Optics and Photonics News* **12**, 57, (2001).
M. J. Ablowitz and J. F. Ladik, J. Math. Phys. **17**, 1011 (1976).
M. Peyrard, and M. D. Kruskal, Physica D **14**, 88 (1984).
A. Yariv, Optical Electronics, Oxford University Press, Fifth Edition, (1997).
S. Darmanyan, A. Kobyakov, E. Schmidt, and F. Lederer, Phys. Rev. E **57**, 3520 (1998).
S. Somekh, E. Garmire, A. Yariv, H. L. Garvin, and R. G. Hunsperger, Appl. Phys. Lett. **22**, 46 (1973).
V. I. Petviashvili, Sov. J. Plasma Phys. **2**, 257 (1976).
M. J. Ablowitz and G. Biondini, Opt. Lett. **23**, 1668 (1998).
M. J. Ablowitz, Z. H. Musslimani, and G. Biondini, Phys. Rev. E **65**, 026602 (2002).
M. J. Ablowitz, Y. Ohta, and D. Trubatch, Phys. Lett. A **253**, 287 (1999).
M. J. Ablowitz, B. Prinari, and D. Trubatch, "Discrete and Continuous Nonlinear Schrödinger Systems", APPM report # 473, Dept. of Applied Mathematics, University of Colorado at Boulder (2001).

I. R. Gabitov and S. K. Turitsyn, Opt. Lett. **21**, 327 (1996).
S. K. Turitsyn, Sov. Phys. JETP Lett. **65**, 845 (1997).
J.H. B. Nijhof, W. Forysiak, and N. J . Doran, IEEE J. Sel. Top. on Quantum Elect. **6**, 330 (2000).
In close analogy to the definition of a chirp in dispersion managed solitons, here, the chirp of a discrete beam $\Phi_n(z) = |\Phi_n(z)| \exp[i\Theta_n(z)]$ is defined to be the coefficient of n^2 in the expansion of $\Theta_n(z)$ in a "Taylor series" around $n = 0$. In other words, if $\Theta_n(z) \approx c_0(z) + c_1(z)n + c_2(z)n^2 + \ldots$, then the chirp is given by $c_2(z)$. This definition is valid for moderately localized solitons and breaks down for strongly localized beams.
H. Feddersen, Lecture Notes in Physics, pp. 159-167 (Springer-Verlag, Berlin, 1991).
D. B. Duncan, J. C. Eilbeck, H. Feddersen, and J. A. D. Wattis, Physica D, **68** 1, (1993).
S. Flach and K. Kladko, Physica D **127**, 61 (1999).
S. Flach, Y. Zolotaryuk and K. Kladko, Phys. Rev. E **59**, 6105 (1999).
S. Aubry and T. Cretegny, Physica D **119**, 34 (1998).
Ch. Claude, Y. S. Kivshar, O. Kluth, and K. H. Spatschek, Phys. Rev. B **47**, 14228 (1993).

Chapter 10

Global Description of Patterns Far from Onset: A Case Study

N. Ercolani[1], R. Indik[1], A.C. Newell[1], and T. Passot[2]

[1] *Department of Mathematics, University of Arizona, Tucson, AZ 85721*
[2] *CNRS, Observatoire de la Côte d'Azur, B.P. 4229, 06304 Nice Cedex 4, France*

Abstract. The Cross-Newell phase diffusion equation $\tau(k)\Theta_T = -\nabla \cdot kB(k), \boldsymbol{k} = \nabla\Omega, |\boldsymbol{k}| = k$, and its regularization describe patterns and defects far from onset in large aspect ratio systems with translational and rotational symmetry. In this paper we show how director field solutions of this equation can be used to describe features of global patterns. The ideas are illustrated in the context of a nontrivial case study of high Prandtl number convection in a large aspect ratio, shallow, elliptical container with heated sidewalls, for which we also have the results of simulation and experiment.

1 Introduction

A macroscopic description of convection patterns far from the onset of the convective instability still presents a considerable challenge for both physicists and mathematicians. The path we have followed to tackle this problem is to study the phase diffusion equation that results from the elimination of the complex three-dimensional structure of the microscopic roll pattern and that focuses on the large-scale dynamics of the phase gradient, which is perpendicular to the rolls.

We recently established [1] rigorous proofs for the existence and form of solutions to the regularized phase diffusion equation in the limit where the inverse aspect ratio ε (ratio of the roll wavelength to the typical size